THE JOURNAL
OF
CHEMICAL PHYSICS

VOLUME 16, NUMBER 7 JULY, 1948

The Molecular Diagram Method

PASCALINE DAUDEL AND RAYMOND DAUDEL
Institut du Radium, Laboratoire Curie, Paris

(Received January 6, 1948)

The "importance" of various valence bond formulas, including monoexcited and diexcited formulas, is calculated for a number of resonating organic molecules By "importance" is meant the square of the coefficient of its wave function Several applications of the derived values are discussed

METHOD OF CALCULATION

OBSERVING that naphthalene is representable by means of the three Kékulé formulas (see Formula 1), Pauling represents[1] naphthalene with the diagram shown in Formula 2, which, for each bond, gives its double-bond character.

The excited formulas are not introduced in this diagram. It is possible to introduce them in the following way. Let us consider a Kékulé or an excited formula representing an aromatic molecule, and possessing a double bond between the two atoms l and m. Let S_i be its importance (proportional to the square of the coefficient of its wave function). The number: $I_{lm}=\sum_i S_i$ represents the importance of the sharing between the atoms l and m; we call it the *indice de liaison* of the bond l—m.[2a] Let S_j be the importance of a formula possessing an ineffective bond (i.e., a bond between two non-adjacent carbons) leading to a certain atom l. The number $J_l=\sum_j S_j$ represents the amount of unshared electrons existing in the atom l. It gives quantitatively the Thiele notion of free half-valence; we call it the *indice de valence libre*[2b] of the atom l. For each molecule it is possible to make a diagram which represents these indices.

If we use the importances calculated by Pauling, we get for benzene the diagram shown in Formula 3. For more complicated molecules the number of the formulas which we must use to construct the diagrams rapidly becomes great and the calculation of the importances is very laborious. The importances of the formulas of naphthalene have been calculated by Sherman.[3] Jonnson[4] and Svartholm[5] have calculated those of anthracene and benzanthracene, but they used only the Kékulé and monoexcited formulas, neglecting the diexcited formulas.

Pauling and Wheland's method has been a little simplified, systematized,[6] and used[7] to determine the importances of the formulas (including the diexcited formulas), which represent anthracene and naphthacene. Table I and the

[1] Linus Pauling, *The Nature of the Chemical Bond* (Cornell University Press, Ithaca, New York, 1944).
[2a] Pauling, Brockway and Beach, J. Am. Chem. Soc. **57**, 2705 (1935).
[2b] R. Daudel and A. Pullman, Comptes Rendus **220**, 888 (1945); *ibid.* **222**, 663 (1946); P. Daudel, R. Daudel, R. Jacques, and M. Jean, Rev. Scientifique (1946); P. Daudel, Comptes Rendus **223**, 947 (1946).
[3] J. Sherman, J. Chem. Phys. **2**, 488 (1934).
[4] Jonnson, Ark. f. Kem. Min. Geol. **15A**, No. 14 (1941).
[5] Svartholm, Ark. f. Kem. Min. Geol. **15A**, No. 13 (1941).
[6] R. Daudel and A. Pullman, J. de Phys. 59–64, 74–83, 105–111 (1946).
[7] A. Pullman, Thèse, Paris, 1946.

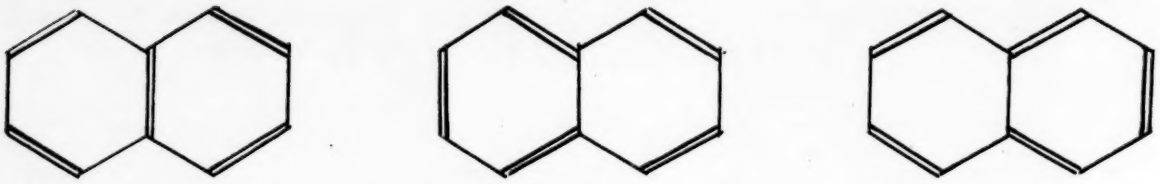

FORMULA 1.

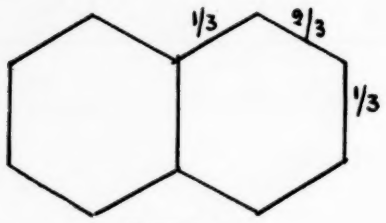

FORMULA 2.

curves of Fig. 1, representing the results obtained, show that the diexcited formulas are very important and that it is not correct to neglect them.

It is pointed out that when the number of rings in an aromatic molecule increases the polyexcited formulas become very important, which leads to very laborious calculations. By using the importances under consideration we obtain the diagram for naphthalene and anthracene shown in Formula 4. Some other diagrams have been calculated in this way.[7]

APPLICATION TO THE STUDY OF THE CHEMICAL PROPERTIES OF MOLECULES

Let us study, for example, the addition of a diatomic molecule AA to an aromatic molecule. Let us consider the approach of AA to the aromatic molecule.

To each formula possessing a double bond between the two atoms C and D (type I, Formula 5) it is possible to associate a formula of type II, Formula 5, using the mesomerism method in order to study the dynamics of the chemical reactions. Let S_i be the importance of the ith formula (type I). If the molecule AA is far from the aromatic molecule, it is possible to admit

TABLE I.

Substances	Unexcited formulas	Importances of monoexcited formulas	Diexcited formulas
Benzene	78	22	0
Naphthalene	54	41	5
Anthracene	10	60	30
Naphthacene	0	40	60

that the part CD is only disturbed; with this condition it is normal to conclude that the importance C_i of the associated formula (type II) is given by the relation

$$C_i = aS_i,$$

where a does not depend on the chosen formula of type I but only on the position of the molecule AA. So, it is possible to write

$$\sum_i C_i = a \sum_i S_i = aI_{cd}.$$

But $\sum_i C_i$ represents roughly the attraction which appears between the molecule AA and the part CD of the aromatic molecule. Since this number is proportionate to I_{CD} we can say:

1. The greater the *indice de liaison* of a bond, the more the molecule which possesses this bond is apt to react by addition.

It is possible to show in the same way that:

2. The addition or the substitution of an atom on a molecule is facilitated by the presence in this molecule of an atom possessing a great *indice de valence libre*.

3. The addition of a diatomic molecule to another molecule is facilitated by the presence in this molecule of two atoms possessing a great *indice de valence libre*.

These are the specific rules of the molecular diagram theory.[8] They have been used in order to study the general reactivity of the aromatic molecules,[8] the diene synthesis,[9] the hydrogena-

TABLE II.

Bond	I_{lm}	J_l	J_m	Y_{lm}	E_{lm}	Number of bond	Energy
$\alpha\beta$	527	123	97	582	30.5	4	122
αO	350	123	67	397	23	4	92
OO	233	67	67	266	17	1	17
$\beta\beta$	376	97	97	424	24.5	2	49
Bond energy of the π-electrons							280

[8] R. Daudel and A. Pullman, Comptes Rendus **221**, 201 (1945).

[9] R. Daudel and A. Pullman, Comptes Rendus **222**, 86 (1946).

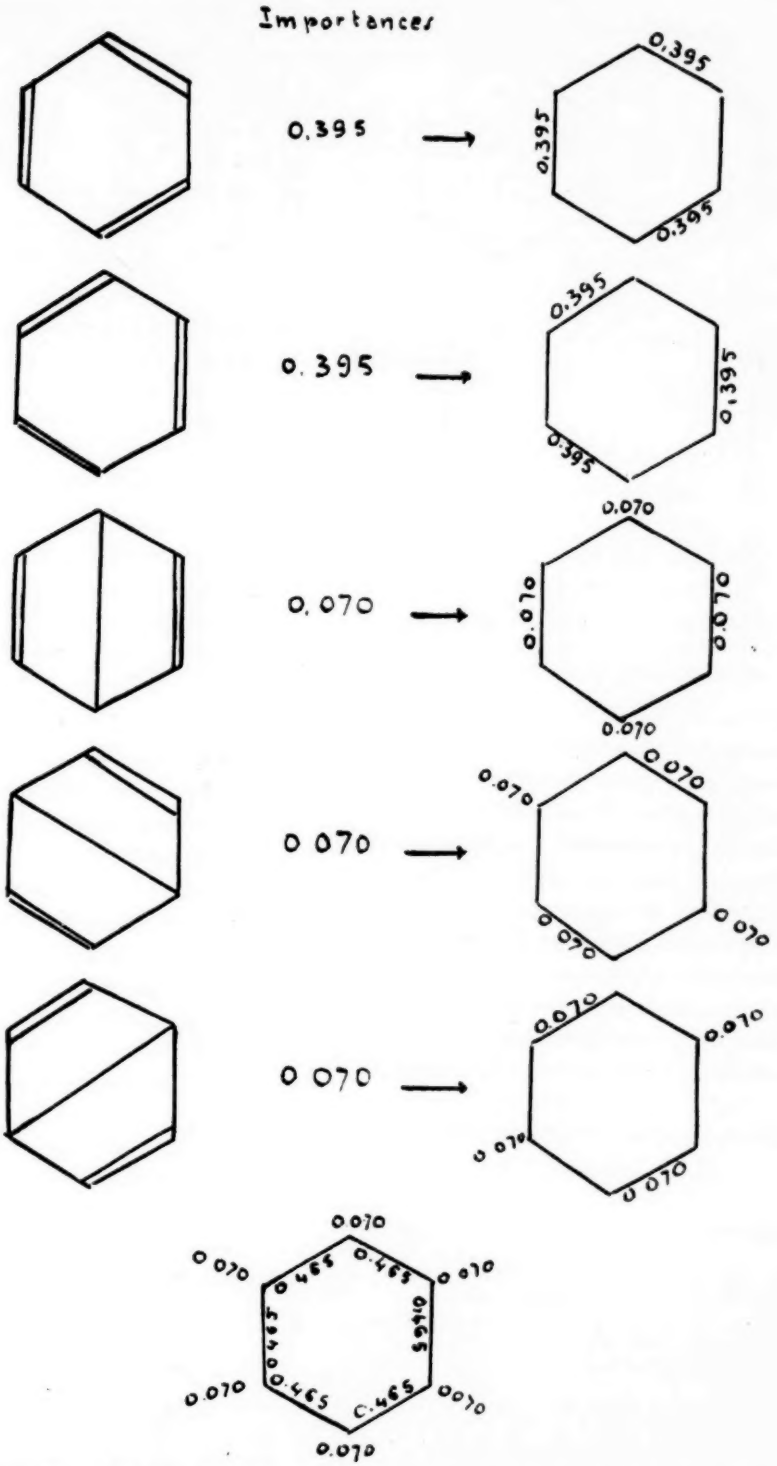
Importances
0.395
0.395
0.395
0.395
0.395
0.395
0.395
0.070
0.070
0.070

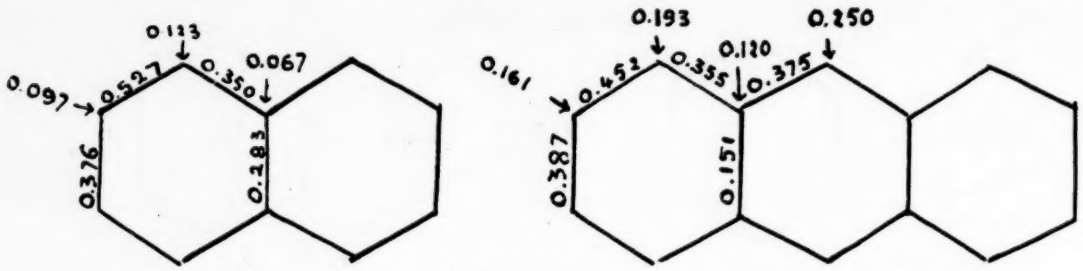

FORMULA 4.

FORMULA 5. The diagram on the left is type I; the one on the right, type II.

double-bond character by the following number:

$$y_{lm} = I_{lm} + a(J_l + J_m/2),$$

which introduces the *indice de liaison* and the *indices de valence libre* in the same time.

In the case of benzene we must obtain $y = \frac{1}{2}$; it is held necessary to take $a = \frac{1}{2}$.

It is possible to establish a relation between the character of a bond and its heat of formation. The consideration of experimental values of the heats of formation of symmetric molecules, such as benzene, leads to the curve shown in Fig. 2.

With it, we can calculate the "*resonance energy*" of aromatic molecules when we know their diagrams. For naphthalene we obtain Table II.

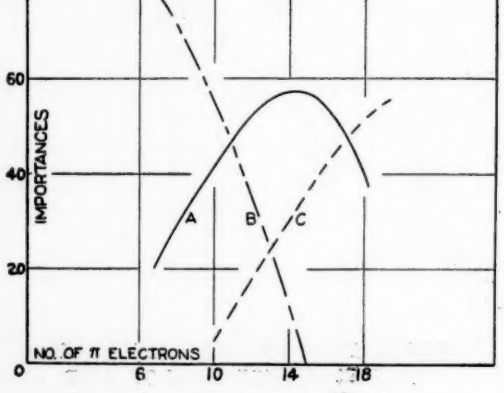

FIG. 1. A—Monoexcited formulas;
B—unexcited formulas;
C—diexcited formulas.

We see that the bond energy of the π-electrons is 280 kcal./mole. If naphthalene could be represented by a Kékulé-like formula this energy would be

$$41.4 \times 5 = 207 \text{ kcal./mole.}$$

The difference (73 kcal./mole) represents the resonance energy, and leads to a good agreement with the experimental value (75 kcal./mole). For anthracene we find a resonance energy of 104.2 kcal./mole and the experimental value is 105.

Using the importances calculated by the mesomerism theory, the molecular diagram leads to better results than those of the simple mesomerism theory because the molecular diagram introduces empirically the variation of the exchange integral α with the interatomic distance.

These interatomic distances can be evaluated with the Pauling curve when we know the molecular diagrams which give the double bond characters y. We obtain, for example, the fol-

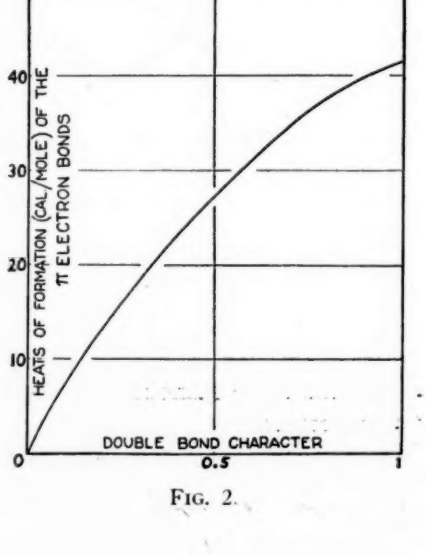

FIG. 2.

TABLE III.

		Double-bond character (direct method)	Double-bond character (Coulson's method)
Benzene		0.465	0.465
Naphthalene	$\alpha\beta$ bond	0.582	0.575
	$\beta\beta$ bond	0.397	0.450
	αO bond	0.266	0.365
	OO bond	0.424	0.400
Anthracene	$\alpha\beta$ bond	0.540	0.590
	αO bond	0.435	0.385
	Om bond	0.467	0.450
	OO bond	0.211	0.340
	$\beta\beta$ bond	0.467	0.435

lowing results:

$\alpha\beta$ bond of naphthalene	1.37A
$\beta\beta$ bond of naphthalene	1.40
$\alpha\beta$ bond of anthracene	1.38
$\beta\beta$ bond of anthracene	1.395

C. A. Coulson has developed another method[12] of determining molecular diagrams, based upon the orbital method. It is possible to establish a correspondence between Coulson's bond orders and the double bond-characters by noting that Coulson finds a bond order of 0.667 for benzene and a bond order of 0.525 for graphite.

Using the bond order diagrams, it is possible to calculate the double-bond characters. Table III compares the results obtained in this way with the numbers directly calculated by the mesomerism method. The agreement is moderately good and it seems that the double-bond character can be placed by decreasing values in the following order:

Naphthalene and anthracene $\alpha\beta$ Benzene
Naphthalene and anthracene $\beta\beta$ and anthracene Om
Naphthalene and anthracene αO
Naphthalene OO
Anthracene OO

GENERALIZATION OF THE METHOD

The method has been generalized by the use of the electro-valency formulas[13] in order to study the substituted and heterocyclic[14] aromatic molecules and inorganic molecules.

This method has been used to study the phenomena of oxidation-reduction,[15] the p_H,[16] the synionie and the free radicals.[17]

TABLE IV.

	Charge of the reactive part*	Carcinogenic power**
5,9,10-methyl-1,2-benzanthracene	2.054	50
9,10-methyl-1,2-benzanthracene	2.043	50
5,6 -methyl-1,2-benzanthracene	2.029	27
10-methyl-1,2-benzanthracene	2.027	23
5-methyl-1,2-benzanthracene	2.016	23
7-methyl-1,2-benzanthracene	2.014	0
8-methyl-1,2-benzanthracene	2.011	0
0-methyl-1,2-benzanthracene	2.000	0

* Calculated by M. Martin.
** These numbers are the index evaluated by Rudali à l'Institut de Radium de Paris (Laboratoire de A. Lacassagne).

APPLICATION TO THE STUDY OF THE PHYSIOLOGICAL PROPERTIES OF THE MOLECULES

O. Schmidt[18] has supposed that the carcinogenic molecules possess a part rich in π-electrons. Svartholm[19] thought that they must tend to react by addition. These two hypotheses[20] have been studied by the molecular diagram method. It seems that there is a good agreement between these hypotheses and the experiments.

With electronic density of the reactive part of the molecules equal, the carcinogenic power increases roughly with the power of addition. With power of addition equal, the carcinogenic power seems to increase with the π-electron charge of the reactive part of the molecule, as is pointed out by Table IV.

[12] For the references see C. A. Coulson, P. Daudel, and R. Daudel, Rev. Scientifique (1947).

[13] P. Daudel and R. Daudel, Comptes Rendus **222**, 738 (1946).

[14] R. Daudel, Comptes Rendus **222**, 798 (1946); Buu Hoi and R. Daudel, Ann. des Pays Bas (1946); R. Daudel, Rev. Scientifique, 229 (1946).

[15] J. Bellugue and R. Daudel, Rev. Scientifique (1946).

[16] Reference 15 and P. Daudel, Comptes Rendus **222**, 799 (1946).

[17] R. Daudel, Trans. Faraday. Soc., "The Labile Molecule" (in press).

[18] For references see R. Daudel. Rev. Scientifique, 37 (1946).

[19] Svartholm, Ark. f. Kem. Min. Geol. **15A**, No. 13 (1941).

[20] Reference 18 and A. Pullman, Thèse, Paris, 1946 and R. Daudel, Bulletin du Cancer (in press).

THE JOURNAL OF CHEMICAL PHYSICS VOLUME 16, NUMBER 7 JULY, 1948

Structure of Micelles of Colloidal Electrolytes. III. A New Long-Spacing X-Ray Diffraction Band, and the Relations of Other Bands*

R. W. MATTOON,** R. S. STEARNS,*** AND W. D. HARKINS
George Herbert Jones Chemical Laboratory, University of Chicago, Chicago 37, Illinois

(Received February 5, 1948)

A newly found x-ray diffraction band, obtained from aqueous solutions of soaps and detergents, gives a Bragg spacing which is independent of concentration and is close to the double-length of the molecule. This is designated as the micelle thickness or M-band. The already known long-spacing band, interpreted here as related to the intermicellar distance, is designated as the I-band. Its spacing d_I increases with decreasing soap concentration. If a hydrocarbon is solubilized in the micelles, these spacings increase by Δd_M and Δd_I. Formerly, Δd_I was supposed to give the mean thickness of the layer of oil dissolved between the ends of the hydrocarbon chains of the soap molecules as a middle layer in the micelle. However, Δd_M seems to be more directly related to this thickness. As measured by d_M, the thickness of the micelle remains constant with increasing soap concentration: e.g., the values are 40.8, 41.5, 40.7, 40.2, 39.5, 39.6, 40.2A for potassium myristate at 25°C at the following respective concentrations: 2.3, 4.5, 7.2, 9.8, 12.0, 13.7, and 16.5 percent. The mean "thickness" increases from 29.7A for potassium caprylate (C_8) to 47.3 for potassium palmitate (C_{16}). By a method explained in the text, the number of molecules in a potassium myristate micelle is calculated as 56 at 9.8 percent by use of the Bragg I-spacing. However, it is probable that a corrected Bragg spacing should be used. A new long-spacing band, designated as an X-band, appears when an I-band is present and oil is solubilized in the micelles. The order of spacing is then $d_I > d_M > d_X$; e.g., in one case the values are $84 > 50 > 27$A.

The "cylindrical" model of the micelle preferred here differs from the lamellar and in some respects from the spherical model. It exhibits the following characteristics: (1) A micelle consists of one double-layer of soap or detergent molecules. These have their polar ends oriented outward toward the water and their non-polar ends inward toward each other. (2) The thickness of the micelle of a pure soap is essentially twice the length of the soap molecule, independent of concentration. (3) Hydrocarbons solubilize inside the micelle between the two layers of soap molecules and thus make he micelle thicker. (4) The area per soap molecule in the micelle remains practically constant, whether or not solubilized hydrocarbons are present. (5) The width or lateral dimension of the micelle and the number of soap molecules per micelle increase with increasing soap concentration and with solubilization of hydrocarbons. (6) From energy considerations the area of contact between the hydrocarbon chains of the detergent molecules and the water must be as small as is compatible with the other conditions imposed upon its structure.

I. INTRODUCTION

ACCORDING to the theory of the mechanism of emulsion polymerization developed in this laboratory,[1] the initial locus of polymerization lies in the monomer solubilized in the soap micelles, so micellar structure is important in this type of polymerization. The present paper presents a structure for the micelle and gives estimates of its size. The discovery of a new x-ray band,[2] which measures the thickness of the micelle, makes it necessary to reconsider the significance of the long-spacing x-ray band investigated earlier. Solubilization data[3] are also used in making certain deductions.

All previous models of micellar structure have been based on the theory of the orientation of molecules in surfaces and interfaces as developed by Harkins[4,5] and by Langmuir,[6] especially on the energy relations developed by the former.[4] The following quotation[5] is specially pertinent if it is kept in mind that the micelles constitute a new phase:

"The general law for surfaces seems to be as follows: *If we suppose the structure of the surface of a liquid to be at first the same as that of the interior of the liquid, then the actual surface is*

* This investigation was carried out under the sponsorship of the Reconstruction Finance Corporation, Office of Rubber Reserve, in connection with the Government's synthetic rubber program.

** Present address: Research Laboratory, Procter and Gamble Company, Cincinnati 17, Ohio.

*** Present address: Chemical and Physical Research Laboratories, Firestone Tire and Rubber Company, Akron 17, Ohio.

[1] W. D. Harkins, J. Am. Chem. Soc. **69**, 1428 (1947).

[2] R. W. Mattoon, R. S. Stearns, and W. D. Harkins, J. Chem. Phys. **15**, 209 (1947).

[3] R. S. Stearns, H. Oppenheimer, E. Simon, and W. D. Harkins, J. Chem. Phys. **15**, 496 (1947).

[4] W. D. Harkins, F. E. Brown, and E. C. H. Davies, J. Am. Chem. Soc. **39**, 354 (1917).

[5] W. D. Harkins, E. C. H. Davies, and G. L. Clark, J. Am. Chem. Soc. **39**, 541 (1917).

[6] I. Langmuir, J. Am. Chem. Soc. **39**, 1848 (1917).

always formed by the orientation of the least active portion of the molecule toward the vapor phase, and at any surface or interface the change which occurs is such as to make the transition to the adjacent phase less abrupt."

"At interfaces the molecules turn so that their *like* parts come together in conformity with the general law. With solutions, the solute molecules orient so that the ends of the molecules toward the liquid *A* are as much like *A* as possible, and the ends toward *B* are as much like *B* as possible. So at interfaces between organic liquids and water, for example, the organic radical sets toward the organic liquid, and the polar group toward the water."

The formation of the micelle is due to the fact that there is a very high interfacial free energy between hydrocarbon and water (*ca.* 50 ergs per sq. cm) and none between hydrocarbon and hydrocarbon. Thus there is a large decrease of free energy if the hydrocarbon chains of the soap molecules leave their environment of water and aggregate to give a hydrocarbon environment. The fact that the micelles are relatively small is due to the repulsion of the polar-ionic ends of the soap molecules, which orient themselves toward the water, or the outside of the micelle, whereas the hydrocarbon chains orient toward the inside. On this basis all earlier models for the micelle and that preferred here agree as to the type of orientation involved, but disagree as to the number of kinds of micelles, their form, and their size.

Probably the oldest theory is that of McBain,[7] who considered that there are two types of micelles, presumably in equilibrium with each other. At low concentrations he assumed a spherical ionic micelle as more prominent, but at higher concentrations, a "non-ionic" micelle. Later he considered this as weakly ionic, "lamellar," and very large, identical in structure[8] with that proposed by a number of German investigators, who also assumed the existence of a small micelle.[9] According to Philippoff the large micelles contain about 10^7 molecules.[9j] Hartley,[10] however, considered that there is only one type of micelle, which is spherical, with a radius in a solution of a pure soap about the length of the soap molecule. He did not have the advantage of knowing the results of x-ray work, but his model agrees moderately well with the properties of soap solutions as known at that time. Its principal defect is that it does not allow the micelle of the pure soap to change in size since the radius is constant; the "cylindrical" model preferred here allows a change in size while still maintaining a constant thickness.

Krishnamurti[11] in early work ascribed to micelles a diffuse, long-spacing x-ray diffraction from sodium oleate solutions. Later, many x-ray and related investigations on soap solutions were carried out in Germany.[9]

On the basis of the x-ray spacings a large lamellar micelle was proposed.[9a] This was assumed to consist of several (*ca.* 4 to 6) parallel double-layers of soap molecules, each double-layer separated from the next by a "bound" layer of water. The x-ray long-spacing, designated by us as d_I, was interpreted as measuring the identity distance from a plane in one double-layer to the corresponding plane of an adjacent one. The water layer, whose thickness was considered as d_I minus twice the length of the soap molecule, became thicker upon dilution, since d_I increased.[9e, i] The solubilization of an oil in a given soap solution increases d_I an amount Δd_I, which was interpreted[9e] as the thickness of the oil layer in the middle of each soap double-layer. The thickness of the water layer was assumed to remain unchanged.

The lamellar model was adopted in the first of two papers from this laboratory[12] on x-ray investigations of aqueous solutions of pure soaps. In a second paper on x-ray spacings with solu-

---

[7] J. W. McBain, *Fourth Colloid Symposium Monograph* (Chemical Catalog Company, New York, 1926), p. 8; Kolloid Zeits. **40**, 1 (1926).

[8] J. W. McBain, *Advances in Colloid Science* (Interscience Publishers, Inc., New York, 1942), Vol. I, pp. 122–144.

[9] [a] K. Hess and J. Gunderman, Ber. **70B**, 1800 (1937); [b] W. Philippoff and K. Hess, Ber. **70B**, 1808 (1937); [c] K. Hess, H. Kiessig, and W. Philippoff, Naturwiss. **26**, 184 (1938); [d] J. Stauff, Naturwiss. **27**, 213 (1939); [e] H. Kiessig and W. Philippoff, Naturwiss. **27**, 593 (1939); [f] K. Hess, W. Philippoff, and H. Kiessig, Kolloid Zeits. **88**, 40 (1939); [g] J. Stauff, Kolloid Zeits. **89**, 224 (1939); [h] J. Stauff, Kolloid Zeits. **96**, 244 (1941); [i] H. Kiessig, Kolloid Zeits. **96**, 252 (1941); [j] W. Philippoff, Kolloid Zeits. **96**, 255 (1941); [k] K. Hess, H. Kiessig, and W. Philippoff, Fette und Seifen **48**, 377 (1941); [l] K. Hess, Fette und Siefen **49**, 81 (1942); [m] H. Kiessig, Kolloid Zeits. **98**, 213 (1942).

[10] G. S. Hartley, *Aqueous Solutions of Paraffin-Chain Salts* (Hermann et Cie, Paris, 1936).

[11] P. Krishnamurti, Ind. J. Phys. **3**, 307 (1929).

[12] W. D. Harkins, R. W. Mattoon, and M. L. Corrin, J. Am. Chem. Soc. **68**, 220 (1946), see corrections on p. 2751 in this volume.

TABLE I. X-ray bands diffracted from clear liquid aqueous solutions of colloidal electrolytes at room temperature.

Band symbol	Bragg spacing symbol	Approximate Bragg spacing, A	Behavior	Tentative interpretation of spacing
W	d_W	31.–3.2	[a, b]	From liquid water
S	d_S	4.5–4.6	[a, c, d]	Side-spacing between soap molecules in micelle
M	d_M	30–60	[e]	Thickness of micelle
	Δd_M	0–15	[f]	Thickness of oil solubilized in middle of micelle
I	d_I	30–100	[e, g]	Intermicelle spacing
	Δd_I	0–30	[f]	Increment of intermicelle spacing due to solubilized oil
X	d_X	25–30	[h]	Uncertain

[a] Spacing remains constant with changing soap concentration and with simple hydrocarbons solubilized.
[b] Intensity becomes weaker with increasing soap concentration.
[c] Intensity becomes stronger with increasing soap concentration.
[d] Intensity remains practically unchanged with simple hydrocarbons solubilized.
[e] Spacing remains nearly constant with changing concentration of a given soap, is larger for longer soap molecules, and is approximately twice the length of the soap molecule; intensity becomes stronger with increasing soap concentration and with simple hydrocarbons solubilized, until this band is overshadowed by the I-band.
[f] Spacing difference increases steadily as a hydrocarbon is solubilized in a given solution up to saturation. The behavior is very specific.
[g] Spacing steadily decreases with increasing soap concentration; intensity becomes stronger with simple hydrocarbons solubilized; this band first appears at a higher soap concentration than does the M-band for the same soap.
[h] Obtained only from solutions of high soap concentration containing much solubilized oil.

bilized hydrocarbons present,[13] predictions of the lamellar model were tested to see if they meet the requirements of the related data.

It was assumed by both the Germans and McBain that (a) the lamellar micelle is very large[14] and (b) that the increase in spacing indicated by Δd_I because of solubilization of an oil, is the thickness of the oil layer. Now if the micelle is very large it should be possible to calculate the thickness τ of the oil layer by dividing the volume V of the oil dissolved in the micelles by the total area of the double-layers. The mean area per soap molecule is approximately 30A^2. Thus

$$\tau = \frac{V}{(N/2)30(10)^{-16}} \text{cm},$$

where N is the number of soap molecules; in the double-layer it takes two molecules of soap to give an area of 30A^2.

On the basis of the large lamellar model $\tau/\Delta d_I$ should be close to unity, since the double-layers are assumed to be so large as to make edge corrections insignificant.

However, the ratio found[13] for n-heptane and triptane in a 25 percent solution of potassium laurate and for ethyl benzene in a 15 percent solution was, at all concentrations of the oils, very close to 0.4. This shows that either: (a) Δd_I does not give the thickness of the oil layer, or (b) the micelle is much smaller than was supposed, so the edge corrections become very large.

Actually, both of these are true.

By assuming spherical micelles, Corrin obtained better, but not perfect, agreement between τ and Δd_I.

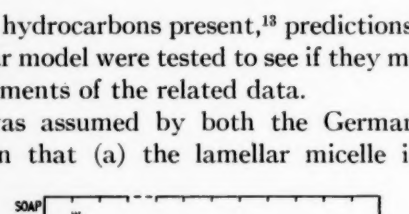

FIG. 1. General illustration of the x-ray bands diffracted from clear liquid aqueous solutions of straight long-chain colloidal electrolytes at room temperature, showing the effects of concentration and solubilized hydrocarbons. The spacings represent only the order of magnitude.

II. GENERAL RELATIONS OF THE X-RAY DIFFRACTION BANDS

Four bands (W, S, M, and I) are obtained from clear, liquid, isotropic, aqueous solutions of pure soaps and detergents, without or with solubilized oils, at room temperature; a fifth band (X) has been obtained only under special conditions. Table I summarizes the order of magnitude of these spacings, the behavior of the bands, and a tentative interpretation. Figure 1 is a general diagram which represents these bands.

The fact that the short-spacing S-band (Fig. 2) is broad indicates a liquid type of arrangement of the soap molecules in the monolayers making up the micelles. The Debye-Keesom equation for

[13] W. D. Harkins, R. W. Mattoon, and M. L. Corrin, J. Colloid Sci. 1, 105 (1946).

[14] Thus in reference 8, p. 124, McBain, in a discussion of the work of Stauff (see reference 9[d, g, h]) states "His 'Grossmizellen' are identical with McBain's neutral or lamellar micelle."

diffraction from liquids

$$\lambda = 0.814(2r)\sin\theta \qquad (1)$$

is derived from the first maximum of the function $(\sin sr)/sr$, where

$$s = 4\pi \sin\theta/\lambda,$$

θ is one-half the scattering angle for the maximum diffraction intensity, and r is the distance between nearest neighbors. Equation (1) combined with Bragg's equation reduces to

$$r = 1.23 d_s. \qquad (2)$$

For soap solutions r is about 5.5 to 5.7A. Assuming close-packed hexagonal arrangement, the area per soap molecule σ is

$$\sigma = (\sqrt{3}/2)r^2 = 1.31 d_s^2.$$

The values of σ vary from 26.5 to 27.5 sq. A.

III. EXPERIMENTAL

The experimental techniques have been described earlier.[12] All long-spacing x-ray photographs were taken in the vacuum small-angle diffraction camera using Ni-filtered CuK_α radiation. An improved brass cell was used which has a capacity of 10 cc, is fitted with two pure beryllium windows 0.1 mm thick and 1 mm apart, and is sealed at the top with a large cap pressed into a rubber-gasketed groove.

The photographic films were held plane and perpendicular to the direct beam 15.00 cm from the sample. This distance was checked by the (200) diffraction from NaCl ($a = 5.628$A), the (002) from graphite ($c = 6.6915$A) and the (001) from lauric acid ($c \sin\beta = 27.4$A).

All soaps, detergents, and oils were purified carefully. The saturated fatty acids were recrystallized repeatedly from ethyl alcohol and acetone, then hydrogenated, and finally distilled twice in a high vacuum. After neutralization the soaps were again recrystallized. All solutions, without and with solubilized oils, were made up fresh and appeared as clear as the distilled water. For solubilization, the solutions were sealed in glass ampulses and shaken mechanically for several days to several weeks.

Since slits were used instead of pinholes to reduce exposure times, the films show straight bands 1.2 cm high instead of rings. Traces made on two different microphotometers showed the usual small zig-zag lines from the emulsion grain (see Fig. 7 in reference 12). A new photoelectric microphotometer was built with a narrow scanning light which covered the complete height of the bands. This averaged over a larger area and gave a very smooth trace. A rotating step-sector was used to convert densities into energies, but since the films were exposed so that the densities of the bands were on the linear part of the density-exposure calibration curve, this conversion was not used throughout.

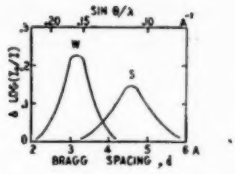

FIG. 2. The water *W*-band and the soap short-spacing *S*-band from 25.0 percent by weight aqueous potassium laurate at 25°C, resolved from the microphotometer trace.

The microphotometer traces give the complete diffraction, coherent plus incoherent, from the colloidal solutions. The shape of the whole curve is significant. To obtain *net* contributions of the bands, three different backgrounds may be applied.

1. The water background, giving the contribution from the non-micellar and the micellar soap.

2. The critical concentration background, giving the contribution from the micellar soap. However, this is not quite correct, since the concentration of non-micellar soap in equilibrium with micelles is not constant.

3. A curve drawn which fits smoothly the general trend of the trace and shows only the deviations caused by the definite bands, giving only the coherent scattering from the micelles. This is I_0 in the ordinates of the figures.

In our analysis background 3 was used. The significance of the particular background used, if any, is important.

IV. THE NEW *M*-BAND RELATED TO MICELLE THICKNESS

Since 1943, it has been noticed that the *I*-band is superimposed on what appears to be a much broader, weak background-scattering, extending from the direct beam outward and having a rather abrupt shoulder. This background pattern, which is clearly evident in an earlier photograph,[9e] remained at soap concentrations below that at which the *I*-band disappeared but not below the critical micelle concentration. From an analysis of microphotometer traces it was suspected that this might be a real band, and a number of crucial test experiments proved its reality.

1. It was thought that the band might be due to weak CuK_β and weak continuous radiation in the incident beam. To eliminate this possibility, strictly monochromatic $CuK_{\alpha 1 \text{ and } 2}$ only, clearly resolved in the direct beam on the films, was obtained from the (200) diffraction from a LiF crystal. However, a 65-hour exposure in the vacuum camera with two lead slits still revealed the band from a 12.2 percent potassium laurate solution.

2. When the soap solution was replaced by pure water, the band disappeared. Consequently, it is due only to the soap in solution; it was not due to any geometrical factors in the slit system or to shielding by the cell.

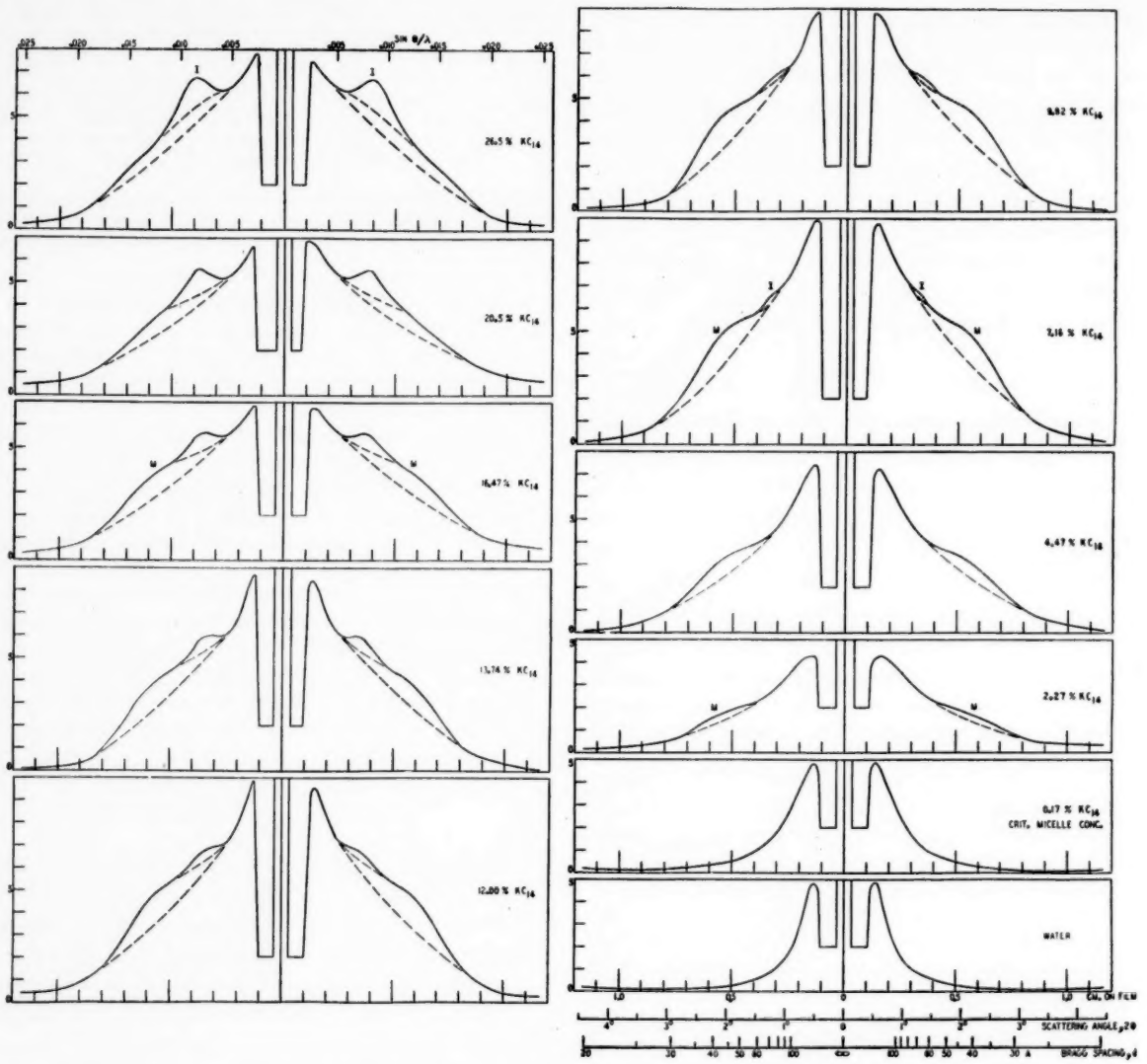

FIG. 3. Microphotometer traces of the long-spacing x-ray diffraction, taken in a vacuum camera, from aqueous solutions of potassium myristate (KC_{14}) at 25°C.

3. The slit system was replaced by two lead pinholes which gave a beam image on the film only 0.9-mm diameter. A 65-hour exposure of Ni-filtered CuK_α to the soap solution again revealed the band, so it is not due to overlapping from slits.

4. Using experimental arrangement 3, when the soap solution was replaced by pure water or by potassium laurate at its critical concentration (0.56 percent), the band disappeared. Again, it was proved to originate from the soap in solution, but only above its critical concentration.

5. Aqueous solutions of potassium laurate when aged develop visible flakes of acid-soap which contribute a very sharp, crystalline line of Bragg spacing 35.6A to the diffraction pattern. To eliminate the presence of even submicroscopic acid-soap particles in fresh solutions, sodium lauryl sulfate was selected, since its solutions remain perfectly clear and have negligible hydrolysis. Experimental arrangement 3, when applied to a 15 percent sodium lauryl sulfate solution, revealed the band similar to that for 12.2 percent potassium laurate, so the band cannot be due to acid-soap. Also, solutions of potassium decyl sulfonate (with no hydrolysis) likewise show the band, and incidentally the *I*-band at high concentrations.

This band will be designated the M-band, since it measures the thickness of the micelle.

Figure 3 presents microphotometer traces of the long-spacing x-ray diffraction from aqueous solutions of potassium myristate. The ordinate is in arbitrary units of intensity as read from the

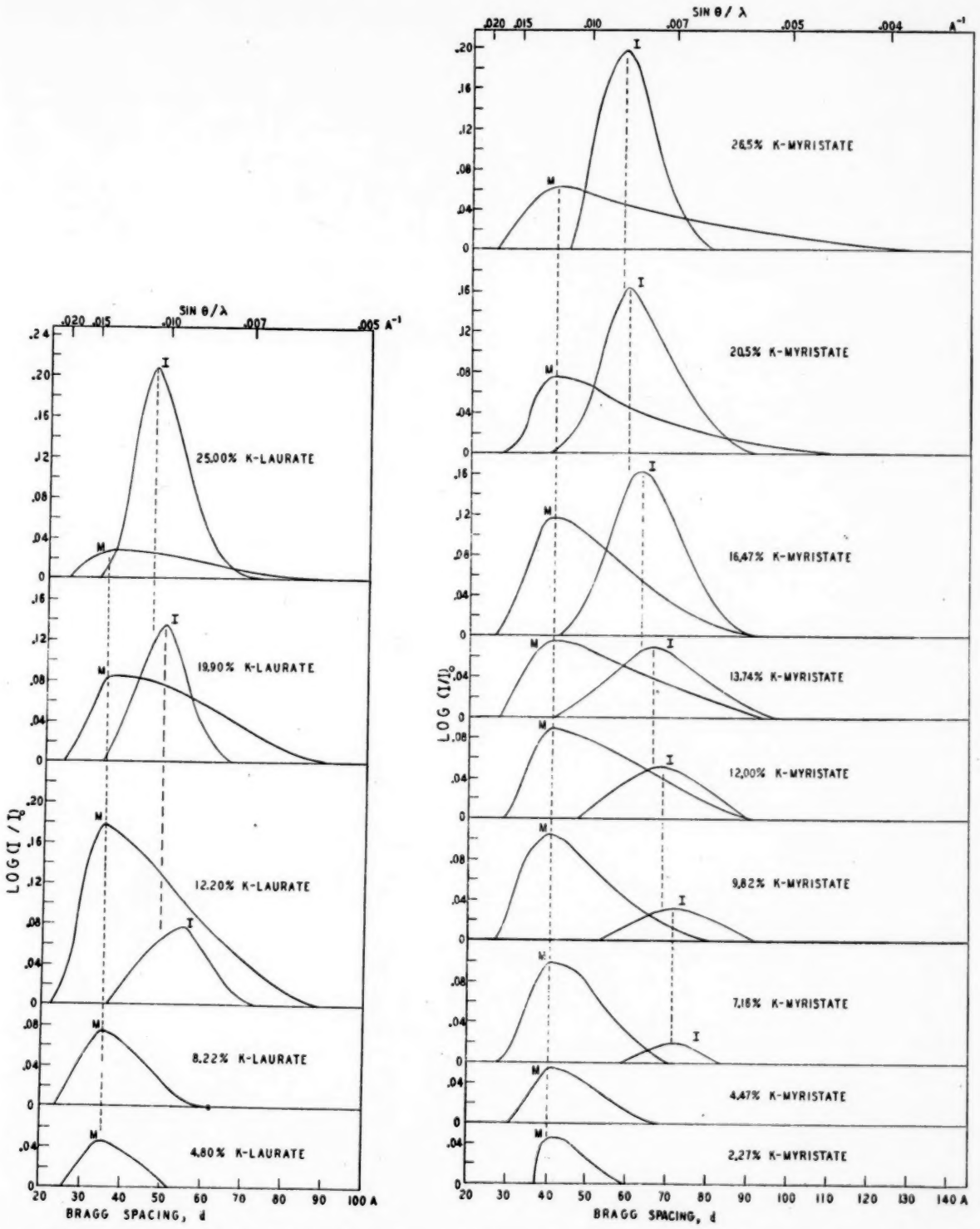

FIG. 4. Resolved *M*-band and *I*-band from aqueous solutions of potassium laurate and potassium myristate.

photoelectric microphotometer. Readings were taken every 0.013 cm across the film, and the intensity variation from the solid line shown was never more than 0.05 of the intensity units shown. The width of the direct beam is shown by the two lines on each side of the center line and

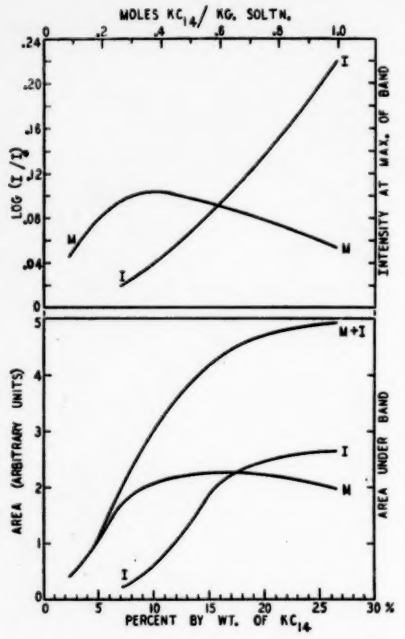

FIG. 5. Intensity at the maximum and total area under the M- and I-bands as a function of the concentration of potassium myristate (KC_{14}) in aqueous solution.

nearest it. The trace at the bottom is the scattering with water. At the critical concentration of potassium myristate (0.17 percent) no micellar M-band appears, even though long exposures were taken to attempt to record it. At 2.27 percent (0.08 molal) the M-band is evident and it becomes more pronounced at higher concentrations.

With the background drawn in, as described in Section III, the diffraction patterns can be resolved into the discrete M- and I-bands. These are shown in Fig. 4 for potassium myristate and potassium laurate. With this particular background the resolved bands come down to zero intensity. With the water or critical concentration background, they would not come down to zero.

In Fig. 5 for potassium myristate, the intensity of the M-band increases up to about 10 percent of this soap and then decreases, whereas that for the I-band steadily increases. The same general behavior holds for the areas under the bands. The concentration at which the I-band first appears (about 5 percent for potassium myristate, about 9 percent for potassium laurate, and about 15 percent for sodium lauryl sulfate) is considerably above the concentration at which the M-band first appears. The intensities of these two bands might have been interpreted as a measure of the relative abundances of two kinds of micelles. However, a single kind of micelle may give the M-band and at higher concentrations, where these micelles are necessarily closer together, the I-band may result from a network of these micelles, giving an intermicelle spacing. At high concentrations the total diffracted intensity would then be partitioned between that from the single micelles (M) and that from the intermicelle arrangement (I). Under this supposition, with increasing concentration the M-spacing should remain constant whereas the I-spacing should decrease. This is what is observed.

TABLE II. M-spacings derived from the position of the peak of the M-band for aqueous soap solutions at 25°C.

	Percent by weight of soap	Bragg M-spacing $d_M \pm 1A$
Potassium caprylate KC_8	6.05	no band
	17.36	29.5 (weak diffraction)
	25.00	30.3
	29.6	30.0
	34.4	29.6
	39.9	30.7
	43.8	28.2
		Av. 29.7
Potassium caprate KC_{10}	7.97	30.3
	9.65	32.8
	10.51	31.2
	11.93	32.5
		Av. 31.7
Potassium laurate KC_{12}	4.80	35.5
	8.22	34.8
	9.10	35.0
	12.10	34.5
	12.20	35.0
	13.20	35.6
	15.00	35.2
	16.70	36.0
	19.90	35.7
		Av. 35.3
Potassium myristate KC_{14}	2.27	40.8
	4.47	41.5
	7.16	40.7
	9.82	40.2
	12.00	39.5
	13.74	39.6
	16.47	40.2
		Av. 40.3
Potassium palmitate KC_{16}	1.28	44.9
	3.44	49.1
	5.01	47.9
		Av. 47.3
Sodium lauryl sulfate	8.6	37.3
	15.0	37.1
	20.0	36.7
	25.0	38.2
		Av. 37.3

Table II presents the M-spacings for a homologous series of soaps at different concentrations.[15] It is at once evident that the M-spacing is very constant for a given soap at all concentrations. The lowest concentration at which the M-band has been measured thus far is 1.28 percent potassium palmitate. A binary soap mixture should have an intermediate M-spacing.

The average M-spacing for each soap is very close to twice the length of that soap molecule as derived from crystal diffraction data or from a scale model of the molecule. Sodium lauryl sulfate falls into line also, d_M being 2.0A longer than potassium laurate. This is reasonable, since the sulfate group is a little larger than the carboxyl group. In passing from one soap to the next longer in Table II and using two soap molecules in line to correspond to d_M, the increment should be $2\times 2.54 = 5.08$A. The successive increments in the average d_M are actually 2.0, 3.6, 5.0, and 7.0A.

The question arises whether the simple Bragg spacing d_M is a measure of the actual spacing. For a spherical liquid molecule the Bragg short-spacing is increased by the factor 1.23, as shown in Eq. (2) Section II, in order to give the diameter. This results from the well-known work by Debye and also of Warren.[16] However, the correction factor for micelles has not been worked out, although Debye has outlined the theoretical calculations to us. The diffraction depends, among other things, upon the total scattering from all the electrons in each molecule integrated over its length with respect to the *density* of scattering electrons distributed along the molecule. Ideally, one should have an atom of high atomic number at the polar *end* of the molecule if d_M is to give the best measure of the double-length. Because of these considerations, the simple Bragg spacings d_M and also d_I will be used until the correction factors are known.

The M-spacing is interpreted as being related to the thickness of the micelle, consisting of only *one* double-layer of soap molecules.

[15] In Tables I, IIIa, and VIa, c of reference 12, the long-spacings given for solutions of sodium and potassium caprylate are now found to be those for the M-band; all other long-spacings given there still remain those for the I-band.

[16] B. E. Warren, Phys. Rev. **44**, 969 (1933).

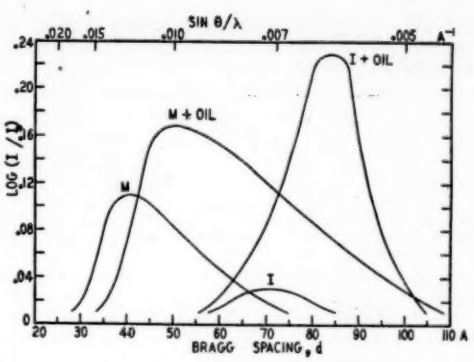

FIG. 6. Example of the increase in intensity and shift to longer spacings of the M- and I-bands from a soap solution caused by the addition of solubilized hydrocarbon. This is a 9.82 percent by weight aqueous solution of potassium myristate saturated with benzene (3.82 g benzene per 100 g soap solution).

V. EFFECT OF SOLUBILIZED OILS ON THE M-BAND

The saturation of a soap solution with a hydrocarbon oil increases both the intensity and the spacing of the M-band, an example of which is shown in Fig. 6.

Figure 7 represents the steady increase of the M-spacing up to saturation with solubilization of increasing amounts of ethyl benzene in a soap solution. With a little more hydrocarbon than the saturation value added, d_M does not increase further.

Hydrocarbons were used to *saturate* solutions of potassium laurate and potassium myristate of various concentrations. These solutions were sealed in ampules and shaken vigorously for 11 days by the use of a mechanical shaker. There

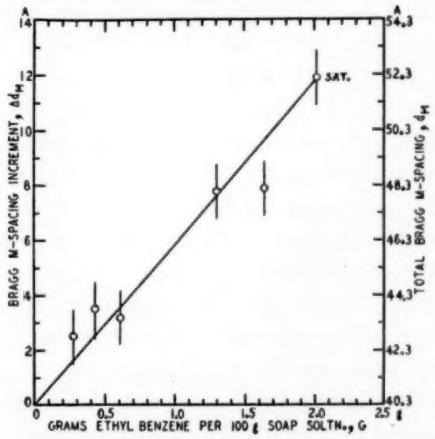

FIG. 7. Increase in the Bragg M-spacing caused by ethyl benzene when solubilized in a 7.16 percent by weight aqueous solution of potassium myristate.

TABLE III. *M*-spacings for aqueous solutions of potassium laurate (KC_{12}) and potassium myristate (KC_{14}) *saturated* with hydrocarbons at 25°C.

Hydrocarbon solubilized	Percent by weight of soap	Bragg *M*-spacing $d_M \pm 1$A	Bragg *M*-spacing increment due to hydrocarbon $\Delta d_{M\,sat} \pm 2$A	Solubility, grams hydrocarbon per 100-g soap solution, G_{sat}
Ethyl benzene	7.00 KC_{12}	40.7	5.4	1.07
	8.84	41.1	5.8	1.48
	10.09	41.5	6.2	1.77
	12.05	41.8	6.5	2.23
	13.60	42.0	6.7	2.63
n-heptane	4.47 KC_{14}	50.0	9.7	0.46
	7.16	51.0	10.7	0.84
	9.82	51.2	10.9	1.24
	12.00	49.2	8.9	1.59
	13.74	48.2	7.9	1.89
Ethyl benzene	4.47 KC_{14}	50.4	10.1	1.13
	7.16	52.2	11.9	2.02
	9.82	51.4	11.1	2.99
	12.00	48.4	8.1	4.03
	13.74	47.8	7.5	4.56
Benzene	4.47 KC_{14}	51.2	10.9	1.57
	7.16	52.0	11.7	2.66
	9.82	49.6	9.3	3.82
	12.00	49.4	9.1	5.08
	13.74	49.0	8.7	5.96

Notes: With no solubilized hydrocarbon, $d_M = 35.3$ for KC_{12} and $d_M = 40.3$A for KC_{14} independent of soap concentration (Table II).

At the higher soap concentrations, the values of Δd_M are less accurate because of the influence of the *I*-band (Fig. 4).

At 25°C the density of *n*-heptane is 0.679, ethyl benzene is 0.862, and benzene is 0.873 g/cc.

At 25°C the solubility in 100 grams of water for *n*-heptane is 0.005, ethyl benzene is 0.015, and benzene is 0.185 grams.

Aqueous solutions of sodium lauryl sulfate saturated with hydrocarbons give similar relations.

remained a small excess of the oil on top of the lower, clear, saturated solution which was x-rayed. Measurements on these solutions are presented in Table III. The variation of the Bragg spacing increment Δd_M for a given oil in different concentrations of a given soap is small. Of importance is the fact that the mean ethyl benzene increment for the 14 carbon atom soap is about twice that for the 12 carbon atom soap. This is in harmony with the effect of different soaps on solubilization of a given oil[3] and agrees with other evidence in suggesting that the *number of soap molecules per micelle* increases as the soap molecules increase in length.

The *M*-spacing increment Δd_M is interpreted as being related to the increase in micelle thickness caused by hydrocarbon which is solubilized in the middle of the micelle.

VI. EFFECT ON THE *M*-BAND BY PENETRATION OF POLAR-NON-POLAR MOLECULES INTO THE SOAP LAYER

In contrast, when long-chain *n*-alcohols, *n*-amines, and similar polar-non-polar molecules are added to an aqueous soap or detergent solution, the *M*-spacing does *not* increase.[17] Here it is postulated that these polar-non-polar molecules *penetrate* a soap monolayer in a micelle, thus not increasing the *M*-spacing thickness but making the micelle larger in lateral extension. The *S*-band short-spacing is not altered by the addition of long straight-chain molecules.

VII. A NEW UNINTERPRETED *X*-BAND

A weak, moderately broad, distinct, long-spacing band (*X*) is clearly evident in an earlier photographic reproduction.[9e] In our work it was found when solubilized small molecules of tetrahedral symmetry[13] were present. The assumed first-order spacing d_X is shorter than d_I or d_M. It has not appeared with any of the soaps used here when dissolved in water up to concentrations at which the solutions cease to be clear, and liquid, nor with dilute soap solutions containing solubilized hydrocarbons which show only the *M*-band, even after long exposures. A 17-hour exposure with 26.5 percent aqueous potassium myristate showed no *X*-band (normal exposure for the *I*-band here is 3 hours). The *X*-band appears only when the *I*-band is fairly intense and when solubilized hydrocarbons are

TABLE IV. Bragg *I*-, *M*-, and *X*-spacings (all assumed first order) from aqueous potassium myristate solutions saturated with hydrocarbons at 25°C.

	Hydrocarbon solubilized				Percent by weight of soap
	None	*n*-heptane	Ethyl benzene	Benzene	
d_I	71A	80	80	84	9.82
d_M	40.2	51.2	51.4	49.6	
d_X	no band	26.6	25.5	26.9	
d_I	68	74	72	77	12.00
d_M	39.5	49.2	48.4	49.4	
d_X	no band	26.4	26.0	27.1	
d_I	66	78	78	78	13.74
d_M	39.6	48.2	47.8	49.0	
d_X	no band	28.0	28.7	29.4	

The hydrocarbon solubilities for these solutions are included in Table III.

[17] W. D. Harkins, R. W. Mattoon, and R. Mittelmann, J. Chem. Phys. **15**, 763 (1947).

present. These conditions mean that the micelles are fairly close together and that they are of larger lateral extension, which is more conducive to a short-range order.

Table IV gives a collection of the I-, M-, and X-spacings for twelve solutions. It may be noted that $d_I - d_M \approx d_X$. In soap crystals odd orders are stronger than even orders. Perhaps d_X is the third order of d_I.

VIII. THE LONG-SPACING I-BAND

The well-known long-spacing band diffracted from aqueous solutions of colloidal electrolytes is called here the I-band. Some new measurements are now presented.

The microphotometer traces in Fig. 3 show the I-band. In Fig. 4 this band is resolved for various concentrations of potassium laurate and potassium myristate. The variation of the intensity and area of the I-band with the concentration of potassium myristate is shown in Fig. 5.

The German workers[9e, i] have shown that the d_I spacing increases with dilution. A more precise description of the functional relationship between d_I and the concentration c (weight fraction of soap) is given here. Table V gives measurements from a very careful analysis of our films.

In Fig. 8 the I-spacing from Table V is plotted against c. A Cartesian plot is obviously not linear. However, a fairly linear plot is obtained by a logarithmic relationship:

$$d_I = k_1 + k_2 \log(1/c)$$

and also by a hyperbolic relationship:

$$d_I = k_3 + k_4[(1/c) - 1].$$

The expression $[(1/c)-1]$ is identical with the grams of water per gram of soap. Both of these equations have a constant spacing (k_1 or k_3) for all soap and no water ($c=1$). With water added (c decreasing), the spacing increases until for all water and no soap ($c=0$) the spacing is infinite. This behavior has some physical reality, although the equations given in Fig. 8 are derived empirically.

The long-spacing from aqueous solutions of hexanolamine oleate has been reported[18] as a linear function of concentration, but they considered a first-order peak to be second order. Our measurements on the same detergent are represented better by a logarithmic function. The hyperbolic relationship has recently been applied to the spacings of non-ionic detergents.[19]

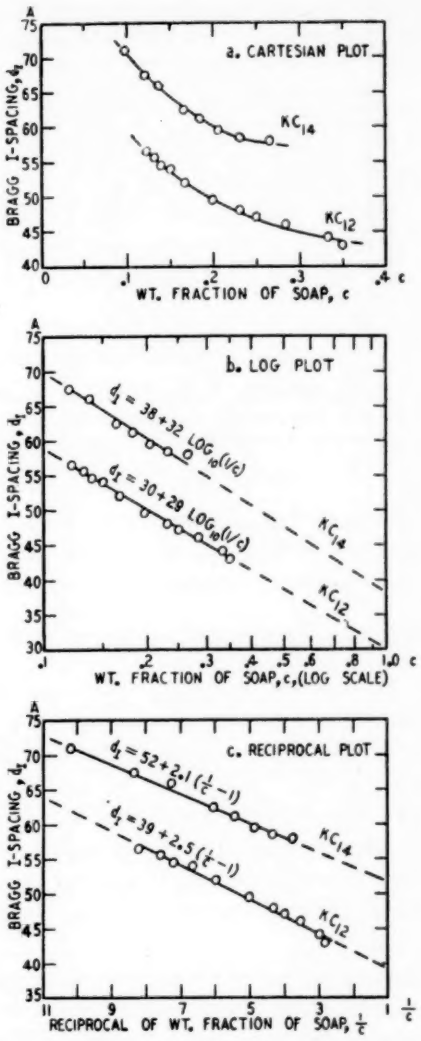
a. CARTESIAN PLOT
KC14
KC12
BRAGG I-SPACING, d_I
WT. FRACTION OF SOAP, c
b. LOG PLOT
$d_I = 38 + 32 \log_{10}(1/c)$
$d_I = 30 + 29 \log_{10}(1/c)$
WT. FRACTION OF SOAP, c, (LOG SCALE)
c. RECIPROCAL PLOT
$d_I = 52 + 2.1(\frac{1}{c} - 1)$
$d_I = 39 + 2.5(\frac{1}{c} - 1)$
RECIPROCAL OF WT. FRACTION OF SOAP, $\frac{1}{c}$

FIG. 8. The Bragg I-spacings for aqueous solutions of potassium laurate (KC_{12}) and potassium myristate (KC_{14}) plotted against the soap concentration, in a Cartesian plot, a logarithmic plot, and a reciprocal plot. The equations shown are those calculated by least squares from Table V.

The I-band looks narrow on a film, but it must be remembered that the change of spacing d with scattering angle 2θ increases very rapidly at smaller angles and d approaches infinity at the direct beam.

$$\partial d/\partial\theta = -\lambda \cos\theta/(2 \sin^2\theta).$$

[18] S. Ross and J. W. McBain, J. Am. Chem. Soc. **68**, 296 (1946).

[19] J. W. McBain and S. S. Marsden, J. Chem. Phys. **15** 211 (1947).

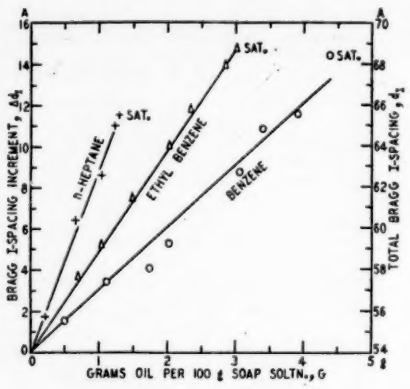

FIG. 9. Increase in the Bragg *I*-spacing caused by oils solubilized in a 15.0 percent by weight aqueous solution of potassium laurate. (The ethyl benzene spacings are given in Table VIII.)

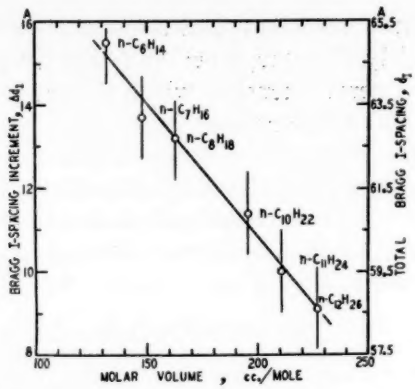

FIG. 10. The Bragg *I*-spacing increment for a 20.0 percent by weight aqueous solution of potassium laurate saturated with *n*-paraffin oils as a function of the molar volume of the oil.

The *I*-band plotted on a spacing basis has considerable width (Fig. 4) which may allow it to be an interparticle diffraction as from liquids.

IX. EFFECT OF SOLUBILIZED OILS ON THE *I*-BAND

An increase in both the intensity and the spacing of the *I*-band from a soap solution due only to the addition of a solubilized oil has been reported earlier.[9e, 20] In Fig. 6 the intensity of both the *I*-band and the *M*-band is increased; (a) the *I*-spacing and (b) the *M*-spacing are also increased. These increases in spacing indicate an increase in (a) the size and (b) the thickness of the micelle.

The presence of solubilized oil makes the *I*-band detectable at a lower soap concentration than in the absence of the oil. This is due to the related increase in thickness and size of the micelle.

With increasing solubilization of a hydrocarbon, the *I*-spacing increases steadily up to saturation. With a little more hydrocarbon than the saturation value added, d_I does not increase further. Figure 9 is an example of this behavior for *n*-heptane, ethyl benzene, and benzene. The solubilities are in this order with *n*-heptane the least soluble. For these three hydrocarbons, the less soluble the oil, the more rapidly the *I*-spacing increases. The volume of hydrocarbon is more significant than the mass in its effect on the form of the micelle. This conversion in Fig. 9 reduces the slopes but does not change the order.

[20] E. W. Hughes, W. M. Sawyer, and J. R. Vinograd, J. Chem. Phys. **13**, 131 (1945).

In Table VI are given the *I*-spacings for potassium laurate solutions *saturated* with each of a series of different hydrocarbons.

The values of Δd_I, taken from Table VI for a 20 percent potassium laurate solution saturated with the *n*-paraffin oils, are plotted in Fig. 10 against the molar volume of the paraffin oil. Hughes, Sawyer, and Vinograd[20] report similar results for the *I*-band. The *I*-spacing increment for *n*-paraffin oils at saturation decreases rapidly with increasing length of the hydrocarbon chain. However, this is caused by the concomitant decrease in solubilization caused by the decrease in activity of the oil with chain length. The vapor pressure of each liquid hydrocarbon is important in solubilization.[21]

For a soap solution *saturated* with a given oil, the *I*-spacing *increment* is somewhat larger for a higher soap concentration (Table VI). An example of this is given in Fig. 11.

X. CALCULATION OF THE NUMBER OF SOAP MOLECULES PER MICELLE ON THE BASIS OF CERTAIN ASSUMPTIONS

Various models for the micelle have been discussed by Dervichian[22] in attempting to explain the properties of soap solutions. He prefers only one kind of micelle which is small and one double-

[21] J. W. McBain and J. J. O'Connor, J. Am. Chem. Soc. **62**, 2855 (1940); *ibid.*, **63**, 875 (1941).

[22] D. G. Dervichian, J. chim. phys. **38**, 59 (1941); Comptes Rendus **217**, 299 (1943); J. Chem. Phys. **11**, 236 (1943); D. Dervichian and F. Lachampt, Bull. Soc. Chim. **12A**, 189 (1945).

TABLE V. *I*-spacings derived from the position of the peak of the *I*-band for aqueous soap solutions at 25°C.

	Percent by weight of soap	Bragg *I*-spacing $d_I \pm 1$A
Potassium caprate KC_{10}	22.9	43.4
	28.6	41.5
	38.0	39.5
Potassium laurate KC_{12}	12.20	56.5
	13.20	55.6
	13.90	54.5
	15.00	54.0
	16.70	52.0
	19.90	49.5
	23.10	48.0
	25.00	47.1
	28.4	46.0
	33.3	44.1
	35.0	42.9
Potassium myristate KC_{14}	9.82	71.0
	12.00	67.5
	13.74	66.0
	16.47	62.5
	18.3	61.2
	20.5	59.5
	23.1	58.5
	26.5	58.0
Sodium lauryl sulfate	20.0	57.8 (weak diffraction)
	25.0	54.1
	30.0	52.9

The weight fraction of soap c is the percent $\div 100$. *I*-spacings for other soaps are given in an earlier paper (see reference 12).

layer thick. He proposes to interpret the long-spacing as the distance between the micelles.

In an endeavor to interpret our own experimental work, it may be assumed that the micelles are distributed in the water in a liquid arrangement, and that the Bragg spacing d_I is the distance between the center of a micelle and that of any one of its nearest neighbors. No special shape for the micelle is necessary in this "point lattice," but it seems probable that the spacing which should be applied is somewhat larger than the Bragg spacing.

The total volume V_T (micelle plus solubilized oil plus surrounding water) associated with each micelle is given by

$$V_T = (6/\pi\sqrt{2})(4/3)\pi(d_I/2)^3,$$

or

$$V_T = d_I^3/\sqrt{2}. \quad (3)$$

This comes from the geometry of close-packed spheres, which are here spheres of water enclosing the micelle, and the factor $[6/(\pi\sqrt{2})]$ accounts for the "empty spaces" among the

TABLE VI. *I*-spacings for aqueous solutions of potassium laurate (KC_{12}) *saturated* with hydrocarbons at 25°C.

Hydrocarbon solubilized	Percent[a] by weight of KC_{12}	Bragg *I*-spacing $d_I \pm 1$A	Bragg *I*-spacing increment due to hydrocarbon $\Delta d_{I\,sat} \pm 2$A	Solubility, grams hydrocarbon per 100-g soap solution G_{sat}	$\frac{\Delta d_{I\,sat}}{G_{sat}}$
None	15	54.0	0		
None	20	49.5	0		
None	25	47.1	0		
n-heptane	15	65.5	11.5	1.31	8.8
n-heptane	20	61.5	12.0	1.99	6.0
n-heptane	25	60.9	13.8	3.62[b]	3.8
Triptane (2, 2, 3 trimethyl butane)	25	61.7	14.6	3.73	3.9
Benzene	15	68.5	14.5	4.38	3.3
Benzene	20	65.7	16.2	6.41	2.5
Ethyl benzene	15	68.8	14.8	3.02	4.9
Cyclohexane	20	63.0	13.5[c]	3.20[c]	4.2
1, 3, 5 trimethyl benzene	20	58.5	9.0[c]	2.92[c]	3.1
n-heptane	15	65.5	11.5	1.31	8.8
n-dodecane	15	61.5	7.5		
n-hexadecane	15	54.0	0		
n-hexane	20	65.1	15.5		
n-heptane	20	61.5	13.7	1.99	6.0
n-octane	20	60.1	13.2		
n-decane	20	59.2	11.4		
n-undecane	20	58.5	10.0		
n-dodecane	20	58.5	9.1		

[a] 15 percent = 0.629; 20 percent = 0.839; 25 percent = 1.049 moles soap/kg. soap solution.
[b] The density method[13] gives 3.62; the turbidity method[3] gives 2.67.
[c] Below saturation.
Additional d_I measurements of hydrocarbons solubilized in aqueous potassium myristate solutions are included in Table IV, with the solubilities given in Table III.

spheres. The reciprocal of Eq. (3) is equivalent to

$$N_M = (\sqrt{2}/d_I^3\rho), \quad (4)$$

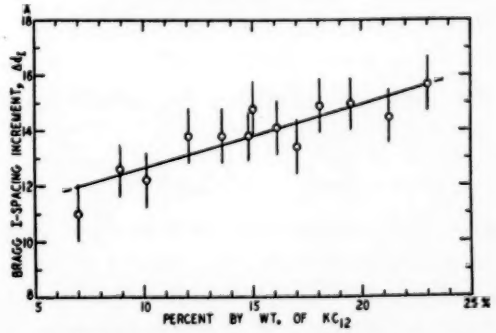

FIG. 11. Effect of soap concentration on the *I*-spacing increment. Each aqueous potassium laurate (KC_{12}) solution is *saturated* with ethyl benzene.

TABLE VII. Approximate distribution and size of micelles based on the Bragg value for d_I.

	Potassium laurate	Sodium lauryl sulfate	Potassium myristate	Sodium oleate	Lauryl ammonium chloride
Molecular wt. m_s	238.4	288.3	266.5	304.5	221.8
Critical micelle concentration, molar	0.0235	0.0061	0.0064	0.001	0.014
Percent by weight of soap	12.2	20.0	9.8	9.4	9.7
Moles of soap per kg. of solution	0.511	0.694	0.368	0.309	0.437
Bragg I-spacing, d_I, ± 1A	56.5	57.8	71.0	92.3	92.8
No. micelles per gram of solution, N_M	$7.8(10)^{18}$	$7.3(10)^{18}$	$4.0(10)^{18}$	$1.8(10)^{18}$	$1.8(10)^{18}$
No. soap molecules per micelle, n_S	39	57	56	103	148
Apparent molecular weight of micelle, M	9,000	16,000	15,000	31,000	33,000
Apparent volume of micelle, V_M, A^3	16,000	27,000	25,000	52,000	56,000

where N_M is the number of micelles per *gram* of total solution and ρ is the solution density (taken as 1.00 g/cc for these dilute solutions).

Let the number of micellar soap molecules per gram of total solution be

$$N_S = c\mathfrak{A}/m_s, \tag{5}$$

where c is the weight fraction of soap of molecular weight m_s and $\mathfrak{A}$ is Avogadro's number. Strictly, c should be reduced by the amount of non-micellar soap, but since this is a relatively small quantity, and not exactly known, it is neglected.

Similarly, let the number of hydrocarbon molecules solubilized per gram of total solution be N_H, calculated from the weight fraction of hydrocarbon of molecular weight m_H. Strictly, this should be reduced by the solubility of the hydrocarbon in the non-micellar phase, but this small correction is also neglected.

The number of soap molecules n_S and hydrocarbon molecules n_H *per micelle* are then given by

$$n_S = N_S/N_M, \tag{6}$$

and

$$n_H = N_H/N_M.$$

The apparent molecular weight of the micelle M would be

$$M = n_S m_s + n_H m_H.$$

The apparent volume of the micelle itself V_M should be approximated by

$$V_M = V_T - (V_w/N_M), \tag{7}$$

where V_w is the volume of water per gram of total solution. Strictly, V_w should include also the volume of the non-micellar soap molecules and the volume of hydrocarbon dissolved in the non-micellar phase, but these small corrections are neglected.

In Table VII are shown several characteristics of micelles as calculated by the use of the equations given above. The values listed are for only the lowest concentration at which the I-spacing could be measured. It is not certain that calculations for higher concentrations have any validity. However, the values obtained indicate that on increasing the soap concentration, the number of micelles per gram of solution, the number of soap molecules per micelle, and the apparent volume of the micelle itself, all increase. These values are specific for each soap and each concentration.

When a certain small volume of hydrocarbon is solubilized in a given soap solution, the total volume is increased, and if the total number of micelles were to remain constant, the micelles would be separated a little farther from each other (center to center). This increase in spacing is readily calculated on a simple dilution basis. *However, the experimental d_I spacing is increased considerably more than this.* If d_I is interpreted as the intermicelle spacing, this would indicate a decrease in the number of micelles per unit volume, which in turn requires that each micelle contain a larger number of soap molecules. This behavior is in agreement with the solubility relations[3] where the rate of change $(\partial s/\partial c)_T$ of the hydrocarbon solubility s increases with increasing soap concentration c.

In Table VIII values are shown as calculated for micelles which contain solubilized ethyl benzene. These show the effects of increasing amounts of ethyl benzene solubilized in the *same* soap solution. The saturation of the soap solution with ethyl benzene apparently halves the number of micelles per gram of solution. This is reflected in a doubling of the number of soap molecules

TABLE VIII. Effects of increasing amounts of ethyl benzene, solubilized in a 15.0 percent aqueous potassium laurate solution, on the approximate distribution and size of micelles.

Grams ethyl benzene solubilized in 100-g soap solution only G	Bragg I-spacing $d_I \pm 1$A	No. micelles per gram of solution N_M	No. soap molecules per micelle n_S	No. oil molecules per micelle n_H	Apparent volume of micelle V_M
0	54.0 ($d_M = 35.3$)	9.0 (10)[18]	42	0	17,000A[3]
0.68	57.8	7.3	51	5	22,000
1.05	59.2	6.8	55	9	23,000
1.51	61.5	6.1	61	14	27,000
2.04	64.1	5.4	69	21	31,000
2.33	66.0	4.9	75	26	34,000
2.86	68.0	4.5	82	35	38,000
3.02 (sat.)	68.8 ($d_M = 42.4$)	4.3	85	38	40,000
n-lauryl alcohol 4.35 (sat.)	73.0 ($d_M = 36.0$)	3.6	99	37	51,000

The apparent average molecular weight of this micelle with no ethyl benzene is 10,000; when saturated with ethyl benzene the soap contribution is 20,000 and the ethyl benzene contribution is 4000, making a total of 24,000.
These spacings are plotted in Fig. 9, and the ethyl benzene density and solubility in water are given in the notes in Table III.

per micelle. When saturated, there are apparently about half as many ethyl benzene molecules as potassium laurate molecules per micelle. The apparent volume of the micelle itself is about doubled by saturation with ethyl benzene.

The ratio of the total micelle molecular weight M converted to grams and the micelle volume V_M gives the apparent micelle density, which ranges between 0.94 and 1.02 g/cc for all entries in Tables VII and VIII. If the micelle is considered a *cylinder* of height d_M and a volume V_M, the lateral diameter would vary between 0.7 d_M and 0.8 d_M for the first three soaps in Table VII and would steadily increase from 0.7 d_M to 0.8 d_M going down in Table VIII for ethyl benzene.

With *n*-lauryl alcohol instead of ethyl benzene, the characteristics of the model are shown in the bottom line of Table VIII. The increment Δd_I is 19.0A and Δd_M is only 0.7A (see Section VI; reference 17 gives other measurements). The calculations indicate this micelle to be thinner than that with ethyl benzene, but to have a larger volume and therefore a larger lateral extension. If considered a *cylinder*, the lateral diameter would be 1.2 d_M.

The addition of simple salt to a soap solution increases the I-spacing (Table VIb of reference 12) which may be interpreted as causing the formation of larger micelles. Also, the addition of a salt increases the solubility of a hydrocarbon,[3] which is presumably a consequence of an increase in size of the micelles.

Substituting Eqs. (4) and (5) in (6) and rearranging gives

$$d_I^3 = (n_s m_s \sqrt{2}/\rho \mathfrak{A})(1/c),$$

which reduces to the working equation

$$d_I^3 = (2.35 n_s m_s)(1/c). \qquad (8)$$

A plot of d_I^3 against $(1/c)$ from Table V yields a fairly straight line, the slope of which may be used for estimating n_s from Eq. (8). The line extrapolated to $c = 1$ gives an intercept whose cube root d_I is close to d_M.

Several investigators[23–25] have determined the rates of diffusion in soap solutions which contain micelles. From the values obtained for cetyl pyridinium chloride at concentrations from 0.002 to 0.05N Hartley calculated on the basis of a spherical micelle that the diameter of the micelle is 52A, and consists of 70 molecules of the detergent. Unfortunately, such determinations have to be made in the presence of a swamping electrolyte, and electrolytes increase the size of the micelle. However, the value obtained by Hartley is in agreement with the idea presented in this paper that the micelle is small in comparison with the size indicated by the lamellar model.

Bernal and Fankuchen[26] observed from solutions of tobacco mosaic virus a long-spacing x-ray diffraction. This spacing increases steadily with

[23] G. S. Hartley and D. F. Runnicles, Proc. Roy. Soc. **A168**, 420 (1938).
[24] O. Lamm, Kolloid Zeits. **98**, 45 (1942).
[25] R. J. Vetter, J. Phys. and Colloid Chem. **51**, 262 (1947).
[26] J. D. Bernal and I. Fankuchen, J. Gen. Physiol. **25**, 111, 157 (1941).

dilution. They interpret this as the interparticle lateral spacing between the parallel virus rods. This two-dimensional relation may be analogous to a three dimensional one for micelles.

ACKNOWLEDGMENTS

Professor P. Debye has given much helpful advice. A number of highly purified soaps have been kindly furnished by the Procter and Gamble Company, Dr. A. W. Ralston of the Armour and Company, Dr. W. C. Ault and Dr. I. E. Knapp of the Eastern and Southern Regional Research Laboratories of the United States Department of Agriculture, the Hercules Powder Company, and Dr. D. A. Shepherd of the Department of Chemistry of the University of Illinois. The close collaboration of Dr. M. L. Corrin and Dr. R. Mittelmann has been of much value.

THE JOURNAL OF CHEMICAL PHYSICS VOLUME 16, NUMBER 7 JULY, 1948

Ultraviolet Absorption Spectrum of Toxicarol and Dehydrotoxicarol

CH'EN SHANG-YI* AND CHAO FENG-CHUAN**
Department of Physics, Yenching University, Peiping, China

(Received February 10, 1948)

The ultraviolet absorption spectra of toxicarol and dehydrotoxicarol in ethyl alcohol solution were studied with a Hilger E-316 quartz spectrograph and a Hilger H-16 sector-photometer. The curve of toxicarol shows a maximum at λ2741 with a molecular extinction coefficient 23,000. The curve drops down vertically at a wave-length λ2801 covering an extinction range from 19,000 to 24,000. The absorption curve of dehydrotoxicarol has two maxima, one being at λ2780 with molecular extinction coefficient 20,250, the other at λ3304 with molecular extinction coefficient 7180. One minimum occurs at λ3114 with coefficient at 5320.

INTRODUCTION

THE introduction of derris root extracts as insecticides[1] has excited the interest of many chemists and entomologists. They found that in the derris extracts, besides rotenone ($C_{23}H_{22}O_6$), there are other materials possessing insecticidal properties. One of these compounds, toxicarol ($C_{23}H_{22}O_6$) is a greenish yellow substance which crystallizes in the form of thin hexagonal plates and rods, has two hethoxyl groups, melts at 218°–220°C,[2] and is toxic to fish.[3]

When toxicarol hydrate, which was obtained by the action of alcoholic alkali upon toxicarol, is boiled with alcoholic hydrochloric acid, it is readily converted to dehydrotoxicarol ($C_{23}H_{20}O_7$). The latter crystallizes in the form of yellow rods and needles and melts at 234°C.[4]

So far, the absorption spectrophotometric study of these compounds has not yet been made. It is the interest of the present work to supply more data for the study of the molecular structure of these compounds by determining their ultraviolet absorption curves.

EXPERIMENTAL

A Hilger E-316 quartz spectrograph and a Hilger H-16 sector-photometer were used in the determination. Iron spark was used as light source. Across the 3-mm spark gap four glass tinfoil condensers of 0.12 microfarad each were connected in series, and the potential was 8000 volts. Twenty-eight strips of photograms were taken on each plate; the time of exposure was increased from 21″ to 8′20″. The photograph thus obtained with the sector-photometer was composed of a pair of spectrograms in close

---

* Now at Institute of Physics, National Academy of Peiping, Peiping, China.

** In Java.

[1] F. Tattersfield and W. A. Roach, Am. Ap. Biol. **10**, 1 (1923).

[2] E. P. Clark, Science **71**, 396 (1930); **73**, 17 (1931); J. Am. Chem. Soc. **52**, 2461 (1930); **56**, 987 (1934).

[3] W. A. Gersdorff, J. Am. Chem. Soc. **53**, 1897 (1931). W. M. Davidson, J. Econ. Entomol. **23**, 878 (1930).

[4] E. P. Clark, J. Am. Chem. Soc. **53**, 2269 (1931).

TABLE I. The molecular extinction coefficient, ϵ, *vs.* wave-length, λ, readings for toxicarol in ethyl alcohol.

λ	ϵ	λ	ϵ
4008	2,000	2801	21,000
3936	2,400	2792	26,000
3905	3,200	2741	28,000
3818	4,000	2640	26,000
2779	4,400	2608	24,000
3472	4,800	2584	21,500
3383	5,200	2569	20,000
3333	5,600	2562	19,000
3300	6,800	2542	18,000
3279	8,000	2524	17,000
3238	9,200	2512	16,000
3197	11,000	2501	15,000
3144	12,000	2490	14,000
3101	13,000	2469	13,000
2960	14,000	2451	12,000
2898	15,000	2419	11,000
2850	16,000	2375	9,200
2823	17,000	2345	8,000
2805	18,000	2318	6,800

TABLE II. The molecular extinction coefficient, ϵ, *vs.* wave-length, λ, readings for dehydrotoxicarol in ethyl alcohol.

	ϵ	λ	ϵ
3958	625	2887	15,600
3773	1,560	2866	16,400
3600	2,500	2838	17,200
3533	3,440	2826	18,750
3472	4,380	2780	20,250
3428	5,320	2710	18,750
3389	6,250	2682	17,200
3304	7,180	2662	16,400
3178	6,250	2652	15,600
3114	5,320	2634	14,820
2955	6,250	2621	14,050
2940	7,180	2604	13,280
2929	8,600	2586	12,500
2926	9,360	2568	11,720
2925	10,930	2543	10,930
2916	13,280	2494	10,150
2908	14,050	2403	9,360
2897	14,820		

juxtaposition. The one that passed through the pure solvent had its density reduced throughout the whole spectrum by changing the sector reading, while the other one that transversed the solution under test was denser than the first in certain parts and less dense in others. The match point, i.e., the wave-length at which the densities of the two are equal, were marked on the spectrogram.

Crude crystals of toxicarol were purified by dissolving it first in hot chloroform. The solution was filtered and heated to its boiling point. Then about 12 volumes of boiling alcohol were added. The solution was maintained in a state of vigorous boiling until it was practically free from chloroform and toxicarol began to crystallize. The crystals were filtered from the boiling liquid.

Finally the pure samples was put in a weighing bottle which was placed in a heater. The bottle and the heater were placed in a vacuum desiccator to allow it to dry in 50°C. The sample was weighed once a day until a constant weight was obtained. Then a portion of the sample was taken out to prepare a solution of desired concentration ready for analysis.

The remainder of the samples were recrystallized and treated the same as that mentioned above. The same spectrophotometric analysis was made again. The process was repeated until the spectra among the successive ones were identical.

The dehydrotoxicarol was purified by adding five volumes of hot methanol to its solution in chloroform. The solution was filtered and dehydrotoxicarol began to crystallize. The purification procedure was then carried out as before.

Several solvents such as distilled water, ethyl ether, ethyl alcohol, chloroform, and benzene were tried to dissolve the compounds. Both of them were found fairly soluble in chloroform, a little in ether, alcohol, and benzene, but none in distilled water. Ethyl alcohol was chosen as solvent because it is very transparent down to $\lambda 2040$ for 1 cm thickness and can be easily prepared and purified.[5]

The proper spectrophotometrical concentration of toxicarol was found to be 5×10^{-5} molar and that of dehydrotoxicarol was 6.4×10^{-5} molar for exposures of about 400 seconds in the present set-up and absorbing thickness of 1.0 cm. The solution of required concentration was prepared by a series of dilutions.

RESULTS

The ultraviolet absorption data of toxicarol in ethyl alcohol were tabulated in Table I and were plotted with molecular extinction coefficient against the wave-length in curve 1, Fig. 1. The curve shows a maximum at $\lambda 2741$ with a molecular extinction coefficient 29,000. It appears

[5] F. Twyman and C. B. Allsopp, *The Practice of Spectrophotometry* (Adam Hilger, London, 1934), p. 67; A. Clow and G. Pearson, Nature **144**, 208 (1939).

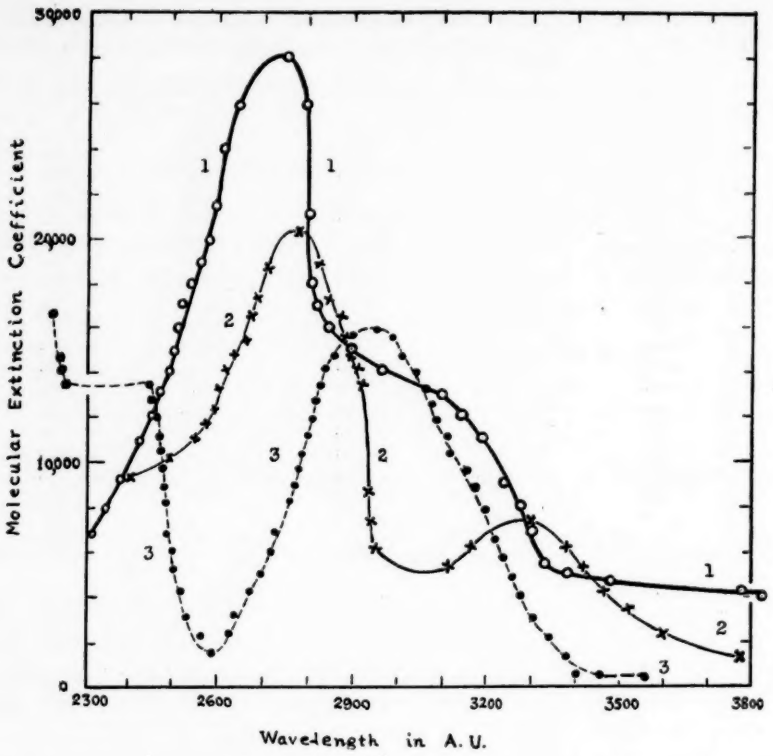

FIG. 1. Ultraviolet absorption curve of toxicarol (curve 1) and dehydratoxicarol (curve 2) in ethyl alcohol and that of rotenone (curve 3) after Ke.

to be vertical at λ2801, covering an extinction range from 19,000 to 24,000.

Likewise, the corresponding data for dehydrotoxicarol were presented in Table II and curve 2, Fig. 1. The curve has two maximum points, one at λ2780 with molecular extinction coefficient 20,250, the other at λ3304 with coefficient 7180. The minimum occurs at λ3114 with coefficient 5320.

The rate of decomposition of toxicarol in ethyl alcohol is imperceptible as shown by the fact that the absorption curves obtained after the solution was allowed to stand for a fortnight and that obtained for the solution newly prepared were identical.

By comparing the ultraviolet absorption curve of toxicarol with that of rotenone[6] (curve 3) it appears that both are flattened in the longer wave-length region but the peak of the one is about above the trough of the other.

The authors wish to thank Professor Liu-Sheng Tsai of the Department of Chemistry for his advice in the purification of chemicals.

[6] Ting-sui Kê, Science **24**, 671 (1940), in Chinese.

THE JOURNAL OF CHEMICAL PHYSICS VOLUME 16, NUMBER 7 JULY, 1948

The Heat and Free Energy of Polymerization of Ethylene

R. S. JESSUP
National Bureau of Standards, Washington, D. C.

(Received March 2, 1948)

Values calculated from available thermochemical and chemical thermodynamic data are given for the heats and free energies of polymerization of gaseous ethylene to gaseous, straight-chain polyethylene (monoolefin) molecules of various lengths. Equations are given expressing these properties at 25°C as functions of n, the number of ethylene units per polymer molecule, for $n \geqq 3$. The limiting values at 25°C for long-chain molecules are $\Delta H_p^\circ = -22.348$ kcal. per ethylene unit, $\Delta F_p^\circ = -12.186$ kcal. per ethylene unit. A preliminary value for the heat of combustion of solid polyethylene at 25°C, $\Delta H_c^\circ = -311.8$ kcal. per ethylene unit, is combined with other data to obtain the value $\Delta H_p^\circ = -25.4$ kcal. per ethylene unit for the heat of polymerization of gaseous ethylene to solid polyethylene. This experimental value and the calculated value for gaseous polyethylene are shown to be consistent within reasonable limits when account is taken of the heat of sublimation of the partly crystalline polyethylene, estimated to be 3.6 kcal. per ethylene unit. Values are given graphically and in tabular form for the equilibrium concentrations of ethylene and all its polymers at various temperatures in a mixture in the ideal gas state at a pressure of 1 atmosphere.

VALUES of heats of polymerization of a number of gaseous unsaturated organic compounds to gaseous polymers, calculated with the aid of various thermochemical data, have been reported by Flory,[1] Evans and Polanyi,[2] and Evans and Tyrrall.[3] The data used were not in all cases sufficient to permit exact calculation of heats of polymerization of long-chain polymer molecules. For example, in some cases the heat of dimerization per mole of dimer was taken as an estimate of the heat of polymerization. This procedure neglects the anomalous increment per CH_2 group in the heats of formation of hydrocarbons of low molecular weight, and also neglects the effect of steric interference between substituent groups attached to the carbon chain of the polymer molecule. The latter effect was also neglected in calculating heats of formation of polymer molecules from heats of formation of long-chain normal paraffin hydrocarbons, together with data on heats of isomerization of octanes, or lower members of the paraffin series. Most of the calculated values of heat of polymerization given in the references cited therefore apply to hypothetical polymer molecules which are free from such steric effects. This fact has been pointed out by Evans and Tyrrall.[3]

It is possible to calculate from data now available, values for the heat and free energy of polymerization of gaseous ethylene to gaseous straight-chain monoolefin molecules of any desired chain length, without introducing any such approximations as those indicated above. The results will therefore apply to the actual polyethylene molecules (in the ideal gas state).

Polymerization is ordinarily considered to be the combination of monomer molecules to form larger molecules, each of which contains an integral number of monomer units. It is doubtful, however, that the actual reactions by which polymers are formed are as simple as this. At high temperatures, at least, the reaction of polymerization, as defined above, would be expected to be accompanied by degradation reactions going on at the same time. Such degradation would be expected to involve, among other things, the breaking of polymer chains at points far removed from the ends, where there is no distinction between the carbon-carbon bonds of the chain which were originally carbon-carbon bonds in monomer molecules and those which are bonds between adjacent monomer units. Some of the resulting polymer molecules would then contain fragments of the original monomer molecules as well as entire monomer units. In particular, it is to be expected that some polyethylene molecules would contain odd numbers

[1] P. J. Flory, J. Am. Chem. Soc. **59**, 241 (1937).
[2] A. G. Evans and M. Polanyi, Nature **152**, 738 (1943).
[3] A. G. Evans and E. Tyrrall, J. Polymer Sci. **2**, 387 (1947).

TABLE I. Values of heat of polymerization of ethylene to polyethylene, both in the ideal gas state at a pressure of 1 atmosphere.

Number of ethylene units in polymer molecule n	Temperature in °K: 0	298.16	300	400	500	600	700	800	900	1000	1100	1200	1300	1400	1500
	Heat of polymerization, kcal per mole of monomer														
1.5	− 8.877	− 9.243	− 9.243	− 9.261	− 9.276	− 9.28	− 9.28	− 9.25	− 9.22	− 9.18	− 9.14	− 9.09	− 9.04	− 8.98	− 8.93
2	−11.943	−12.356	−12.355	−12.311	−12.246	−12.17	−12.08	−11.99	−11.89	−11.79	−11.69	−11.58	−11.47	−11.36	−11.26
2.5	−14.114	−14.496	−14.496	−14.426	−14.34	−14.24	−14.13	−14.02	−13.90	−13.78	−13.66	−13.53	−13.39	−13.26	−13.13
3	−15.420	−15.817	−15.817	−15.74	−15.63	−15.53	−15.41	−15.29	−15.15	−15.02	−14.87	−14.73	−14.59	−14.43	−14.29
4	−17.032	−17.450	−17.449	−17.36	−17.24	−17.12	−16.98	−16.84	−16.69	−16.54	−16.38	−16.21	−16.04	−15.87	−15.72
5	−17.999	−18.430	−18.428	−18.33	−18.21	−18.08	−17.92	−17.77	−17.62	−17.45	−17.28	−17.10	−16.92	−16.73	−16.57
10	−19.934	−20.389	−20.386	−20.27	−20.14	−19.99	−19.81	−19.64	−19.46	−19.27	−19.08	−18.88	−18.67	−18.46	−18.28
100	−21.675	−22.152	−22.148	−22.01	−21.88	−21.71	−21.51	−21.31	−21.12	−20.90	−20.70	−20.48	−20.24	−20.02	−19.82
1000	−21.849	−22.328	−22.324	−22.19	−22.06	−21.88	−21.68	−21.48	−21.29	−21.07	−20.86	−20.64	−20.40	−20.17	−19.97
∞	−21.868	−22.348	−22.344	−22.21	−22.08	−21.90	−21.70	−21.50	−21.31	−21.09	−20.88	−20.66	−20.42	−20.19	−19.99

of carbon atoms, that is, half-odd integral numbers of ethylene units.

In accordance with these considerations, the term "polymerization" is here used to mean the process by which ethylene molecules react to form larger normal monoolefin molecules, which may contain either even or odd numbers of carbon atoms. The restriction to the normal monoolefin compounds is made because the data necessary for the treatment of more complicated monoolefin molecules above hexene are not available.

Values of heat of polymerization of ethylene at 25°C can be calculated using data on the heats of formation of the lower monoolefin hydrocarbons reported by Prosen and Rossini,[4] and the following equation given by Prosen, Johnson, and Rossini:[5]

$$\Delta H_f^\circ = 9.740 - 4.926m, \quad (1)$$

where ΔH_f° is the heat of formation in kilocalories per mole of the normal monolefin hydrocarbon $H(CH_2)_mCH=CH_2$, in the ideal gas state at 1 atmosphere at 25°C. This equation is valid for $m \geqq 4$.

If the independent variable in (1) is changed to $n=(m+2)/2$, where n represents the number of ethylene units in the molecule, the equation for heat of formation at 25°C becomes

$$\Delta H_f^\circ = 19.592 - 9.852n. \quad (2)$$

Combination of Eq. (2) with the value $\Delta H_f^\circ = 12.496$ kcal. per mole[4] for the heat of formation of gaseous ethylene at 25°C yields for the heat of the reaction:

$$n CH_2=CH_2(g) \rightarrow H(CH_2)_{2n-2}CH=CH_2(g), \quad (3)$$

$$\Delta H^\circ = 19.592 - 22.348n, \quad (4)$$

where ΔH° is in kilocalories per mole of polymer. This equation is valid for $n \geqq 3$. Values of ΔH° for $n<3$ can be calculated directly from the appropriate values of ΔH_f° given in reference 4.

In a similar manner values of heats and free energies of polymerization of ethylene at various temperatures can be calculated from data reported by Kilpatrick, Prosen, Pitzer, and Rossini.[6] The equation obtained in this manner for the free energy change accompanying reac-

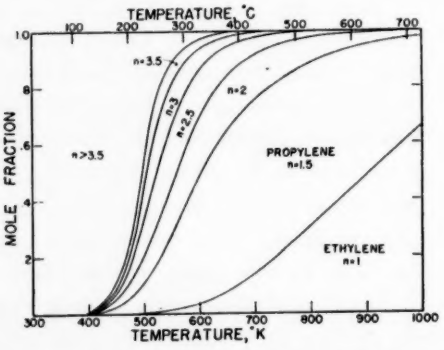

FIG. 1. Equilibrium concentrations of all the normal monoolefin hydrocarbons in a mixture in the ideal gas state at a pressure of 1 atmosphere. The difference between the ordinates of two adjacent curves at any temperature measures the mole fraction of the indicated compound at that temperature. The symbol n represents the number of ethylene units per molecule.

[4] E. J. Prosen and F. D. Rossini, J. Research Nat. Bur. Stand. **36**, 269 (1946).

[5] E. J. Prosen, W. H. Johnson, and F. D. Rossini, J. Research Nat. Bur. Stand. **37**, 51 (1946).

[6] J. E. Kilpatrick, E. J. Prosen, K. S. Pitzer, and F. D. Rossini, J. Research Nat. Bur. Stand. **36**, 559 (1946).

TABLE II. Values of free energy of polymerization of ethylene to polyethylene, both in the ideal gas state at a pressure of 1 atmosphere.

Number of ethylene units in polymer molecule n	Temperature in °K: 0	298.16	300	400	500	600	700	800	900	1000	1100	1200	1300	1400	1500
	Free energy of polymerization, kcal per mole of monomer														
1.5	− 8.877	− 6.289	− 6.271	−5.268	−4.278	−3.28	−2.28	−1.28	−0.29	+0.70	1.69	2.68	3.65	4.63	5.60
2	−11.943	− 7.674	− 7.645	−6.073	−4.530	−2.99	−1.47	+0.03	+1.54	3.02	4.50	5.96	7.42	8.86	10.31
2.5	−14.114	− 8.767	− 8.733	−6.811	−4.933	−3.06	−1.20	+ .63	2.45	4.26	6.06	7.85	9.65	11.41	13.16
3	−15.420	− 9.350	− 9.308	−7.12	−5.01	−2.90	−0.80	+1.29	3.34	5.38	7.41	9.43	11.45	13.46	15.44
4	−17.032	−10.059	−10.013	−7.52	−5.10	−2.69	− .30	+2.08	4.43	6.76	9.08	11.39	13.69	15.99	18.27
5	−17.999	−10.485	−10.435	−7.76	−5.16	−2.56	+ .01	2.56	5.09	7.59	10.08	12.56	15.03	17.50	19.96
10	−19.934	−11.335	−11.280	−8.25	−5.27	−2.31	+ .62	3.52	6.40	9.25	12.08	14.91	17.72	20.52	23.35
100	−21.675	−12.101	−12.040	−8.69	−5.37	−2.08	+1.16	4.37	7.58	10.75	13.88	17.02	20.14	23.24	26.40
1000	−21.849	−12.177	−12.117	−8.73	−5.38	−2.06	+1.22	4.46	7.69	10.89	14.06	17.23	20.38	23.52	26.71
∞	−21.868	−12.186	−12.125	−8.74	−5.39	−2.06	+1.22	4.47	7.71	10.91	14.08	17.25	20.41	23.55	26.74

tion (3) at 25°C is

$$\Delta F^\circ = 8.507 - 12.186n. \quad (5)$$

This equation is also valid only for $n \geqq 3$.

Values of heat and free energy of polymerization per mole of monomer will be obtained by dividing values of ΔH° and ΔF°, obtained as indicated above, by n. Thus for $n \geqq 3$, at 25°C,

$$\Delta H_p^\circ = \Delta H^\circ/n = -22.348\left(1 - \frac{1}{1.1407n}\right), \quad (6)$$

$$\Delta F_p^\circ = \Delta F^\circ/n = -12.186\left(1 - \frac{1}{1.4325n}\right). \quad (7)$$

Values of ΔH_p° and ΔF_p° are given in Tables I and II, respectively, for various values of n, and for various temperatures. Equation (6) and the data in Table I will given an idea of the effect of short-chain polymers on the results of measurements of heats of polymerization.

The limiting value given in Table I for the heat of polymerization at 298.16°K for $n = \infty$ may be compared with a preliminary value derived by combining other data with the results of two measurements, by Donald E. Roberts of the National Bureau of Standards, of the heat of combustion of a sample of polyethylene which, according to the manufacturer, was 100 percent pure. That the material was of relatively high purity was also indicated by the fact that the ratio of the mass of carbon dioxide formed in its combustion checked that calculated stoichiometrically from the mass of sample burned within less than 0.01 percent.

The value obtained by Roberts for the heat of combustion of the sample of polyethylene at 25°C is

$$\Delta H_c^\circ/n = -311.8 \text{ kcal. per ethylene unit,}$$

the products of combustion bring gaseous carbon dioxide and liquid water. Combination of this with the value reported by Prosen and Rossini[4] for the heat of combustion of gaseous ethylene at 25°C,

$$\Delta H_c^\circ = -337.234 \text{ kcal. per mole}$$

yields the value

$$\Delta H_c^\circ = -25.4 \text{ kcal. per ethylene unit,}$$

for the heat of polymerization of gaseous ethylene to solid polyethylene at 25°C.

An estimate of the heat of sublimation of the partly crystalline polyethylene to the ideal gas at atmospheric pressure was obtained by combining the limiting value, 2.36 kcal. per C_2H_4

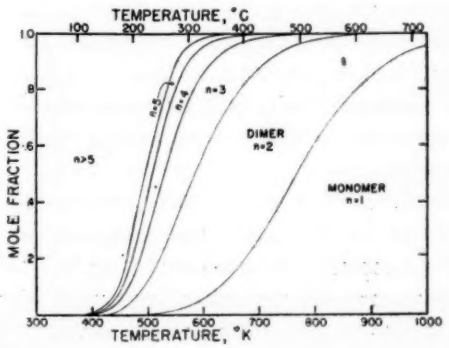

FIG. 2. Equilibrium concentrations of ethylene and all its polymers which contain integral numbers of ethylene units per molecule, in a mixture in the ideal gas state at a pressure of 1 atmosphere. The difference between the ordinates of two adjacent curves at any temperature measures the mole fraction of the indicated polymer at that temperature. The symbol n represents the number of ethylene units per polymer molecule.

TABLE III. Equilibrium concentrations of the normal monoolefin hydrocarbons in the ideal gas state at a pressure of 1 atmosphere.

Temperature	Number of ethylene units per molecule, n					$\frac{c_{n+\frac{1}{2}}}{c_n}$
	1	1.5	2	2.5	3	
	Mole fraction, c_n					for $n \geqq 3$
°K						
300	1.47×10^{-9}	4.01×10^{-7}	2.97×10^{-7}	6.64×10^{-8}	6.99×10^{-6}	0.9999993
400	1.88×10^{-5}	1.43×10^{-3}	1.22×10^{-3}	2.33×10^{-3}	2.19×10^{-3}	0.9978
500	0.0031	0.1100	0.0874	0.1310	0.1096	0.8361
600	0.0373	0.4459	0.2112	0.1641	0.0767	0.4580
700	0.1400	0.6139	0.1624	0.0634	0.0155	0.2410
800	0.3091	0.5768	0.0914	0.0196	0.0026	0.1363

unit, derived from data reported by Prosen and Rossini,[7] for the difference between the heats of combustion of liquid and gaseous normal paraffin hydrocarbons, with the value 1.21 kcal. per ethylene unit for the heat of fusion of polyethylene at 25°C. The latter value was derived from data reported by Raine, Richards and Ryder[8] on the heat content of solid and liquid polyethylene over the temperature range from 20° to 115°C.

The value for the heat of sublimation of solid polyethylene at 25°C obtained in the manner indicated is 3.6 kcal. per ethylene unit. When this is subtracted from the limiting value given in Table I for the heat of polymerization of gaseous ethylene to gaseous polyethylene at 25°C, there is obtained the value,

$$\Delta H_p^\circ = -25.9 \text{ kcal. per ethylene unit,}$$

for the heat of polymerization at 25°C of gaseous ethylene to solid polyethylene. The difference between this and the experimental value given above may be due in part to error in the estimated value of heat of sublimation of polyethylene, and in part to the presence of molecules of low molecular weight in the sample of polyethylene used in the measurement of heat of combustion.

As stated previously, the data given in Tables I and II are for polymers consisting of straight-chain monoolefin hydrocarbons only, because data necessary for the exact treatment of other types of polymer molecule are lacking. Estimates based on available information indicate that the effect of branching of the polyethylene on the heat and free energy of polymerization may be of the order of 0.1 kcal. per ethylene unit or less. The effect of end groups other than the assumed methyl group at one end of the chain and vinyl group at the other is probably negligible for sufficiently long molecules.

The data on free energy of polymerization may be used to calculate the equilibrium concentrations of ethylene and its polymers in a mixture in the ideal gas state at a pressure of 1 atmosphere. The values calculated for all the normal monoolefin hydrocarbons at several temperatures are given in Table III, and are shown graphically in Fig. 1. Similar data are shown in Fig. 2 for a mixture of all polymers containing integral numbers of ethylene units in the molecule.

As a consequence of the linear relation connecting free energy of formation at any one temperature with n, the number of ethylene units per molecule, for $n \geqq 3$, the ratio, $c_{n+\frac{1}{2}}/c_n$, of mole fractions of molecules having $n+\frac{1}{2}$ and n ethylene units each is a constant for $n>3$. At high temperatures c_n is relatively large for $n \leqq 3$, and the constant ratio $c_{n+\frac{1}{2}}/c_n$ is small, so that only molecules of low molecular weight are present in appreciable amounts in the equilibrium mixture. At lower temperatures the mole fractions are all low, and the ratio $c_{n+\frac{1}{2}}/c_n$ for $n \geqq 3$ is only slightly less than unity, so that c_n is comparable with c_3 for a large number of values of $n>3$.

The data reported here are of particular interest, since the polymerization of ethylene to normal monoolefin hydrocarbons is perhaps the simplest polymerization reaction involving hydrocarbons. The data are not affected by steric interference between substituent groups attached to the carbon chain, or by other effects of such groups. It may be noted that the heat of polymerization of ethylene is higher than any of the values which have been reported for vinyl derivatives.[3, 9, 10]

[7] E. J. Prosen and F. D. Rossini, J. Research Nat. Bur. Stand. **34**, 263 (1946).
[8] H. C. Raine, R. B. Richards, and H. Ryder, Trans. Faraday Soc. **41**, 56 (1945).
[9] D. E. Roberts, W. W. Walton, and R. S. Jessup, J. Research Nat. Bur. Stand. **38**, 627 (1947).
[10] L. K. J. Tong and W. O. Kenyon, J. Am. Chem. Soc. **67**, 1278 (1945); **68**, 1355 (1946); **69**, 1402 (1947).

THE JOURNAL OF CHEMICAL PHYSICS VOLUME 16, NUMBER 7 JULY, 1948

Note on a Relation between the Order of a Phase Transition and Discontinuities in the Distribution Functions of Molecules

JOSEPH E. MAYER
Institute for Nuclear Studies, University of Chicago, Chicago, Illinois
(Received February 23, 1948)

It is pointed out that in a phase transition of the n'th order the distribution functions for n molecules change discontinuously at the transition point.

DISTRIBUTION FUNCTIONS

THERE exists a relation between the order of a phase transition and the lowest number of molecules involved in the distribution functions which show discontinuity at the transition. This note serves to point out the relationship which is apparently not generally known.

Consider any chemical system consisting of σ-components, s, $1 \leq s \leq \sigma$, for which the symbol z_s is used to indicate the fugacity or activity of the s'th component; where z_s is so normalized that it becomes equal to the number density, ρ_s, of molecules of component s per unit volume, when all densities approach zero and the system becomes a perfect gas. Thus, for a system of low vapor pressure, z_s is essentially the number density of component s in the vapor in equilibrium with the system. We use z to indicate the set of numbers:

$$z = z_1, z_2, \cdots, z_s, \cdots, z_\sigma \tag{1}$$

of all fugacities of all components.

Let n represent a set:

$$n = n_1, n_2, \cdots, n_s, \cdots, n_\sigma \tag{2}$$

of numbers, n_s, of molecules of component s, and $\{n\}$ be used as a symbol to indicate all the coordinates necessary to describe the positions of these molecules, including at least three Cartesian coordinates for each molecule, and, in addition, any necessary internal coordinates. We use $d\{n\}$ to indicate a volume element in this multidimensional space, and if normal coordinates are used, rather than the Cartesian coordinates of the individual atoms composing the molecules, it is assumed that $d\{n\}$ includes the Jacobian of transformation to the volume element in the Cartesian space. We also use the short-hand notation:

$$\rho^n = \rho_1^{n_1} \rho_2^{n_2} \cdots \rho_s^{n_s} \cdots \rho_\sigma^{n_\sigma}, \tag{3}$$

and later,

$$z^n = z_1^{n_1} z_2^{n_2} \cdots z_s^{n_s} \cdots z_\sigma^{n_\sigma}, \tag{4}$$

$$n! = n_1! n_2! \cdots n_s! \cdots n_\sigma!. \tag{5}$$

One may define distribution functions $F_n\{n\}$, that depend on the temperature T and on the fugacity set z and are functions of the coordinates $\{n\}$ necessary to specify the positions, orientations, and internal coordinates of the set n of molecules. These functions are described by the statement that $\rho^n F_n d\{n\}$ is the probability that in the system there will be the appropriate set, n, of molecules found at the position $\{n\}$ in the volume element $d\{n\}$.

Thus, the function $F_s(i_s)$ for a single molecule of type s, depending on the coordinates (i_s) of a molecule of this species, will not depend on the Cartesian coordinates x_{is}, y_{is}, z_{is}, of the position of the center of mass if the system is in a glass, liquid, or gaseous state and when averaged over any internal coordinates, it has the value unity. If the molecule has no internal coordinates then $F_s(i_s)$ is the trivial function unity for a fluid or glassy system. If the system is crystalline, $F_s(i_s)$ is triply periodic, with the periodicity of the lattice, having sharp maxima at the positions where molecules of species s normally reside.

The functions for two molecules, $F_{ss}((i_s), (j_s))$ or $F_{st}((i_s), (j_t))$ depending on the coordinates (i_s), (j_s) of two molecules of the same species s, or on those, (i_s), (j_t), of two molecules of different species, s and t, will asymptotically approach the product $F_s(i_s)F_s(j_s)$ or $F_s(i_s)F_t(j_t)$ in value if the distance r_{ij} between the two molecules becomes large. For small distances they deviate from this product, the deviation depending on r_{ij} as well as the internal coordinates.

For molecules without internal degrees of freedom and for fluid systems (glass, liquid, or gaseous) the functions for two molecules F_{ss} or F_{st} depend only on r_{ij} and are the usual distribution functions for pairs discussed by many authors and measured by x-ray diffraction.

The functions for three (or more) molecules also approach the products of the single-molecule functions when all distances between molecules are large. For small distances they are often assumed to be given to a good approximation by the product of the function for all the pairs,[1] an approximation which is certainly not exact but may be very valuable.

At a given temperature T the functions for zero values of the fugacity $z=0$, i.e., $z_s=0$ for all s, which will be denoted by F_n^*, are given by:

$$F_n^*\{n\}=\exp -U_n\{n\}/kT, \tag{6}$$

which may be regarded as a definition of the function $U_n\{n\}$. If the system is classical in behavior, U_n is the potential energy of the set n of molecules at the position $\{n\}$. For systems having significant quantum-mechanical deviations from classical behavior, F_n^* must be calculated from a Slater sum, and U_n, defined by (6), is different from the classical potential, and is, in general, temperature dependent. In any case, U_n is a continuous function of temperature.

PHASE TRANSITIONS

Now we consider a system of σ-components whose thermodynamic state is determined by the σ-different fugacities, $z_1, \cdots, z_\sigma$, and by the temperature T. The boundaries of the regions of thermodynamic stability of single phases are σ-dimensional hyper-surfaces in the $(\sigma+1)$-dimensional space of the fugacities and temperature. That is, for instance, for a one-component system the state is determined by a single z and the temperature T, and a line in the z, T plane separates the region of gas and liquid phase or of any other two phases. The thermodynamic potentials of the system, such as energy, free energy, or PV, and the probability densities $\rho^n F_n$, all vary continuously in the $(\sigma+1)$-dimensional region for which a single phase is stable, with continuous derivatives of all these quantities with respect to z_s or T.

At the hyper-surface dividing the stability limits of two different phases, however, there are discontinuities in some of the thermodynamic functions or their derivatives, and in some of the probability densities $\rho^n F_n$.

Now the thermodynamic function whose "natural" variables are T and the set z, is the quantity P/kT. Its derivatives are the simple quantities:

$$(\partial(P/kT)/\partial \ln z_s)_{T,z_t}=\rho_s \tag{7}$$

$$(\partial(P/kT)/\partial \ln T)_z=(N/V)(\epsilon-\epsilon_0)/kT, \tag{8}$$

where $N/V=\sum_s \rho_s$ is the total number of molecules per unit volume, ϵ is the average energy per molecule, and ϵ_0 is the average energy per molecule in the perfect gas state at infinite dilution.

The pressure P is always continuous across the surface of equilibrium of two phases, that is, two phases are in equilibrium at the same T, z, and P. If there is a phase change, however, some derivatives of P are discontinuous at the boundary. If the phase change is an ordinary one of the first order (liquid to crystalline, liquid to gas, or gas to crystalline, etc.) the first derivatives, that is, the densities ρ_s and energies ϵ, are discontinuous across the boundary (and generally also all higher derivatives). If the phase change is one of the second order, the first derivatives are continuous but the second (and higher) derivatives are discontinuous. Similarly, higher order phase changes, which have never been definitely observed, may be defined by discontinuity of all derivatives of order n or greater, but continuous values of the derivatives of order less than n.

DISTRIBUTION FUNCTIONS AND PHASE TRANSITIONS

Now if the phase change is of the first order, the probability density functions $\rho_s F_s(i_s)$ for the single molecules are discontinuous across the boundary in the z, T space. More precisely stated, let z', T' represent any value of the set z, T lying on the hyper-surface of stability of two phases a and b, that is, z', T' represent values of the activity and temperature for which both

[1] See for instance: M. Born and H. S. Green, Proc. Roy. Soc. **A188**, 10 (1947); J. G. Kirkwood and E. M. Boggs, J. Chem. Phys. **10**, 394 (1942).

phases a and b are stable and can coexist in equilibrium. The function $\rho_s F_s(i_s)$ approaches a definite function, $\rho_s^{(a)} F_s^{(a)}$, as the point z', T' is approached from the side in which phase a is stable, and approaches a definite function $\rho_s^{(b)} F_s^{(b)}$ as z', T' is approached from the side in which b is stable, but the two functions are *not* equal. This statement is rather trivial, since in general the two densities $\rho_s^{(a)}$ and $\rho_s^{(b)}$ are not equal.

If the phase change is of the second order, however, the two limiting values $\rho_s^{(a)} F_s^{(a)}$ and $\rho_s^{(b)} F_s^{(b)}$ are equal, but the corresponding limiting values for two molecules, $[\rho_s^{(a)}]^2 F_{ss}^{(a)}$ and $[\rho_s^{(b)}]^2 F_{ss}^{(b)}$, or $\rho_s^{(a)} \rho_t^{(a)} F_{st}^{(a)}$ and $\rho_s^{(b)} \rho_t^{(b)} F_{st}^{(b)}$, are *not* equal. Since the densities $\rho_s^{(a)}$, $\rho_s^{(b)}$ are equal, the difference lies in the distribution functions $F_{ss}^{(a)}$ and $F_{ss}^{(b)}$ for two molecules. *In a second-order phase transition the distribution functions for pairs of molecules are discontinuous as functions of z and T across the boundary between the regions in the z, T space for which the two phases are stable.*

The general statement for any phase transition of higher order may be made: *In a phase transition of order n the distribution functions for n molecules change discontinuously in value as the thermodynamic state crosses the boundary of the phase transition.* Although there is presumptive evidence for the converse statement that in a phase transition of order n the distribution functions involving $n-1$ molecules are always continuous across the transition, the author does not see a completely rigorous proof of this.

PROOF OF THE RULE

The proof of the italicized statements above follows simply from Eq. (70) in a paper[2] by W. G. McMillan and the author, namely:

$$P(z+\Delta z) = P(z) + kT \sum_{m=0} b_m(z) (\Delta z \rho(z)/z)^m, \quad (9)$$

for the pressure $P(z+\Delta z)$ at an activity set $z+\Delta z$ in terms of a power series in Δz with coefficients $b_m(z)$, which are integrals over the distribution functions at the activity set z. Differentiating (9) with respect to

$$\partial^n / \partial \Delta z^n = \partial^{n_1} / \partial z_1^{n_1} \cdots \partial^{n_\sigma} / \partial z_\sigma^{n_\sigma}, \quad (10)$$

and setting $\Delta z = 0$, we find:

$$(\partial^n P / \partial z^n)_T = n! b_n (\rho/z)^n, \quad (11)$$

where the short-hand notation (3), (4), and (5) is employed.

The quantity b_n is

$$b_n = (1/V) \int\int \cdots \int \Big[\sum_{k=1}^{k=n} (\{k\{\nu_i\}_n\}_u)(-)^{k-1} \times (k-1)! \prod_{i=1}^{i=k} F_\nu\{\nu_i\} \Big] d\{n\}, \quad (12)$$

where $\sum\{k\{\nu_i\}_n\}_u$ means summation, for all k from unity to n, over all partitions of the set n into k unconnected subsets ν_i, $1 \leq i \leq k$, where by unconnected subsets we mean that every molecule of the set n occurs once and only once in one of the subsets ν_i. The integrand of (12) thus involves F_n, when $k=1$, and all distribution functions of sets of molecules smaller than n.

If the n'th derivative of P changes discontinuously as the phase change occurs, it follows from (11) that b_n changes discontinuously, and since if the phase change is of order n the $(n-1)$st derivatives are continuous, it follows that the integral of all the additive terms in the integrand of (12), except that of F_n, are continuous. The function, F_n must therefore be discontinuous across the phase transition.

DISCUSSION

It is to be noted that one can only prove that the *integral* of F_{n-1} is continuous across the phase transition of order n, and not that the function itself cannot be discontinuous. However, one may assume the plausibility that F_{n-1} itself is continuous. Indeed, a number of rather rigorous conditions would have to be satisfied by the two functions $F_{n-1}^{(a)}$ and $F_{n-1}^{(b)}$ if they were not identical in an n'th order phase transition.

There are, however, some conditions imposed on the values which the distribution functions approach as the thermodynamic boundary of any second-order phase transition is approached from the two different sides. For instance, in a second-order transition the densities $\rho_s^{(a)} = \rho_s^{(b)}$ and the energy $\epsilon^{(a)} = \epsilon^{(b)}$ for the two phases (a) and (b) at equilibrium. The average energy per molecule, ϵ, is determined by an integral of

[2] W. G. McMillan and J. E. Mayer, J. Chem. Phys. **13**, 276 (1945).

the potentials between pairs of molecules multiplied by the distribution functions for pairs F_{ss} and F_{st}. Thus, although $F_{ss}^{(a)} \neq F_{ss}^{(b)}$ etc., an integral involving these functions must be equal for the two phases (a) and (b).

There is one application of these results to the second-order transition, occurring in crystals such as the ammonium halides, commonly ascribed to the onset of free rotation of the groups within the crystal. Since the transition is second order, the integral of the distribution functions $F_{ss}((i_s), (j_s))$ for two molecules must be different across the phase boundary. However, one might think of the integration as being carried out in two stages: first over the internal coordinates of i_s and j_s and then over the Cartesian coordinates of the centers of mass of the two molecules. After the first part of the integration one obtains a function $F_{ss}'(x_{is},y_{is},z_{is},x_{js}, y_{js},z_{js})$ of the Cartesian coordinates only. Since the integrals of these functions, F_{ss}', are different for the two phases (a) and (b) it follows, of course, that the functions must be different, $F_{ss}'^{(a)} F_{ss}'^{(b)}$.

Thus, *in a phase transition of the second order, the distribution functions for the centers of mass of two molecules must be discontinuous across the transition as functions of the thermodynamic variables z and T.*

This means, of course, that even without looking at the rotational coordinates of the molecules there must be a fundamental difference in the behavior of the molecules with respect to their centers of mass in the two phases. This casts considerable doubts on attempts to treat phase transitions of this sort without consideration of the coupling between the frequencies concerned with movements of the centers of mass of the molecules and those only due to rotations. It does not deny, however, that the fundamental cause of the transition is connected with the molecule's ability to rotate.

Errata: The Infra-Red Spectrum and Structure of Aluminum Trimethyl

[J. Chem. Phys. 16, 552 (1948)]

KENNETH S. PITZER AND RAYMOND K. SHELINE
Department of Chemistry, University of California, Berkeley, California

AND

Low Frequency Raman Spectrum of Calcite

[J. Chem. Phys. 16, 555 (1948)]

L. GIULOTTO AND G. OLIVELLI
Instituto di Fisica "A. Volta" dell'Universita di Pavia, Pavia, Italy

THROUGH an unfortunate error the figures in these two Letters to the Editor were reversed in printing.

The figure appearing on page 552 and captioned "Fig. 1. The infra-red absorption of $Al_2(CH_3)_6$. Cell length, 9 cm. Pressure, 11.5 min." should have appeared on page 556 with the caption "Fig. 1. Microphotometer curves of Raman spectra of calcite relative to the electric vector (a) parallel and (b) perpendicular to the optic axis." accompanying the Letter "Low Frequency Raman Spectrum of Calcite" by L. Giulotto and G. Olivelli.

The figure appearing on page 556 and captioned "Fig. 1. Microphotometer curves of Raman spectra of calcite relative to the electric vector (a) parallel and (b) perpendicular to the optic axis" should have appeared on page 552 and captioned "Fig. 1. The infra-red absorption of $Al_2(CH_3)_6$. Cell length, 9 cm. Pressure, 11.5 min." accompanying the Letter "The Infra-Red Spectrum and Structure of Aluminum Trimethyl" by Kenneth S. Pitzer and Raymond K. Sheline. The scale on this figure was omitted in publication. The corrected figure is reprinted here.

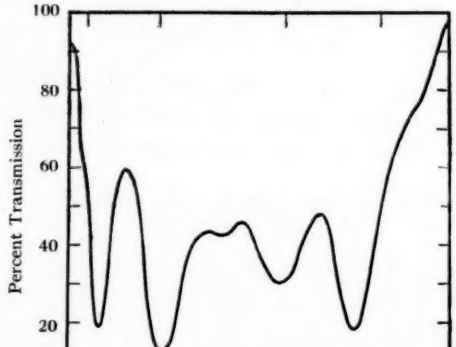

FIG. 1. The infra-red absorption of $Al_2(CH_3)_6$. Cell length, 9 cm; pressure, 11.5 mm.

The Stark Effect for a Rigid Asymmetric Rotor*

S. GOLDEN** AND E. BRIGHT WILSON, JR.
Mallinckrodt Chemical Laboratory, Harvard University, Cambridge, Massachusetts

(Received March 18, 1948)

The Stark effect, arising from the interaction of a uniform electric field with a permanent electric dipole that is arbitrarily oriented within a rigid asymmetric rotor, and with a dipole induced in the rotor by the field, has been evaluated by perturbation methods. Tables are given for the perturbation of the energy levels so that, for $J \leq 2$, the rotational energies of an asymmetric molecule in an electric field may be readily approximated to terms quadratic in the electric field.

The effect of accidental degeneracy upon the Stark effect and line intensities has been considered. A qualitative discussion of certain features of Stark patterns is given that may be useful in the identification of rotational spectral lines.

INTRODUCTION

THE recent progress in microwave spectroscopy has made it possible to observe the Stark effect in the pure rotational spectra of many molecules.[1] The formulas for the influence of an homogeneous electric field upon the rotational energy levels of linear[2] and symmetric-rotor[3] molecules are well known. The case of the rigid asymmetric rotor has been treated by Penney.[4] The purpose of the present paper is to extend this treatment, to give certain general rules that may facilitate the identification of spectral lines and to provide tables from which the Stark effect may be approximated for rotational energy levels up to and including $J=2$. The results are accurate to and including terms quadratic in the electric field strength.

I. THE PERTURBATION OPERATOR

When an homogeneous electric field is applied to a molecule having a permanent electric dipole moment μ and a polarizability tensor $\mathcal{P}$, the Hamiltonian operator will contain the following terms in addition to those involving rotation-vibration.

$$\mathbf{H}' = -E\sum_g \Phi_{Zg}\mu_g - \tfrac{1}{2}E^2\sum_{g,h}\Phi_{Zg}\Phi_{Zh}P_{gh} = E\mathbf{H}^{(1)}+E^2\mathbf{H}^{(2)}, \quad (1)$$

where E is the electric field, assumed to be along the space-fixed Z axis; g, h refer to the molecule-fixed principal axes of inertia x, y, z; μ_g are the components of the permanent dipole moment along the principal axes; P_{gh} are the components of the polarizability tensor referred to the principal axes of inertia; Φ_{Zg} are the direction cosines between the space fixed Z axis and the rotating molecule-fixed principal axes.

The first term in this expression is the orientational energy of the permanent dipole in the field, while the second is that of the induced dipole.

II. PERTURBATION THEORY NON-DEGENERATE CASE

Even when the asymmetric-rotor energy levels are otherwise distinct, they are nevertheless $(2J+1)$-fold degenerate in the quantum number M. Here J is the total angular-momentum quantum number and M is the magnetic quantum number. However this M degeneracy offers no difficulty to the application of the conventional perturbation theory.

To apply the conventional perturbation theory the matrix elements of Eq. (1) must be evaluated in terms of a basis of asymmetric-rotor wave

* The support by the Navy Department of the computational work herein reported is gratefully acknowledged. It was carried out under Task Order V of Contract N5ori-76, Office of Naval Research. The authors extend their appreciation to Mrs. Dorothy A. H. Brown, Mrs. Grace C. Ek, Mr. F. C. Merriam and Mr. J. A. Hayman, for carrying out the computations.

** National Research Council Predoctoral Fellow. Present address: Hydrocarbon Research, Inc., 115 Broadway, New York, N. Y.

[1] Various molecules are: OCS, T. W. Dakin, W. E. Good, D. K. Coles, Phys. Rev. **70**, 560 (1946); NH_3 D. K. Coles, W. E. Good, Phys. Rev. **70**, 979 (1946); SO_2, B. P. Dailey, S. Golden, E. B. Wilson, Jr., Phys. Rev. **72**, 871 (1947); H_2O, S. Golden, T. Wentink, M. W. P. Strandberg, Phys. Rev. **73**, 92 (1948).

[2] See, for example, J. H. Van Vleck, *Electric and Magnetic Susceptibilities* (Oxford Press, 1932), p. 152.

[3] See, for example, C. Mannebeck, Physik. Zeits. **28**, 72 (1927).

[4] W. G. Penney, Phil. Mag. **11**, 602 (1931).

TABLE I. The structure of the perturbation energy matrix, $\mathbf{H}^{(1)}$, due to a permanent dipole.

Species	A	B_x	B_y	B_z
A	···	$\mu_x\Phi_{Zx}$	$\mu_y\Phi_{Zy}$	$\mu_x\Phi_{Zx}$
B_x	$\mu_x\Phi_{Zx}$	···	$\mu_z\Phi_{Zx}$	$\mu_y\Phi_{Zy}$
B_y	$\mu_y\Phi_{Zy}$	$\mu_z\Phi_{Zx}$	···	$\mu_z\Phi_{Zz}$
B_z	$\mu_x\Phi_{Zx}$	$\mu_y\Phi_{Zy}$	$\mu_z\Phi_{Zz}$	···

TABLE II. The structure of the perturbation energy matrix, $\mathbf{H}^{(2)}$, due to an induced dipole.

Species	A	B_x	B_y	B_z
A	$\Sigma_g P_{gg}(\Phi_{Zg})^2$	$P_{xy}(\Phi_{Zx})(\Phi_{Zy})$	$P_{xz}(\Phi_{Zx})(\Phi_{Zz})$	$P_{yz}(\Phi_{Zy})(\Phi_{Zz})$
B_x	$P_{xy}(\Phi_{Zx})(\Phi_{Zy})$	$\Sigma_g P_{gg}(\Phi_{Zg})^2$	$P_{yz}(\Phi_{Zy})(\Phi_{Zz})$	$P_{xz}(\Phi_{Zx})(\Phi_{Zz})$
B_y	$P_{xz}(\Phi_{Zx})(\Phi_{Zz})$	$P_{yz}(\Phi_{Zy})(\Phi_{Zz})$	$\Sigma_g P_{gg}(\Phi_{Zg})^2$	$P_{xy}(\Phi_{Zx})(\Phi_{Zy})$
B_z	$P_{yz}(\Phi_{Zy})(P_{Zz})$	$P_{xz}(\Phi_{Zx})(\Phi_{Zz})$	$P_{xy}(\Phi_{Zx})(\Phi_{Zy})$	$\Sigma_g P_{gg}(\Phi_{Zg})^2$

functions. The latter may be expressed as linear combinations of symmetric-rotor wave functions,[5] all having the same values of J and M. The matrix elements of the direction cosines Φ_{Zg} evaluated in terms of a symmetric-rotor wave function basis are diagonal in M.[6] Hence it follows that in terms of the asymmetric-rotor functions the direction-cosine matrix elements are also diagonal in M, and the problem can be treated for each value of M separately.

Now, the asymmetric rotor wave functions belong to the representations A, B_x, B_y, B_z of the Four-Group.[7] The direction cosines Φ_{Zg} belong to the representations B_x, B_y, and B_z for $g=x$, y and z, respectively. Since non-vanishing matrix elements can be obtained only if the product of the direction cosine and the wave functions of the connected states belongs to representation A, the results of Table I are obtained for the non-vanishing matrix elements of $\mathbf{H}^{(1)}$.

Similarly, and by use of the fact that $(\Phi_{Zg})^2$ belongs to representation A, $\Phi_{Zx}\Phi_{Zy}$ to B_z, $\Phi_{Zz}\Phi_{Zx}$ to B_y, $\Phi_{Zy}\Phi_{Zz}$ to B_x, the results of Table II are obtained for the non-vanishing elements of $\mathbf{H}^{(2)}$.

From Table I it is seen that there are no diagonal elements of $\mathbf{H}^{(1)}$. Hence if the energy levels of the unperturbed asymmetric rotor are distinct and widely separated compared to the magnitude of the coupling perturbation, there are no contributions from terms linear in the field. Any first-order effect must arise from degeneracy between two or more levels of the unperturbed rotor. In the non-degenerate second-order perturbation treatment $\mathbf{H}^{(2)}$ will contribute only diagonal elements. A proof is given in Appendix A which shows that terms cubic in the field vanish in the non-degenerate case.

[5] S. C. Wang, Phys. Rev. **34**, 243 (1929).
[6] See, for example, P. C. Cross, R. M. Hainer, G. W. King, J. Chem. Phys. **12**, 210 (1944).
[7] See, for example, G. W. King, R. M. Hainer, P. C. Cross, J. Chem. Phys. **11**, 27 (1943).

The formula for the energy levels correct to the second order is, in the absence of accidental degeneracy, the usual perturbation result and is identical with the expression in Eq. (11) below.

III. PERTURBATION THEORY-DEGENERATE CASE

In order to provide a useful tabulation of the Stark effect that will be applicable to most asymmetric molecules, it is necessary to examine the cases of accidental degeneracy that may occur. The energy of the J_τ'th level of the asymmetric rotor is[7]

$$W^0{}_{J\tau}=\frac{(a-c)}{2}E_\tau{}^J(\kappa)+\frac{(a+c)}{2}J(J+1), \quad (2)$$

where $a=\hbar^2/2I_a$, $b=\hbar^2/2I_b$, $c=\hbar^2/2I_c$; $I_a\leq I_b\leq I_c$ are the principal moments of inertia;

$$\kappa=(2b-a-c)/(a-c),$$

the asymmetry parameter; $E_\tau{}^J(\kappa)$ is a characteristic value of the asymmetric-rotor problem. It is convenient to write Eq. (2) as

$$W^0{}_{J\tau}=\frac{(a+c)}{2}[\alpha E_\tau{}^J(\kappa)+J(J+1)], \quad (3)$$

where

$$\alpha=\frac{a-c}{a+c} \quad \text{and} \quad 0\leq\alpha\leq+1.$$

The lower limit corresponds to the spherically symmetric case while the upper limit corresponds to the linear case. It is readily observed that the terms in brackets in Eq. (3) are dimensionless; they may be thought of as a reduced energy.

Now for degeneracy between a number of unperturbed levels

$$W^0{}_{J\tau}=W^0{}_{J'\tau'}=W^0{}_{J''\tau''}=\cdots$$

or

$$\alpha E_\tau{}^J(\kappa)+J(J+1)=\alpha E_{\tau'}{}^{J'}(\kappa)+J'(J'+1)=\cdots,$$

for $J\neq J'$, $J\neq J''$, etc.,

$$\alpha=\frac{J'(J'+1)-J(J+1)}{E_\tau{}^J(\kappa)-E_{\tau'}{}^{J'}(\kappa)}=\frac{J''(J''+1)-J(J+1)}{E_\tau{}^J(\kappa)-E_{\tau''}{}^{J''}(\kappa)}=\cdots. \quad (4)$$

In particular for $J=J'$

$$\alpha[E_\tau{}^J(\kappa)-E_{\tau'}{}^{J'}(\kappa)]=0. \quad (5)$$

In this case ($J=J'$) the degeneracy is never exact except in the symmetric rotor limits but it can be very nearly exact for many pairs of levels even for molecules with the maximum asymmetry.

Equation (4) has been applied to the energy levels for $J\leq 3$ to determine which *pairs* of levels may become accidentally degenerate in the asymmetric rotor. Table III indicates which component of the permanent dipole becomes important in the accidental degeneracy.

From Table III it is clear that as both κ and α are varied, the frequent appearance of accidental degeneracy, even at low values of J,[8] makes it impractical to apply conventional perturbation theory. By a modification of the conventional perturbation theory, such as that employed by Van Vleck[9] and Jordahl,[10] an entirely satisfactory manner of handling these cases is obtained.

Briefly, the method consists in applying to the matrix to be diagonalized (*viz.* $\mathbf{W}^0+\mathbf{H}'$, where $\mathbf{W}^0$ is the diagonal energy matrix of the asymmetric rotor and $\mathbf{H}'$ is the matrix of Eq. (1) evaluated with asymmetric-rotor wave functions) the following matrix.

$$\mathbf{S}=\mathbf{I}+\lambda\mathbf{S}^{(1)}+\lambda^2\mathbf{S}^{(2)}, \quad (6)$$

where λ is a parameter of smallness (to be associated with the electric field in the present case); $\mathbf{S}$ is unitary to second order in λ. This requires

$$\mathbf{S}^{(1)\dagger}=-\mathbf{S}^{(1)}, \quad \mathbf{S}^{(2)}=\tfrac{1}{2}[\mathbf{S}^{(1)}]^2. \quad (7)$$

With no loss of generality, $\mathbf{S}^{(2)}$ may be taken to be hermitian. Now define $\mathbf{S}^{(1)}$ as follows.

$$S_{ij}{}^{(1)}=H_{ij}{}^{(1)}/W_i{}^0-W_j{}^0 \quad (8a)$$

for those values of i and j for which $W_i{}^0$ is not near $W_j{}^0$; for all other values k, l (i.e. the degenerate levels)

$$S_{kl}{}^{(1)}=0. \quad (8b)$$

With this definition, the application of $\mathbf{S}\cdots\mathbf{S}^\dagger$ to $(\mathbf{W}^0+\mathbf{H}')$ gives, for results correct to second order, the following matrix to be diagonalized:

$$\mathfrak{IC}=(\mathbf{W}^0+E\mathbf{H}_0{}^{(1)}+E^2\mathbf{H}^{(2)}+E^2\mathbf{H}^{(3)}). \quad (9)$$

Here $\mathbf{H}_0{}^{(1)}$ consists of those elements of $\mathbf{H}^{(1)}$ coupling degenerate levels, and

$$H_{jk}{}^{(3)}=\tfrac{1}{2}\sum_m{}'\left(\frac{H_{jm}{}^{(1)}H_{mk}{}^{(1)}}{W_j{}^0-W_m{}^0}+\frac{H_{jm}{}^{(1)}H_{mk}{}^{(1)}}{W_k{}^0-W_m{}^0}\right), \quad (10)$$

TABLE III. Appearances of accidental degeneracy in the asymmetric rotor. *a*, *b*, *c*, denote dipole-moment components along principal axes of least, intermediate, and greatest moment of inertia, respectively. The asterisk denotes no coupling term. Blanks indicate no accidental degeneracy possible.

J_τ	0_0	1_{-1}	1_0	1_{+1}	2_{-2}	2_{-1}	2_0	2_{+1}	2_{+2}
0_0									
1_{-1}									
1_0		c							
1_{+1}			a						
2_{-2}			b	c					
2_{-1}					c				
2_0						a			
2_{+1}							c		
2_{+2}								a	
3_{-3}						c	b	*	a
3_{-2}							*	c	b
3_{-1}								b	c
3_0									
3_{+1}									
3_{+2}									
3_{+3}									

[8] The formula given by Penney for $J=1$, must be restricted to case of non-degeneracy.

[9] J. H. Van Vleck, Phys. Rev. **33**, 467 (1929). See also E. C. Kemble, *Fundamental Principles of Quantum Mechanics* (McGraw-Hill Book Company, Inc., New York, 1937), p. 394.

[10] O. M. Jordahl, Phys. Rev. **45**, 87 (1934).

the prime indicating that the summation extends only over levels W_m^0 not degenerate with W_j^0 or W_k^0.

In diagonalizing $\mathcal{H}$, off-diagonal elements connecting non-degenerate levels will be ignored, since the transformation **S** has reduced them to second order and they therefore contribute no terms below fourth order to the energy. Consequently, $\mathcal{H}$ factors into small matrices, each associated with one group of degenerate levels. The diagonalization of these factors involves the solution of secular equations, usually no larger than second degree.

A. Diagonal Elements of $\mathcal{H}$

The diagonal elements of $\mathcal{H}$ are given by[11]

$$\mathcal{H}(J\tau M)=W^0{}_{J\tau}+E^2\sum_{J',\tau',g}{}'\frac{\mu_g{}^2[(\Phi_{Zg})_{J,\tau,M;J',\tau',M}]^2}{W^0{}_{J\tau}-W^0{}_{J'\tau'}}$$

$$-E^2\sum_{J'\tau'g}\tfrac{1}{2}P_{gg}[(\Phi_{Zg})_{J,\tau,M;J'\tau',M}]^2, \quad (11)$$

where the prime over the summation indicates that the summation is to extend only over those values of $J'\tau'$ for which $W^0{}_{J'\tau'}$ is not near $W^0{}_{J\tau}$.

No cross products of the dipole moments occur because of symmetry restrictions (see Tables I and II). Consequently, the perturbation energy may be separated according to the components of the permanent and induced dipoles. The second-order perturbation arising from the gth component of the permanent dipole (to the degree of approximation indicated in Eq. (11)) is

$$[W_g{}^{(2)}]_{J\tau M}=(\mu_g)^2E^2\sum_{J',\tau'}{}'\frac{[(\Phi_{Zg})_{J,\tau,M;J',\tau'M}]^2}{W^0{}_{J\tau}-W^0{}_{J'\tau'}} \quad (12)$$

and that arising from the ggth component of the induced dipole is

$$[W_{gg}{}^{(2)}]_{J\tau M}=\tfrac{1}{2}P_{gg}E^2\sum_{J',\tau'}[(\Phi_{Zg})_{J,\tau,M;J',\tau',M}]^2, \quad (13)$$

so that Eq. (11) may be written as

$$\mathcal{H}(J\tau M)=W_{J\tau}{}^0+\textstyle\sum_g[W_g{}^{(2)}-W_{gg}{}^{(2)}]_{J\tau M}.$$

Making use of Table I of reference (6)

$$[W_g{}^{(2)}]_{J\tau M}=\mu_g{}^2E^2\Bigg[\frac{(J^2-M^2)}{4J^2(4J^2-1)}\sum_{\tau'}{}'\left\{\frac{[(\Phi_{Zg})_{J,\tau;J-1,\tau'}]^2}{W^0{}_{J\tau}-W^0{}_{J-1,\tau'}}\right\}+\frac{M^2}{4J^2(J+1)^2}\sum_{\tau'\neq\tau}{}'\left\{\frac{[(\Phi_{Zg})_{J,\tau;J,\tau'}]^2}{W^0{}_{J\tau}-W^0{}_{J\tau'}}\right\}$$

$$+\frac{(J+1)^2-M^2}{4(J+1)^2(2J+1)(2J+3)}\sum_{\tau'}{}'\left\{\frac{[(\Phi_{Zg})_{J,\tau;J+1,\tau'}]^2}{W^0{}_{J\tau}-W^0{}_{J+1,\tau'}}\right\}\Bigg]. \quad (14)$$

Similarly

$$[W_{gg}{}^{(2)}]_{J\tau M}=\tfrac{1}{2}P_{gg}E^2\Bigg[\frac{J^2-M^2}{4J^2(4J^2-1)}\sum_{\tau'}[(\Phi_{Zg})_{J,\tau;J-1,\tau'}]^2$$

$$+\frac{M^2}{4J^2(J+1)^2}\sum_{\tau'}[(\Phi_{Zg})_{J,\tau;J,\tau'}]^2+\frac{(J+1)^2-M^2}{4(J+1)^2(2J+1)(2J+3)}\sum_{\tau'}[(\Phi_{Zg})_{J,\tau;J+1,\tau'}]^2\Bigg]. \quad (15)$$

For computational purposes it is convenient to separate out the coefficient of M^2 and remove the $\frac{1}{2}(a+c)$ from the W^0's (see Eq. (3)). One then obtains for the contribution of the second-order perturbation to the diagonal elements of $\mathcal{H}$

$$[W_g{}^{(2)}]_{J\tau M}=\frac{2\mu_g{}^2E^2}{a+c}[A_{J\tau}(\kappa,\alpha)+M^2B_{J\tau}(\kappa,\alpha)] \quad (16)$$

and

$$[W_{gg}{}^{(2)}]_{J\tau M}=\tfrac{1}{2}P_{gg}E^2[C_{J\tau}(\kappa)+M^2D_{J\tau}(\kappa)]. \quad (17)$$

In Appendix D the quantities A and B are tabulated for various values of the parameters κ and α. The quantities C and D have not been tabulated since, as shown in Appendix B, the terms arising from induced polarization are extremely small compared to those arising from

[11] The notation of reference 6 will be used.

the permanent dipole, and may be safely neglected.

B. Energy Calculations

By means of these tabulated quantities, the $\mathcal{H}(J\tau M)$'s may be obtained. In order to determine energy levels when degeneracy occurs a secular equation must be solved. When, as will probably most frequently be the case, the degeneracy occurs simply between a pair of levels, simple second-degree secular equations are obtained. These have the solutions

$$2W=\mathcal{H}(J\tau M)+\mathcal{H}(J'\tau' M)$$
$$\pm\{[\mathcal{H}(J\tau M)-\mathcal{H}(J'\tau' M)]^2+4|\xi^2|E^2\}^{\frac{1}{2}}. \quad (18)$$

The value of the off-diagonal element ξ is determined by the two states under consideration and will be discussed below.

Except for the fact that the $\mathcal{H}$'s are functions of E, Eq. (18) is virtually identical with that given by Penney for cases of slight symmetry.

A discussion of the ξ's requires the consideration of four separate cases. (Induced polarization terms are neglected.)

(1) $\quad |\Delta J|=0$

Only one type of degeneracy need be considered under this case and that is the limiting symmetric-rotor degeneracy. It must be emphasized, however, that the rotor may be quite asymmetric and still have this near-degeneracy occur. Since these states are adjacent to one another[12] in the energy scale they have different symmetries. Therefore there will be a non-vanishing coupling term from $\mathbf{H}_0^{(1)}$ so that

$$E\xi=\mathcal{H}_{kl}=EH_{kl}^{(1)}+\frac{E^2}{2}\sum_m{}' H_{km}^{(1)}H_{ml}^{(1)}$$
$$\times\left(\frac{1}{W_k^0-W_m^0}+\frac{1}{W_l^0-W_m^0}\right), \quad (19)$$

where k, l, m refer to the unperturbed levels. From Table I, all terms vanish for which m has the same species representation as either k or l. Consequently, the non-vanishing terms of Eq. (19) contains $H_{kl}^{(1)}$, $H_{km}^{(1)}$, $H_{ml}^{(1)}$ corresponding to the three different direction cosines or dipole components. By Table I, reference 6, one of these only is a pure imaginary while the other two are real. Therefore, no first-order terms appear in $|\xi|^2$ and it reduces to

$$|\xi|^2=(H_{kl}^{(1)})^2=\frac{M^2}{4J^2(J+1)^2}\mu_g^2|(\Phi_{Zg})_{J\tau;\,J\tau'}|^2, \quad (20)$$

if second-order terms are neglected. g is determined by the symmetry of the two states. It is seen that there is no "mixing" of the dipole components for this case. Two expansions of Eq. (18) are possible. When $|\mathcal{H}_{(J\tau M)}-\mathcal{H}_{(J\tau' M)}| \gg 2|\xi E|$ the conventional second-order result is obtained. When the converse is true a term linear in E appears which is proportional to $|M|$.

(2) $|\Delta J|=1$; *unperturbed states have different symmetries*

The results are similar to the previous case except that now

$$|\xi|^2=|H_{kl}^{(1)}|^2=\frac{(J^{*2}-M^2)\mu_g^2|(\Phi_{Zg})_{J\tau;\,J'\tau'}|^2}{4J^{*2}(4J^{*2}-1)}, \quad (21)$$

where J^* is the larger of the two J's involved, g is determined by the symmetry of the two states.

Here, also, there is no "mixing" of the dipole-moment components. The usual second-order result is obtained when $|\mathcal{H}_{(J\tau M)}-\mathcal{H}_{(J'\tau' M)}| \gg 2|\xi E|$. When the converse is true a term linear in E appears which is proportional to $(J^{*2}-M^2)^{\frac{1}{2}}$.

(3) $|\Delta J|=1$; *unperturbed states have the same symmetry*

In this case $H_{kl}^{(1)}$, as well as terms for which m has the same species representation as k or l, will vanish. The sum in Eq. (19) will consist of a real linear combination of the squares of the dipole-moment components. Moreover since the direction-cosine matrix elements vanish for $|\Delta J|>1$, the following form for ξ is obtained

$$\xi=EM[J^{*2}-M^2]^{\frac{1}{2}}\sum_g \mu_g^2 R_g(J, J', \tau, \tau'), \quad (22)$$

where J^* is the larger of J, J', g refers to the principal axes of inertia, and R_g depends upon the

[12] See, for example, Appendix I of reference 7. Also, G. H. Dicke and G. B. Kistiakowsky, Phys. Rev. **45**, 4 (1934).

quantities indicated (for a given asymmetric rotor).

When $M=0$, ξ vanishes, so that Eq. (18) gives the conventional second-order result. When the unperturbed energy levels are distinct (i.e. $|W_{J\tau}{}^0-W_{J'\tau'}{}^0|\gg 2|\xi E|$) the conventional second-order result is also obtained. However when there is degeneracy, no general conclusions may be drawn regarding the expansion of Eq. (18), This is seen from the fact that $[\mathcal{H}_{(J\tau M)}-\mathcal{H}_{(J'\tau' M)}]$ reduces to terms in E^2, so that all terms under the radical are of the same order, E^4. Then only terms quadratic in the electric field are introduced from the radical, so that this case of degeneracy does not give rise to a first-order Stark effect.

(4) $\qquad |\Delta J|=2$

This case will not be considered in any great detail except to note that for its dependence upon M and E,

$$|\xi|^2 \propto E^2[(J+1)^2-M^2][(J+2)^2-M^2] \quad (23)$$

where J is the lower of the two J's involved.

Degeneracies for which $|\Delta J|\geq 3$ result in vanishing ξ.

In actual practice the effect of degeneracy may not be as complicated as might be supposed from the foregoing. For example, when the dipole moment lies along one of the principal axes it is easy to show that the sum in Eq. (19) vanishes for states having different symmetries. Another simplification occurs when only certain states are allowed by virtue of nuclear-symmetry restrictions. Then certain degeneracies cannot occur.

IV. INTENSITIES

The intensities of the various component lines in the presence of an electric field involve the elements of the dipole-moment matrix, evaluated in terms of the basis of functions which diagonalize the energy, when the field is applied. For transitions involving non-degenerate levels these matrix elements are simply obtained from $\mathbf{SH}^{(1)}\mathbf{S}^{\dagger}$. They will contain small terms linear and quadratic in E which are added to $\mathbf{H}^{(1)}$. Only quite small changes in intensity are to be expected due to the field. It is interesting to observe, however, that non-vanishing elements may be expected, for finite fields, between states having the same symmetry; they may likewise occur as terms linear in E when $|\Delta J|\leq 3$. The selection rule on M is, of course, unchanged.

An important modification of the selection rules (with the exception of those on M) becomes possible when an accidental degeneracy occurs. Consider a pair of degenerate levels that have a non-vanishing element $-EH_{kl}{}^{(1)}$ connecting them. Then the proper linear combinations of asymmetric-rotor wave functions $A_k{}^0$ and $A_l{}^0$ are

$$\begin{cases} A_1=\dfrac{1}{\sqrt{2}}\left(A_k{}^0-\dfrac{H_{kl}{}^{(1)}}{|H_{kl}{}^{(1)}|}A_l{}^0\right), \\ A_2=\dfrac{1}{\sqrt{2}}\left(\dfrac{H_{kl}{}^{(1)}}{|H_{kl}{}^{(1)}|}A_k{}^0+A_l{}^0\right). \end{cases} \quad (24)$$

The elements of the dipole-moment matrix coupling either of these two states to some other state with wave function $A_m{}^0$ are

$$\begin{cases} H_{1m}{}^{(1)}=\dfrac{1}{\sqrt{2}}H_{km}{}^{(1)}-\dfrac{1}{\sqrt{2}}\dfrac{H_{kl}{}^{(1)}}{|H_{kl}{}^{(1)}|}H_{lm}{}^{(1)}, \\ H_{2m}{}^{(1)}=\dfrac{1}{\sqrt{2}}\dfrac{H_{kl}{}^{(1)}}{|H_{kl}{}^{(1)}|}H_{km}{}^{(1)}+\dfrac{1}{\sqrt{2}}H_{lm}{}^{(1)}. \end{cases} \quad (25)$$

To make the case non-trivial, it may be assumed that neither $H_{km}{}^{(1)}$ nor $H_{lm}{}^{(1)}$ vanishes, which corresponds to a permitted transition between the unperturbed state m and the unperturbed states k or l. Since $H_{kl}{}^{(1)}\neq 0$, by hypothesis, k and l correspond to states having different species representations. Only when m corresponds to a state having a species representation that differs from both the states corresponding to k and l will all of the terms in Eqs. (25) be non-vanishing. Then, application of the line of argument immediately following Eq. (19), indicates that the three dipole-moment components must be involved in Eqs. (25). Since only one of these components is a pure imaginary while the other two are real, Eqs. (25) can differ only in phase. If either $H_{km}{}^{(1)}$ or $H_{lm}{}^{(1)}$ vanish, again Eqs. (25) differ only in phase.

Since the absolute values of the dipole-moment matrix elements are involved in the expression for the line intensity, either of Eqs. (25) will give

the same value. This means, if transitions are normally permitted between, say, state m and state l but not between state m and state k, that transitions between the latter become possible if states k and l are degenerate. Furthermore, since degeneracy may occur between states for which $|\Delta J|=1$, it is clear that transitions having non-vanishing field-independent probabilities are now possible for $|\Delta J|=2$.

Other cases of degeneracy require the examination of the secular equation involving the degenerate levels, but will not be carried out here. It is important to observe that the change in selection rules which may be brought about by degeneracy results in a doubling (or, more generally, splitting) of the Stark components of a spectral line. When a first order term is introduced by the degeneracy a symmetrical Stark pattern results. When the degeneracy introduces only second-order terms, a splitting of the Stark components may be expected at higher fields.

V. APPLICATION TO ANALYSIS

Even though quantitative theoretical calculations for $J>2$ may not be available, it is nevertheless possible to utilize observed Stark effects to advantage in analyzing rotational spectra.

In what follows the effects due to induced polarization will be disregarded. Also, the discussion will be restricted to representative cases of non-degeneracy and of degeneracy[13] with first-order Stark effect (i.e. cases (1) and (2) above). Second-order terms will be neglected when first-order terms arise.

A. Formulas for Transition Frequencies, $\Delta M=0$

For those transitions in which the electric vector of the radiation is parallel to the electric field the following formulas may be obtained for the frequency displacement of each component, measured relative to the position of the unsplit line.

(a) *No Degeneracy*

$$\Delta\nu_M=(A'+B'M^2)E^2; \tag{26a}$$

(b) *Degeneracy*,[13] $|\Delta J|=0$

$$\Delta\nu_M=\pm F'|M|E; \tag{26b}$$

(c) *Degeneracy*,[13] $|\Delta J|=1$

$$\Delta\nu_M=\pm\{G'[J^{*2}-M^2]^{\frac{1}{2}}\}E; \tag{26c}$$

where A', B', F', G' are coefficients that are independent of M; J^* is the larger of the two J's involved in the degeneracy. A spectral line will, under the influence of an electric field, exhibit significant differences in appearance according to whether case (a), (b), or (c) applies.

Since $|M|\leq J$, a completely resolved spectral line will have $(J+1)$ components for case (a), where J is the smaller of the two J's involved in the transition. When degeneracy occurs, there will be $(2J+1)$ components.[14] If complete resolution is not attained it is nevertheless possible to determine the $|M|$ value of certain of the resolved components. From this information a good estimate of $|M|_{\max}$ may usually be determined, with the result that the smaller of the two J's involved is determined. How this may be accomplished depends upon which of Eq. (26a)–(26c) is applicable. The necessary formulas are given below.

(a) Observe that successive components, when resolved, must differ by unity in their value of M. For two such components, therefore

$$\begin{aligned}\Delta\nu_M-\Delta\nu_{M\pm1}&=B'E^2[M^2-(M\pm1)^2],\\&=\mp B'E^2(2M\pm1).\end{aligned} \tag{27a}$$

If there are at least three components then, ordering the components so that M corresponds to one extreme, $M\pm1$ to the intermediate and $M\pm2$ to the other extreme, one obtains

$$r=\frac{\Delta\nu_M-\Delta\nu_{M\pm1}}{\Delta\nu_{M\pm1}-\Delta\nu_{M\pm2}}=\frac{2M\pm1}{2M\pm3}. \tag{27b}$$

Solving,

$$M=\pm\left(\frac{3r-1}{2-2r}\right). \tag{27c}$$

Consistency of the solution may be determined by evaluating $B'E^2$ and then determining the frequency displacement of the component cor-

[13] Specifically, discussion of degeneracy will be restricted to transitions which either involve one non-degenerate level or two degenerate levels whose energy dependence on M is precisely the same.

[14] Not all components may be observable; for example when $\Delta J=0$, the $M=0$ transition will be forbidden.

responding to some other value of M and comparing with observation.

In general, experimental errors may be such that Eq. (27c) may not lead to an integral value for M, particularly if M is very large. In such a case, however, certain limits may be imposed upon the smaller J involved in the transition.

(b) For this case one may observe that

$$\Delta\nu_M - \Delta\nu_{M\pm1} = \pm F'E, \tag{28a}$$

so that

$$M = \pm\frac{\Delta\nu_M}{\Delta\nu_M - \Delta\nu_{M\pm1}}. \tag{28b}$$

As under case (a) consistency should be established by comparing the frequency displacement computed for another value of M with the observed spectrum.

(c) For this case one readily obtains

$$(\Delta\nu_M)^2 - (\Delta\nu_{M\pm1})^2 = \pm G'^2E^2(2M\pm1). \tag{29a}$$

Proceeding as in case (a),

$$s = \frac{(\Delta\nu_M)^2 - (\Delta\nu_{M\pm1})^2}{(\Delta\nu_{M\pm1})^2 - (\Delta\nu_{M\pm2})^2} = \frac{2M\pm1}{2M\pm3}. \tag{29b}$$

Solving,

$$M = \pm\frac{3s-1}{2-2s}. \tag{29c}$$

B. Formulas for Transition Intensities, $\Delta M = 0$

To facilitate the analysis, the dependence of the intensity upon the quantum number M may be employed. For the selection rule $|\Delta M| = 0$, the following relationships are obtained (neglecting changes due to frequency).[15]

(I) $|\Delta J| = 0$ transitions.

For these transitions it is known that the line strength is

$$I_M = PM^2; \tag{30}$$

(II) $|\Delta J| = 1$ transitions.

For these transitions it is known that the line strength is

$$I_M = Q(J^{*2} - M^2), \tag{31}$$

where P, Q are parameters depending upon the quantum numbers (other than M) and the asymmetry of the molecule; J^* is the larger of the two quantum numbers of the levels involved in the transition.

A factor of $\frac{1}{2}$ must be applied to those transitions for which $M = 0$.

The results previously considered must be modified for case (*I*). From Eq. (30) it is seen that the component for which M equals zero has a vanishing line strength. Hence, under conditions of complete resolution only J components will be observed for case (a), and $2J$ components for cases (b) and (c), above.

The following relations may be obtained.

(I) $|\Delta J| = 0$ transitions

$$M = \pm\frac{(I_M/I_{M\pm1})^{\frac{1}{2}}}{1-(I_M/I_{M\pm1})^{\frac{1}{2}}}. \tag{32}$$

(II) $|\Delta J| = 1$ transitions

$$M = \pm\left(\frac{3t-1}{2-2t}\right), \tag{33}$$

where

$$t = \left(\frac{I_M - I_{M\pm1}}{I_{M\pm1} - I_{M\pm2}}\right).$$

These relationships together with those given above for the frequency displacements permit the quantum number M to be evaluated by two independent methods. In practice, the formulas involving frequency displacements may be expected to yield somewhat better results since the frequencies are generally capable of being measured more accurately. Equations (32) and (33) may then serve as a convenient means of checking the results so obtained.

The formulas presented above have been arrayed to give a value of the quantum number M corresponding to a particular component of a partially or completely solved line. It should be emphasized, however, that to determine M one must know which of the above cases is actually applicable to a given line. In general, this may not be known beforehand, so it will be necessary to apply each of the formulas until a pair of equations (*viz.* for frequency displacements and relative intensities) is found that describe the experimental data adequately.

It should be borne in mind that the frequency

[15] Here field-free intensities are employed. See, for example, Table I, reference 6.

displacements and relative intensity measurements give two entirely different kinds of information about the transition giving rise to the spectral line under observation. The frequency displacement measurements give information dealing with the degeneracies among the asymmetric-rotor levels and information leading to a determination of a quantum number J, which is the smaller of the two involved in the transition. The relative intensity measurements give more pertinent information pertaining to the transition itself (i.e. whether $|\Delta J|=0$ or $|\Delta J|=1$).

C. Formulas for Transition Frequencies, $|\Delta M|=1$

For transitions in which the electric vector of the radiation is perpendicular to the electric field, the Stark pattern is moderately more complex than in the cases previously considered. A certain simplification is obtained when it is realized that transitions corresponding to

$$(-|M|\rightarrow-|M|-1) \text{ and } (|M|\rightarrow|M|+1)$$

give rise to the same frequency. Similarly for

$$(-|M|\rightarrow-|M|+1) \text{ and } (|M|\rightarrow|M|-1).$$

Accordingly, the frequency displacements may be classified into two groups, as indicated. The following formulas result.

(*a'*) *No degeneracy*

$$\begin{aligned}\Delta\nu_M^{(+)}&=\{A'+B'M^2+B''|M|\}E^2,\\ \Delta\nu_M^{(-)}&=\{A'+B'M^2-B''|M|\}E^2;\end{aligned}\tag{34a}$$

(*b'*) *Degeneracy*,[13] $|\Delta J|=0$

$$\begin{aligned}\Delta\nu_M^{(+)}&=\pm\{F'|M|+F''\}E,\\ \Delta\nu_M^{(-)}&=\pm\{F'|M|-F''\}E;\end{aligned}\tag{34b}$$

(*c'*) *Degeneracy*,[13] $|\Delta J|=1$

$$\begin{aligned}\Delta\nu_M^{(+)}&=\pm\{G'(J^{*2}-M^2)^{\frac{1}{2}}\\ &\quad+G''(J^{*2}-(|M|+1)^2)^{\frac{1}{2}}\}E\\ \Delta\nu_M^{(-)}&=\pm\{G'(J^{*2}-M^2)^{\frac{1}{2}}\\ &\quad+G''(J^{*2}-(|M|-1)^2)^{\frac{1}{2}}\}E\end{aligned}\tag{34c}$$

where $\Delta\nu_M^{(+)}$ corresponds to $|M|\rightarrow|M|+1$; $\Delta\nu_M^{(-)}$ correspond to $|M|\rightarrow|M|-1$.

Since $|M|\leq J$, a completely resolved spectral line will have $(2J+1)$ component for case (a') where J is the smaller of the two J's involved in the transition. For case (b') there will be $(4J+2)$ components if $F''\neq0$ and $(2J+1)$ components otherwise. A similar statement applies to case (c'), depending upon whether or not G'' vanishes. Presumably, the more frequently occurring cases of (c') will have $G''=0$, corresponding to a transition that involves at least one nondegenerate level.

D. Formulas for Transition Intensities, $|\Delta M|=1$

The explicit formulas permitting a solution for $|M|$ can be obtained readily if the $\Delta\nu^{(+)}$ and $\Delta\nu^{(-)}$ groups of components can be distinguished from one another. Fortunately, this can be done on the basis of the relative strengths of the lines. The following relations hold.

(*I'*) $|\Delta J|=0$ *transitions*

$$I_M^{(+)}=P\{J^2-J-M^2+|M|\},\tag{35a}$$

$$I_M^{(-)}=P\{J^2-J-M^2-|M|\}.\tag{35b}$$

From these equations it is readily seen that the $\Delta\nu^{(+)}$ group of components have intensities that are greater than that of the $\Delta\nu^{(-)}$ group (except for $M=0$, when they are the same).

(*II'*) $\Delta J=-1$ *transitions*

$$I_M^{(+)}=Q(J-|M|)(J-|M|-1),\tag{36a}$$

$$I_M^{(-)}=Q(J+|M|)(J+|M|-1);\tag{36b}$$

(*II''*) $\Delta J=+1$ *transitions*

$$I_M^{(+)}=Q(J+|M|)(J+|M|+1),\tag{37a}$$

$$I_M^{(-)}=Q(J-|M|)(J-|M|+1).\tag{37b}$$

Here J is the larger of the two J's involved in the transition. Note that in each case the $\Delta\nu^{(+)}$ and $\Delta\nu^{(-)}$ groups may be distinguished from each other on the basis of intensities. However, in case (II') the $\Delta\nu^{(-)}$ group is the more intense group, while in case (II'') it is the $\Delta\nu^{(+)}$ group. The $M=0$ components of both groups will have the same intensity and frequency displacement.

No detailed formulas will be given from which the M's corresponding to the various components may be determined. However, it may be noted that the mean frequency displacement ($\Delta\nu_M^{(+)}$

$+\Delta\nu_M^{(-)}$) reduces (for cases (a′) and (b′) above) to formulas already given for $\Delta M=0$ transitions. When it is possible to effect this combination for a number of different M values, those formulas may be used. In addition the frequency displacement differences $(\Delta\nu_M^{(+)}-\Delta\nu_M^{(-)})$ may serve to check a determination of M. In the particular case where F'' and G'' are zero, the formulas pertaining to $\Delta M=0$ are applicable insofar as frequency displacements are concerned.

APPENDIX A

Proof That the Third-Order Perturbation Terms Vanish in the Non-Degenerate Case

It may be shown that for the non-degenerate case the coefficient of the term cubic in the field strength is

$$W_{ii}^{(3)}=-\sum_{j\neq i}\frac{H_{ii}H_{ij}H_{ji}}{(W_i^0-W_j^0)^2}+\sum_{j\neq i}\sum_{k\neq i}\frac{H_{ij}H_{jk}H_{ki}}{(W_i^0-W_j^0)(W_i^0-W_k^0)},$$

where i, j, k refers to the pairs of quantum numbers J, τ, and H is the matrix element of the dipole moment matrix (see Eq. (1)). For the present case $H_{ii}=0$, so

$$W_{ii}^{(3)}=\sum_{j\neq i}\sum_{k\neq i}\frac{H_{ij}H_{jk}H_{ki}}{(W_i^0-W_j^0)(W_i^0-W_k^0)}.$$

Since H is hermitian, this becomes

$$W_{ii}^{(3)}=\sum_{j>k}\sum_{k}\frac{(H_{ij}H_{jk}H_{ki})+(H_{ij}H_{jk}H_{ki})^*}{(W_i^0-W_j^0)(W_j^0-W_k^0)},$$

since those terms for which $j=k$ must vanish (i.e. $H_{jj}=0$).

Now those terms for which any two of i, j, or k correspond to the same species of wave function must also vanish. Consequently, only these terms remain for which i, j, and k correspond to different species of functions. Consequently, H_{ij}, H_{jk}, H_{ki}, must correspond to the three different direction cosines (or dipole-moment components), as indicated in Table I.

Since one of these only[6] (depending upon the representation) is pure imaginary, while the other two are real, it follows that

$$W_{ii}^{(3)}=0.$$

APPENDIX B

Estimate of the Order of Magnitude of Polarization Terms

Any contribution attributable to polarization will depend upon the departure of the polarizability ellipsoid from a sphere. To make an estimate of the effect under the most favorable conditions, imagine the polarizability ellipsoid degenerating into a line. Then the contribution to the energy is

$$W_p<\tfrac{1}{2}\alpha\langle\cos^2\theta\rangle_{Av}E^2,$$

where α is the polarizability, θ is the angle between the line of polarization and the direction of the applied electric field E.

To contribute to the Stark effect we require

$$\Delta W_p<\tfrac{1}{2}\alpha E^2\Delta\langle\cos^2\theta\rangle_{Av},$$

where Δ refers to the difference in the values in the upper and lower states. Clearly, since $\cos^2\theta<1$

$$\Delta W_p\ll\tfrac{1}{2}\alpha E^2.$$

Since $\alpha=10^{-24}$ e.s.u. in order of magnitude, the frequency displacement for $E=10^4$ volts/cm.

$$\Delta\nu_p\ll 0.08\text{ mc/sec.},$$

which can be safely neglected.

APPENDIX C

Use of Tabulated Line Strengths to Evaluate the Direction-Cosine Matrix Elements

When extension to larger values of J of the present tables of Stark coefficients is desired, use may be made of the tables of line strengths of reference 6. From Eq. (14), above, it is seen that the only quantities needed are $(\Phi_{Z0})^2_{J\tau;J'\tau'}$. From Eq. (19) of reference 6, the line strength is defined as

$$\lambda=\sum_{FMM'}|\Phi_{F0}|^2_{J\tau M;J'\tau'M'}=3|\Phi_{Z0}|^2_{J;J'}\times|\Phi_{Z0}|^2_{J\tau;J'\tau'}\times\sum_{M,M'}|\Phi_{Z0}|^2_{J,M;J'M'}.$$

Two cases need be considered.

(*a*) $|J-J'|=1$. In this case, solving for $|\Phi_{Z0}|^2_{J\tau;J'\tau'}$ and substituting for $|\Phi_{Z0}|^2_{J;J'}$ and $\sum_{M,M'}|\Phi_{Z0}|^2_{JM;J'M}$

making use of Table I of reference 6,

$$|\Phi_{Z_0}|^2_{J\tau;J'\tau'}=4J^*\lambda,$$

where J^* is the larger of the pair (J, J').

(*b*) $|J-J'|=0$. In this case

$$|\Phi_{Z_0}|^2_{J\tau;J\tau'}=\frac{4J(J+1)}{2J+1}\lambda.$$

Substitution into Eq. (14), above with the frequencies determined from term values, or computed, gives immediately $W^{(2)}$.

APPENDIX D

Tables of Reduced Stark Coefficients

In preparing the tables of $A(\kappa, \alpha)$ and $B(\kappa, \alpha)$ the energy matrix of the asymmetric rotor was evaluated in terms of the type I^r representation of symmetric-rotor basis functions, making use of the results given in reference 7. The Wang transformation **X** was then applied. Since the energy levels of the asymmetric rotor are known as explicit functions of the parameter $\kappa(J\leq 3)$, it was possible to solve for the elements of the orthogonal transformation matrix **T** as explicit functions of κ. These elements were then evaluated for $\kappa=-1(0.1)+1$. The calculations were carried out independently for each element to eight significant figures. The magnitude of the characteristic vectors of T differed from unity by no more than four in the eighth place. The values of the elements were rounded off to the seventh decimal place.

Next, the direction-cosine matrices were evaluated by applying $\mathbf{T}\cdots\mathbf{T}'$ to the matrices $\|(\Phi_{Z_0})_{JK;J'K'}\|$.[11] The rules of spectroscopic stability[6] were applied to check the transformation. The deviations from the sum rule were no more than three in the seventh figure. An additional check was made through the symmetry of the transformed direction-cosine matrices: these matrices for negative κ values have the same numerical values as for positive values, but have the labelling of the rows and columns inverted.[6] The deviations between several computed values and those obtained by symmetry did not exceed two in the seventh place.

The reduced energy levels (see Eq. (3)) of the asymmetric rotor were calculated from the explicit formulas for $\kappa=-1(0.1)+1$. To obtain the energy values for positive κ, use was made of the relation

$$E_\tau^J(\kappa)=-E_{-\tau}^J(-\kappa).$$

The calculations were carried out to eight significant figures and were rounded off to seven. Differences were formed between the various energy levels.

The reduced second-order Stark coefficients were then evaluated with the aid of Eq. (14) for $\kappa=-1(0.2)+1$ and $\alpha=0.1(0.2)0.9$. A separate computation was carried out for the accidentally degenerate levels so that Eq. (18) may be applied when degeneracy does occur. The final tabulation was rounded off to six decimal places, and fifth differences taken and smoothed.

In using the tables, the factor $(2/a+c)$ must be applied to take into account the fact that *reduced* energies have been employed (see Eq. (16)). The various A's and B's are given for each level and dipole-moment component. In addition, a separate tabulation is given for the accidentally degenerate levels which will permit of easier interpolation (*viz.* interpolation of reciprocal) in regions of degeneracy. To get the entire reduced Stark coefficient for no degeneracy it is necessary to add the contributions from the accidentally degenerate parts to that given for the individual level. The signs given are for the first indicated level of the pair. For the remaining one, the signs should be reversed. For degeneracy, Eq. (18) must be applied.

Reduced Stark coefficients for dipole-moment component along principal axis of smallest moment of inertia.

Level		$\alpha\backslash\kappa$	−0.9	−0.7	−0.5	−0.3	−0.1	+0.1	+0.3	+0.5	+0.7	+0.9
0_0	A_a	0.1	−.184162	−.182149	−.180180	−.178253	−.176367	−.174520	−.172712	−.170940	−.169205	−.167504
		0.3	−.233100	−.223714	−.215054	−.207039	−.199601	−.192678	−.186220	−.180180	−.174520	−.169205
		0.5	−.317460	−.289855	−.266667	−.246914	−.229885	−.215054	−.202020	−.190476	−.180180	−.170940
		0.7	−.497512	−.411523	−.350877	−.305810	−.271003	−.243309	−.220751	−.202020	−.186220	−.172712
		0.9	−1.149425	−.709220	−.512820	−.401606	−.330033	−.280112	−.243309	−.215054	−.192678	−.174520

Reduced Stark coefficients for dipole-moment component along principal axis of smallest moment of inertia.—*Continued.*

Level		$\alpha \backslash \kappa$	−0.9	−0.7	−0.5	−0.3	−0.1	+0.1	+0.3	+0.5	+0.7	+0.9
		0.1	.110496	.109278	.108075	.106888	.105717	.104561	.103420	.102294	.101183	.100086
		0.3	.139843	.134088	.128671	.123564	.118742	.114182	.109860	.105758	.101858	.098142
	A_a	0.5	.190401	.173343	.158650	.145856	.134604	.124620	.115685	.107628	.100310	.093618
		0.7	.298186	.244913	.206427	.177239	.154294	.135714	.120298	.107243	.095985	.086120
		0.9	.687107	.416573	.294253	.224222	.178605	.146318	.122077	.103037	.087524	.074486
1_{-1}												
		0.1	−.165745	−.163931	−.162154	−.160412	−.158704	−.157030	−.155389	−.153779	−.152199	−.150650
		0.3	−.209786	−.201307	−.193458	−.186171	−.179386	−.173054	−.167130	−.161575	−.156354	−.151439
	B_a	0.5	−.285696	−.260727	−.239662	−.221649	−.206065	−.192445	−.180436	−.169764	−.160213	−.151610
		0.7	−.447681	−.369870	−.314762	−.273667	−.241826	−.216410	−.195638	−.178326	−.163661	−.151064
		0.9	−1.033846	−.636058	−.458179	−.357260	−.292176	−.246664	−.213001	−.187050	−.166390	−.149511
		0.1	−.055402	−.055096	−.054795	−.054496	−.054201	−.053908	−.053619	−.053333	−.053050	−.052770
		0.3	−.070671	−.069204	−.067797	−.066445	−.065147	−.063898	−.062696	−.061539	−.060423	−.059347
	A_a	0.5	−.097561	−.093023	−.088889	−.085106	−.081633	−.078431	−.075472	−.072727	−.070175	−.067797
		0.7	−.157480	−.141844	−.129032	−.118343	−.109290	−.101523	−.094787	−.088889	−.083682	−.079051
		0.9	−.408163	−.298508	−.235294	−.194175	−.165289	−.143885	−.127389	−.114286	−.103627	−.094787
1_0												
		0.1	.013850	.013774	.013699	.013624	.013550	.013477	.013405	.013333	.013263	.013193
		0.3	.017668	.017301	.016949	.016611	.016287	.015974	.015674	.015385	.015106	.014837
	B_a	0.5	.024390	.023256	.022222	.021277	.020408	.019608	.018868	.018182	.017544	.016949
		0.7	.039370	.035461	.032258	.029586	.027322	.025381	.023697	.022222	.020921	.019763
		0.9	.102041	.074627	.058824	.048544	.041322	.035971	.031847	.028571	.025907	.023697
		0.1	−.055096	−.054201	−.053333	−.052493	−.051680	−.050891	−.050125	−.049383	−.048662	−.047962
		0.3	−.069204	−.065147	−.061539	−.058309	−.055402	−.052770	−.050378	−.048193	−.046189	−.044346
	A_a	0.5	−.093023	−.081633	−.072727	−.065574	−.059702	−.054795	−.050633	−.047059	−.043956	−.041237
		0.7	−.141844	−.109290	−.088889	−.074906	−.064725	−.056980	−.050891	−.045977	−.041929	−.038536
		0.9	−.298508	−.165289	−.114286	−.087336	−.070671	−.059347	−.051151	−.044944	−.040080	−.036166
1_1												
		0.1	.013774	.013550	.013333	.013123	.012920	.012723	.012531	.012346	.012166	.011990
		0.3	.017301	.016287	.015385	.014577	.013850	.013193	.012595	.012048	.011547	.011087
	B_a	0.5	.023256	.020408	.018182	.016393	.014925	.013699	.012658	.011765	.010989	.010309
		0.7	.035461	.027322	.022222	.018727	.016181	.014245	.012723	.011494	.010482	.009634
		0.9	.074627	.041322	.028571	.021834	.017668	.014837	.012788	.011236	.010020	.009042
		0.1	.026284	.025775	.025012	.023958	.022605	.020984	.019157	.017210	.015234	.013308
		0.3	.033264	.031617	.029771	.027697	.025422	.023001	.020520	.018079	.015768	.013658
	A_a	0.5	.045274	.040759	.036457	.032298	.028296	.024498	.020982	.017831	.015111	.012856
		0.7	.070819	.057088	.046408	.037683	.030374	.024224	.019129	.015047	.011940	.009747
		0.9	.162326	.094060	.061305	.041255	.027418	.017391	.010156	.005209	.002218	.000895
2_{-2}												
		0.1	−.013218	−.013670	−.014960	−.017317	−.020893	−.025690	−.031531	−.038088	−.044954	−.051731
		0.3	−.016668	−.016168	−.015965	−.016122	−.016688	−.017666	−.019009	−.020619	−.022373	−.024149
	B_a	0.5	−.022689	−.020826	−.019421	−.018439	−.017861	−.017663	−.017799	−.018201	−.018788	−.019479
		0.7	−.035560	−.029561	−.025469	−.022595	−.020592	−.019259	−.018457	−.018072	−.018002	−.018156
		0.9	−.082252	−.051154	−.037352	−.029650	−.024831	−.021731	−.019755	−.018576	−.017982	−.017816
		0.1	.013191	.013115	.013036	.012956	.012873	.012788	.012701	.012612	.012521	.012429
		0.3	.016822	.016436	.016033	.015616	.015186	.014747	.014300	.013847	.013388	.012925
	A_a	0.5	.023211	.021981	.020739	.019498	.018270	.017060	.015872	.014708	.013568	.012453
		0.7	.037409	.033124	.029225	.025692	.022487	.019565	.016888	.014419	.012128	.009988
		0.9	.096327	.066911	.048725	.036288	.027204	.020186	.014548	.009868	.005871	.002375
2_{-1}												
		0.1	−.009160	−.009110	−.009059	−.009008	−.008958	−.008908	−.008858	−.008809	−.008759	−.008710
		0.3	−.011685	−.011438	−.011198	−.010964	−.010736	−.010513	−.010297	−.010086	−.009880	−.009679
	B_a	0.5	−.016129	−.015362	−.014650	−.013987	−.013368	−.012789	−.012246	−.011735	−.011254	−.010800
		0.7	−.026029	−.023381	−.021168	−.019291	−.017678	−.016274	−.015041	−.013948	−.012970	−.012089
		0.9	−.067393	−.048894	−.038094	−.031002	−.025980	−.022227	−.019309	−.016969	−.015045	−.013429
		0.1	.013118	.012901	.012689	.012480	.012274	.012072	.011874	.011679	.011487	.011298
		0.3	.016473	.015474	.014558	.013714	.012933	.012208	.011531	.010897	.010300	.009736
	A_a	0.5	.022130	.019302	.017011	.015112	.013508	.012128	.010923	.009856	.008898	.008027
		0.7	.033699	.025617	.020395	.016724	.013985	.011846	.010113	.008668	.007429	.006340
		0.9	.070609	.038016	.025357	.018575	.014309	.011344	.009133	.007394	.005962	.004737
2_0												
		0.1	−.009110	−.008961	−.008817	−.008677	−.008542	−.008410	−.008281	−.008156	−.008035	−.007917
		0.3	−.011442	−.010768	−.010165	−.009622	−.009132	−.008686	−.008278	−.007904	−.007560	−.007241
	B_a	0.5	−.015379	−.013483	−.011991	−.010787	−.009793	−.008958	−.008246	−.007631	−.007094	−.006619
		0.7	−.023445	−.018026	−.014612	−.012262	−.010543	−.009230	−.008192	−.007349	−.006649	−.006057
		0.9	−.049305	−.027181	−.018691	−.014194	−.011405	−.009503	−.008119	−.007064	−.006229	−.005550
		0.1	−.026309	−.026021	−.025740	−.025465	−.025195	−.024931	−.024673	−.024420	−.024172	−.023929
		0.3	−.033300	−.031959	−.030722	−.029577	−.028514	−.027525	−.026603	−.025740	−.024931	−.024172
	A_a	0.5	−.045352	−.041408	−.038095	−.035273	−.032841	−.030722	−.028860	−.027211	−.025740	−.024420
		0.7	−.071073	−.058789	−.050125	−.043687	−.038715	−.034758	−.031536	−.028860	−.026603	−.024673
		0.9	−.164204	−.101317	−.073260	−.057372	−.047148	−.040016	−.034758	−.030722	−.027525	−.024931
2_1												
		0.1	.002993	.003617	.005149	.007830	.011813	.017094	.023471	.030614	.038066	.045416
		0.3	.003723	.003793	.004177	.004953	.006173	.007833	.009868	.012160	.014564	.016938
	B_a	0.5	.005053	.004746	.004691	.004919	.005452	.006278	.007354	.008604	.009936	.011265
		0.7	.007907	.006636	.005897	.005569	.005589	.005908	.006466	.007192	.008010	.008850
		0.9	.018253	.011338	.008394	.006930	.006240	.006038	.006166	.006514	.006990	.007521

Reduced Stark coefficients for dipole-moment component along principal axis of smallest moment of inertia.—*Continued.*

Level		$\alpha \backslash \kappa$	−0.9	−0.7	−0.5	−0.3	−0.1	+0.1	+0.3	+0.5	+0.7	+0.9
		0.1	−.026272	−.025672	−.024761	−.023585	−.022193	−.020614	−.018879	−.017028	−.015122	−.013222
		0.3	−.033239	−.031433	−.029316	−.027045	−.024711	−.022362	−.020016	−.017702	−.015458	−.013326
	A_a	0.5	−.045220	−.040376	−.035671	−.031322	−.027420	−.023933	−.020788	−.017928	−.015329	−.012983
		0.7	−.070677	−.056316	−.045287	−.036893	−.030469	−.025429	−.021336	−.017910	−.014986	−.012472
		0.9	−.161622	−.092777	−.061682	−.044575	−.034022	−.026910	−.021739	−.017752	−.014545	−.011910
2_2												
		0.1	.002915	.002812	.002628	.002364	.002021	.001608	.001139	.000633	.000113	−.000399
		0.3	.003690	.003457	.003154	.002789	.002374	.001918	.001435	.000940	.000453	−.000010
	B_a	0.5	.005021	.004456	.003874	.003294	.002728	.002175	.001639	.001125	.000644	.000203
		0.7	.007850	.006231	.004953	.003936	.003106	.002403	.001788	.001240	.000753	.000325
		0.9	.017956	.010285	.006783	.004807	.003531	.002615	.001900	.001312	.000816	.000396
		0.1	25.000000	8.333333	5.000000	3.571428	2.777778	2.272727	1.923076	1.666667	1.470588	1.315789
		0.3	8.333333	2.777778	1.666667	1.190476	.925926	.757576	.641025	.555555	.490196	.438596
1_1-1_0	B_a	0.5	5.000000	1.666667	1.000000	.714286	.555556	.454545	.384615	.333333	.294118	.263158
		0.7	3.571429	1.190476	.714286	.510204	.396825	.324675	.274725	.238095	.210084	.187970
		0.9	2.777778	.925926	.555556	.396825	.308642	.252525	.213675	.185185	.163399	.146199
		0.1	.925926	.308642	.185185	.132275	.102881	.084175	.071225	.061728	.054466	.048733
		0.3	.308642	.102881	.061728	.044092	.034294	.028058	.023742	.020576	.018155	.016244
2_0-2_{-1}	B_a	0.5	.185185	.061728	.037037	.026455	.020576	.016835	.014245	.012346	.010893	.009747
		0.7	.132275	.044092	.026455	.018896	.014697	.012025	.010175	.008818	.007781	.006962
		0.9	.102881	.034294	.020576	.014697	.011431	.009353	.007914	.006859	.006052	.005415
		0.1	288.88888	30.453380	10.370598	4.993661	2.843947	1.789652	1.204169	.850946	.624897	.473659
		0.3	96.296296	10.151128	3.456866	1.664553	.947983	.596551	.401390	.283649	.208299	.157886
2_2-2_1	B_a	0.5	57.777778	6.090677	2.074120	.998732	.568789	.357930	.240834	.170189	.124979	.094732
		0.7	41.269829	4.350483	1.481514	.713380	.406278	.255665	.172024	.121564	.089271	.067666
		0.9	32.098765	3.383710	1.152289	.554851	.315994	.198850	.133797	.094550	.069433	.052629
		0.1	−.000012	−.000104	−.000247	−.000362	−.000395	−.000343	−.000242	−.000133	−.000049	−.000005
		0.3	−.000029	−.000226	−.000500	−.000702	−.000747	−.000642	−.000452	−.000251	−.000094	−.000011
2_2-3_3	A_a	0.5	.000073	.001380	.022416	−.011169	−.006789	−.004939	−.003503	−.002263	−.001213	−.000357
		0.7	.000016	.000170	.000478	.000803	.000958	.000867	.000609	.000322	.000111	.000011
		0.9	.000009	.000091	.000242	.000388	.000447	.000399	.000280	.000150	.000053	.000006
2_2-3_{-3}	B_a	0.1	.000001	.000012	.000027	.000040	.000044	.000038	.000027	.000015	.000005	.000001
		0.3	.000003	.000025	.000056	.000078	.000083	.000071	.000050	.000028	.000010	.000001
		0.5	−.000008	−.000153	−.002491	.001241	.000754	.000549	.000389	.000252	.000135	.000040
		0.7	−.000002	−.000019	−.000053	−.000089	−.000106	−.000096	−.000068	−.000036	−.000012	−.000001
		0.9	−.000001	−.000010	−.000027	−.000043	−.000050	−.000044	−.000031	−.000017	−.000006	−.000001

Reduced Stark coefficients for dipole-moment component along principal axis of intermediate moment of inertia.

Level		$\alpha \backslash \kappa$	−0.9	−0.7	−0.5	−0.3	−0.1	+0.1	+0.3	+0.5	+0.7	+0.9
		0.1	−.166667									
		0.3	−.166667									
0_0	A_b	0.5	−.166667	→								
		0.7	−.166667									
		0.9	−.166667									
		0.1	−.052632									
		0.3	−.058824									
	A_b	0.5	−.066667	→								
		0.7	−.076923									
		0.9	−.090909									
1_{-1}												
		0.1	.013158									
		0.3	.014706									
	B_b	0.5	.016667	→								
		0.7	.019231									
		0.9	.022727									
		0.1	.120398	.123372	.126692	.130296	.134076	.137894	.141601	.145066	.148195	.150945
		0.3	.124601	.127676	.131049	.134647	.138355	.142034	.145543	.148763	.151620	.154085
	A_b	0.5	.128105	.131201	.134549	.138068	.141641	.145133	.148413	.151379	.153973	.156180
		0.7	.131070	.134141	.137423	.140828	.144243	.147539	.150597	.153329	.155690	.157677
		0.9	.133611	.136632	.139825	.143103	.146356	.149461	.152314	.154837	.156998	.158799
1_0												
		0.1	−.155099	−.155843	−.156673	−.157574	−.158519	−.159474	−.160400	−.161266	−.162049	−.162736
		0.3	−.156150	−.156919	−.157762	−.158662	−.159589	−.160509	−.161386	−.162191	−.162905	−.163521
	B_b	0.5	−.157026	−.157800	−.158637	−.159517	−.160410	−.161283	−.162103	−.162845	−.163493	−.164045
		0.7	−.157768	−.158535	−.159356	−.160207	−.161061	−.161885	−.162649	−.163332	−.163923	−.164419
		0.9	−.158403	−.159158	−.159956	−.160776	−.161589	−.162365	−.163078	−.163709	−.164249	−.164700
		0.1	−.047619									
		0.3	−.043478									
	A_b	0.5	−.040000	→								
		0.7	−.037037									
		0.9	−.034483									
1_{+1}												
		0.1	.011905									
		0.3	.010870									
	B_b	0.5	.010000	→								
		0.7	.009259									
		0.9	.008621									

Reduced Stark coefficients for dipole-moment component along principal axis of intermediate moment of inertia.—*Continued.*

Levels		$\alpha \backslash \kappa$	−0.9	−0.7	−0.5	−0.3	−0.1	+0.1	+0.3	+0.5	+0.7	+0.9
		0.1	−.031035	−.031957	−.032971	−.034054	−.035173	−.036284	−.037344	−.038317	−.039180	−.039923
		0.3	−.036285	−.037494	−.038771	−.040077	−.041359	−.042565	−.043644	−.044564	−.045314	−.045897
	A_b	0.5	−.043673	−.045367	−.047098	−.048796	−.050381	−.051773	−.052912	−.053770	−.054350	−.054678
		0.7	−.054842	−.057439	−.060023	−.062459	−.064601	−.066319	−.067530	−.068211	−.068403	−.068187
		0.9	−.073686	−.078280	−.082771	−.086852	−.090195	−.092527	−.093705	−.093749	−.092822	−.091161
2_{-2}												
		0.1	.003448	.003551	.003663	.003784	.003908	.004032	.004149	.004257	.004353	.004436
		0.3	.004032	.004166	.004308	.004453	.004596	.004729	.004849	.004952	.005035	.005100
	B_b	0.5	.004853	.005041	.005233	.005422	.005598	.005753	.005879	.005974	.006039	.006075
		0.7	.006094	.006382	.006669	.006940	.007178	.007369	.007503	.007579	.007600	.007576
		0.9	.008187	.008698	.009197	.009650	.010022	.010281	.010412	.010417	.010314	.010129
		0.1	.030784	.034885	.038807	.042148	.044760	.046699	.048109	.049129	.049874	.050426
		0.3	.037205	.041682	.045837	.049271	.051874	.053751	.055075	.056007	.056669	.057147
	A_b	0.5	.045272	.050091	.054422	.057892	.060466	.062236	.063466	.064311	.064899	.065315
		0.7	.055748	.060876	.065340	.068810	.071293	.072990	.074131	.074899	.075425	.075790
		0.9	.069949	.075359	.079920	.083365	.085767	.087373	.088433	.089135	.089609	.089935
2_{-1}												
		0.1	−.010730	−.011186	−.011622	−.011993	−.012283	−.012499	−.012655	−.012769	−.012852	−.012913
		0.3	−.012304	−.012801	−.013263	−.013644	−.013934	−.014142	−.014289	−.014393	−.014467	−.014520
	B_b	0.5	−.014290	−.014825	−.015306	−.015692	−.015976	−.016174	−.016311	−.016405	−.016470	−.016517
		0.7	−.016878	−.017448	−.017944	−.018329	−.018605	−.018794	−.018921	−.019006	−.019064	−.019105
		0.9	−.020398	−.021000	−.021506	−.021889	−.022156	−.022334	−.022452	−.022530	−.022583	−.022619
		0.1	−.023810									
		0.3	−.023810									
	A_b	0.5	−.023810	→								
		0.7	−.023810									
		0.9	−.023810									
2_0												
		0.1	.002646									
		0.3	.002646									
	B_b	0.5	.002646	→								
		0.7	.002646									
		0.9	.002646									
		0.1	.014388	.015000	.015806	.016881	.018326	.020264	.022806	.025974	.029595	.033284
		0.3	.013980	.014614	.015436	.016513	.017935	.019808	.022218	.025163	.028462	.031754
	A_b	0.5	.013480	.014116	.014929	.015983	.017356	.019140	.021403	.024127	.027132	.030083
		0.7	.012950	.013575	.014368	.015386	.016701	.018391	.020510	.023031	.025779	.028444
		0.9	.012419	.013028	.013796	.014774	.016028	.017625	.019611	.021952	.024476	.026902
2_1												
		0.1	−.008213	−.008281	−.008370	−.008489	−.008650	−.008865	−.009148	−.009500	−.009902	−.010312
		0.3	−.007592	−.007663	−.007754	−.007873	−.008032	−.008240	−.00850	−.008835	−.009201	−.009567
	B_b	0.5	−.007053	−.007124	−.007214	−.007331	−.007484	−.007682	−.007934	−.008236	−.008570	−.008898
		0.7	−.006583	−.006652	−.006741	−.006854	−.007000	−.007188	−.007423	−.007703	−.008008	−.008305
		0.9	−.006169	−.006237	−.006322	−.006431	−.006570	−.006748	−.006968	−.007228	−.007509	−.007778
		0.1	.013028	.010569	.007820	.004848	.001760	−.001316	−.004253	−.006945	−.009331	−.011386
		0.3	.012555	.010004	.007187	.004183	.001103	−.001921	−.004766	−.007337	−.009580	−.011484
	A_b	0.5	.012029	.009450	.006638	.003676	.000678	−.002228	−.004926	−.007334	−.009409	−.011151
		0.7	.011496	.008928	.006160	.003277	.000392	−.002374	−.004914	−.007156	−.009070	−.010664
		0.9	.010978	.008446	.005742	.002955	.000194	−.002428	−.004814	−.006903	−.008673	−.010137
2_2												
		0.1	−.007874	−.007188	−.006421	−.005590	−.004722	−.003850	−.003009	−.002229	−.001529	−.000921
		0.3	−.007237	−.006527	−.005746	−.004912	−.004055	−.003208	−.002404	−.001672	−.001025	−.000471
	B_b	0.5	−.006692	−.005976	−.005198	−.004381	−.003551	−.002743	−.001988	−.001308	−.000718	−.000218
		0.7	−.006221	−.005510	−.004746	−.003953	−.003158	−.002393	−.001686	−.001057	−.000517	−.000064
		0.9	−.005811	−.005110	−.004366	−.003601	−.002843	−.002120	−.001459	−.000876	−.000379	−.000034
		0.1	−.020951	−.023914	−.027223	−.030815	−.034585	−.038393	−.042090	−.045545	−.048666	−.051407
		0.3	−.031394	−.033904	−.036800	−.039988	−.043341	−.046710	−.049944	−.052920	−.055559	−.057827
	A_b	0.5	−.062588	−.058228	−.056771	−.056936	−.058034	−.059626	−.061400	−.063144	−.064726	−.066081
		0.7	−.830826	−.206071	−.124148	−.098817	−.087799	−.082414	−.079677	−.078265	−.077516	−.077083
		0.9	.063395	.133895	.664525	−.373715	−.180240	−.133399	−.113446	−.102908	−.096606	−.092479
1_0-2_{-2}												
		0.1	.005238	.005979	.006806	.007704	.008646	.009598	.010523	.011386	.012167	.012852
		0.3	.007848	.008476	.009200	.009997	.010835	.011677	.012486	.013230	.013890	.014457
	B_b	0.5	.015647	.014557	.014193	.014234	.014509	.014906	.015350	.015786	.016182	.016520
		0.7	2.457708	.051518	.031037	.024704	.021950	.020604	.019919	.019566	.019379	.019271
		0.9	−.015849	−.033474	−.166131	.093429	.045060	.033350	.028361	.025727	.024152	.023120
		0.1	1.250000									
		0.3	.416667									
1_1-1_{-1}	B_b	0.5	.250000	→								
		0.7	.178571									
		0.9	.138889									
		0.1	−.018443	−.022539	−.026455	−.029792	−.032399	−.034334	−.035739	−.036755	−.037497	−.038045
		0.3	−.025850	−.030071	−.034014	−.037271	−.039724	−.041471	−.042682	−.043515	−.044090	−.044490
	A_b	0.5	−.043202	−.045165	−.047619	−.049762	−.051328	−.052353	−.052974	−.053322	−.053498	−.053565
		0.7	−.131405	−.090681	−.079365	−.074849	−.072509	−.070977	−.069805	−.068836	−.068008	−.067289
		0.9	.126148	11.634484	−.238095	−.150943	−.009168	−.110171	−.102314	−.097081	−.093318	−.090468
$2_{-1}-3_{-3}$												
		0.1	.002049	.002504	.002939	.003310	.003600	.003815	.003971	.004084	.004166	.004227
		0.3	.002872	.003341	.003779	.004141	.004414	.004608	.004742	.004835	.004899	.004943
	B_b	0.5	.004800	.005018	.005291	.005529	.005703	.005817	.005886	.005925	.005944	.005952
		0.7	.014601	.010076	.008818	.008317	.008057	.007886	.007756	.007648	.007556	.007477
		0.9	−.014017	−1.292720	.026455	.016772	.001019	.012241	.011368	.010787	.010369	.010052

Reduced Stark coefficients for dipole-moment component along principal axis of intermediate moment of inertia.—*Continued.*

Levels		$\alpha \backslash \kappa$	−0.9	−0.7	−0.5	−0.3	−0.1	+0.1	+0.3	+0.5	+0.7	+0.9
		0.1	.385824	.326893	.272357	.223059	.179694	.142657	.111948	.087171	.067634	.052491
		0.3	.128608	.108964	.090786	.074353	.059898	.047552	.037316	.029057	.022545	.017497
2_0-2_{-2}	B_b	0.5	.077165	.065379	.054471	.044612	.035939	.028532	.022390	.017434	.013527	.010498
		0.7	.055118	.046699	.038908	.031866	.025671	.020380	.015993	.012453	.009662	.007499
		0.9	.042869	.036322	.030262	.024784	.019966	.015851	.012439	.009686	.007515	.005832
		0.1	.046296									
		0.3	.015432									
2_1-2_{-1}	B_b	0.5	.009259	→								
		0.7	.006614									
		0.9	.005144									
		0.1	−.003224	−.003831	−.004632	−.005701	−.007143	−.009076	−.011614	−.014778	−.018396	−.022081
		0.3	−.005989	−.006272	−.006833	−.007709	−.008973	−.010716	−.013019	−.015873	−.019095	−.022320
	A_b	0.5	−.042052	−.017290	−.013024	−.011900	−.012065	−.013079	−.014810	−.017143	−.019849	−.022564
		0.7	.008375	.022854	−.242173	−.026073	−.018409	−.016780	−.017172	−.018634	−.020665	−.022813
		0.9	.003808	.006880	.016041	.136436	−.038821	−.023401	−.020431	−.020408	−.021551	−.023068
2_1-3_{-1}												
		0.1	.000358	.000426	.000515	.000634	.000794	.001009	.001291	.001642	.002044	.002454
		0.3	.000666	.000697	.000759	.000857	.000997	.001191	.001447	.001764	.002122	.002480
	B_b	0.5	.004672	.001921	.001447	.001322	.001341	.001453	.001646	.001905	.002205	.002507
		0.7	−.000931	−.002539	.026908	.002897	.002045	.001864	.001908	.002070	.002296	.002535
		0.9	−.000423	−.000764	−.001782	−.015160	.004314	.002600	.002270	.002268	.002395	.002563
		0.1	.052491	.067634	.087171	.111948	.142657	.179694	.223059	.272357	.326893	.385824
		0.3	.017497	.022545	.029057	.037316	.047552	.059898	.074353	.090786	.108964	.128608
2_2-2_0	B_b	0.5	.010498	.013527	.017434	.022390	.028532	.035939	.044612	.054471	.065379	.077165
		0.7	.007499	.009662	.012453	.015993	.020380	.025671	.031866	.038908	.046699	.055118
		0.9	.005832	.007515	.009686	.012439	.015851	.019966	.024784	.030262	.036322	.042869
		0.1	−.002792	−.002382	−.001935	−.001480	−.001050	−.000677	−.000384	−.000179	−.000058	−.000006
		0.3	−.005501	−.004578	−.003651	−.002757	−.001944	−.001253	−.000715	−.000337	−.000111	−.000011
	A_b	0.5	−.186936	−.058776	−.032184	−.020158	−.013102	−.008448	−.005226	−.002974	−.001420	−.000375
		0.7	.005845	.005423	.004722	.003795	.002763	.001782	.000984	.000436	.000131	.000012
		0.9	.002878	.002592	.002199	.001734	.001250	.000806	.000450	.000203	.000063	.000006
2_2-3_{-2}												
		0.1	.000310	.000265	.000215	.000164	.000117	.000075	.000043	.000020	.000006	.000001
		0.3	.000611	.000509	.000406	.000306	.000216	.000139	.000079	.000038	.000012	.000001
	B_b	0.5	.020771	.006531	.003576	.002240	.001456	.000939	.000581	.000330	.000158	.000042
		0.7	−.000650	−.000603	−.000525	−.000422	−.000307	−.000198	−.000109	−.000049	−.000015	−.000001
		0.9	−.000320	−.000288	−.000244	−.000193	−.000139	−.000090	−.000050	−.000023	−.000007	−.000001

Reduced Stark coefficients for dipole-moment component along principal axis of largest moment of inertia.

Level		$\alpha \backslash \kappa$	−0.9	−0.7	−0.5	−0.3	−0.1	+0.1	+0.3	+0.5	+0.7	+0.9
		0.1	−.165838	−.164204	−.162602	−.161031	−.159490	−.157978	−.156494	−.155039	−.153610	−.152207
		0.3	−.164204	−.159490	−.155039	−.150830	−.146843	−.143062	−.139470	−.136054	−.132802	−.129702
0_0	A_c	0.5	−.162602	−.155039	−.148148	−.141844	−.136054	−.130719	−.125786	−.121212	−.116959	−.112994
		0.7	−.161031	−.150830	−.141844	−.133869	−.126743	−.120337	−.114548	−.109290	−.104493	−.100100
		0.9	−.159490	−.146843	−.136054	−.126743	−.118623	−.111483	−.105152	−.099502	−.094429	−.089847
		0.1	−.052219	−.051414	−.050633	−.049875	−.049140	−.048426	−.047733	−.047059	−.046404	−.045767
		0.3	−.057307	−.054496	−.051948	−.049628	−.047506	−.045558	−.043764	−.042105	−.040568	−.039139
	A_c	0.5	−.063492	−.057971	−.053333	−.049383	−.045977	−.043011	−.040404	−.038095	−.036036	−.034188
		0.7	−.071174	−.061920	−.054795	−.049140	−.044543	−.040733	−.037523	−.034783	−.032415	−.030349
		0.9	−.080972	−.066445	−.056338	−.048900	−.043197	−.038685	−.035026	−.032000	−.029455	−.027285
1_{-1}												
		0.1	.013055	.012854	.012658	.012469	.012285	.012107	.011933	.011765	.011601	.011442
		0.3	.014327	.013624	.012987	.012407	.011877	.011390	.010941	.010526	.010142	.009785
	B_c	0.5	.015873	.014493	.013333	.012346	.011494	.010753	.010101	.009524	.009009	.008547
		0.7	.017794	.015480	.013699	.012285	.011136	.010183	.009381	.008696	.008104	.007587
		0.9	.020243	.016611	.014085	.012225	.010799	.009671	.008757	.008000	.007364	.006821
		0.1	−.047506	−.047281	−.047059	−.046838	−.046620	−.046404	−.046189	−.045977	−.045767	−.045558
		0.3	−.043197	−.042644	−.042105	−.041580	−.041068	−.040568	−.040080	−.039604	−.039139	−.038685
	A_c	0.5	−.039604	−.038835	−.038095	−.037383	−.036697	−.036036	−.035398	−.034783	−.034188	−.033613
		0.7	−.036563	−.035651	−.034783	−.033956	−.033168	−.032415	−.031696	−.031008	−.030349	−.029718
		0.9	−.033956	−.032949	−.032000	−.031104	−.030257	−.029455	−.028694	−.027972	−.027285	−.026631
1_0												
		0.1	.011877	.011820	.011765	.011710	.011655	.011601	.011547	.011494	.011442	.011390
		0.3	.010799	.010661	.010526	.010395	.010267	.010142	.010020	.009901	.009785	.009671
	B_c	0.5	.009901	.009709	.009524	.009346	.009174	.009009	.008850	.008696	.008547	.008403
		0.7	.009141	.008913	.008696	.008489	.008292	.008104	.007924	.007752	.007587	.007429
		0.9	.008489	.008237	.008000	.007776	.007564	.007364	.007174	.006993	.006821	.006658
		0.1	.117019	.112960	.108978	.105191	.101720	.098674	.096122	.094081	.092516	.091360
		0.3	.119637	.112772	.106291	.100294	.094886	.090147	.086116	.082774	.080054	.077858
	A_c	0.5	.121606	.112112	.103463	.095693	.088847	.082950	.077988	.073891	.070550	.067834
		0.7	.123076	.111126	.100597	.091402	.083489	.076802	.071257	.066729	.063064	.060096
		0.9	.124156	.109911	.097754	.087416	.078713	.071492	.065593	.060832	.057014	.053943
1_1												
		0.1	−.153633	−.151393	−.149196	−.147071	−.145047	−.143152	−.141401	−.139799	−.138336	−.136995
		0.3	−.153062	−.147810	−.142852	−.138196	−.133854	−.129833	−.126131	−.122734	−.119615	−.116741
	B_c	0.5	−.152353	−.144307	−.136977	−.130306	−.124253	−.118777	−.113837	−.109382	−.105357	−.101704
		0.7	−.151542	−.140904	−.131532	−.123252	−.115929	−.109453	−.103725	−.098650	−.094136	−.090099
		0.9	−.150656	−.137610	−.126479	−.116911	−.108646	−.101485	−.095263	−.089835	−.085075	−.080871

Reduced Stark coefficients for dipole-moment component along principal axis of largest moment of inertia.—*Continued*.

Levels		$\alpha \backslash \kappa$	−0.9	−0.7	−0.5	−0.3	−0.1	+0.1	+0.3	+0.5	+0.7	+0.9
		0.1	−.029919	−.028576	−.027265	−.026030	−.024911	−.023943	−.023146	−.022525	−.022070	−.021757
		0.3	−.034085	−.031087	−.028419	−.026075	−.024060	−.022375	−.021011	−.019945	−.019138	−.018545
	A_z	0.5	−.039583	−.034089	−.029687	−.026135	−.023279	−.021011	−.019245	−.017899	−.016895	−.016160
		0.7	−.047195	−.037736	−.031082	−.026205	−.022555	−.019810	−.017756	−.016236	−.015124	−.014319
		0.9	−.058434	−.042261	−.032619	−.026279	−.021879	−.018742	−.016482	−.014856	−.013689	−.012854
2_{-2}												
		0.1	.003324	.003175	.003029	.002892	.002768	.002660	.002572	.002503	.002452	.002417
		0.3	.003787	.003454	.003158	.002897	.002673	.002486	.002335	.002216	.002126	.002061
	B_z	0.5	.004398	.003788	.003299	.002904	.002567	.002334	.002138	.001989	.001877	.001796
		0.7	.005244	.004193	.003454	.002912	.002506	.002201	.001973	.001804	.001680	.001591
		0.9	.006493	.004696	.003624	.002920	.002431	.002082	.001831	.001651	.001521	.001428
		0.1	−.023691	−.023458	−.023229	−.023004	−.022784	−.022568	−.022356	−.022148	−.021944	−.021744
		0.3	−.023458	−.022784	−.022148	−.021547	−.020978	−.020437	−.019924	−.019436	−.018971	−.018529
	A_z	0.5	−.023229	−.022148	−.021164	−.020263	−.019436	−.018674	−.017969	−.017316	−.016708	−.016152
		0.7	−.023004	−.021547	−.020263	−.019124	−.018106	−.017191	−.016364	−.015613	−.014928	−.014300
		0.9	−.022784	−.020978	−.019436	−.018106	−.016946	−.015926	−.015022	−.014215	−.013490	−.012835
2_{-1}												
		0.1	−.040125	−.032774	−.025319	−.018181	−.011792	−.006506	−.002517	.000172	.001712	.002346
		0.3	−.011646	−.009262	−.006839	−.004518	−.002444	−.000734	.000547	.001397	.001866	.002035
	B_z	0.5	−.005970	−.004615	−.003229	−.001896	−.000705	.000272	.000997	.001466	.001711	.001780
		0.7	−.003552	−.002660	−.001734	−.000838	−.000035	.000622	.001104	.001408	.001555	.001579
		0.9	−.002219	−.001600	−.000941	−.000293	.000291	.000768	.001114	.001325	.001418	.001418
		0.1	.026619	.022384	.018756	.015989	.014062	.012792	.011977	.011457	.011123	.010904
		0.3	.031722	.025637	.020589	.016789	.014124	.012329	.011129	.010314	.009743	.009326
	A_z	0.5	.037924	.029281	.022476	.017526	.014136	.011884	.010389	.009377	.008668	.008148
		0.7	.045623	.033396	.024423	.018209	.014106	.011458	.009739	.008596	.007806	.007234
		0.9	.055436	.038087	.026438	.018843	.014045	.011053	.009164	.007935	.007100	.006504
2_0												
		0.1	−.010211	−.009628	−.009117	−.008704	−.008388	−.008147	−.007961	−.007809	−.007681	−.007568
		0.3	−.011484	−.010418	−.009503	−.008758	−.008168	−.007698	−.007315	−.006994	−.006717	−.006472
	B_z	0.5	−.013032	−.011305	−.009905	−.008806	−.007957	−.007294	−.006766	−.006333	−.005968	−.005654
		0.7	−.014955	−.012311	−.010324	−.008848	−.007754	−.006931	−.006294	−.005786	−.005369	−.005019
		0.9	−.017406	−.013460	−.010762	−.008885	−.007560	−.006601	−.005883	−.005326	−.004880	−.004517
		0.1	.013846	.013295	.012792	.012341	.011945	.011608	.011331	.011114	.010956	.010854
		0.3	.013317	.012568	.011889	.011283	.010753	.010299	.009921	.009618	.009385	.009218
	A_z	0.5	.012741	.011862	.011073	.010375	.009768	.009251	.008822	.008476	.008207	.008010
		0.7	.012164	.011200	.010343	.009592	.008944	.008395	.007941	.007576	.007293	.007083
		0.9	.011607	.010590	.009693	.008913	.008245	.007683	.007220	.006849	.006561	.006348
2_1												
		0.1	−.008137	−.008044	−.007957	−.007877	−.007802	−.007735	−.007674	−.007621	−.007574	−.007534
		0.3	−.007479	−.007319	−.007169	−.007029	−.006899	−.006779	−.006669	−.006569	−.006479	−.006397
	B_z	0.5	−.006916	−.006712	−.006521	−.006345	−.006182	−.006033	−.005897	−.005773	−.005660	−.005559
		0.7	−.006430	−.006196	−.005980	−.005782	−.005601	−.005435	−.005285	−.005149	−.005026	−.004915
		0.9	−.006006	−.005753	−.005522	−.005310	−.005119	−.004945	−.004788	−.004646	−.004519	−.004404
		0.1	.015148	.017160	.019063	.020717	.021971	.022703	.022880	.022616	.022158	.021769
		0.3	.014675	.016529	.018201	.019554	.020449	.020792	.020582	.019965	.019203	.018555
	A_z	0.5	.014120	.015834	.017431	.018437	.019072	.019147	.018690	.017866	.016942	.016168
		0.7	.013542	.015132	.016458	.017397	.017838	.017726	.017109	.016164	.015158	.014325
		0.9	.012971	.014451	.015647	.016441	.016736	.016491	.015770	.014757	.013713	.012860
2_2												
		0.1	.034293	.026356	.018335	.010680	.003859	−.001745	−.005927	−.008690	−.010221	−.010800
		0.3	.006432	.003468	.000507	−.002279	−.004714	−.006655	−.008030	−.008855	−.009218	−.009239
	B_z	0.5	.001289	−.000645	−.002550	−.004311	−.005811	−.006959	−.007715	−.008100	−.008183	−.008055
		0.7	−.000668	−.002141	−.003572	−.004869	−.005943	−.006728	−.007199	−.007380	−.007335	−.006639
		0.9	−.001598	−.002804	−.003958	−.004985	−.005811	−.006385	−.006691	−.006756	−.006640	−.006408
		0.1	1.315789	1.470588	1.666667	1.923077	2.272727	2.777778	3.571429	5.000000	8.333333	25.000000
		0.3	.438596	.490196	.555556	.641026	.757576	.925926	1.190476	1.666667	2.777778	8.333333
1_0-1_{-1}	B_z	0.5	.263158	.294118	.333333	.384615	.454545	.555556	.714286	1.000000	1.666667	5.000000
		0.7	.187970	.210084	.238095	.274725	.324675	.396825	.510204	.714286	.190476	3.571428
		0.9	.146199	.163399	.185185	.213675	.252525	.308642	.396825	.555556	.925926	2.777778
		0.1	−.018016	−.014829	−.011716	−.008792	−.006181	−.003989	−.002286	−.001087	−.000360	−.000037
		0.3	−.027275	−.021635	−.016563	−.012106	−.008329	−.005285	−.002990	−.001410	−.000465	−.000047
	A_z	0.5	−.056106	−.039986	−.028249	−.019430	−.012768	−.007830	−.004323	−.002005	−.000654	−.000066
		0.7	.982747	−.263412	−.095945	−.049179	−.027335	−.015102	−.007797	−.003466	−.001103	−.000110
		0.9	.050357	.057418	.068712	.092589	.193987	−.211759	−.039729	−.012798	−.003527	−.000331
1_1-2_{-2}												
		0.1	.004504	.003707	.002929	.002198	.001545	.000997	.000572	.000272	.000090	.000009
		0.3	.006819	.005409	.004141	.003027	.002082	.001321	.000748	.000353	.000116	.000012
	B_z	0.5	.014027	.009997	.007062	.004857	.003192	.001958	.001081	.000501	.000163	.000016
		0.7	−.245687	.065853	.023986	.012295	.006834	.003776	.001949	.000867	.000276	.000027
		0.9	−.012589	−.014355	−.017178	−.023147	−.048497	.052940	.009932	.003199	.000882	.000083
		0.1	.473659	.624897	.850946	1.204169	1.789653	2.843947	4.993661	10.372655	30.453386	288.888889
		0.3	.157886	.208299	.283649	.401390	.596551	.947983	1.664554	3.457552	10.151128	96.296286
$2_{-1}-2_{-2}$	B_z	0.5	.094732	.124979	.170189	.240834	.357931	.568790	.998732	2.074531	6.090677	57.777778
		0.7	.067666	.089271	.121564	.172024	.255665	.406278	.713380	1.481808	4.350483	44.269839
		0.9	.052629	.069433	.094550	.133797	.198850	.315994	.554851	1.152517	3.383710	32.098765
		0.1	−.014358	−.010277	−.006803	−.004190	−.002414	−.001296	−.000633	−.000263	−.000078	−.000007
		0.3	−.020502	−.014457	−.009524	−.005891	−.003436	−.001879	−.000939	−.000402	−.000123	−.000012
	A_z	0.5	−.035839	−.024367	−.015873	−.009918	−.005956	−.003413	−.001820	−.000849	−.000291	−.000033
		0.7	−.142277	−.077483	−.047619	−.031360	−.022335	−.018577	−.029454	.007603	.000807	.000044
		0.9	.072227	.065674	.047619	.026993	.012761	.005394	.002076	.000694	.000169	.000013
2_0-3_{-2}												
		0.1	.001595	.001142	.000756	.000466	.000268	.000144	.000070	.000029	.000009	.000001
		0.3	.002278	.001606	.001058	.000655	.000382	.000209	.000104	.000045	.000014	.000001
	B_z	0.5	.003982	.002708	.001764	.001102	.000662	.000379	.000202	.000094	.000032	.000004
		0.7	.015809	.008609	.005291	.003484	.002482	.002064	.003273	−.000845	−.000090	−.000005
		0.9	−.008025	−.007297	−.005291	−.002999	−.001418	−.000599	−.000231	−.000077	−.000019	−.000002

Reduced Stark coefficients for dipole-moment component along principal axis of largest moment of inertia.—*Continued.*

Level		$\alpha \backslash \kappa$	−0.9	−0.7	−0.5	−0.3	−0.1	+0.1	+0.3	+0.5	+0.7	+0.9
		0.1	.048733	.054466	.061728	.071225	.084175	.102881	.132275	.185185	.308642	.925926
		0.3	.016244	.018155	.020576	.023742	.028058	.034294	.044092	.061728	.102881	.308642
2_1-2_0	B_c	0.5	.009747	.010893	.012346	.014245	.016835	.020576	.026455	.037037	.061728	.185185
		0.7	.006962	.007781	.008818	.010175	.012025	.014697	.018896	.026455	.044092	.132275
		0.9	.005415	.006052	.006859	.007914	.009353	.011431	.014697	.020576	.034294	.102881
		0.1	−.002693	−.002163	−.001684	−.001260	−.000896	−.000593	−.000354	−.000177	−.000063	−.000007
		0.3	−.005305	−.004143	−.003145	−.002301	−.001604	−.001044	−.000613	−.000303	−.000106	−.000011
	A_c	0.5	−.175669	−.048888	−.023771	−.013249	−.007648	−.004334	−.002290	−.001044	−.000341	−.000035
		0.7	.005647	.004988	.004276	.003527	.002763	.002014	.001320	.000724	.000278	.000033
		0.9	.002779	.002373	.001962	.001556	.001170	.000817	.000512	.000269	.000099	.000011
2_1-3_{-2}												
		0.1	.000299	.000240	.000187	.000140	.000100	.000066	.000039	.000020	.000007	.000001
		0.3	.000590	.000460	.000349	.000256	.000178	.000116	.000068	.000034	.000012	.000001
	B_c	0.5	.019519	.005432	.002641	.001472	.000850	.000482	.000255	.000116	.000038	.000004
		0.7	−.000627	−.000554	−.000475	−.000392	−.000307	−.000224	−.000147	−.000081	−.000031	−.000004
		0.9	−.000309	−.000264	−.000218	−.000173	−.000130	−.000091	−.000057	−.000030	−.000011	−.000001
		0.1	−.003094	−.003301	−.003428	−.003415	−.003194	−.002718	−.002002	−.001169	−.000443	−.000048
		0.3	−.005750	−.005420	−.005093	−.004676	−.004091	−.003296	−.002324	−.001313	−.000478	−.000051
	A_c	0.5	−.040563	−.015134	−.009904	−.007413	−.005686	−.004186	−.002769	−.001496	−.000520	−.000056
		0.7	.008026	.018433	−.178707	−.017879	−.009319	−.005733	−.003426	−.001739	−.000570	−.000061
		0.9	.003652	.005855	.011139	.043408	−.025827	−.009095	−.004490	−.002076	−.000630	−.000067
2_2-3_{-1}												
		0.1	.000344	.000367	.000381	.000379	.000355	.000302	.000222	.000130	.000049	.000005
		03.	.000639	.000602	.000566	.000520	.000455	.000366	.000258	.000146	.000053	.000006
	B_c	0.5	.004507	.001681	.001100	.000824	.000632	.000465	.000308	.000166	.000058	.000006
		0.7	−.000892	−.002122	.019856	.001987	.001035	.000637	.000381	.000193	.000063	.000007
		0.9	−.000406	−.000651	−.001238	−.004823	.002870	.001011	.000499	.000231	.000070	.000008

Cyclotron Targets: Preparation and Radiochemical Separation. III.* Na^{22}**

JOHN W. IRVINE, JR.,
Department of Chemistry, Massachusetts Institute of Technology, Cambridge, Massachusetts

AND

E. T. CLARKE,
Department of Physics, Massachusetts Institute of Technology, Cambridge, Massachusetts

(Received March 15, 1948)

Two methods for separating Na^{22} from magnesium cyclotron targets are described. The first is a direct precipitation of $NaMg(UO_2)_3(C_2H_3O_2)_9\cdot 6H_2O$ or $NaZn(UO_2)_3(C_2H_3O_2)_9\cdot 6H_2O$ from an acetic acid solution of the target utilizing the normal sodium contamination of the magnesium for carrier. This is effective for as little as 1 mg Na in 5 g of Mg. If the sodium contamination is too small for precipitation, the bulk of the magnesium can be removed as $Mg(NH_4)_2(CO_3)_2\cdot 4H_2O$ which does not carry sodium. Deuteron excitation functions for $Mg^{26}(d,\alpha)Na^{24}$ and $Mg^{24}(d,\alpha)Na^{22}$ and thick target yields for the two sodium isotopes are given. The maximum values of the cross sections are $\sigma_{Na^{24}}=0.095\times10^{-24}$ cm² at 8.5 Mev and $\sigma_{Na^{22}}=0.16\times10^{-24}$ at 9.5 Mev. With 14-Mev deuterons the thick target yields are $Na^{24}=8.7rd/\mu ah$ and $Na^{22}=65mrd/\mu ah$.

THE radionuclide,[1] Na^{22}, can be prepared with high specific activity by the reaction $Mg^{24}(d,\alpha)$, $Ne^{21}(d,n)$, and $Ne^{22}(d,2n)$, and by $F^{19}(\alpha,n)$.[2] From a practical standpoint the first reaction is the most important and is the subject of this discussion. However, because metallic magnesium and most magnesium compounds contain inactive sodium contamination (0.1–0.01 percent), carrier-free Na^{22} is probably best prepared by deuteron bombardment of neon gas with collection of the active material on a charged wire.[3]

TARGETS

The most satisfactory target for outside beam bombardment is a thick, water-cooled magnesium block. Powdered magnesium, magnesium oxide, or magnesium carbonate spread on a grooved water-cooled copper plate are useful for short, low intensity bombardments.

A probe target can be prepared by powder metallurgy techniques. Layers of copper powder, equal parts copper and magnesium powder, and magnesium powder are compressed and sintered in pure hydrogen. The resulting target is about 2 mm thick and can be fastened to a probe with soft solder. These targets will not stand a beam current of more than $100\mu a/cm^2$ without excessive evaporation of the target surface with consequent loss of the Na^{22} activity.

After bombardment the targets should be allowed to age for about a week to allow the Na^{24} to decay, thus reducing the radiation hazard.

CHEMICAL TREATMENT OF TARGETS

The aged target is weighed and dissolved in 50 percent excess of glacial acetic acid. With the metal the reaction is slow in starting but becomes very vigorous as it proceeds. After the reaction subsides, the solution is diluted with an equal volume of 50 percent alcohol. The last traces of metal are dissolved after 15–30 minutes. If any insoluble residue remains, it is removed by filtration.

After the solution has cooled to room temperature 15 ml of a solution containing 0.01 of a mole of $UO_2(C_2H_3O_2)_2\cdot 2H_2O$ in $6M$ $H(C_2H_3O_2)$ (uranyl acetate dihydrate in $6M$ acetic acid) is added. The solutions are mixed thoroughly and divided between two 100-ml centrifuge tubes and placed in a refrigerator (~6°C) for 10–12 hours. The Na^{23} contamination provides suffi-

* Contribution from the Department of Chemistry, Department of Physics, and the Laboratory for Nuclear Science and Engineering, Massachusetts Institute of Technology. This paper is also number III in the series "Nuclear excitation functions."

** The work here reported was supported in part by the Office of Naval Research.

[1] T. P. Kohman, Am. J. Phys. **15**, 356 (1947).
[2] G. T. Seaborg, Rev. Mod. Phys. **16**, 1 (1944).
[3] J. G. Hamilton, private communication.

cient carrier for the formation of a precipitate of $NaMg(UO_2)_3(C_2H_3O_2)_9 \cdot 6H_2O$. The precipitate forms slowly.

Centrifugation and decantation give a good separation of the precipitate. The two portions of the precipitate are dissolved in 2 ml of warm 0.1*M* $H(C_2H_3O_2)$ and the solutions combined in a 50-ml centrifuge tube. After the addition of 15 ml of 95 percent alcohol, 15 ml of zinc uranyl acetate reagent solution[4] is added and the precipitate again allowed to form in a refrigerator. Three to four hours are sufficient for the second precipitation. After centrifugation and decantation the $NaZn(UO_2)_3(C_2H_3O_2)_9 \cdot 6H_2O$ is washed once with 5 ml of cold 95 percent alcohol containing 0.5 ml of the zinc uranyl acetate reagent, then washed once with 10 ml of ether, dried at 40°C in a current of air and weighed.

Zinc and uranium are removed by dissolving the precipitate in 20 ml of 0.1*M* $NH_4(C_2H_3O_2)$ solution and precipitating with an alcoholic solution of 8-hydroxyquinoline at a *p*H of 7–8. After removing the precipitate of mixed zinc and uranyl 8-hydroxyquinolates by centrifuging, the supernate is evaporated to dryness on a steam bath with NH_4OH to remove the excess 8-hydroxyquinoline. The $NH_4(C_2H_3O_2)$ is removed by repeated evaporations on a steam bath with concentrated HNO_3. The Na^{22} is finally obtained as a neutral solution of $NaNO_3$.

All waste solutions and precipitates should be monitored for Na^{22} by γ-ray measurements with a suitable counter. Over-all recovery of Na^{22} is approximately 95 percent from 5 g of Mg metal containing 1 mg of Na^{23}.

In an earlier experiment it was found that $Mg(NH_4)_2(CO_3)_2 \cdot 4H_2O$ did not carry sodium and could be used to remove the large excess of Mg^{++}. In this procedure the large bulk of precipitate necessitated repeated precipitations with a volume reduction at each step. A final chloride residue of unknown composition weighing 126 mg was obtained from 8 g of Mg metal. It contained 5.5 mg of sodium as determined by a $NaZn(UO_2)_3(C_2H_3O_2)_9 \cdot 6H_2O$ precipitation. Over-all recovery with this procedure was about 90 percent. This method of removal of large quantities of magnesium can be used where the Na^{23} concentration in the magnesium is too low to permit direct precipitation of the triple acetate and the addition of carrier is undesirable.

Rough measurements of the solubility of $NaZn(UO_2)_3(C_2H_3O_2)_9 \cdot 6H_2O$ in an excess of the precipitating reagent indicated a sodium concentration in the solution of approximately 0.1μg/ml. This extremely low solubility indicates the feasibility of precipitating quantities of Na as small as 0.1 mg. This corresponds to 6.6 mg of $NaZn(UO_2)_3(C_2H_3O_2)_9 \cdot 6H_2O$ which can be handled with ease.

DEUTERON EXCITATION FUNCTIONS—EXPERIMENTAL

Normal magnesium, composed of 77.4 percent Mg^{24}, 11.5 percent Mg^{25}, and 11.1 percent Mg^{26}, when bombarded with high energy deuterons will produce only two known radionuclides possessing half-lives longer than a few minutes. These two activities, both isotopes of sodium, are produced by emission of alpha-particles from the compound nuclei $(Mg^{24}+d)$ and $(Mg^{26}+d)$. The resulting Na^{22} and Na^{24} isotopes exhibit periods of 3.0 years and 14.8 hours, respectively, and emit radiations whose characteristics are known.[5]

Since rolled foils of magnesium metal, of the order of 5 mg/cm^2 thickness, are unobtainable, about 5 grams of high purity metal*** were evaporated in high vacuum from a molybdenum boat. The resulting layer of metal deposited on the inner wall of the enclosing bell jar was carefully peeled off, and from a section almost free from pinholes thirty disks $\frac{3}{4}''$ in diameter were punched. By keeping a record of the weights and relative positions of the disks on the original sheet it was possible to select and use only those disks originating in regions of low thickness gradient. Thus, even though individual thicknesses varied as much as 20 percent, the data could be corrected for these variations to reduce errors from this source to about 2 percent. The magnesium disks, because of their fragility, were sealed between layers of aluminum foil (0.00025″)

[4] F. J. Welcher, *Organic Analytical Reagents* (D. Van Nostrand Company, Inc., New York, 1947), Vol. II, p. 7.

[5] L. G. Elliott, M. Deutsch, and A. Roberts, Phys. Rev. **63**, 386 (1943); W. M. Good, D. Peaslee, and M. Deutsch, Phys. Rev. **69**, 313 (1946).

*** The high purity magnesium metal was obtained through the courtesy of Dow Chemical Company, Midland, Michigan.

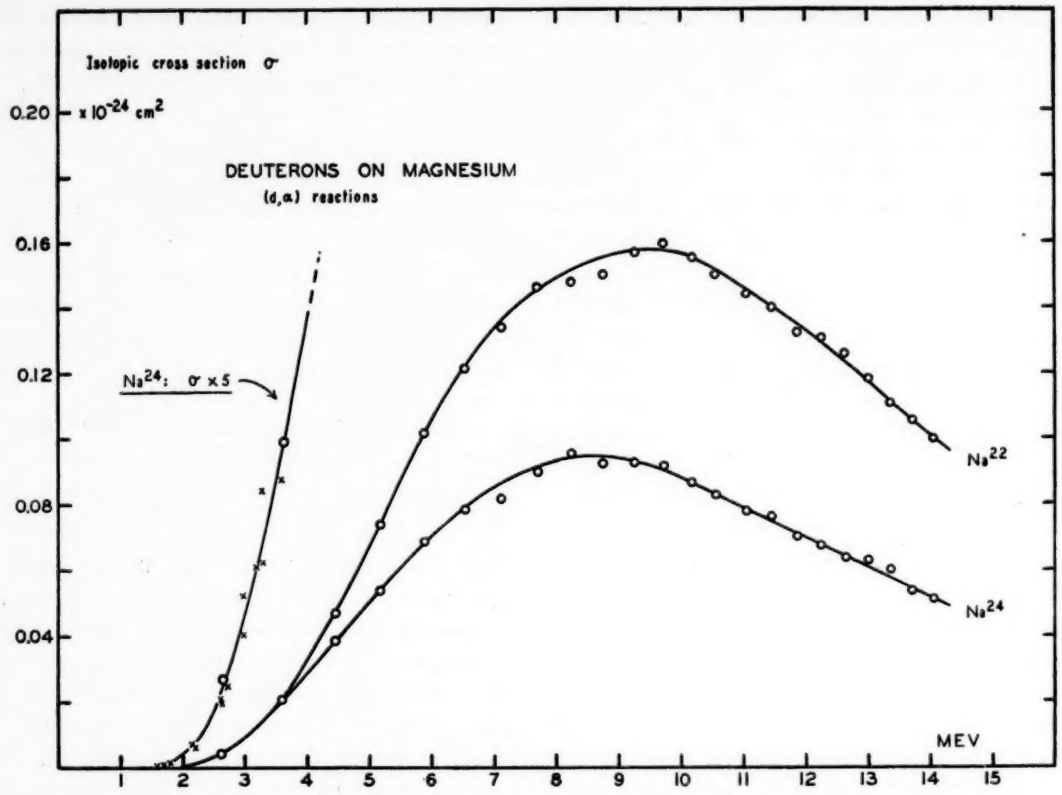

FIG. 1. Excitation functions of the reactions $Mg^{26}(d,\alpha)Na^{24}$ and $Mg^{24}(d,\alpha)Na^{22}$, in terms of the isotopic cross section σ. Circles represent present data; crosses are those reported by Henderson[10] for Na^{24}, ordinates arbitrarily fitted at 3.5 Mev.

and stacked, resulting in a series of 24 absorbers whose average individual thickness was 7.7 mg/cm² and whose total thickness, 185 mg/cm², was approximately equal to the distance of penetration of the 14-Mev deuterons used.

The stack of foils was bombarded for 1½ hours, 47.5-microampere minutes, with a deuteron beam whose initial energy was 14.20 Mev (range 184.5 mg/cm² Al), using the bombarding arrangement and beam energy measurement method already described.[6] Average deuteron energies traversing each foil were calculated, neglecting the difference in stopping power between Mg and Al (2 percent).

About 12 hours after the end of bombardment only the two activities Na^{24} (14.8 hours) and Na^{22} (3.0 years) remained in the magnesium samples. The intact foils were measured for gamma-radiation during the first few days after bombardment, then allowed to decay for a month, after which only the 3-year activity remained to be detected by its positron emission. Gamma-radiation from the Na^{22} was too weak to interfere with the measurement of the 14.8-hour activity.

Gamma-ray activities from the Na^{24} generated in the individual foils were measured on a calibrated platinum screen wall counter[7] shielded with $\frac{1}{16}$" lead, and compared with a 10-microgram radium standard to obtain the absolute disintegration rates. Decays of several foils were also followed for a few days as a check on the identity of the activity. The Na^{22} positrons in the foils were measured with a bell-type thin-window counter[8] after the shorter-lived component had died away. Absolute disintegration rates were obtained by calibration of the counter with a known quantity of Na^{22} made up into a

[6] E. T. Clarke and J. W. Irvine, Jr., Phys. Rev. 66, 231 (1944).

[7] A. Roberts, J. R. Downing, and M. Deutsch, Phys. Rev. 60, 544 (1941).

[8] W. M. Good, S. C. Brown, and A. F. Kip, Rev. Sci. Inst. 17, 262 (1946).

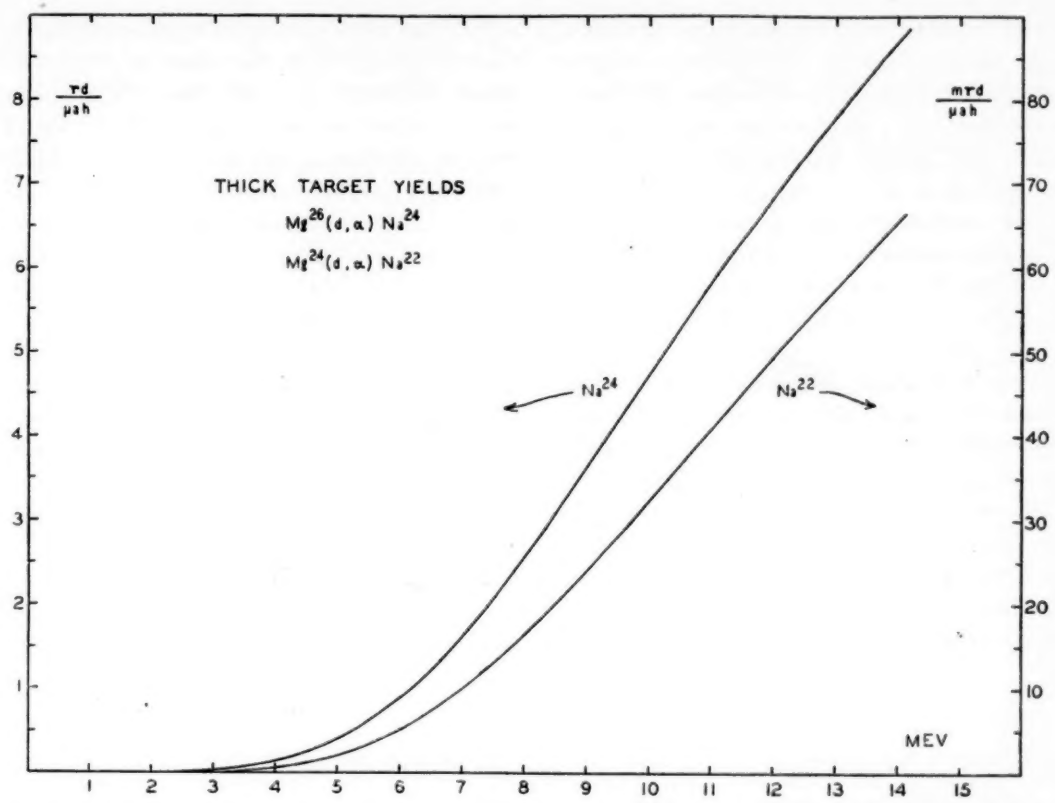

FIG. 2. Thick target yields for deuterons on magnesium metal. Ordinates for Na^{24} given in rutherfords per microampere hour bombardment, on the left; those for Na^{22} are in millirutherfords per microampere hour, plotted on the right.

sample having approximately the same geometrical characteristics as those of the foils. The Na^{22} standard, prepared by Dr. W. C. Peacock of the M.I.T. Radioactivity Center, had been calibrated by coincidence methods. The results of these measurements, corrected for decay since bombardment, were plotted as a function of the average deuteron energy traversing each foil.

DEUTERON EXCITATION FUNCTIONS—RESULTS

The results of these measurements, when plotted against deuteron energy, showed that while the Na^{22} excitation function exhibited the familiar rise and fall of cross section with increasing bombardment energy, the Na^{24} function was anomalous in that, after beginning to decrease in cross section, it suddenly rose again above energies of about 11 Mev. Investigation of the cause of this anomaly disclosed that the added activity was contributed by the aluminum foil enclosing the magnesium. A stacked foil experiment using aluminum alone was therefore carried out, the results of which have already been reported,[9] and the effects of this source of Na^{24} activity subtracted from the observed curve obtained from the magnesium foil bombardment. The final isotopic cross sections for the reactions $Mg^{26}(d,\alpha)Na^{24}$ and $Mg^{24}(d,\alpha)Na^{22}$ were then calculated by means of Eq. (4) in reference 6 and plotted in Fig. 1.

An excitation function for the reaction $Mg^{26}(d,\alpha)Na^{24}$ extending to 3.5 Mev has been reported by Henderson.[10] His data, with the topmost point arbitrarily fitted to the present curve (resulting in a cross section within 25 percent of his rough estimate) are included in Fig. 1. The agreement checks the energy scale calculated for the present results, since errors in the range-energy relationship of deuterons in magnesium would be greatly magnified at the low energy end of the curve.

[9] E. T. Clarke, Phys. Rev. **71**, 187 (1947).
[10] M. C. Henderson, Phys. Rev. **48**, 855 (1935).

The two excitation functions have the characteristic shape observed in deuteron-induced reactions in the lighter elements when bombardments are made at energies considerably above threshold. The initial, low energy ends of the curves are limited by the penetrability both of the target nucleus by the deuteron, and the barrier of the compound nucleus by the emergent particle. Since the two curves are almost coincident at very low energies, the deuteron penetrability is probably the governing factor in this region, particularly since this is independent of the particular target isotope involved. Though the magnitudes of the cross sections at higher energies are governed mainly by competition for decay of the compound nucleus ($Mg+d$), the energies at which the maxima occur may be expected to bear the same relation to each other as the thresholds of the reactions. Thus the excitation of $Mg^{26}(d,\alpha)Na^{24}$ with a threshold of -2.7 Mev rises to a maximum cross section at a lower energy than does that of $Mg^{24}(d,\alpha)Na^{24}$ whose threshold is -1.1 Mev. Not enough is yet known about the factors entering into competitive disintegration of compound nuclei to yield an explanation for the magnitudes of the cross sections, which differ by a factor of two and which are about an order of magnitude less than those for the (d,p) reactions in this region of the periodic table.

By integration of the excitation functions, using Eq. (5) in reference 6 thick target yield curves (total activity per microampere hour of bombardment as a function of deuteron energy) were calculated and are given in Fig. 2. Yields are given in rutherfords ($1\ rd=10^6$ disintegrations per second) per microampere hour, following the recommendations of Curtiss and Condon.[11]

[11] E. U. Condon and L. F. Curtiss, Phys. Rev. 69, 672 (1946).

THE JOURNAL OF CHEMICAL PHYSICS VOLUME 16, NUMBER 7 JULY, 1948

Some Characteristic Frequencies in the Raman Spectra of Saturated Aliphatic Hydrocarbons*

N. SHEPPARD
School of Chemistry and Physics, The Pennsylvania State College, State College, Pennsylvania
(Received March 29, 1948)

An analysis of the data presented in a recent compilation of Raman spectra of saturated hydrocarbons has been carried through with a view to the determination and assignment of vibration frequencies that are characteristic of particular molecular groups.

Suggested approximate assignments have been made for the rocking and wagging modes of CH_2 groups (720–760 cm^{-1} and 1300–1340 cm^{-1}, respectively) and for the deformation modes of CH groups (1330–1360 cm^{-1}) in such hydrocarbon molecules.

Assignments previously made for the analysis of the Raman spectra of isobutane (trimethyl methane) and neopentane (tetramethyl methane) have been reviewed, and the results applied to the interpretation of observed characteristic frequencies of singly and double branched paraffins. Single branching of the hydrocarbons gives rise to characteristic frequencies in the regions 1180–1140 cm^{-1} and 830–790 cm^{-1}, whereas double branching gives similar frequencies in the regions 1260–1190 cm^{-1} and 760–710 cm^{-1}. These can probably be assigned to C—C stretching modes of vibration of the molecules. Other characteristic frequencies in the regions 970–950 cm^{-1} and 930–910 cm^{-1} occur in the spectra of single and doubly branched hydrocarbons, respectively, when these have at least two methyl groups attached to the branching carbon atom. They are probably caused by methyl wagging modes of these groups.

INTRODUCTION

THE interpretation of the vibrational spectra of hydrocarbon molecules is a matter of fundamental importance in the application of this branch of spectroscopy to the structural problems of organic chemistry. However, some of the methods which are available for the interpretation of the infra-red and Raman spectra of the first few symmetrical molecules in the hydrocarbon series, e.g., the use of selection rules

* This research was carried out on Contract N6onr-269, Task V, of the Office of Naval Research.

or the band contours in infra-red spectra of gaseous hydrocarbons, have considerably less power in deciding questions of frequency assignment when applied to the spectra of larger molecules. Any means of replacing or supplementing these methods are obviously of great value. The work of Kohlrausch[1] and his coworkers has amply demonstrated the value of examining the spectra of series of related molecules with a view to the determination and assignment of frequencies characteristic of different structural groups. This method has already been applied to the interpretation of the infra-red spectra of hydrocarbons.[2] In the present communication the same method will be applied to the analysis of a recent compilation of the Raman spectra of saturated hydrocarbons obtained in these laboratories under the direction of Dr. Fenske and Dr. Rank. The spectra and experimental details have recently been published elsewhere.[3,4]

We follow the method of classification adopted by Sutherland and Simpson,[2] and arrange the spectra under the following headings:

(1) Straight chain hydrocarbons.

(2) Singly branched hydrocarbons of the 2-methyl type—i.e., having the common structural grouping $CH_3—\underset{\displaystyle CH_3}{\overset{\displaystyle |}{CH}}—R$, where R is an alkyl group, C_nH_{2n+1}, with $n>1$.

(3) Singly branched hydrocarbons of the 3-methyl type: $CH_3—\underset{\displaystyle R}{\overset{\displaystyle |}{CH}}—R'$.

(4) Other singly branched hydrocarbons:

$$R—\underset{\displaystyle R''}{\overset{\displaystyle |}{CH}}—R'.$$

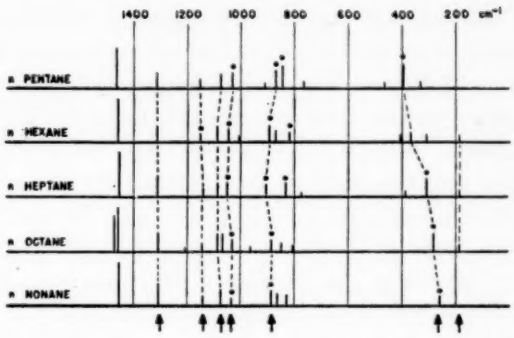

FIG. 1. The Raman spectra and observed characteristic frequencies in long chain paraffins.

(5) Doubly branched hydrocarbons of the 22-dimethyl type: CH_3, CH_3, C, CH_3, R.

(6) Doubly branched hydrocarbons of the 33- and 44-dimethyl types: CH_3, R, C, CH_3, R', and other doubly branched hydrocarbons.

The collected spectra below 1500 cm^{-1} are shown in Figs. 1 to 6. Highly polarized lines in the spectra ($\rho<0.5$) are indicated by o.

Most of the data have been taken from the tables of frequencies published in the compilation of Raman spectra,[3] but in several cases extra qualitative data on the polarization of weak lines have been obtained by examination

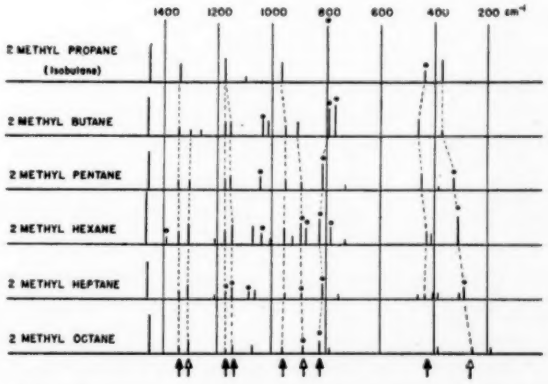

FIG. 2. The Raman spectra and observed characteristic frequencies in singly branched paraffins of the 2-methyl type.

[1] K. W. F. Kohlrausch, "Ramanspektren," *Hand und Jahrbuch der Chemischen Physik* (Leipzig, 1943).

[2] G. B. B. M. Sutherland and D. M. Simpson, J. Chem. Phys. **15**, 153 (1947); also the joint report by the Oxford and Cambridge infra-red laboratories, Institute of Petroleum Report XI (February, 1946).

[3] M. R. Fenske, W. G. Braun, R. V. Wiegand, D. Quiggle, R. H. McCormick, and D. H. Rank, Ind. Eng. Chem. Anal. **19**, 700 (1947).

[4] D. H. Rank, Ind. Eng. Chem. Anal. **19**, 766 (1947).

of the original curves.[5] The spectra of the simplest branched hydrocarbons, isobutane and neopentane, are shown in Figs. 2 and 5 with the spectra of the 2-methyl and 22-dimethyl hydrocarbons, respectively. They have been taken from another source[6] and are not on the same uniform intensity scale as the rest of the spectra. Lines marked *X* in the diagrams are of greater intensity than our diagrams can show and reference must be made to the original paper for the precise values of these. In Figs. 2 to 6 the characteristic frequencies of the branched hydrocarbons are indicated at the bottom by black-headed arrows; the white arrows indicate frequencies which are probably caused by the straight chain parts of the molecules.

The characteristic frequencies that have been picked out from the spectra obey one or the other of the following criteria: (i) they remain relatively invariant in position on passing from one spectrum to the next (the first members of a series may deviate to a small extent from the rest), or (ii) they have a considerable degree of polarization and exhibit gradual changes in position in passing from one molecule to the next.

DISCUSSION OF THE SPECTRA

1. The Straight Chain Hydrocarbons

The Raman spectra of a similar series of straight chain hydrocarbons have been examined by Kohlrausch and Köppl[7] (see also reference 1, p. 206) and these spectra are in good agreement with the earlier work. To a first approximation the spectrum of a long chain hydrocarbon <1500 cm^{-1} can be regarded as comprised of frequencies caused by deformation vibrations of the CH_2 groups, and other series caused by the valence and deformation modes of the zig-zag carbon chain. As has been shown by the calculations of several authors (see later discussions), the stretching and bending modes of the carbon chains probably lie in the regions 1200–800 cm^{-1} and <500 cm^{-1}, respectively. Several of the characteristic frequencies in these regions, e.g., those at *ca.* 1140, 1080, 1040, 890, and 190 cm^{-1}, can probably be attributed to these vibrations. Other frequencies in these regions which show greater variations in position from molecule to molecule, e.g., the Raman lines between 200 and 400 cm^{-1}, can probably also be assigned to such modes. Kohlrausch and Köppl assigned the frequencies below 1100 cm^{-1} to the carbon skeletal vibrations and those above this figure to the deformation modes of the CH_2 groups. It will be shown later that such a rigid subdivision of frequency types is not strictly correct, but it is probably a fair approximation to the truth as far as the Raman spectra of the long chain molecules are concerned. At the present time, agreement between experiment and theory is not sufficiently good to give specific assignments to any of the Raman lines in the skeletal regions in the case of these large molecules.

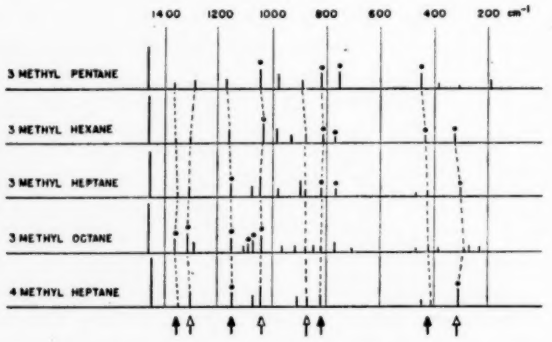

FIG. 3. The Raman spectra and observed characteristic frequencies in singly branched paraffins of the 3-methyl type.

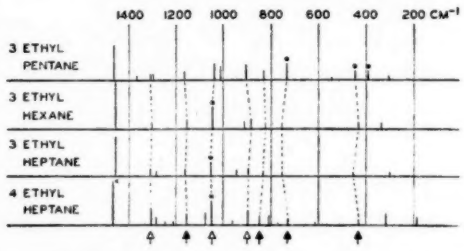

FIG. 4. The Raman spectra and observed characteristic frequencies in singly branched paraffins of the 3-ethyl and 4-ethyl types.

The assignment of the deformation modes of vibration of CH_2 groups in hydrocarbon mole-

[5] Report on the Raman Spectra of Hydrocarbons, Petroleum Refining Laboratory, School of Chemistry and Physics, The Pennsylvania State College (May, 1947).

[6] K. S. Pitzer and J. E. Kilpatrick, Chem. Rev. **39**, 435 (1946).

[7] K. W. F. Kohlrausch and F. Köppl, Zeits. f. physik. Chemie **B26**, 209 (1934).

cules has not previously been discussed systematically. An isolated CH_2 group attached to a heavy framework would have four deformation modes of vibration which we designate as shown in Fig. 7. This figure shows the relative amplitudes of the hydrogen atoms only. We have changed slightly the original nomenclature of Linnett[8] so that the description "deformation" can be applied to the whole group of vibrations.

It has been well established that the bending mode of CH_2 groups in paraffins gives a very characteristic frequency in the region[9] 1440–1470 cm^{-1}, and it seemed worth while to see whether any of the other vibrations could be similarly characterized.

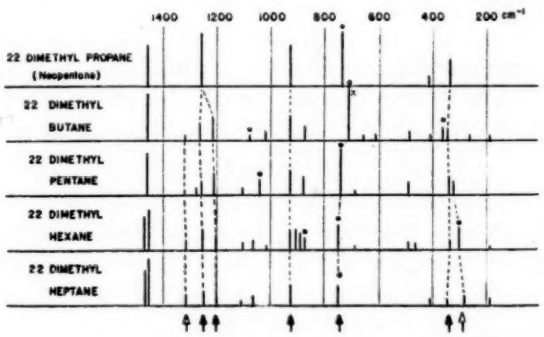

FIG. 5. The Raman spectra and observed characteristic frequencies in doubly branched paraffins of the 22-dimethyl types.

There is one prominent line in the Raman spectra of the long chain hydrocarbons which is well beyond the highest limit for skeletal vibrations and which can safely be assigned to a hydrogen deformation mode—that lying in the region 1300–1310 cm^{-1}. Furthermore, this line remains prominent in the largest molecules studied and can therefore be assigned as a CH_2 (and not CH_3) vibration. This line persists in butane but not in propane, although in the spectrum of the latter hydrocarbon (which appears to have been reliably assigned by Pitzer[10]) a Raman line appears at 1278 cm^{-1} and an infra-red band at 1338 cm^{-1}. The 1278-cm^{-1} line has been assigned to the CH_2 twisting mode in propane, and the band at 1338-cm^{-1} to the wagging mode. It is clear that the 1300- to 1310-cm^{-1} characteristic frequency of the normal paraffins can be assigned to the one or the other of these vibrations of the CH_2 group. We suggest assigning it to the wagging mode on the grounds that this frequency in normal pentane and several other straight chain hydrocarbons shows appreciable polarization[3] and that in general the more symmetrical vibration (i.e., the vibration symmetrical with respect to the C_3 plane of neighboring carbon atoms) is likely to be stronger in the Raman scattering. The twisting mode cannot be identified with certainty in the Raman spectra of the long chain hydrocarbons, although the propane case suggests that it will be a fairly high frequency—say between the limits 1100–1350 cm^{-1}.

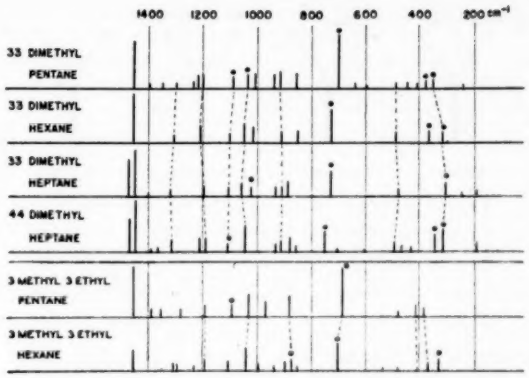

FIG. 6. The Raman spectra and observed characteristic frequencies in doubly branched paraffins of the 33-dimethyl, 44-dimethyl, and 3-methyl, 3-ethyl types.

The rocking mode of vibration of the CH_2 groups cannot be identified in the Raman spectra either, but it has been shown recently[11] that a characteristic absorption near 720 cm^{-1} in the infra-red spectra of straight chain paraffins can be identified as a CH_2 deformation vibration. This fact was established by the observation that the absorption had moved by a factor of $1/\sqrt{2}$ in the spectrum of a deuterated paraffin compared to its hydrogen analog. It appears that this frequency must be the remaining rocking mode of the CH_2 groups, and this is confirmed by the contour of the infra-red band at 748 cm^{-1} in propane,[12] which is of such a form that the

[8] J. W. Linnett, J. Chem. Phys. 6, 692 (1938).
[9] See, for example, G. Herzberg's *Infra-red and Raman Spectra of Polyatomic Molecules* (D. Van Nostrand Company, Inc., New York, 1945), p. 195.
[10] K. S. Pitzer, J. Chem. Phys. 12, 310 (1944).
[11] N. Sheppard and G. B. B. M. Sutherland, Nature 159, 739 (1947).
[12] V. L. Wu and E. F. Barker, J. Chem. Phys. 9, 487 (1941).

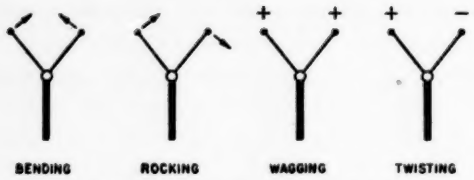

FIG. 7. Schematic diagram of the deformation modes of the CH_2 group.

vibration involved must be perpendicular to the plane of the C_3 triangle. Vallance-Jones and Sutherland[13] have also shown by the use of polarized infra-red radiation on an orientated Polythene (polyethylene) sample that the change in electric moment occurring during this vibration at 720 cm^{-1} is perpendicular to the carbon chain—again in agreement with the assignment of this absorption to the CH_2 rocking mode. It should be noted that the value of 720 cm^{-1} for the infra-red absorption applies to long chain hydrocarbons only ($n \geqslant 5$), and that the first few members of the series, e.g., propane, have higher frequencies than this. However, the region 720–760 cm^{-1} would appear to be a reasonable range within which we can expect the occurrence of the CH_2 rocking modes.

From the study of these characteristic frequencies we can conclude that the CH_2 deformation frequencies lie in the ranges 1440–1470 cm^{-1} (bending), 1300–1340 cm^{-1} (wagging), 720–760 cm^{-1} (rocking). From the assignment of propane it seems likely that the twisting frequency will also have a fairly high value (1100–1350 cm^{-1}). For CH_2 groups in long chain molecules the lower values in the ranges given should be taken for the wagging and rocking modes. It should be noted that these correlations apply strictly only to CH_2 groups in paraffins, but it is probable that they do not differ greatly in other non-cyclic hydrocarbon molecules in which the CH_2 group is in a saturated part of the molecule. Greater disagreement with the above assignments must be expected in molecules with skeletal atoms other than carbon, e.g., the alkyl halides, etc. In the case of both the 1300–1310-cm^{-1} Raman line and the 720-cm^{-1} infra-red absorption, the intensity increases in rough proportion to the relative number of CH_2 groups in the molecule.

[13] A. Vallance-Jones and G. B. B. M. Sutherland, Nature **160**, 567 (1947).

2. The Branched Chain Hydrocarbons

As a preliminary to the discussion of the characteristic frequencies that are found in the Raman spectra of the various types of branched hydrocarbons, we shall review the assignments of the symmetrical molecules isobutane (trimethyl methane) and neopentane (tetramethyl methane). These have recently been considered by Pitzer and Kilpatrick.[6]

In the case of neopentane there are (below 1450 cm^{-1}) Raman lines at 1252 (20,*dp*), 925 (15,*dp*), 733 (20,*p*), 414 (3,*dp*) and 335 cm^{-1} (10,*dp*)—the polarizations have been added from our own unpublished data on the spectrum. There can be little doubt about the assignment of the 733-cm^{-1} line to the "breathing" frequency of the C_5 tetrahedron. The 414- and 335-cm^{-1} lines are also clearly the bending skeletal modes. Further, the remaining lines at 925 cm^{-1} and 1252 cm^{-1} must be triply degenerate modes because of their appearance in the infra-red spectrum. Pitzer and Kilpatrick assign the 925- and 1252-cm^{-1} lines specifically to the methyl wagging and asymmetrical C—C stretching vibrations. This, perhaps, is the most likely assignment as several normal coordinate treatments of the molecule are in agreement with this interpretation (see later).

The assignment of the Raman lines of isobutane can also be made with fair confidence[6] except for the two at 965 and 1172 cm^{-1}. Both of these are depolarized and, hence, correspond to doubly degenerate vibrations. There are three possible modes of vibration which could be used to assign these lines, *viz.*, two methyl wagging modes and an asymmetrical C—C stretching vibration. Pitzer and Kilpatrick assign the two Raman lines to the two methyl wagging vibrations whereas Sutherland and Simpson[2] suggest that the 1172-cm^{-1} line (which occurs also in the infra-red) should be assigned to the C—C stretching mode. This would seem to be more consistent with the assumption that the 1252-cm^{-1} line in neopentane corresponds to the C—C vibration, and so we favor a slight modification of Pitzer and Kilpatrick's assignment, *viz.*, 1172 (C—C vibration), 965 (methyl wag), and 925 cm^{-1} (methyl wag). This latter frequency occurs in the infra-red spectrum. It will be noticed

that this merely represents a change of the assignments within a given symmetry class and thus can invalidate no selection rule or band contour data, nor make any difference to the thermodynamic functions deduced from these data.

Having clarified the position with respect to the smaller molecules in the series we are now in a position to discuss the characteristic frequencies observed in the more complex molecules.

A. The Singly Branched Paraffins

These all have a common feature with isobutane, *viz.*, a 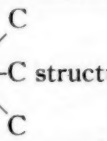 structural unit, and most of the characteristic frequencies can be identified immediately by analogy with the isobutane assignment, as shown in Table I. The value in brackets beside each isobutane frequency gives the degeneracy of the vibration, and the *underlined* frequencies have been reported also in the infra-red spectra.[2,**] The quoted average figures for the substituted paraffins can be taken as correct within the limits ± 20 cm^{-1}, and in the majority of cases with considerably greater precision as can be seen by examination of the appropriate figures.

The assignments appear to be very satisfactory and are in most cases self-explanatory. In the case of the 2-methyl and 3-methyl compounds the C—C stretching frequency near 800 cm^{-1} can usually be picked out by its strength and polarization characteristics. However, in several cases there are other polarized lines in the vicinity which might be possible alternative assignments, and this is particularly true of the 3-ethyl compounds where two frequencies at 750 and 830 cm^{-1} are listed. It is probable that these extra lines are due to essentially the same vibrations of the other rotational isomers that are present in the liquid (see reference 1, p. 234 *et seq.*, for a discussion of this phenomenon in similar flexible molecules). It should be noted that of the three lines which persist throughout the whole series of spectra of the singly branched hydrocarbons, two almost certainly correspond to skeletal vibrations (at *ca.* 430 and 830 cm^{-1}) and it is hence probable that the third one near 1160 cm^{-1} can be similarly assigned, i.e., to a C—C stretching mode. This is independent evidence in favor of our earlier assignment for the 1172-cm^{-1} mode of isobutane to such a vibration.

TABLE I. Observed characteristic frequencies of singly branched paraffins.

Assignment	Isobutane	2-methyl compounds	3-methyl compounds	3-ethyl compounds
C—C deformation	371 (2)	—	—	—
C—C deformation	*437* (1)	430	425	440
C—C stretching	*795* (1)	820	820	750 830
Methyl wagging	965 (2)	950	—	—
C—C stretching	*1172* (2)	*1150* *1175*	*1160* (see reference**)	*1160* (see reference**)
C—H deformation	*1339* (2)	1345	1355	—

It is clear that the frequency near 1350 cm^{-1} in these branched paraffins is to be assigned to the bending mode of the lone CH group in all these hydrocarbons. Its non-appearance in the case of some of the 3-ethyl compounds is probably due to weakness caused by the smaller proportion of such groups in these molecules. In the case of the 2-methyl hydrocarbons the C—C stretching frequency near 1160 cm^{-1} splits into two components at *ca.* 1150 and 1175 cm^{-1}. As pointed out by Sutherland and Simpson[2] in their discussion of the infra-red spectra, this is to be explained as caused by the decrease in symmetry of these molecules compared with isobutane. The fact that other doubly degenerate modes of isobutane do not appear to split in a similar fashion in the spectra of the less symmetrical paraffins is probably due to either the small magnitude of the splitting, or to weakness of some of the components.

The frequencies at 965 and 950 cm^{-1} in the respective spectra of isobutane and the 2-methyl compounds are probably caused by a methyl wagging mode. Such an assignment would appear to correlate well with their apparent disappearance when there are less than two methyl groups attached to the branching carbon atom. They probably correspond to modes of vibration in which the "wagging" motions of the several methyl groups are coupled together. In the case of the 3-methyl and 3-ethyl hydrocarbons two extra frequencies appear in the regions 1050–

** The author is indebted to Dr. D. M. Simpson for unpublished data on the infra-red spectra of certain of these hydrocarbons, Institute of Petroleum Report XI, reference 2.

TABLE II. Observed characteristic frequencies of doubly branched paraffins.

Assignment	Neopentane	22-dimethyl compounds	33-dimethyl compounds	3-methyl 3-ethyl compounds
C—C bending	335 (2)	340	—	—
C—C bending	414 (3)	—	—	375 410
C—C stretching	733 (1)	750	725	690
Methyl wagging	*925* (3)	*930* (see reference**)	*910* (see reference**)	—
C—C stretching	*1252* (3)	*1210* *1250*	*1200* (see reference**)	*1190*

TABLE III. Comparison of some observed and calculated skeletal frequencies of branched paraffins.

Type of compound	Observed frequency	Calculated (1)	Calculated (2)
2-methyl	820 cm^{-1}	0.791ν	835 cm^{-1}
3-methyl	820 cm^{-1}	0.780ν	825 cm^{-1}
3-ethyl	830 cm^{-1}	0.774ν	816 cm^{-1}
22-dimethyl	750 cm^{-1}	0.693ν	731 cm^{-1}
33-dimethyl	725 cm^{-1}	0.688ν	727 cm^{-1}

1040 cm^{-1} and 900–870 cm^{-1} which do not fit in with the assignment scheme of Table I. However, both these types of hydrocarbons have the ethyl group as a common structural feature, and it is probable that these lines are to be ascribed to vibrations of this group.

B. The Doubly Branched Paraffins

These hydrocarbons have a common structural feature with neopentane—a 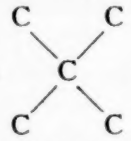 group—and once again many of the characteristic frequencies can be assigned with the help of the spectrum of the smaller molecule, as shown in Table II.

In all of these compounds the "breathing" frequency of the C_5 unit near 730 cm^{-1} is very easily picked out on account of its great strength and high degree of polarization, and the other C—C stretching modes in the region 1250–1190 cm^{-1} again carry right through the spectra of the whole series of doubly branched molecules. The identification of the C—C stretching frequency near 730 cm^{-1} is unambiguous for all these molecules in contrast to the behavior of the corresponding frequency near 800 cm^{-1} in the singly branched hydrocarbons. This is in agreement with the fact that the 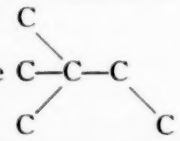 "unit" probably has only one stable rotational configuration (cf., Kohlrausch's discussion of neopentyl chloride on page 236 of his book[1]). The methyl wagging frequency in the region 930–910 cm^{-1} again becomes uncertain when there are less than two methyl groups attached to the central carbon atom, and at the same time new frequencies appear near 1030 and 880 cm^{-1} in the 3-methyl, 3-ethyl hydrocarbons which can probably be attributed to ethyl groups in these molecules. The assignment of the 480-cm^{-1} frequency of the 33 dimethyl compounds is less certain, although it is almost certainly a bending frequency of the carbon skeleton.

The strength of the highly polarized symmetrical C—C stretching frequencies in the region 850–650 cm^{-1}, and the variation of their positions with the type of branching present in the hydrocarbons makes them very suitable for the determination of molecular structure. By a more detailed study of the data presented in the original compilation of spectra[3] it is possible to characterize complex groupings such as 223-, 224-, 233-trimethyl derivatives, etc., with the help of these frequencies.

COMPARISON OF SOME OF THE ASSIGNED C—C FREQUENCIES WITH THE RESULTS OF THEORETICAL CALCULATIONS

Several attempts have been made to calculate the skeletal frequencies of hydrocarbon molecules, but in no case with convincing over-all agreement with experiment. However, some success has been achieved and it is interesting to compare out conclusions on the assignment of such frequencies with the results of the theoretical work.

The earliest attempts were made to calculate the stretching frequencies of zig-zag chains while assuming that no angle changes took place.[14] This showed that these vibrations could be expected between 1200 and 800 cm^{-1} and it was on the basis of these calculations that Kohl-

[14] E. Bartholomé and E. Teller, Zeits. f. physik. Chemie **B19**, 366 (1932).

rausch and Köppl made their suggested subdivision of the observed long chain hydrocarbon frequencies into skeletal and hydrogen deformation types. Although it has since been shown that several hydrogen deformation modes occur below 1200 cm^{-1}, more exact calculations[15–17] still agree on the approximate range of the skeletal stretching modes. Mecke[18] studied the problem of the skeletal frequencies of the branched chain hydrocarbons and showed that these gave calculated frequencies below 800 cm^{-1} which could be correlated with observed Raman frequencies. Recently Stepanov[19] has considerably extended this work and has given calculated values for the lowest skeletal stretching modes of many branched hydrocarbons as multiples of a frequency (ν), which characterizes a single C—C bond. In Table III Stepanov's predictions for 2-methyl, 3-methyl, 3-ethyl, 22-dimethyl, and 33-dimethyl hydrocarbons are given alongside the observed symmetrical C—C stretching frequencies. The observed frequencies are given in the second column, Stepanov's values in terms of ν in the third column, and the calculated values on the assumption of a ν value of 1055 cm^{-1} in the last column.

The agreement is good considering the approximations involved in the calculations. Similar calculations have also been made by Kellner.[20] However, although good agreement has been obtained for these low frequencies, this method of calculation gives little agreement of higher frequencies with the observed spectra. In particular these methods give a calculated value in the region of 1100 cm^{-1} for the asymmetrical triply degenerate C—C stretching mode of neopentane—almost exactly half way between the observed lines at 1252 and 925 cm^{-1}.

However, as already mentioned, calculations by Sutherland and Simpson[2] show that the corresponding vibrations of 2-methyl and 22-dimethyl compounds can be explained as C—C vibrations with a reasonable value for the force constant. In addition, more detailed calculations on the neopentane molecule by Wall and Eddy,[21] and by Silver,[22] agree in assigning the 1252-cm^{-1} line of this compound to the asymmetrical C—C stretching vibration. Also, recent calculations of the chain frequencies of a series of hydrocarbons by Ahonen,[16] in which both valence bond and angle deformations are taken into account, have shown that branched chain molecules may have frequencies up to 1350 cm^{-1} as well as down to 650 cm^{-1}, although the earlier more approximate calculations gave 1200 cm^{-1} as the upper limit of skeletal frequencies in these types of molecules.

In the light of these calculations then we can conclude that our assignments of both the low and high C—C frequencies in the branched chain hydrocarbons are in agreement with theoretical expectations.

The author would like to thank Dr. D. H. Rank, Dr. D. M. Simpson, and Dr. G. B. B. M. Sutherland for much helpful discussion and criticism.

[15] E. Bauermeister and W. Weizel, Physik. Zeits. **37**, 169 (1936).
[16] C. O. Ahonen, J. Chem. Phys. **14**, 625 (1946).
[17] J. Barriol and J. Chapelle, J. de phys. et rad. (viii) **8**, 8 (1947).
[18] R. Mecke, Zeits. f. physik. Chemie **B36**, 347 (1937).
[19] B. Stepanov, J. Phys. Chem. (U.S.S.R.) **14**, 474 (1940).
[20] L. Kellner, Trans. Faraday Soc. **41**, 217 (1945).
[21] F. T. Wall and C. R. Eddy, J. Chem. Phys. **6**, 107 (1938).
[22] S. Silver, J. Chem. Phys. **8**, 919 (1940).

Fine Structure of Raman Lines Due to Chlorine Isotopes*

D. H. RANK, N. SHEPPARD, AND G. J. SZASZ
Department of Physics, The Pennsylvania State College, State College, Pennsylvania
(Received March 29, 1948)

In continuation of previous work the isotopic fine structures of polarized lines in the Raman spectra of trichloroethylene, tetrachloroethylene, 1,2-dichloroethane, methyl chloroform, 1,1,2-trichloroethane, and 1,1,2,2-tetrachloroethane have been studied. Observed and computed contours are compared. In the majority of cases the results are according to theoretical expectations based on the number of chlorine atoms in the molecule, and the relative abundance of the two isotopes. The fine structure pattern obtained for the "*trans*" form of 1,1,2,2-tetrachloroethane is anomalous. It is possible that this anomaly is caused by weak mechanical coupling between the motions of the two $-CCl_2$ groups in this molecule, or by the presence of a weak combination band that distorts the contour. Experimental methods of checking these explanations are discussed.

I. INTRODUCTION

IN a previous paper by one of us[1] which appeared several years ago, methods were described which produced Raman spectra under high resolution. The isotopic fine structure of two molecules (CCl_4 and $CHCl_3$) was investigated in the above-mentioned work. The results obtained agreed with theoretical expectations. The chlorine atoms in CCl_4 and $CHCl_3$ are all attached to the same carbon atom. It seemed desirable to investigate some simple molecules having the chlorine atoms attached to different carbons.

H. D. Rix,[2] in collaboration with one of us, obtained some photographs of symmetrical tetrachloroethane under high resolution. These photographs showed an anomalous intensity distribution in the isotopic fine structure pattern of the $\nu = 353\text{-cm}^{-1}$ line of the above-mentioned molecule. This anomaly suggested further more extensive investigation of isotopic fine structures. Symmetrical tetrachloroethane is particularly interesting because of the fact that Langseth and Bernstein[3] have shown it to consist of two rotational isomers.

Unfortunately, the Raman spectra of most molecules are somewhat weaker than those of $CHCl_3$ and CCl_4. The weakness of the spectrum of symmetrical tetrachloroethane and other molecules of this type presented some experimental difficulties because of the appearance of grating ghosts which tended to mask the fine structure when sufficiently strong exposures were made. It was found that the grating ghosts would have to be eliminated if satisfactory photographs of these spectra were to be obtained.

II. EXPERIMENTAL

Spectrograph

The grating spectrograph was essentially the same as that used by Rank and Van Horn.[1] The grating and collimating mirror were identical with those used before, while a 16-foot focal length objective mirror and shorter focus cylindrical lens were substituted for the 30-foot mirror and cylindrical lens used previously. The fine structure of the 992-cm^{-1} frequency shift of benzene could be photographed with a one-hour exposure when excited by λ4358A, using the second order of the grating (dispersion 1.7A/mm).

Dispersion Filter

The elimination of overlapping orders with a diffraction grating is a very old problem which first received attention in Fraunhofer's time. Wadsworth[4] in a paper entitled, "A simple device for completely isolating or cutting out any desired portion of the diffraction spectrum" has

* This research was carried out on Contract N6onr-269, Task V, of the Office of Naval Research.
[1] D. H. Rank and J. A. Van Horn, J. Opt. Soc. Am. **36**, 454 (1946).
[2] H. D. Rix, M.S. Thesis, Pennsylvania State College (1947).
[3] A. Langseth and H. J. Bernstein, J. Chem. Phys. **8**, 410 (1940).
[4] F. L. O. Wadsworth, Astrophys. J. **3**, 169 (1896).

given the general principles on which such a dispersion filter must operate. Schematically the device described by Wadsworth is practically identical with the arrangement described below. Wadsworth's instrument, however, will not be sharp cutting since the prisms are operating in convergent light which introduces large aberrations due to oblique incidence. The construction of "prism filters" of this general type has also been discussed by Lehmann.[5] The devices described by him suffer from the objections that they also are not sharp cutting and are only capable of isolating general regions of the spectrum. The present modification of Wadsworth's device has overcome all the objections which prevent sharp cut-off and lack of achromatization.

The optical layout of the dispersion filter is shown in Fig. 1. It can be seen that the instrument consists of two single monochromators working in opposition. White light focused on slits S and S' will produce spectra at A which are exactly superimposed. Therefore, white light focused on S will produce a white light image of S'. In practice it is, of course, unnecessary to have a slit at S' since the slit of the high dispersion instrument takes its place. Lenses L_2 and L_3 must be of the same focal length so that the spectra are in register. Of course the prisms must also produce identical angular dispersion. Lenses L_1 and L_4 do not need to have the same focal length or to have the same focal length as L_3 and L_2.

From inspection of Fig. 1 it can be seen that the spectrum can be cut off at either end by suitable adjustment of the diaphragm at A. The instrument which was constructed had a clear aperture of 2 inches. With L_2 and L_3 of approximately 8-inch focal length, it is possible to cut off at the end of the spectrum in the blue to within 10 or 15 angstroms of a strong line in a practical case. The present instrument is equipped with a straight slit at S. This produces a straight line image at S'. The spectrum lines produced at A are, of course, curved. It would be possible to produce any predetermined curvature at S' by using a suitably curved entrance slit S.

The major uncorrected aberration of this

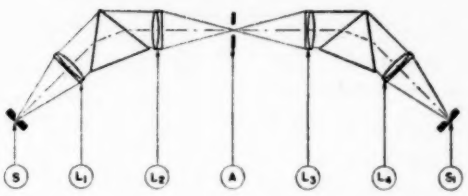

FIG. 1. Dispersion filter. S, S', slits; L_1, L_2, L_3, L_4, lenses; A, aperture.

optical system when non-anastigmatic lenses are used is curvature of field at A which prevents exact register of the real and virtual spectra produced by the two monochromators. This aberration is, however, too small in the present apparatus to show any lack of achromatization which is of practical importance for the present purpose.

A device of the type described above might be of considerable use in the ultraviolet region of the spectrum. It would be possible to isolate selected regions of the ultraviolet and thus enable the use of higher orders of gratings than the first for certain problems. The rather common production of synthetic fluorite takes the use of quartz fluorite achromats out of the realm of speculation. The design of this type of "achromatic spectrograph" for the infra-red region of the spectrum becomes rather complex in practice if mirrors are used exclusively as the image producing devices.

In conclusion, the dispersion filter allows mechanical rejection of undesired regions of the spectrum in a manner which is completely at the control of the investigator over the whole region of the spectrum which the filter is able to pass. The transmission of the filter is determined by the absorption properties of the

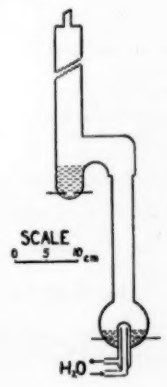

FIG. 2. Water-cooled, low pressure, mercury arc.

[5] H. Lehmann, Ann. d. Physik **39**, 53 (1912).

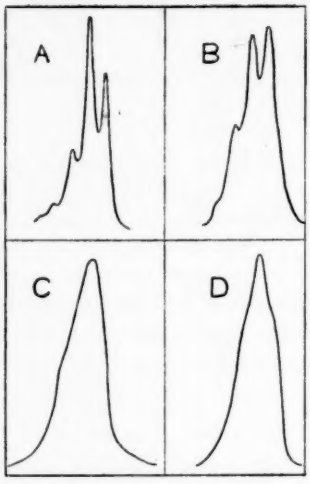

FIG. 3. Smoothed microphotometer curves of Raman lines under high dispersion. A—carbon tetrachloride, $\nu = 459$ cm^{-1}; B—chloroform, $\nu = 366$ cm^{-1}; C—trichloroethylene, $\nu = 380$ cm^{-1}; D—tetrachloroethylene, $\nu = 447$ cm^{-1}.

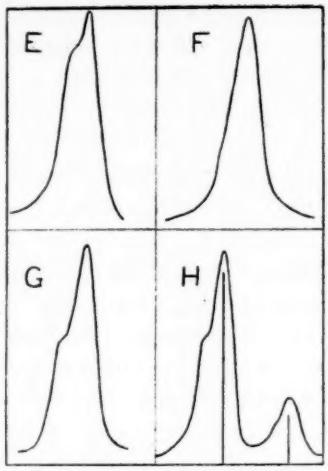

FIG. 4. Smoothed microphotometer curves of Raman lines under high dispersion. E—1,2-dichloroethane, $\nu = 301$ cm^{-1}; F—methyl chloroform, $\nu = 342$ cm^{-1}; G—1,1,2-trichloroethane, $\nu = 332$ cm^{-1}; H—1,1,2,2-tetrachloroethane, $\nu = 353$ cm^{-1}, and 366 cm^{-1}.

refracting materials used, and the usual Fresnel and scattering losses. It should be emphasized that strict register of the spectra from the two monochromators is only obtainable when the lenses used are achromatic.

Apparatus

The general disposition of the apparatus used for excitation of the spectra has been described previously.[6] Recently we have been using water cooled Pyrex mercury lamps of a new design. A diagram of these lamps is shown in Fig. 2. The water-cooled end of the lamp is constructed in the manner described by Welsh and Crawford.[7]

TABLE I. Frequencies and polarizations of the Raman lines studied.

Compound	Frequency shift, cm^{-1}	ρ
Carbon tetrachloride	459	0.013
Chloroform	366	0.145
Trichloroethylene	380	0.31
Tetrachloroethylene	447	0.36
1,2-dichloroethane	301	0.35
Methyl chloroform	342	0.43
1,1,2-trichloroethane	332	0.30
1,1,2,2-tetrachloroethane	353 366	0.20

[6] D. H. Rank and R. V. Wiegand, J. Opt. Soc. Am. **36**, 325 (1946).

[7] H. L. Welsh and M. F. Crawford, paper presented at the Montreal Meeting of the American Physical Society, 1947.

The two lamps used are operated in series on a 110-volt d.c. line, at a current of 30 amperes with a potential drop across each lamp of about 27 volts. Cooling of the upper electrode section is by means of an air blast directed against the long straight section above the arc stream. The continuous background of this arc is very weak and the lines are very sharp, since they show beautiful hyperfine structure even at the large current used.

All the spectra were obtained under high dispersion using the "dispersion filter" previous to analysis by the grating spectrograph. Exposure times varied from 1 to 3 days duration using Eastman II-0 plates. The samples used were Eastman organic chemicals. They were distilled in a simple distilling flask, just before exposure, mainly to eliminate any impurity that might cause fluorescense.

III. RESULTS

The particular vibrational frequencies which can be expected to show isotope effects of observable magnitude will be the more symmetrical C—Cl bending vibrations. For most molecules the bending modes are experimentally found to be more mass sensitive than the stretching modes. The molecules studied in this investigation, together with the frequencies examined and the polarizations, are given in Table

I. The relevant data are also given for the two previously studied compounds, CCl_4 and $CHCl_3$.

The depolarization factors (ρ) were measured using the photoelectric spectrograph essentially in the manner described by Rank.[8] The ρ values are corrected for convergence errors making use of convergence corrections described by Douglas and Rank.[9,10]

Figures 3 and 4 show the intensity contours of the lines investigated. The plates were microphotometered with a Leeds and Northrup microphotometer, and for comparison purposes the intensities measured were converted to a linear scale.

IV. DISCUSSION OF RESULTS

In addition to the aforementioned paper by Rank and Van Horn,[1] previous investigations on the study of the fine structure in the Raman spectra of chlorine compounds were made by Langseth,[11] Hagerty,[12] and Menzies.[13] These have been principally concerned with the isotope effect in the Raman spectrum of carbon tetrachloride. Wu and Sutherland[14] have discussed the interpretation of the carbon tetrachloride results in terms of the force field of this molecule.

Let a represent the fraction of the chlorine atoms having an atomic weight 35 and b the fractional part of the chlorine atoms which have an atomic weight of 37. Then if there are n chlorine atoms in the molecule the relative abundances of the isotopic molecules will be proportional to the magnitude of the different terms in the expansion of $(a+b)^n$. The intensities of the lines caused by the different isotopic molecules should be to a first approximation proportional to the abundances mentioned above.

From previous work on chloroform and carbon tetrachloride[1] it was known that the separation of the Raman lines of the different isotopic molecules for these low frequencies is of the order of magnitude of 3 cm^{-1}.

We have constructed synthetic intensity contour diagrams for $n=2$, 3, and 4, making use of the following reasonable but arbitrary assumptions. In doing this we are following the general procedure of Menzies.[13] It is assumed that (a) each component line has a half-intensity width equal to the separation of the lines; (b) the contribution of intensity drops to zero at a distance equal to or greater than the distance to the center of the neighboring line of the pattern; (c) the separation of centers of neighboring lines is assumed to be 3 cm^{-1}; (d) the line shape for each individual component is symmetrical about its center.

Figure 5 shows these synthetic intensity distribution curves plotted on the same wave number scale as the line contour patterns shown in Figs. 3 and 4.

The following considerations should be taken into account when comparing the computed and experimental contours. (a) Even in the case of very poor resolution it should be possible to identify a "four" pattern in that it will have a fairly symmetrical structure as compared with the other patterns. (b) In all cases the precise contours will depend markedly on the assumed shape of the component lines. In the case of the "three" pattern a slightly greater intensity half-width than we have assumed would give a single maximum. The apparent strength of shoulders will also depend on this assumption. (c) The absence of the weakest components in the experimental curves, when compared with the computed ones, is not significant. The original microphotometer curves showed considerable fluctuation caused by graininess in the plates, and this would obscure these weak components. The figures have been constructed from smoothed microphotometer curves.

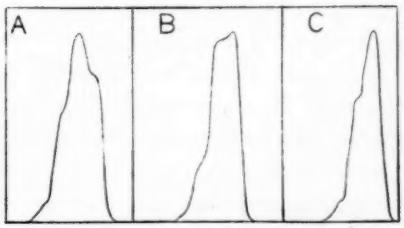

FIG. 5. Computed intensity contour diagrams. A—contour of "four" pattern; B—contour of "three" pattern; C—contour of "two" pattern.

[8] D. H. Rank, J. Opt. Soc. Am. **37**, 798 (1947).
[9] A. E. Douglas and D. H. Rank, J. Opt. Soc. Am. **38**, 281 (1948).
[10] A. E. Douglas, Ph.D. Thesis, Pennsylvania State College (1948).
[11] A. Langseth, Zeits. f. Physik **72**, 350 (1931).
[12] A. A. Hagerty, M.S. Thesis, Pennsylvania State College (1937).
[13] A. C. Menzies, Proc. Roy. Soc. **A172**, 89 (1939).
[14] C. K. Wu and G. B. B. M. Sutherland, J. Chem. Phys. 6, 114 (1938).

It can be seen that a much smaller line width must be used to reproduce a synthetic contour to match the experimental line contours for carbon tetrachloride and chloroform (cf. Fig. 3, A and B with Fig. 5, A and B, respectively). In these cases it can be seen that the line width is small enough so that the resolution of the isotopic lines is practically complete. The question, of course, arises as to why the effective resolution is so much worse in the present series of compounds than in $CHCl_3$ and CCl_4. The answer to this question is probably to be found in the rotational structure of the lines in question. On the basis of theory it is to be expected that the rotational branches of these lines will be depolarized. It can be seen by reference to Table I and Fig. 3 that small ρ values and good resolution of the fine structure correlate very well. For example, the best resolved pattern of the present investigation is that of 1,1,2,2-tetrachloroethane, which is the most highly polarized line of all of the present group of molecules. Experimental proof of the depolarization of rotational vibration wings has been given by Douglas and Rank[9] in the case of the strong lines of CS_2. It seems to be a necessary consequence of theory and experiment that very sharp Raman lines can probably only be expected when these lines are highly polarized.

The intensity contours of trichloroethylene, tetrachloroethylene, 1,2-dichloroethane and methylchloroform (Fig. 3, C and D and Fig. 4, E and F) seem to conform to the appropriate contours in Fig. 5. Figure 3C is similar to an $n=3$ pattern; Fig. 3D has all the characteristics of an $n=4$ pattern; Fig. 4E is a good reproduction of an $n=2$ pattern; Fig. 4F shows very poor resolution but does not seem to be inconsistent with an $n=3$ pattern. We are now left with Fig. 4G and H.

Langseth and Bernstein[3] have shown that symmetrical tetrachloroethane consists of two rotational isomers and that $\nu=353$ cm^{-1} and $\nu=366$ cm^{-1} each belong to a different configuration. It would be expected that these two lines should give rise to identical isotopic fine structures. It is immediately apparent from an inspection of Fig. 4H that the intensity contours of these two lines are totally different. The contour for the weaker line is poorly resolved but could easily be interpreted as an $n=4$ pattern, in view of its symmetrical shape. However, the strong line shows a fine structure contour which is very different from the expected $n=4$ pattern. The line contour is definitely unsymmetrical. In the case of 1,2-dichloroethane there are also two rotational isomers, and the line that we have studied belongs to the *trans*-form.[15] The corresponding vibration of the "gauche" form gives in this case a very weak line at 264 cm^{-1}, and its fine structure could not be obtained with our present exposure times.

The intensity contour of the $\nu=332$-cm^{-1} line of 1,1,2-trichloroethane is likewise somewhat anomalous since the line contour shows a low frequency shoulder somewhat more intense than would be expected for an $n=3$ pattern. On the other hand the height of such shoulders is rather dependent on the exact line shape assumed for the component lines.

It should be noted that visual examination of these last two lines shows a much better apparent resolution than does the microphotometer tracing, and thus accentuates the anomalous contours. The visual appearance of the $\nu=353$-cm^{-1} pattern of 1,1,2,2-tetrachloroethane is a rather completely resolved line pair.

It is not possible to give a definite explanation of the distinct anomaly in 1,1,2,2-tetrachloroethane on the basis of the available experimental evidence. However, two possible explanations suggest themselves.

(a) It was noticed that the anomalous contour for the strong line in 1,1,2,2-tetrachloroethane (Fig. 3H) bears a marked resemblance to the computed "two" pattern (Fig. 5C). Such a "two" pattern might be explained if the two $-CCl_2$ groups were to vibrate in an essentially independent manner. An analogous mechanism could also explain the less certain anomaly in the contour of the 1,1,2-trichloroethane line. However, in several other cases the contours are in agreement with the expected normal patterns. In particular, the contours of 1,2-dichloroethane (Fig. 4E) and the "gauche"[16] form of 1,1,2,2-tetrachloroethane (Fig. 4H) gave very satis-

[15] S. Mizushima and Y. Morino, Bull. Chem. Soc. Japan **13**, 182 (1938).

[16] G. Herzberg, *Infrared and Raman spectra of Polyatomic Molecules* (D. Van Nostrand Company, Inc., New York, 1945), p. 347.

factory "two" and "four" patterns, respectively (cf. Fig. 5C and A).

It is possible that in the case of a large molecule in which $-CCl_2$ groups are separated from each other by several linkages they might vibrate in an essentially independent fashion. In terms of frequency of vibration this means that, under conditions of weak mechanical coupling between the two groups, the symmetrical and unsymmetrical modes (in which the $-CCl_2$ groups perform vibrations in and out of phase) will tend towards the same frequency which would be that a single $-CCl_2$ group in similar surroundings. At the same time it is probable that the contour caused by the isotopic splitting will also tend to that of a single $-CCl_2$ group, i.e., assume a "two" pattern. At first sight, however, it is not easy to imagine such an extreme effect with adjoining $-CCl_2$ groups as in 1,1,2,2-tetrachloroethane. Such phenomena are a matter of degree and without a detailed calculation in each case it is difficult to make definite predictions. Nevertheless we might expect that uncoupling effects would be more pronounced in the "internal" vibrations of a group, than in the "external" ones (in which the group is moving as a whole). Thus if the line at $\nu = 353$ cm^{-1} in 1,1,2,2-tetrachloroethane is caused by the "internal" bending mode of the $-CCl_2$ groups it is understandable why it should behave in a different manner from the corresponding vibration of 1,2-dichloroethane ($\nu = 301$ cm^{-1}). This latter frequency is necessarily of the "external" type. A similar mechanism does not explain very satisfactorily the apparent "four" contour of the line at $\nu = 366$ cm^{-1} of the "gauche" isomer of 1,1,2,2-tetrachloroethane, although in this case (on the assumption that the stable isomer is the "*trans*" one) increased "coupling" may be caused by the closer proximity of the Cl atoms in the two $-CCl_2$ groups. In the case of the chlorinated ethylenes, the fact that the contours observed were in accord with predictions made without taking "uncoupling" effects into account points to the fact that the $-CCl_2$ and $-CCl$ groups at either end of the double bond are strongly coupled together. This seems very reasonable on mechanical grounds in view of the greater strength of the intervening double bond compared to the single bond in the chlorinated ethanes.

It should be noticed that if this explanation of the anomalous contours in the 1,1,2,2-tetrachloroethane is correct, the same effect should be reflected in the separation of the symmetrical and unsymmetrical bending frequencies of these molecules, i.e., a greater separation would be expected for the two frequencies in 1,2-dichloroethane than in 1,1,2,2-tetrachloroethane. Unfortunately, insufficient experimental data are available to settle this point because of the lack of infra-red spectra in this region.

(b) Another weak Raman band at about this same frequency would greatly alter the appearance of the contours. In the case of 1,1,2,2-tetrachloroethane such a possibility would be provided by the difference band of $646 - 289 = 357$ cm^{-1}. Both of these Raman lines are strong, but nevertheless the difference band would not be expected to be of appreciable intensity. Furthermore, the summation band $646 + 289 = 935$ cm^{-1} is missing, despite the fact that it should probably be stronger than the difference band of the same two frequencies.[17] There are, however, a few difference bands listed by Herzberg in the detailed assignments for various molecules, several of which appear without the simultaneous appearance of the corresponding summation band.[18]

A crucial test of this explanation would be the determination of the contour of the analogous line in the spectrum of deuterated 1,1,2,2-tetrachloroethane. The spectrum of this compound has been obtained by Langseth and Bernstein[3] and the corresponding difference line would lie at a considerably lower frequency than the C—Cl bending mode discussed.

[17] See reference 16, p. 267

[18] See reference 16, pp. 311, 329, 341, 352, 358.

Spectroscopic Studies of Rotational Isomerism. I. Liquid *n*-Butane and the Assignment of the Normal Modes of Vibration*

G. J. Szasz, N. Sheppard, and D. H. Rank
Department of Physics, The Pennsylvania State College, State College, Pennsylvania

(Received March 29, 1948)

The Raman spectrum of *n*-butane has been investigated over the temperature range 147°K to 305°K. The results clearly show the presence of two rotational isomers in the liquid. These are the planar, *trans*-form (symmetry C_{2h}) and probably the gauche form obtained by a rotation of 120° about the central C—C bond (symmetry C_2). The photoelectric spectrograph was used for quantitative intensity measurements on the line pair at 432 cm^{-1} and 325 cm^{-1} over the temperature range studied. These lines belong to the two rotational isomers and the results were used to give a value of 770±90 cal. $mole^{-1}$ for the energy difference, $-\Delta H$, between the two forms of *n*-butane in the liquid phase. This result is shown to be in good agreement with a value assumed by Pitzer in his treatment of long chain paraffins. A detailed assignment has been made of the vibrational spectrum of the *trans*-rotational isomer.

I. INTRODUCTION

THE first spectroscopic evidence for the existence of rotational isomers in liquids was obtained by Kohlrausch[1,2] in his study of the Raman spectrum of 1,2-dichloroethane and other halogenated ethanes. Such rotational isomers are possible when different stable configurations can be obtained by rotation of the groups at either end of a single bond. This will be true when, as for example in 1,2-dichloroethane, the C_3 symmetry of both end groups is destroyed.

As normal butane is the simplest hydrocarbon in which such a situation occurs, a detailed understanding of its vibrational spectra is necessary before complete interpretations can be made of the spectra of more complex hydrocarbons. For this reason we undertook a detailed reinvestigation of its Raman spectrum.

The first investigation of this nature was carried out by Kohlrausch and Köppl[3] who favored the existence of more than one rotational isomer for normal butane on the basis of their study of the Raman spectrum. However, they pointed out that the infra-red spectrum could apparently be interpreted in terms of one form only. Mizushima, Morino, and Nakamura[4] also favored the presence of more than one form, and showed that several weak lines in the Raman spectrum of the liquid disappeared on solidification—presumably corresponding to a reversion to the single isomeric (*trans*) form in the crystal. Although their work seemed to be well substantiated from studies of this and related molecules, the determination of weak lines in the Raman spectrum of a solid is usually a hazardous procedure in view of the increased scattering background. Other investigations of the Raman spectrum of normal butane at room temperature have been made by Bhagavantam,[5] Ananthakrishnan,[6] and Murray and Andrews.[7] These are in substantial agreement with the work discussed above. The infra-red absorption spectrum of gaseous normal butane was originally obtained by Coblentz,[8] and has been studied more recently by several laboratories under the auspices of the American Petroleum Institute.[9] Pitzer[10] has obtained good agreement with the measured ther-

* This research was carried out on Contract N6onr269, Task V, of the Office of Naval Research.

[1] K. W. F. Kohlrausch, Zeits. f. physik. Chemie. **B18**, 61 (1932).

[2] K. W. F. Kohlrausch, "Ramanspectren," *Hand und Jahrbuch der Chemischen Physik; Akademische Verlagsges* (Leipzig, 1943), pp. 234 *et seq.*

[3] K. W. F. Kohlrausch and F. Köppl, Zeits. f. physik. Chemie **B26**, 209 (1934).

[4] S. Mizushima, Y. Morino, and S. Nakamura, Sci. Pap. Inst. Phys. Chem. Res. (Tokyo) **37**, 208 (1940).

[5] S. Bhagavantam, Ind. J. Phys. **6**, 595 (1932).

[6] R. Ananthakrishnan, Proc. Ind. Acad. Sci. **5**, 285 (1937).

[7] J. W. Murray and D. H. Andrews, J. Chem. Phys. **1**, 406 (1933).

[8] W. W. Coblentz, *Investigations of Infrared Spectra* (Carnegie Institute of Washington, D. C.), No. 17, **35**, Part I (1905).

[9] American Petroleum Institute Research Project 44. Spectrogram No. 438, contributed by the Shell Development Company, Emeryville, California.

[10] K. S. Pitzer, J. Chem. Phys. **8**, 711 (1941).

modynamic properties of the gas by making certain assumptions with respect to the amounts of different isomers present, whereas Aston, Isserow, Szasz, and Kennedy[11] were able to obtain similar results on the assumption of a single molecular species.

This research was thus undertaken with the following objectives:

(i) To determine whether or not there is more than one rotational isomer present in normal butane at room temperature. This was investigated by comparing the Raman spectra of liquid normal butane at room temperature with that near, but above, the freezing point. Any lines due to less stable (higher energy) rotational isomers should decrease in intensity on going to the lower temperature.

(ii) If rotational isomers were found to be present, to determine the energy difference between them by the method of Langseth and Bernstein.[12] This involves measuring the relative intensities of pairs of Raman lines caused by two molecular species, over a range of temperatures.

(iii) To determine as far as possible the symmetries of the separate isomers and to assign the lines caused by the separate isomers to their respective modes of vibration. The low temperature spectrum obtained as described in (i) will distinguish between lines caused by the different isomers; the usual selection rules, polarizations, etc., can then be used to attempt an answer to question (iii).

II. EXPERIMENTAL

Both of the spectrographs used in this investigation have already been adequately described.[13,14] The photoelectric recording Raman spectrograph of Rank and Wiegand was found to be almost ideal for a study of the relative intensities of line pairs in the Raman spectrum. Its main drawback lies in the strong secondary excitation of the 4358A Hg line of the source. In making these quantitative studies of individual lines, use was made of the best combination of speed, time constant, and amplification ratio available in this instrument. At the speeds used, it took approximately 45 minutes to scan the spectral region of the line pair used.

The prism spectrograph, together with our new recently described,[15] low background sources, was used to obtain complete Raman spectra in the various temperature ranges investigated.

In both spectrographs sodium nitrite solutions were used both as filters and as condensing lenses. Praseodymium nitrate solutions were used to reduce the background intensity in the neighborhood of the exciting line. In the photographic work Eastman-I plates were used after suitable backing with Fe_2O_3 paste to reduce halation caused by Rayleigh scattering. Exposure times ranged from two to eight hours. The microphotometer traces were made with the Leeds and Northrup recording microphotometer.

The *n*-butane used was made by The Ohio Chemical Company and was obtained from the Petroleum Refining Laboratory of this College. It was stated to be 99+ percent pure. The material was handled in a high vacuum system and was dried by passing over phosphorus pentoxide. At temperatures in the neighborhood of the freezing point the small amount of impurity present froze out of the liquid. However, it formed relatively few large particles and did not interfere appreciably with the measurements.

The low temperature measurements were made by placing the sample tube in a Dewar vessel and cooling it with cold air. The temperature in the Dewar was measured by the indications of a single junction copper-constantan thermocouple, and the sample was kept at a constant temperature by proper adjustment of the flow of cold air. The Dewar was an unsilvered Pyrex glass vessel, with two plane glass windows on the bottom, of 38-mm and 48-mm diameter, respectively. It was evacuated to a high vacuum and sealed off. The system was closed by a rubber stopper, with a center hole for the sample tube and appropriate small openings for air inlet, air outlet, and thermocouple. The source of dry air was a liquid air boiler of 20-liter capacity, made of steel, insulated by rock wool, and housed in a wooden box. A resistance heater of

[11] J. G. Aston, S. Isserow, G. J. Szasz, and R. M. Kennedy, J. Chem. Phys. **12**, 336 (1944).
[12] A. Langseth and H. J. Bernstein, J. Chem. Phys. **8**, 410 (1941).
[13] D. H. Rank and R. Wiegand, J. Opt. Soc. Am. **36**, 325 (1946).
[14] D. H. Rank, R. Scott, and M. R. Fenske, Ind. Eng. Chem. Anal. Ed. **14**, 816 (1942).
[15] D. H. Rank, N. Sheppard, and G. J. Szasz, J. Chem. Phys. **16**, 698 (1948).

TABLE I. Observed Raman and infra-red frequencies in *n*-butane (below 1500 cm^{-1}).

Raman lines (cm^{-1})		Infra-red frequencies (cm^{-1})
Low energy form	High energy form	
1455 (*dp*)	(1455)	1466 (*S*)
		1390 (*S*)
(1370)		
		1340 (*W*)
1304 (*p*)	1282	
		1297 (*S*)
		1244 (*W*)
1148 (*p*)	1167	
		1134 (*M*)
1058 (*p*)	1077 (*p*)	
	981 (*p*)	
		970 (*S*)
		959 (*S*)
956 (*dp*)		
835 (*p*)	789 (*p*)	
		795 (*W*)
		751 (*M*)
		734 (*M*)
432 (*p*)	325 (*p*)	

45 ohms was wound on the outside of the boiler to make controlled rates of flow possible. The boiler required about six liters of liquid air to cool it down, and the rate of evaporation thereafter was found to be less than one liter per hour. The evaporated air was cooled by passage through a coil immersed in liquid air, before entering the Dewar. All lines conducting cold air were insulated with felt and thus the temperature of the air entering the Dewar was probably close to 100°K.

III. THE RESULTS AND THEIR INTERPRETATION

A. The Raman Spectra at 302° and 147°K

In Fig. 1 are shown the Raman spectra below 1500 cm^{-1} for the higher and lower temperatures, respectively. These have been traced directly from the microphotometer curves except that short range fluctuations caused by grain on the original plate have been smoothed out. It can be seen at once that a considerable number of the lines have decreased in intensity relative to the others. The most notable changes are the apparent disappearance, at the low temperature, of the 325-cm^{-1} line and the reversal in intensity of the 956-cm^{-1} and 981-cm^{-1} lines, presumably due to the weakening of the latter. If one takes a line of medium strength, such as those at 956 cm^{-1} or 1148 cm^{-1} as a standard, it is an easy matter to pick out those lines which have weakened considerably at the low temperature. These are presumably the lines due to the less stable (high energy) rotational isomer, as the concentration of the latter will decrease with temperature. The fact that each strong line of the stable isomer is accompanied by only one such weak companion is evidence for the presence of a single high energy form. In Table I are listed the Raman spectra due to the two forms, together with the observed infra-red bands.

The weak Raman line near 730 cm^{-1}, which is not listed in Table I is caused by triple excitation of the 835-cm^{-1} line. The broad, ill defined line near the 1370-cm^{-1} line may also be due to multiple excitation or may be a weak line of the stable isomer. It is inserted in brackets in Table I. The ease with which the two sets of lines can be separated is indisputable evidence for the existence of two rotational isomers in liquid *n*-butane.

Our Raman spectra are in good agreement with those of Mizushima *et al.*,[4] and we used their exact wave numbers throughout. In separating the Raman lines belonging to the two forms, our results again agree with those of the Japanese investigators, with the exception of their erroneous assignment of the 956-cm^{-1} line to the high energy isomer. Careful examination of our plates shows that the very strong 1450-cm^{-1} band splits into two components at the low temperature, in agreement with Mizushima's analogous observation on the solid spectrum.

The polarization data listed in Table I are those of Ananthakrishnan,[6] as given by Kohlrausch.[2] We redetermined the polarization of the 1304-cm^{-1} line, however, because it seemed difficult to assign this shift to a depolarized

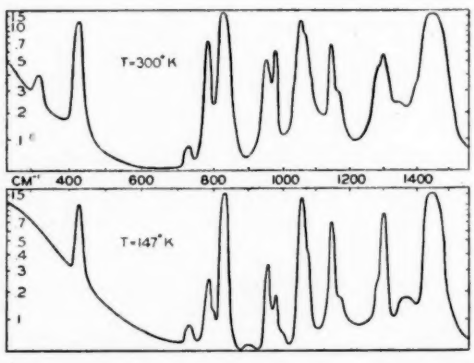

FIG. 1. Smoothed microphotometer curves of the Raman spectrum of liquid *n*-butane at 300°K and at 147°K.

mode. We found the correct depolarization to be about 0.6. The lines at 1167 cm^{-1} and 1282 cm^{-1} were too weak for polarization measurements.

The infra-red spectrum was obtained from the American Petroleum Institute's compilation of infra-red spectra.[9] These data refer to *n*-butane in the vapor phase. The infra-red bands are generally broad because of their rotational structure and this probably obscures the doubling of lines due to the two forms in most cases. Except where otherwise stated we have quoted the center of the band, and further subdivision must await the determination of the infra-red absorption spectrum of liquid *n*-butane at low temperatures. The infra-red band near 965 cm^{-1} has a complex contour and we have assumed that there are two separate frequencies of the same isomer corresponding to the differently shaped peaks at 970 cm^{-1} and 959 cm^{-1}. The infra-red band near 740 cm^{-1} also has two separate peaks at 751 cm^{-1} and 734 cm^{-1}. These are both of similar shape and therefore probably correspond to frequencies of the same general type. We have assumed them to be related frequencies of the two rotational isomers, and have arbitrarily assigned the 751-cm^{-1} frequency to the *trans*-form.

B. The Determination of the Energy Difference between the Rotational Isomers

A choice was made of well separated line pairs which probably correspond to related vibrations of the two isomers, with the purpose of carrying out quantitative measurements on their relative intensities at several temperatures according to the method of Langseth and Bernstein.[12] Most of the line pairs are unsuitable because of the relatively small separation between the two components, and the consequent failure of the photoelectric spectrograph to resolve them. With these considerations in mind the most profitable pairs to study appeared to be those at 325 and 432 cm^{-1}, and 789 and 835 cm^{-1}. The study of the 325- and 432-cm^{-1} line pair proved to be a straightforward matter, and a typical pair of curves obtained at the lower and higher temperatures is given in Fig. 2. On the other hand, it was found to be impossible to utilize the line pair at 789 and 835 cm^{-1} as a quantitative check on our results with the lower line pair, because the secondary excitation of the stronger 835-cm^{-1} line almost obliterates the 789-cm^{-1} line at low temperatures. Quantitative measurements on this line pair were finally abandoned, although it was concluded that within the large limits of error introduced by this difficulty the behavior of this line pair was consistent with the result obtained from the 432- and 325-cm^{-1} line pair.**

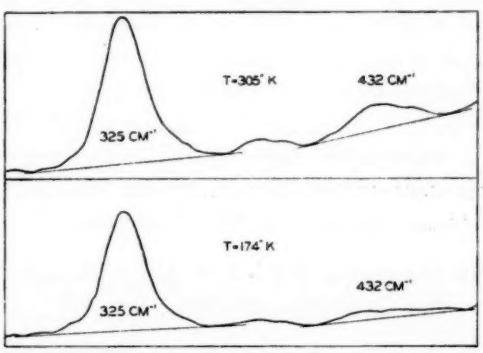

FIG. 2. Photoelectric intensity recording of the 325-cm^{-1} and 432-cm^{-1} Raman shifts in liquid *n*-butane at 305°K and at 174°K.

TABLE II. The intensity ratio of the 432-cm^{-1} to 325 cm^{-1} line pair as a function of temperature.

T°K	174	184	184	217	301	301	305
I/I'	14.60	14.70	14.10	10.00	6.05	6.50	5.92
$(1/T)\times10^3$	5.75	5.43	5.43	4.61	3.32	3.32	3.28
$\log I/I'$	1.164	1.167	1.149	1.000	0.782	0.813	0.772

The quantitative results are summarized in Table II where the first row lists the temperatures and the second row gives the corresponding intensity ratios, intensity of 432-cm^{-1} line/intensity of 325 cm^{-1} line.

The equation used to determine the difference in energy between the two forms was the integrated form of the standard Van't Hoff equation

$$\log(K_1/K_2)=(\Delta H/2.303R)[(1/T_2)-(1/T_1)] \quad (1)$$

with the usual assumptions. The observed intensity of a line is given by $I=C\alpha$, where C is the concentration of molecules and α is the line intensity per molecule.

Thus

$$K_1=(C/C')_{T_1}=((I/I')\cdot(\alpha'/\alpha))_{T_1}, \quad (2)$$

** *Note added in proof:* Recently we have been able to obtain a quantitative value for the energy difference from the 835- and 789-cm^{-1} line pair by using the low pressure source described in reference 15. The value obtained was 800 ± 150 cal. $mole^{-1}$.

TABLE III. Designation, character, species, and activity of the normal vibrations of *n*-butane.

Description \ C_{2h}	$A_g(R.p)$	$A_u(I.R.)$	$B_g(R.dp)$	$B_u(I.R.)$	Expected freq. range	Reference
CH_2 stretching	ν_1	ν_{12}	ν_{20}	ν_{27}	2800–3000 cm^{-1}	17
CH_3 non-symm. stretching	ν_2	ν_{13}	ν_{21}	ν_{28}		
CH_3 symm. stretching	ν_3	—	—	ν_{29}		
CH_2 bending	ν_4	—	—	ν_{30}	*ca.* 1450 cm^{-1}	18
CH_3 non-symm. deformation	ν_5	ν_{14}	ν_{22}	ν_{31}		
CH_3 symm. deformation	ν_6	—	—	ν_{32}	*ca.* 1370 cm^{-1}	18
CH_2 wagging	ν_7	—	—	ν_{33}	1290–1340 cm^{-1}	19
CH_2 twisting	—	ν_{15}	ν_{23}	—	1100–1350 cm^{-1}	19
C—C (skeletal) stretching	$\nu_{8,9}$	—	—	ν_{34}	800–1200 cm^{-1}	19
CH_2 rocking	ν_{10}	ν_{16}	ν_{24}	ν_{35}	900–1200 cm^{-1}	18
CH_2 rocking	—	ν_{17}	ν_{25}	—	720–760 cm^{-1}	19
Skeletal bending	ν_{11}	—	—	ν_{36}		
Skeletal torsion	—	ν_{18}	—	—	<650 cm^{-1}	19
Methyl torsion	—	ν_{19}	ν_{26}	—		
C_{2v}	$A_1(R.p;I.R.)$	$A_2(R.dp)$	$B_1(R.dp;I.R.)$	$B_2(R.dp;I.R.)$		
C_2	$A(R.p;I.R.)$		$B(R.dp;I.R.)$			

and assuming α'/α to be independent of temperature

$$K_1/K_2=(I/I')_{T_1}/(I/I')_{T_2}. \quad (3)$$

The experimental results are shown in Fig. 3 in which $\log I/I'$ is plotted against $1/T$. In accordance with Eq. (1) the best straight line is drawn through the points, and its slope determines ΔH. The scattering of the points is an indication of the consistency of our results. It will be noticed that the scattering is somewhat greater for the points at the lowest temperatures, as in these cases the accuracy of measurement of the weak line is considerably reduced (cf. Fig. 2).

From the slope of the straight line the value of $-\Delta H=770\pm90$ cal. mole^{-1} was obtained. In estimating our error we have allowed for the spread of values that could be obtained by taking extreme slopes of the line between the upper and lower temperatures. No explicit correction has been made for the variation with temperature of the relative distribution of molecules between the ground state and the vibrational state studied in each molecular species. Calculations showed that such a correction would be but a fraction of our experimental error.

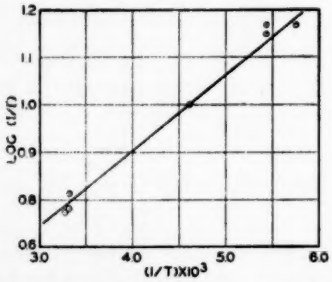

FIG. 3. Plot of intensity ratio of the 325-cm^{-1} and 432-cm^{-1} Raman shifts in liquid *n*-butane *vs.* temperature.

In his discussion of the partition function for long chain hydrocarbons Pitzer[10] assumed the presence of rotational isomers. He calculated the fraction of a particular isomer (1) from the expression $a_1 \exp(-E_1/kT) \sum_{i=1}^{i=n} a_i \exp(-E_i/kT)$ where n is the total number of isomeric species. The various a's are statistical factors determined by the geometry of the molecule, and the E's are the appropriate integral multiples (including zero) of 800 cal. mole^{-1}. In the case of normal butane this 800 cal. mole^{-1} was regarded as the energy difference between the two rotational isomers. Our value of $-\Delta H=770$ cal. mole^{-1} could be directly compared with the above value of 800 cal. mole^{-1} if the assumption were made, with Pitzer, that the products of the remaining partition functions for the two isomers are identical, and further that there is little change in this value in passing from the liquid to the vapor phase. Although these assumptions are not strictly correct the agreement can be taken as good confirmation of Pitzer's treatment.

C. The Symmetry of the Rotational Isomers and the Assignment of Their Spectra

1. The Symmetry of the Isomers

If the assumption is made that the configuration of the rotational isomers is determined by

TABLE IV. Assignment of the normal vibrations of the *trans*-isomer of *n*-butane.

CH_2 stretching	$\nu_1 = 2860\ cm^{-1}$,	$\nu_{12} = (2935)$,	$\nu_{20} = 2934$,	$\nu_{27} = (2860)$,
CH_3 non-symm. stretching	$\nu_2 = (2950)$,	$\nu_{13} = (2960)$,	$\nu_{21} = 2964$,	$\nu_{28} = (2950)$,
CH_3 symm. stretching	$\nu_3 = 2880$,	$\nu_{29} = (2880)$,		
CH_2 bending	$\nu_4 = 1455$,	$\nu_{30} = 1466$,		
CH_3 non-symm. deformation	$\nu_5 = (1455)$,	$\nu_{14} = (1466)$,	$\nu_{22} = (1455)$,	$\nu_{31} = (1466)$,
CH_3 symm. deformation	$\nu_6 = 1370$,	$\nu_{32} = 1390$,		
CH_2 wagging	$\nu_7 = 1304$,	$\nu_{33} = 1297$,		
CH_2 twisting	$\nu_{15} = 1244$,	$\nu_{23} = (1250)$,		
CH_3 wagging	$\nu_{10} = 1148$,	$\nu_{35} = 1134$,	$\nu_{16} = 959$,	$\nu_{24} = 956$
CH_2 rocking	$\nu_{17} = 751$,	$\nu_{25} = (740)$,		
Skeletal stretching	$\nu_8 = 1058$,	$\nu_9 = 835$,	$\nu_{34} = 970$,	
Skeletal bending	$\nu_{11} = 432$,	$\nu_{26} = (365)$,		
Skeletal torsion	$\nu_{18} = ?$			
Methyl torsion	$\nu_{19} =$ or	$\nu_{36} = (200?)$,		

repulsion between the groups at either end of the central C—C bond of butane, the most likely configurations are an essentially *trans*-(C_{2h}) form and two optically isomeric (and therefore spectroscopically identical) C_2 forms. On the other hand, if the restricted rotation is caused by attraction between the groups at either end, we would expect three "eclipsed" forms, one of symmetry C_{2v} (*cis*) and two optical isomers of symmetry C_2. An analogous discussion is given by Herzberg[16] for the 1,2-dichloroethane molecule.

n-Butane will have 36 normal modes of vibration and these can be further subdivided as shown in Table III. In this table the selection rules and symmetry types are given for the different possible molecular configurations, together with the regions of the spectrum where the various molecular vibrations will probably occur. These rules are derived from several sources and an appropriate reference is given in each case.[17–19] Table III has been further subdivided into broad frequency ranges which can be investigated fairly independently from the point of view of the number of observed vibrations. The most interesting regions are those lying between 1500 cm^{-1} and 700 cm^{-1} and $<650\ cm^{-1}$.

First of all let us consider the spectrum of the most stable isomer whose Raman lines below 1500 cm^{-1} are given in the first column of Table I. If this molecule has the symmetry C_{2h} (*trans*), C_{2v} (*cis*) or C_2 (gauche) it will have, respectively, 11, 21, and 21 allowed Raman fundamentals in the region 1500–650 cm^{-1}. Although all the Raman lines may not have been detected, it should be noticed that the observation of the triple excitation of the 835-cm^{-1} line on both microphotometer traces, at *ca.* 730 cm^{-1}, shows that a line of one-hundredth of the strength of the strongest line of the more stable isomer could be observed. Table I shows that, at the most, eight distinct lines can be detected in the Raman spectrum of this region and this is clearly strong evidence for the C_{2h} (*trans*) configuration for the molecule. In the infra-red spectra the number of allowed lines for the C_{2h}, C_{2v}, and C_2 configurations are 10, 17, and 21, respectively, whereas there are only nine well established lines, including several weak ones. This again is very good evidence for the C_{2h} symmetry and we can thus conclude that the more stable rotational isomer has undoubtedly the *trans*-configuration. In the region below 650 cm^{-1} the isomeric configurations C_{2h}, C_{2v}, and C_2 would require 2, 5, and 5 Raman lines, and if we exclude the restricted rotation of the methyl groups, which, in general, seem to be difficult to observe in Raman scattering, the above would reduce to 1, 3, and 3, respectively. The fact that a single line at 432 cm^{-1} is observed in the Raman spectrum of the more stable isomer is therefore further evidence for the C_{2h} (*trans*) configuration. The infra-red spectrum has not so far been examined in this region.

With regards to the configuration of the other rotational isomer we cannot reach any very

[16] G. Herzberg, *Infrared and Raman Spectra of Polyatomic Molecules* (D. Van Nostrand Company, Inc., New York, 1945), p. 347.
[17] J. J. Fox and A. E. Martin, Proc. Roy. Soc. London **A175**, 208 (1940).
[18] G. Herzberg, reference 16, p. 195, and discussions of individual hydrocarbon spectra.
[19] N. Sheppard, J. Chem. Phys. **16**, 690 (1948).

definite conclusions, as all the Raman lines observed have been relatively weak. These presumably correspond to the most symmetrical modes and it is clear that the small concentration of this isomer is such that we cannot expect to detect the weaker lines caused by the less symmetrical vibrations. However, as there is no doubt about the *trans*-configuration of the more stable isomer, it is probable that the other rotational isomer has also a "staggered" configuration, which will be of symmetry C_2.

2. General Methods of Assignment

In Table IV an assignment has been made of the observed vibrational frequencies of the trans form of *n*-butane to the normal modes of vibration. In drawing up this assignment the following points have been taken into account.

(a) Polarization data on the Raman lines can be used to distinguish between A_g and B_g type vibrations.

(b) Infra-red active frequencies of symmetry A_u give rise to a change in electric moment during the vibration which is perpendicular to the plane of symmetry, i.e., along the greatest axis of inertia. They should thus have band contours exhibiting a Q branch under conditions of sufficiently high resolution. Vibrations of type B_u will have "hybrid" contours which cannot be easily predicted.

(c) Many assignments can be made with the help of the correlation rules listed in Table III. These have been derived from the study of series of related molecules.

(d) Because of the center of symmetry in the molecule, closely related stretching and bending modes of the CH_2 and CH_3 groups occur in pairs, one being active in infra-red absorption and the other in Raman scattering. In several cases the application of rules (a)–(c) show that these occur with very similar frequencies in the two types of spectra, and this fact has been used to assign approximate values to non-observed members of other frequency pairs.

(e) A Raman active skeletal stretching mode, on the other hand, will probably not have any such corresponding frequency in the infra-red spectrum, and vice-versa.

When the above points are taken into account the reasons for many of the assignments are clear, but some less evident points are discussed below.

3. The Spectrum in the Region of 3000 cm^{-1}

The frequencies in this region are caused by C—H stretching modes of vibration. Fox and Martin[17] have shown, from a study of infra-red spectra, that CH_2 groups have symmetric and non-symmetric CH stretching modes near 2850 and 2925 cm^{-1}, respectively, and that CH_3 groups have corresponding symmetric and non-symmetric modes near 2870 and 2960 cm^{-1}. They also showed that an overtone of the hydrogen deformation frequency near 1450 cm^{-1} occurs near 2900 cm^{-1}. In the Raman spectrum, Mizushima and his co-workers[4] give the following frequencies for liquid and solid *n*-butane:—liquid; 2667(2,*p*), 2703(3,*p*), 2733(4,*p*), 2860(10,*p*), 2880 (10,*p*), 2909(8,*p*), 2937(10,*p*), 2964(9,*dp*?); solid 2703(1), 2725(1), 2853(8), 2872(8), 2896(10), 2912(4), 2931(1), 2950(4), 2965(9). The polarization data on the room temperature spectrum were taken from Ananthakrishnan's work.[6]

The assignments given in Table IV have been made with the help of Fox and Martin's rules, and taking into account the polarization data and the persistence of frequencies in the spectra of both liquid and solid butane. The infra-red frequencies have been assigned in a schematic fashion with the help of the Raman assignments and the correlation rules.

4. The Spectrum in the Region 1500–650 cm^{-1}

The polarized Raman lines in the region 1500–1300 cm^{-1} can be assigned with the help of the correlation rules, and there remains only the identification of the 1148-, 1058- and 835-cm^{-1} lines to be made to one or the other of the modes ν_8, ν_9, or ν_{10}. It seems likely that the 1148-cm^{-1} frequency corresponds to the only hydrogen deformation frequency of the three, *viz.*, an in-plane CH_3 wagging mode, as there is a corresponding infra-red band at 1134 cm^{-1} (see C 2 d). We therefore assign $\nu_{10}=1148$ cm^{-1} (and $\nu_{35}=1134$ cm^{-1}), and thus the 1058- and 835-cm^{-1} lines are, respectively, ν_8 and ν_9. These seem to be very reasonable values for C—C stretching modes, and obey point C 2 e, in

that there are no neighboring frequencies in the infra-red spectrum. The single observed depolarized Raman line in this region at 954 cm^{-1} can be assigned to ν_{24}, an out-of-plane CH_3 wagging mode, on the basis of the correlation data. Nearly all the strong lines in the infra-red spectrum of this region can be immediately assigned with the help of the correlation rules and the previous interpretation of the Raman frequencies. The exceptions are bands at 1340 cm^{-1} (weak), 970 cm^{-1} (strong), 795 cm^{-1} (weak), and 734 cm^{-1} (medium). The 734-cm^{-1} line is probably the analogue of the 751-cm^{-1} frequency in the spectrum of the less stable rotational isomer. The 970-cm^{-1} frequency corresponds to the strongest band left and is almost certainly the remaining C—C stretching mode, ν_{34}. It is possible that the 1340- and 795-cm^{-1} bands correspond to the less stable isomeric form, or, on the other hand, they may be summation or difference bands. If they are summation bands, the 795-cm^{-1} frequency can be most easily explained as $\nu_{11}+\nu_{36}$, giving $\nu_{36}=365$ cm^{-1}. This is in satisfactory agreement with Pitzer's calculation[10] of 380 cm^{-1} for this mode, but must await confirmation from the infra-red spectrum before being accepted. The 1340-cm^{-1} line seems to be rather anomalous with respect to the correlation rules, and hence can also be most probably explained as a combination level. It is, however, difficult to assign this band satisfactorily with the help of fundamentals that have already been identified. The most likely explanation would appear to be a combination level involving either ν_{10} or ν_{35} near 1140 cm^{-1} together with a frequency near 200 cm^{-1} (ν_{18}, ν_{19}, or ν_{22}). Such a frequency, if it were assigned to the methyl torsion modes ν_{19} or ν_{26}, would give a reasonable value for the barrier to rotation of the methyl groups of between 2000 and 3000 cal. $mole^{-1}$.

5. The Spectrum in the Region below 650 cm^{-1}

Unfortunately, the infra-red data in this region are not available. The polarized Raman line at 432 cm^{-1} is clearly the bending mode, ν_{11}.

6. The Spectrum of the C_2 Isomer

Only a few of the strongest Raman lines of the molecule have been observed and they have been listed earlier in Table I. In most cases they occur as weaker satellites to strong Raman lines of the *trans*-isomer and can be assigned to the same vibrations of the less symmetrical molecule (see Table I). The line at 981 cm^{-1} of the less stable (C_2) isomer is anomalous in that its polarization is different from that of the neighboring 956-cm^{-1} line of the *trans*-form, and it is more intense than the latter. It seems probable that it corresponds to a different mode of vibration in the less stable rotational isomer, and it may be the third C—C stretching mode, ν_{34}, which is allowed in the Raman spectrum of this molecule and occurs at 970 cm^{-1} in the infra-red spectrum of the *trans*-molecule.

ACKNOWLEDGMENTS

We wish to thank Dr. J. G. Aston, Director of the Cryogenic Laboratory in this College, for suggesting the investigation, for helpful discussions, and for making available generous supplies of liquid air during the course of the measurements. Our thanks are also due to Dr. M. R. Fenske, Director of the Petroleum Refining Laboratory, for the *n*-butane sample. The figures were prepared by Mr. E. Shull.

Vibrational Frequency Assignments for Paraffin Hydrocarbons; Infra-Red Absorption Spectra of the Butanes and Pentanes

R. S. RASMUSSEN*
Shell Development Company, Emeryville, California
(Received April 6, 1948)

The infra-red absorption spectra from 2 to 15μ are given for *n*-butane, isobutane, *n*-pentane, isopentane, and neopentane. Vibrational assignments for these molecules and for propane are deduced. The band positions correlatable with particular types of vibration of various hydrocarbon groupings are discussed.

COMPLETE or almost complete vibrational frequency assignments are known for the hydrocarbons methane, ethane, ethylene, acetylene, methylacetylene, and dimethylacetylene.[1,1a] Pitzer[2a] has discussed the assignment for propane, isobutane and neopentane have been discussed by Pitzer and Kilpatrick[2b] and neopentane by Young, Koehler, and McKinney.[2c] In this paper, the assignments for propane, the butanes, and the pentanes are considered, with some modifications of the previous assignments, and an attempt is made to generalize these results toward the understanding of more complex paraffin spectra.

I. GENERAL CONSIDERATIONS

The general problem is to correlate observed infra-red and Raman frequencies with specific vibrations of groups. Strictly speaking, a given normal mode of vibration involves motion of all the atoms in a molecule. However, to a certain approximation, the normal modes may be assigned to particular vibrations of small groups of atoms, the motions of these atoms being only weakly coupled with other atoms in the molecule.[3]

From the vibrational assignments of the simpler molecules referred to in the introduction and from a comparative examination of the spectra of a much larger number of other organic molecules, certain general frequency regions have come to be recognized. Thus, the vibrations involving principally the stretching of CH bonds give rise to the numerous infra-red bands and Raman shifts in the interval 2900 to 3100 cm^{-1}. Similarly, vibrations due mainly to changes in HCH angle give rise to frequencies near 1400 cm^{-1}. These frequencies appear as the well marked infra-red bands near 6.8μ and 7.2μ present in the spectra of all paraffin hydrocarbons[4] and as the strong shift near 1460 cm^{-1} present in their Raman spectra.[5] Specifically, the three HCH bending vibrations of a methyl group combine to give a "symmetric" methyl bending vibration (symmetry representation A_1 of the C_{3v} point group about the carbon atom) which appears near 1380 cm^{-1} and is strong in the infra-red but weak or missing in the Raman; and a doubly degenerate "antisymmetric" pair of vibrations (symmetry representation E) appearing near 1460 cm^{-1} and strong in both the Raman and infra-red.[6] The methylene group of

* Present address: Shell Chemical Company, San Francisco, California.

[1] References for and discussions of these cases are given by G. Herzberg, *Infra-Red and Raman Spectra of Polyatomic Molecules* (D. Van Nostrand Company, Inc., New York, 1945), Ch. III.

[1a] Recently Pitzer and co-workers have given assignments based on careful consideration of recent spectra, of propylene and certain butenes [J. Res. Nat. Bur. Standards **38**, 191 (1947)], of cyclopentane [J. Am. Chem. Soc. **69**, 2483 (1948)], and of cyclohexane and some substituted cyclohexanes [J. Am. Chem. Soc. **69**, 2488 (1948)].

[2a] K. S. Pitzer, J. Chem. Phys. **12**, 310 (1944).

[2b] K. S. Pitzer and J. E. Kilpatrick, Chem. Rev. **39**, 435 (1946).

[2c] C. W. Young, J. S. Koehler, and D. S. McKinney, J. Am. Chem. Soc. **69**, 1410 (1947).

[3] G. Herzberg, *Infra-Red and Raman Spectra of Polyatomic Molecules* (D. Van Nostrand Company, Inc., New York, 1945), pp. 192–201.

[4] See references to spectra of paraffins given by R. S. Rasmussen and R. R. Brattain, J. Chem. Phys. **15**, 120 (1947); also American Petroleum Institute Research Project 44, Infra-Red Absorption Spectrograms.

[5] K. W. F. Kohlrausch and F. Köppl, reference 12b.

[6] These symmetry designations apply to the local symmetry of the methyl group and are used here merely as descriptive devices. The over-all molecular symmetry may cause the degeneracy to disappear or may create new degeneracies involving more than one methyl group.

the system $C-CH_2-C$ gives rise to a single HCH bending vibration of frequency near 1460 cm^{-1}, as judged from cycloparaffins.

The region from 1350 cm^{-1} to 650 cm^{-1} includes two further types of vibration, *viz.*, CC stretching vibrations and motions involving changes of HCC angles, while the low frequency region (<700 cm^{-1}) includes the CCC bending vibrations. It will be desirable to consider separately the skeletal vibrations (CC stretching and CCC bending) and the HCC bending vibrations. The former will, in general, be more highly dependent on the geometry of the molecule, with normal vibrations not being localized in particular bonds but involving motion of the whole skeleton. This follows from the near equality of force constants and masses of the vibrating groups, leading to a large amount of coupling between motions of adjacent bonds and bond angles.

In contrast, the HCC bending vibrations might be expected to exhibit a certain amount of regularity irrespective of the particular carbon skeleton involved. This follows from the fact that the motions are essentially those of light hydrogen nuclei attached to the heavy carbon skeleton and presumably would not couple strongly with or through the skeleton. As has been already the practice of the Harvard group in normal frequency calculations of simpler molecules, the HCC bending motions will be described as shown in Fig. 1. The methyl rocking vibrations are essentially equivalent motions at right angles to each other, as are the two tertiary CH wagging vibrations. These motions correspond to the correct orthogonal combinations of the angle displacement coordinates $\Delta\beta$, consistent with the local symmetry about the carbon atom of interest. In the notation of Fig. 1, these combinations are (exclusive of normalization factors):

methyl group rocking:
$$\Delta\beta_1-\Delta\beta_2,\ \Delta\beta_1+\Delta\beta_2-2\Delta\beta_3;$$
methylene group rocking:
$$\Delta\beta_{11}-\Delta\beta_{12}+\Delta\beta_{21}-\Delta\beta_{22};$$
methylene group twisting:
$$\Delta\beta_{11}-\Delta\beta_{12}-\Delta\beta_{21}+\Delta\beta_{22};$$
methylene group wagging:
$$\Delta\beta_{11}+\Delta\beta_{12}-\Delta\beta_{21}-\Delta\beta_{22};$$

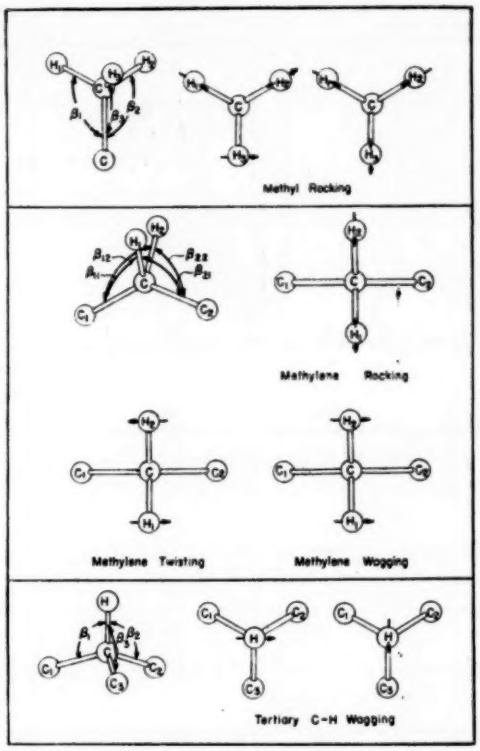

FIG. 1. Types of HCC vibrations.

tertiary CH wagging:
$$\Delta\beta_1-\Delta\beta_2,\ \Delta\beta_1+\Delta\beta_2-2\Delta\beta_3.$$

The apparent degeneracy in the two methyl rocking and the two tertiary CH wagging vibrations may, of course, be removed when the remainder of the molecule is taken into account. Particularly for the methyl rocking frequencies, the two motions shown may occur with quite different frequencies because of different interactions with other groups of the molecule (e.g., see propane below).

The remainder of this paper is concerned with the assignment for these frequencies in the range less than 1350 cm^{-1}, i.e., the skeletal frequencies and HCC bending frequencies.

II. METHOD AND EXPERIMENTAL DATA

The molecules whose frequency assignments are considered here in detail are propane, *n*-butane, isobutane, *n*-pentane, isopentane, and neopentane.

The general method used is to make as complete an assignment as possible for the simpler molecules, where infra-red and Raman selection

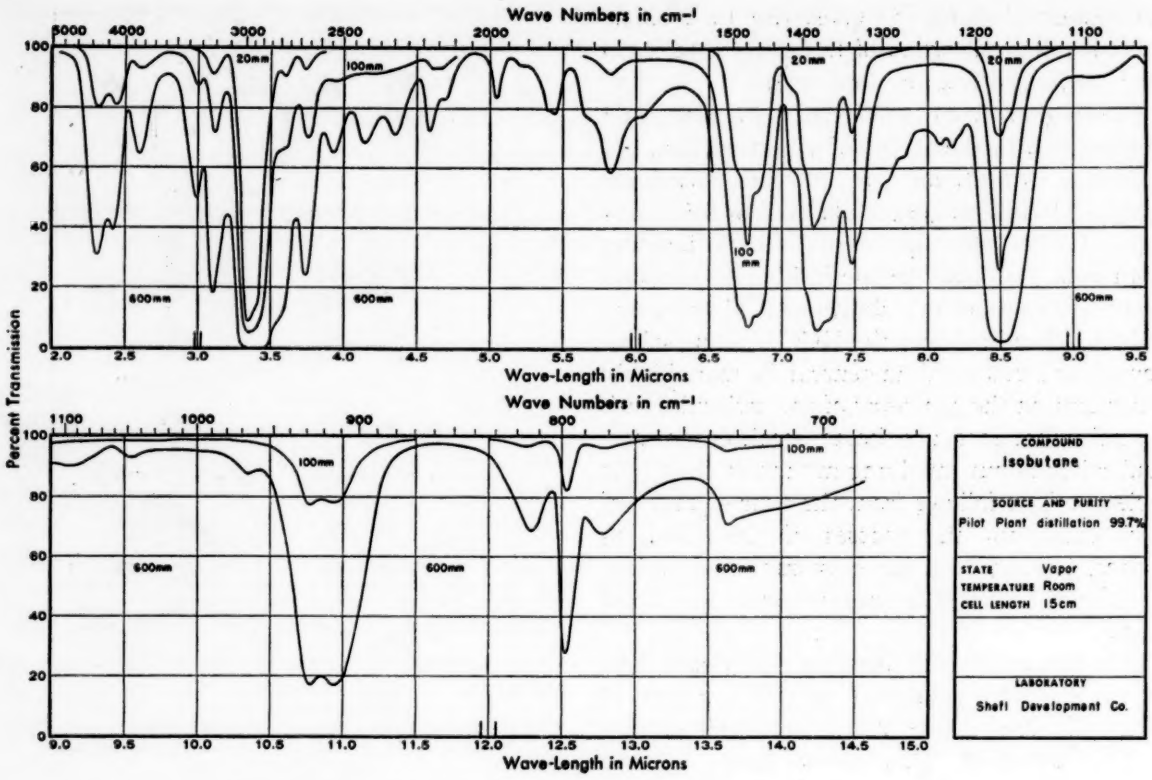

FIG. 2. Isobutane.

rules can be used to advantage. Simplified force constant treatments have been made on certain models. It was not expected that these calculations would give close agreement with experiment, but they were used merely to give indications of the general regions in which given types of vibrations were to be expected. The results on these simpler molecules are then compared with spectra of higher molecules of the same type and thus afford some guide as to the interpretation of groups of frequencies even where specific assignments of individual infra-red bands or Raman lines are impossible.

No attempt has been made to carry out complete force-constant treatments. Improved methods of setting up and solving the secular determinants[7,8] and the demonstrated validity of the transfer of physically similar force constants from one molecule to another[9] have brought such calculations within reason for molecules of the complexity of those considered here. However, lack of *a priori* knowledge of the correct cross term interactions to include in the potential function and of the effect of anharmonicity made it seem more worth-while to follow a more empirical approach for the present. However, further elucidation of some of the unknown or doubtful frequencies will ultimately require force constant calculations.

Experimental infra-red data used are, for propane, the high resolution grating absorption spectrum given by Wu and Barker,[10] and, for the butanes and pentanes, the vapor spectra shown in Figs. 2 to 6, obtained by means of the rocksalt prism spectrograph of this laboratory.[11] Wave-lengths, frequencies, and intensities are given in Tables I to V.

[7] E. B. Wilson, Jr., J. Chem. Phys. **7**, 1047 (1939); **9**, 76 (1941).

[8] B. L. Hicks, J. Chem. Phys. **8**, 569 (1940).

[9] B. L. Crawford, Jr., and S. R. Brinkley, Jr., J. Chem. Phys. **9**, 69 (1941).

[10] V. L. Wu and E. F. Barker, J. Chem. Phys. **9**, 487 (1941). Since it is difficult to estimate intensities from the grating curves, those shown in Fig. 7 have been taken from salt-prism spectra from this laboratory.

[11] This instrument, the methods used in obtaining curves, and the accuracy achieved are described by R. S. Rasmussen and R. R. Brattain, J. Chem. Phys. **15**, 120 (1947).

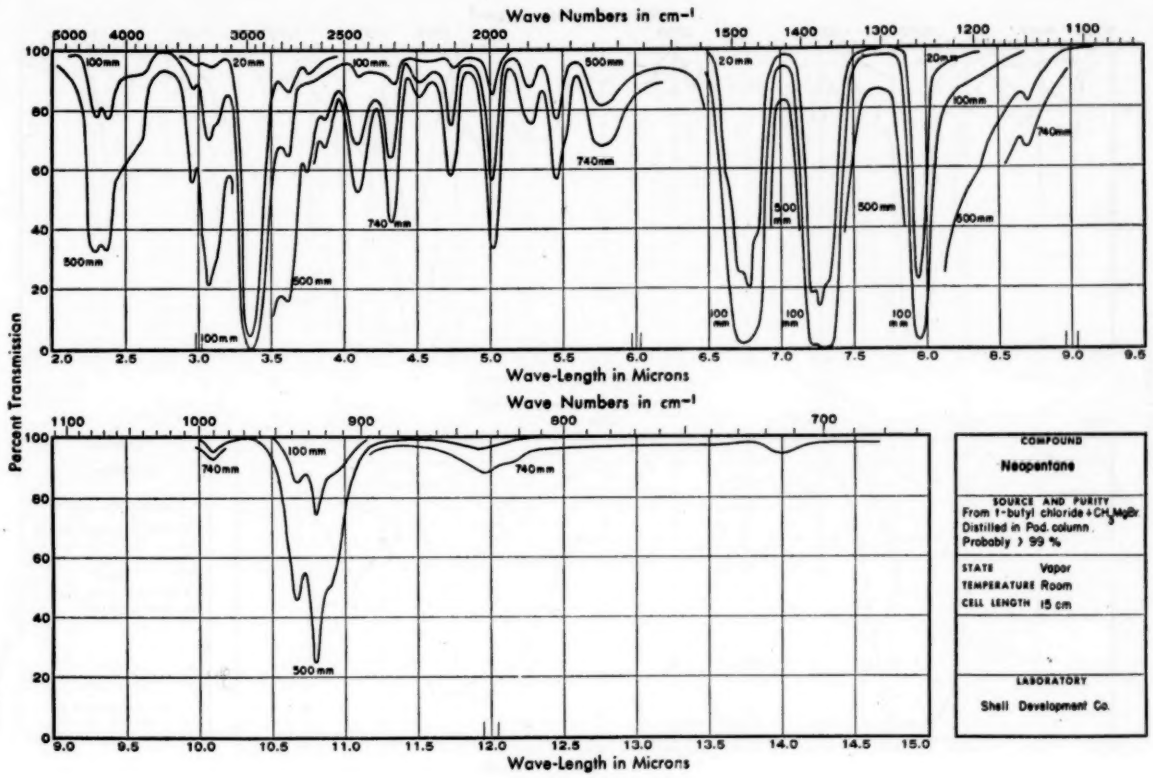

FIG. 3. Neopentane.

Raman data were taken from various literature sources,[12] average values being used. All Raman data refer to the liquid state. Infra-red and Raman data are plotted together for easy comparison in Fig. 7. Since the resolution was not sufficient to deduce the centers of infra-red bands with certainty in all cases, the band positions shown are reasonable estimates, taking into account probable envelope shapes.

III. PROPANE

Pitzer[2] has discussed the frequency assignment for propane, with which that advanced here agrees in the main. However, the present assignment differs in a significant point, so that further discussion is required. As indicated in Fig. 7, there are nine infra-red bands in the region of interest (700 to 1350 cm^{-1}). Except for the extremely weak band at 1250 cm^{-1}, observed in high pressure spectra and certainly an overtone, the symmetry types of these bands are unambiguously determined from the spectrum given by Wu and Barker.[10] The symmetry designations shown in Fig. 7 have the following meanings:

	Symmetry to reflection through: CCC plane	Central CH_2 plane	Activity
A_1	+	+	*IR, R*
A_2	−	−	*R*
B_1	+	−	*IR, R*
B_2	−	+	*IR, R*

In accord with Kohlrausch and Köppl[12b] and Pitzer, the 870-cm^{-1} and 1053-cm^{-1} bands may be assigned as the symmetric and antisymmetric CC stretching frequencies. This follows from their intensities in the Raman spectrum, their symmetries from the infra-red, and simple valence-type force constant considerations. The

[12a] S. Bhagavantam, Ind. J. Phys. **6**, 595 (1931): propane, *n*-butane, isobutane.
[b] K. W. F. Kohlrausch and F. Köppl, Zeits. f. physik. Chemie **26B**, 209 (1934): propane, *n*-butane, isobutane, *n*-pentane, neopentane.
[c] J. W. Murray and D. H. Andrews, J. Chem. Phys. **1**, 406 (1933): *n*-butane.
[d] R. Ananthakrishnan, Proc. Ind. Acad. Sci. **5A**, 285 (1937): *n*-butane; *ibid.* **3A**, 527 (1936): isobutane.
[e] P. A. Bazhulin, A. F. Platé, O. P. Solovova, and B. A. Kazanskii, Bull. Acad. Sci. U.R.S.S., Classe de sci. chim. 1941 (1), 13; Survey For. Pet. Literature, Sept. 5, 1941: *n*-pentane, isopentane.
[f] H. Kopper, R. Seka, and K. W. F. Kohlrausch, Monats. 61, 397 (1932): isopentane.
[g] D. H. Rank and E. R. Bordner, J. Chem. Phys. **3**, 248 (1935): neopentane.

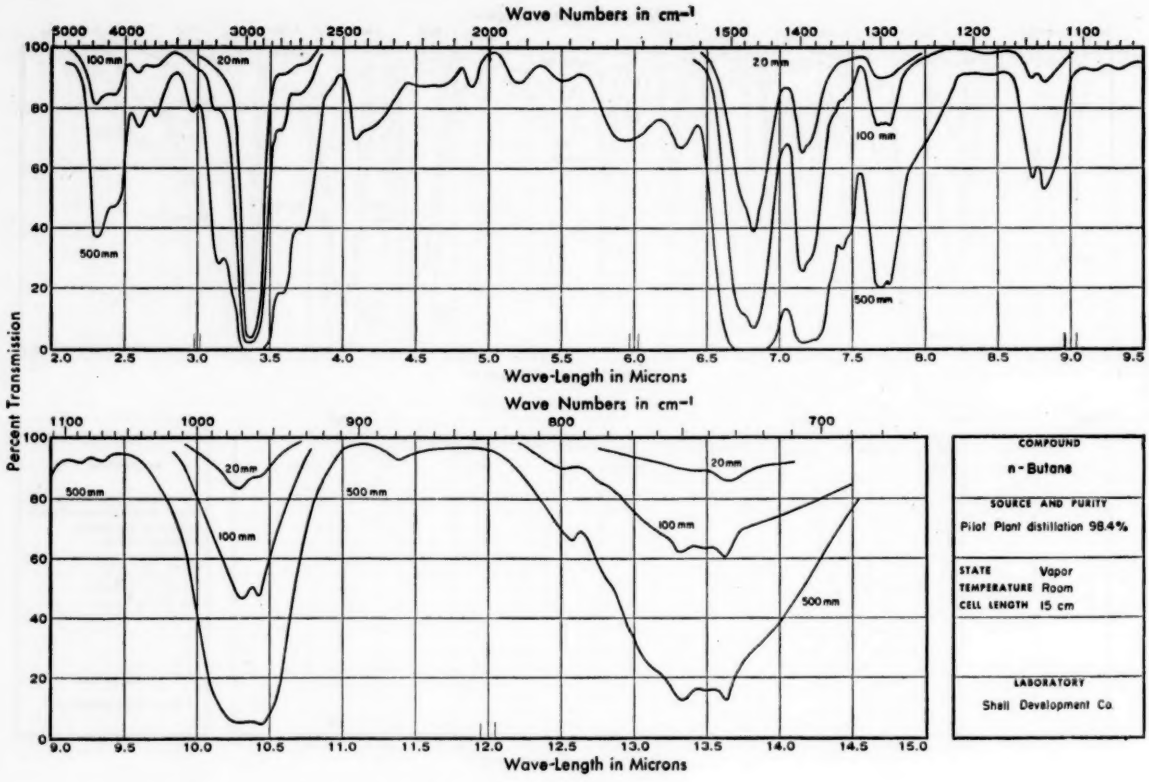

FIG. 4. *n*-Butane.

CCC bending frequency lies at 374 cm^{-1}, from Raman work.[12] Wu and Barker[10] failed to find an analogous band in the infra-red, presumably because of its unexpectedly low intensity. As discussed by Pitzer, the weak 720-cm^{-1} band is taken to be a difference band from an excited methyl torsion level.

There remain the four methyl rocking frequencies (A_1, A_2, B_1, B_2) and the three methylene frequencies (A_2, B_1, B_2) to be assigned. Empirical evidence indicates that the 748-cm^{-1} infra-red band and the 1278-cm^{-1} Raman line are associated with the CH_2 group. This follows from the fact that all aliphatic hydrocarbons containing CH_2 groups show infra-red bands at 700 to 800 cm^{-1}, which appear stronger the more CH_2 groups are present,[4] and similarly for the Raman spectral lines near 1300 cm^{-1}, of which the propane 1278 cm^{-1} is the prototype.[12b] A force constant calculation for the CH_2X_2-type molecule, where X = methyl, using force constants from independent sources, yields the following values for the CH_2 frequencies: rocking (B_2), 761 cm^{-1}; twisting (A_2), 1175 cm^{-1}; wagging (B_1), 1205 cm^{-1} (see Appendix B for details of calculation). By using these approximate values as a guide, the observed 748 cm^{-1}, 1278 cm^{-1}, and 1338 cm^{-1} frequencies are to be assigned to these vibrations, in keeping with the symmetry types of the observed 748-cm^{-1} and 1338-cm^{-1} bands, and with the fact that the A_2 frequency at 1278-cm^{-1} should appear in the Raman but not the infra-red. Any other assignment consistent with the symmetries of the infra-red bands would lead to disagreements with the calculated results of the order of 400 cm^{-1}, which is unlikely.

The remaining unassigned bands at 922 cm^{-1} (B_1), 1160 cm^{-1} (A_1), and 1179 cm^{-1} (B_2) must be assigned as the methyl rocking frequencies of the indicated symmetries. The fourth methyl rocking frequency, of type A_2 and hence infra-red inactive, has not been observed. It is noteworthy that the two methyl rocking vibrations which involve the close approach of the methyl groups are the A_1 (in the carbon plane) and B_2 (out of the carbon plane) and that these two exhibit the higher frequency values, near 1170 cm^{-1}. The

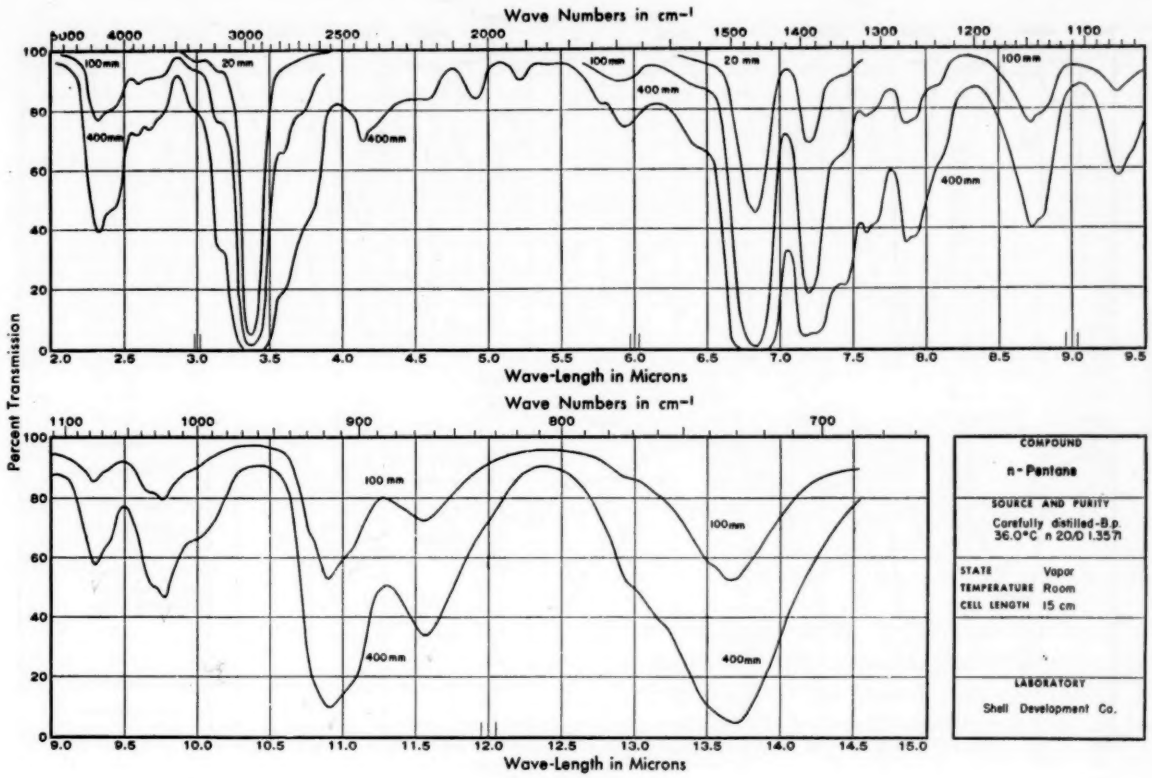

FIG. 5. *n*-Pentane.

B_1 vibration, in which one methyl group moves away from and the other toward the twofold axis, has the lower value of 922 cm^{-1}. If the higher values of the A_1 and B_2 frequencies are attributed to steric repulsion of the methyl groups, it would be anticipated that the A_2 frequency would be in the 900-cm^{-1} region; like the B_2, it is a vibration in which the methyl groups do not approach each other closely, one moving out of the carbon plane on one side while the other moves out on the other.

The important point in the above conclusions is the assignment of the low 748-cm^{-1} frequency to the methylene rocking vibration. Previously, this band had been considered as a carbon-stretching frequency or a methyl-rocking frequency. The former possibility, besides being implausible on other grounds, has been rather definitely contraindicated by recent work by Sheppard and Sutherland[13] on completely deuterated hydrocarbons. It was shown that the ~720-cm^{-1} band of long chain paraffins, which is the analog of the propane 748-cm^{-1} band, arose from a CH and not a C–C type of vibration. Pitzer[2] considered the two B_2 vibrations (CH_2 wagging and CH_3 out-of-plane wagging) to interact strongly, so that the two B_2 frequencies (748 cm^{-1} and 1179 cm^{-1}) each corresponded to a mixed vibration involving both motions.**

[13] N. Sheppard and G. B. B. M. Sutherland, Nature **159**, 739 (1947).

** At the suggestion of Dr. Pitzer, the present point of view is further elucidated here. To a certain extent, the names given to these frequencies are merely a matter of convenient labeling, since certainly there is interaction of some extent between them, neither corresponding to a pure vibration of the one sort or other. In order accurately to assess the participation of each motion in each of the true normal coordinates corresponding to the observed frequencies, a normal coordinate analysis of reasonable accuracy would have to be made. However, it is felt by the author that there is good ground for the proposed assignment, and that actually the 748-cm^{-1} band corresponds to a vibration essentially only of the CH_2 group, and the 1179-cm^{-1} band similarly for the CH_3 groups. The reasons follow: (1) The frequency calculation made on the simplified model CH_2X_2 ($X=CH_3$; see Appendix B) indicated the CH_2 wagging frequency to be in the 750-cm^{-1} region, so it is not necessary to adduce any large amount of interaction with CH_3 vibrations to explain the observed position at 748 cm^{-1}. (2) As described later, and as also suggested by Sutherland,[13] the strong bands of higher paraffins at 720–780 cm^{-1} are attributable to vibrations of CH_2 chains. The 748-cm^{-1} band of propane seems clearly the prototype of these, and its occurrence in the same region

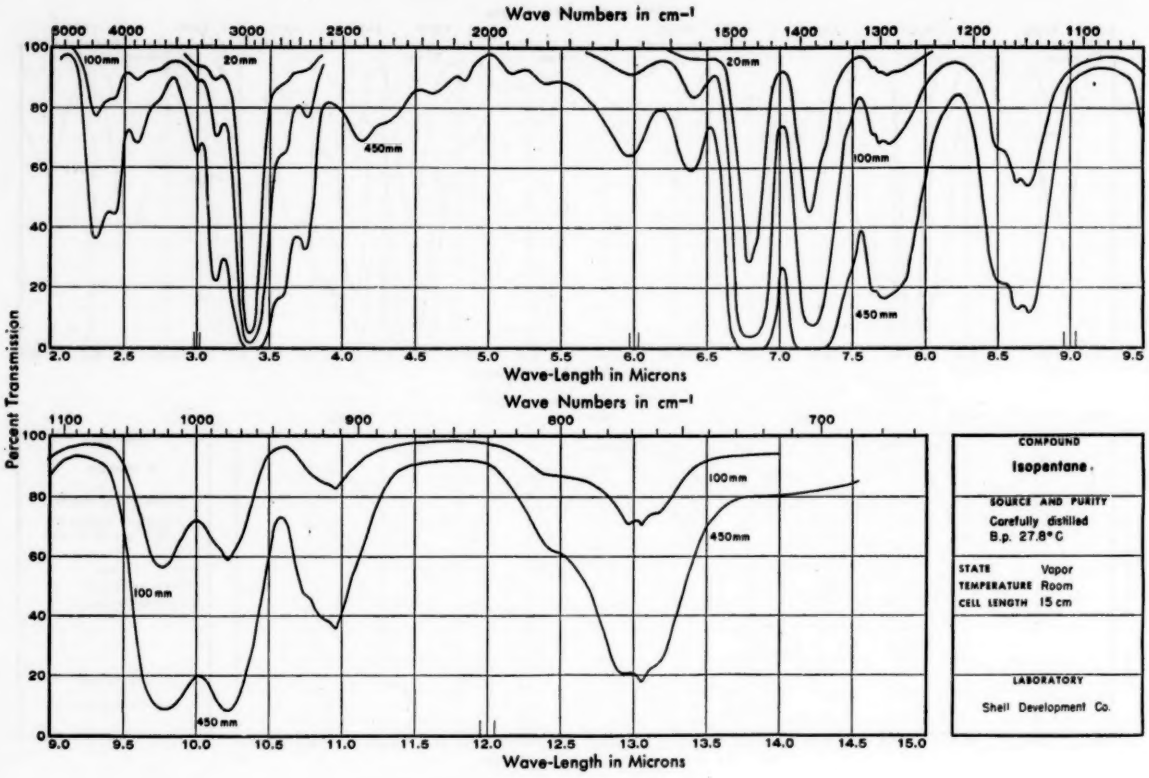

FIG. 6. Isopentane.

IV. ISOBUTANE AND NEOPENTANE

Isobutane and neopentane will be considered next, since there is no ambiguity in their structures and since with ethane and propane they form a related series obtained by successive substitution of methyl groups on methane.

Isobutane (symmetry C_{3v}) has vibrations of three symmetry types, A_1, A_2, and E, of which all three are Raman active and the A_1 and E infra-red active. Aside from the CH stretching and HCH bending vibrations and the methyl torsional oscillations, the following vibrations have to be assigned:

Skeletal:	CC stretching	A_1, E,
	CCC bending	A_1, E.
HCC bending:	CH_3 rocking (in planes through axis)	A_1, E,
	CH_3 rocking (perpendicular to planes through axis)	A_2, E,
	Tertiary CH wagging	E.

The observed frequencies are 371 (4) D, 437 (1) P (Raman[12]), and those given in Fig. 7. The Raman polarization data shown are from Ananthakrishnan.[12d] The infra-red band envelopes are unfortunately of little use in fixing the symmetry types of the absorption bands, since the molecule is sufficiently close to a spherical rotator that no

would indicate only a small interaction with the CH_3 vibrations. (3) Further, the exact position of these CH_2 chain bands are a function of the CH_2 chain length, irrespective of the groups (methyl or otherwise) that terminate the chain; whereas, an 1179-cm^{-1} band is observed with great constancy for all molecules of the type $(CH_3)_2CHR$(R = H or primary radical). (4) We have recently obtained spectra of 1-deutero- and 2-deuteropropane, and find for the 2-*d* compound a disappearance of the 748 cm^{-1}, a new band at 667 cm^{-1} appearing ascribable to the C − D wagging; whereas, for the 1-*d* compound a band is found with two Q branches at 743 and 702 cm^{-1}. While this splitting is not understood, it is clear that the deuterium substitution which has the profoundest effect on the 748-cm^{-1} band is that on the 2 position, not the 1.

The reason for Pitzer's assignment of the 748-cm^{-1} band as involving, at least partly, a CH_3 vibration follows mainly from a consideration of the ethane spectrum. It is definitely known that one of the CH_3 rocking motions of ethane is rather low (827 cm^{-1}), so it seems reasonable to expect analogous motions of the methyl groups of propane to be in this region. That this is seemingly not the case to any large extent must be ascribed simply to unforeseeable differences in kinetic interactions, and possibly also potential interactions, between the vibrations in the two cases.

TABLE I. Wave-length, frequencies, and intensities of absorption maxima of isobutane vapor. Intensities estimated in units of 10 percent absorption; s = shoulder.

$\lambda(\mu)$	$\omega(cm^{-1})$	I	$\lambda(\mu)$	$\omega(cm^{-1})$	I
2.31	4330	2	7.05	1418	1s
2.43	4115	1	7.16	1397	
2.61	3830	0	7.22	1385	9
3.00	3335	0	7.32	1361	
3.11	3215	1	7.475	1338	5
3.35	2985	9	7.53	1328	
3.40	2940		7.72	1295	0s
3.59	2785	1s	7.83	1277	0s
3.74	2675	1	8.08	1238	0
3.93	2545	0	8.16	1225	0
4.15	2410	0	8.21	1218	0s
4.36	2295	0	8.48	1179	7
4.59	2180	0	8.56	1168	
4.69	2130	0s	*ca.* 9.18	*ca.* 1090	0
5.04	1984	0	9.55	1047	0
5.21	1919	0	10.34	967	0
5.39	1855	1	10.77	929	2
5.44	1838		10.94	914	
5.67	1764	0s	12.29	814	
5.82	1718	1	12.52	799	1
6.04	1656	0s	12.77	783	
6.69	1495		13.62	734	
6.76	1479	9	*ca.* 14.1	*ca.* 710	1
6.83	1464				

TABLE II. Wave-length, frequencies, and intensities of absorption maxima of neopentane vapor. Intensities estimated in units of 10 percent absorption; s = shoulder.

$\lambda(\mu)$	$\omega(cm^{-1})$	I	$\lambda(\mu)$	$\omega(cm^{-1})$	I
2.31	4330	2	5.75	1739	0
2.38	4200	2	5.85	1709	
2.58	3875	0s	6.63	1508	
2.96	3380	1s	6.72	1488	10
3.085	3240	2	6.78	1475	
3.14	3185	0s	6.85	1460	
3.37	2965	10	7.22	1385	
3.63	2755	2s	7.27	1376	10
3.76	2660	0s	7.33	1364	
3.88	2575	0s	7.955	1257	9
4.10	2440	0	*ca.* 8.35	*ca.* 1200	1s
4.335	2305	1	8.71	1148	0
4.52	2210	0	10.105	990	0
4.74	2110	0	10.675	937	
5.025	1990	1	10.80	926	2
5.28	1894	0	10.91	917	
5.46	1832	1	11.98	835	0
5.53	1808	0s	12.16	822	
			14.03	713	0

significant difference is to be expected between parallel (A_1) and perpendicular (E) bands on the basis of Gerhard and Dennison's work[14] (moments of inertia: $A=B=83$, $C=110$ at wt. units$\times A^2$).

A skeletal vibrational assignment which is thought by the present author to be correct has been given by Ananthakrishnan.[12d] The polarization characters of the low frequency Raman lines indicate that the A_1 bending vibration is of frequency 437 cm^{-1} and the E of frequency 371 cm^{-1}. From its high Raman intensity and polarization character, the 799-cm^{-1} frequency corresponds to the symmetrical (A_1) CC stretching vibration. The antisymmetrical (E) CC stretching vibration was assigned to the moderately strong, depolarized 965-cm^{-1} Raman line on the basis of a central force calculation by Kohlrausch and Köppl.[12b] Since Bonner[15] had assigned the 1169-cm^{-1} line to this vibration, a more detailed force constant calculation was made here, using constants from ethane and propane and using the isobutane skeletal bending frequencies (see Appendix A for details). As illustrated in Fig. 8, the trend of calculated skeletal frequencies in the sequence ethane-propane-isobutane-neopentane offers a strong indication that the isobutane E vibration is to be assigned to the 965-cm^{-1} frequency and not the 1169-cm^{-1} one, despite the lack of close agreement between calculation and observation. A further point of interest is the extreme weakness of the CC stretching band in the infra-red at 965 cm^{-1}. In contradistinction to the Raman spectrum, where skeletal vibrations generally give rise to the strongest lines in the spectrum below 1350 cm^{-1}, these vibrations often give fairly weak infra-red bands. The HCC bending types, which are usually weak or missing in the Raman, are relatively strong in the infra-red.

Of the four methyl rocking frequencies, the 1169-cm^{-1} Raman line may be assigned, in view of its high Raman intensity, to the A_1 methyl rocking vibration. This is not contradictory to the fact that the line is depolarized, since El'yashevich and Vol'kenshtein[16] have indicated that totally symmetric bending vibrations may be highly depolarized. If the same explanation be applied here as was used for propane (i.e., that the higher methyl rocking frequencies are those in which the methyl groups approach each other most closely), then the A_1 vibration should be found, as suggested by the propane assignment, in the 1170 cm^{-1} region, since all methyl groups

[14] S. L. Gerhard and D. M. Dennison, Phys. Rev. **43**, 197 (1933).
[15] L. G. Bonner, J. Chem. Phys. **5**, 293 (1937).
[16] M. A. El'yashevich and V. V. Vol'kenshtein, Comptes rendus Acad. Sci. U.R.S.S. **41**, 366 (1943).

TABLE III. Wave-lengths, frequencies, and intensities of absorption maxima of *n*-butane vapor. Intensities estimated in units of 10 percent absorption; *s* = shoulder.

λ(μ)	ω(cm⁻¹)	*I*	λ(μ)	ω(cm⁻¹)	*I*
2.31	4330	2	7.43	1346	1
2.42	4130	1*s*	7.49	1335	
2.60	3845	0	7.67	1304	
2.71	3690	0	7.71	1297	2
2.96	3380	0*s*	7.76	1289	
3.14	3185	1*s*	*ca.* 8.04	*ca.* 1244	0
3.25	3075	0*s*	8.43	1186	0
3.37	2965	10	8.74	1144	1
3.59	2785	1*s*	8.82	1134	
3.73	2680	1*s*	8.89	1125	
3.93	2545	0	9.18	1089	0
4.09	2445	1	9.33	1072	0
ca. 4.26	*ca.* 2350	0*s*	*ca.* 10.1	*ca.* 990	5
ca. 4.54	*ca.* 2200	0	10.31	970	
4.70	2130	0	10.43	959	
4.89	2045	0	11.38	879	0
5.21	1919	0	12.58	795	0
5.52	1812	0	*ca.* 12.78	*ca.* 782	0*s*
ca. 5.95	*ca.* 1680	1	*ca.* 13.12	*ca.* 762	4
6.33	1580	0	13.32	751	
6.74	1484	9	13.50	741	
6.82	1466		13.63	734	
6.89	1451		*ca.* 13.98	*ca.* 715	
7.16	1397	7			
7.23	1383				

TABLE IV. Wave-lengths, frequencies, and intensities of absorption maxima of *n*-pentane vapor. Intensities estimated in units of 10 percent absorption; *s* = shoulder.

λ(μ)	ω(cm⁻¹)	*I*	λ(μ)	ω(cm⁻¹)	*I*
2.32	4310	2	7.19	1391	7
2.44	4100	1*s*	7.38	1355	1*s*
2.58	3875	0	7.44	1344	
2.68	3730	0	7.58	1319	2
2.76	3625	0*s*	7.65	1307	
2.96	3380	0*s*	7.85	1274	2
3.14	3185	1*s*	7.92	1263	
3.365	2970	10	8.07	1239	0*s*
3.59	2785	1*s*	8.71	1148	2
3.75	2665	1*s*	8.79	1138	
4.04	2475	0	9.30	1075	1
4.13	2420	1	9.40	1064	
4.23	2365	0*s*	9.67	1034	2
4.60	2175	0	9.78	1022	
4.91	2035	0	10.01	999	0*s*
5.21	1919	0	10.78	928	4
5.41	1848	0	10.915	916	
5.77	1733	0	11.09	902	
5.93	1686	1	11.58	864	2
6.42	1558	1*s*	12.94	773	0*s*
6.78	1475	10	13.52	740	4
6.83	1464		13.69	730	

approach each other simultaneously. The *E* vibrations involve approach of some groups but avoidance by others, so that their positions cannot be predicted. One of these must be the moderately intense 920-cm^{-1} infra-red band. The other is probably the strong 1179-cm^{-1} band. However, there is the possibility that this band represents the A_1 frequency, the difference from the Raman position being due to liquid-vapor shift. In this event, the other *E* frequency would probably be represented by one of the very weak bands in the 1000- to 1100-cm^{-1} region. The A_2 methyl rocking vibration, which is infra-red inactive and does not appear in the Raman spectrum although allowed, is of the type where methyl group hydrogens do not approach closely to one another and hence is probably of a frequency near 900 cm^{-1}.

The final vibration to be considered is the tertiary CH wagging. Since the propane CH_2 wagging vibration is found at 1338 cm^{-1}, the frequency represented by the Raman line at 1324 cm^{-1} and the infra-red band at 1335 cm^{-1} may logically be taken for this vibration. The fact that the Raman line is depolarized is consistent with this assignment. A force constant calculation similar to that for the methylene group of propane shows that this frequency is indeed expected to be high although, because of the approximations in the calculation, no significance can be given to the calculated value, 1113 cm^{-1} (details of the calculation are given in Appendix B).

The above assignment is presented in Table VI. The remainder of the weak infra-red bands shown in Figs. 2 and 7 are presumably overtones or different bands. No attempt has been made to assign these, since the existence of the two methyl torsional vibrations of very low and uncertain frequency makes this pointless.

For neopentane (symmetry T_d) the following vibrations are to be assigned:

Skeletal: CC stretching	A_1, T_2,
CCC bending	E, T_2,
HCC bending: CH_3 rocking	E, T_1, T_2,
Infra-red active:	T_2,
Raman active:	A_1, E, T_2,
Inactive:	T_1.

From central force field calculations and analogy with carbon tetrachloride, Kohlrausch[12b] and Rank and Bordner[12a] have assigned the four skeletal frequencies from Raman work as: stretching, 731 (A_1), 924 (T_2); bending, 332 (E),

415 (T_2). The infra-red spectrum is consistent with this (Figs. 3 and 7) in that the 731-cm^{-1} frequency does not appear, whereas the 924-cm^{-1} one does. Also an extension of the skeletal force constant calculations made for isobutane confirms the assignment, the calculated frequencies showing a trend in agreement with the above assignment (Fig. 8; see Appendix A for details of calculation).

Of the methyl rocking frequencies, the T_2 is clearly present as the strong infra-red band at 1257 cm^{-1} (Fig. 7). If it is assumed that the strong Raman line at 1250 cm^{-1} represents the same frequency, the other Raman-active rocking frequency (E) is unobserved, as is the inactive T_1. From the propane and isobutane assignments, one of these might be expected in the 900-cm^{-1} region and the other probably in the 1200-cm^{-1} region.

The assignment is recapitulated in Table VI. The remainder of weak infra-red bands are to be attributed to overtone or difference bands.

V. NORMAL BUTANE AND NORMAL PENTANE

These compounds introduce an additional possibility of uncertainty in that the carbon skeleton may be capable of existence in more than one configuration due to rotation about CC bonds. The question has not been settled as to whether, in *n*-butane for example, there are truly three potential minima (stable *trans*-form and two equivalent metastable skew-*cis*-forms) or whether due to the repulsion of the end methyl groups there is only one minimum (*trans*-form). The former assumption has been used by Pitzer[17] and by Aston and co-workers[18] in statistical calculations of thermodynamic functions. However, more recent attempts by Aston and coworkers to deduce the true form of the barrier to internal rotation indicate the possibility that there is only a single very shallow minimum corresponding to the *trans*-form.[19]

It is clear from the Raman work on liquid *n*-butane (e.g., see Fig. 7) that no single configuration will fit the spectrum, since many more lines are observed than are to be expected on the centrosymmetric *trans*-structure. Kohlrausch and Köppl[12b] and Pitzer[17] have assigned the observed lines on the basis of a mixture of the two stereoisomeric forms. However, it must be pointed out that conclusions from the Raman spectrum may be vitiated because of liquid-state interactions. Even if one assumes with Aston a single minimum potential curve in which the valley is very broad and shallow, it is to be expected that the molecule in the liquid will not oscillate freely in this valley but will be constrained by neighboring molecules to certain portions of the valley. Since the internal rotations do not separate in the kinetic energy from the other skeletal vibrations, this will result in a complex and ill defined liquid spectrum such as is actually observed in hydrocarbons with skeletal torsion.

The infra-red spectra of the vapors present a contrastingly simpler picture. In the region in which the skeletal stretching vibrations of normal paraffins are expected (roughly 800 to 1100 cm^{-1}),[20] *n*-butane has only a single band of appreciable intensity, at 962 cm^{-1} (Figs. 4 and 7). This is to be expected if the *trans*-structure is assumed as the only one present, since the sym-

TABLE V. Wave-lengths, frequencies, and intensities of absorption maxima of isopentane vapor. Intensities estimated in units of 10 percent absorption; s = shoulder.

$\lambda(\mu)$	ω(cm^{-1})	I	$\lambda(\mu)$	ω(cm^{-1})	I
2.27	4405	0s	7.21	1387	9
2.31	4330	2	7.32	1366	
2.43	4115	1s	7.49	1335	0s
2.59	3860	0	7.635	1310	3
2.73	3665	0	7.68	1302	
3.00	3335	0s	7.74	1292	
3.13	3195	1s	7.84	1276	
3.24	3085	0s	8.50	1176	
3.36	2975	10	8.63	1159	4
3.59	2785	1s	8.71	1148	
3.75	2665	1s	9.78	1022	
4.14	2415	1	10.13	987	4
4.35	2300	0s	10.225	978	
4.62	2165	0	10.77	929	
4.83	2070	0	10.87	920	2
5.15	1942	0	10.97	912	
5.89	1698	0	12.42	805	1s
5.97	1675	1	12.97	771	3
6.40	1563	1	13.065	765	
6.795	1472	10	13.18	759	
6.84	1462				

[17] E.g., K. S. Pitzer, J. Chem. Phys. **8**, 711 (1940).

[18] E.g., J. G. Aston and G. H. Messerly, J. Am. Chem. Soc. **62**, 1917 (1940).

[19] J. G. Aston, S. Isserow, G. J. Szasz, and R. M. Kennedy, J. Chem. Phys. **12**, 336 (1944).

[20] The limits of these vibrations for normal paraffins have been calculated, using various simplifying assumptions, by Pitzer (reference 17) and L. Kellner, Trans. Faraday Soc. **41**, 217 (1945), among others. Inspection of the Raman spectra given by Kohlrausch and Köppl (reference 12b) leads to the limits quoted, with which the calculations are in approximate agreement.

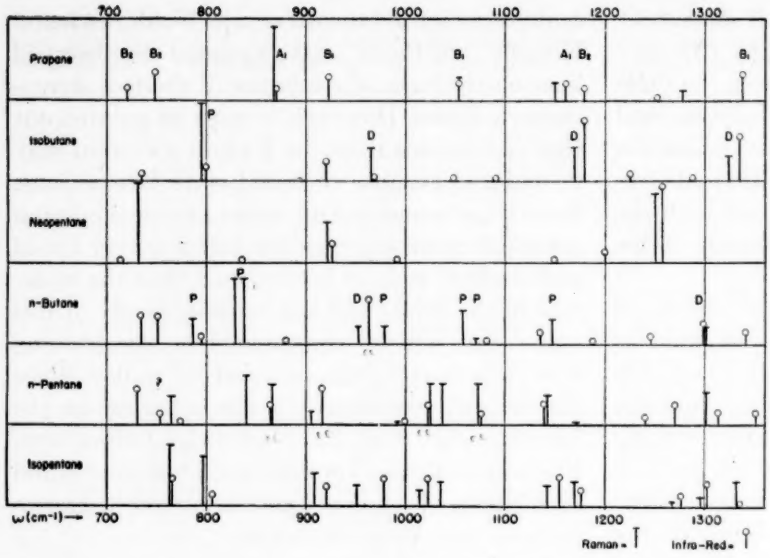

FIG. 7. Observed infra-red and Raman frequencies.

metry (C_{2h}) allows only the B_u CC stretching frequency to appear in the infra-red, the other two (A_g) frequencies being forbidden. Similarly, *n*-pentane, which—like *n*-butane—exhibits more Raman lines in the liquid than can be accounted for by any single structure, has the correct number of infra-red bands in the vapor if the all-*trans*-planar structure is assumed; all four CC stretching frequencies should be infra-red active, and four bands are found (864, 916, 1022, and 1075 cm^{-1}; Figs. 5 and 7). However, assignment of these four bands as the four skeletal frequencies is highly uncertain, since one or more may be overtone or difference bands, or methyl rocking fundamentals. Interpolation between these *n*-pentane frequencies and the propane skeletal frequencies leads to probable values of 865 cm^{-1} and 1070 cm^{-1} for the vapor-phase frequencies of the two infra-red inactive *n*-butane skeletal vibrations.

The HCC bending frequencies in both *n*-butane and *n*-pentane fit rather well with the pattern indicated by the propane assignment. On the basis of the *trans*-forms for these two molecules in the vapor state, frequencies of the following symmetries are expected:

	n-butane (C_{2h})	*n*-pentane (C_{2v})
CH_2 rocking	A_u, B_g	A_2, $2B_2$
CH_2 twisting	A_u, B_g	$2A_2$, B_2
CH_2 wagging	A_g, B_u	A_1, $2B_1$
CH_3 rocking (in-plane)	A_g, B_u	A_1, B_1
CH_3 rocking (out-of-plane)	A_u, A_g	A_2, B_2
IR active	A_u, B_u	A_1, B_1, B_2
Raman active	A_g, B_g	A_1, A_2, B_1, B_2

Symmetry designations for *n*-butane:

	Reflection	Inversion
A_g	+	+
A_u	−	−
B_g	−	+
B_u	+	−

Symmetry designations for *n*-pentane: same as for propane (see Section III).

For *n*-butane, one CH_2 rocking frequency is expected in the infra-red, in the 750 cm^{-1} region. The band observed here is of a peculiar shape, exhibiting two *Q* branch-like maxima and seeming to be a superposition of two close bands of A_u symmetry.[21] It is possible that one of these is the true fundamental and the other a band of the $(\nu+\nu_t)-\nu_t$ type, where ν_t is, say, the thermally excited methyl torsion frequency of A_u symmetry, which might interact strongly with the A_u CH_2 rocking vibration. For *n*-pentane, two infra-red bands are to be expected in this region. The observed absorption shows a single strong maximum, but some asymmetrical broadening on the short wave-length side indicates a possible weaker band here (Fig. 5). For both *n*-butane and *n*-pentane, the Raman lines shown at 760 to 800 cm^{-1} in Fig. 7 are believed to be caused by skeletal vibrations of non-planar forms and not to CH_2 rocking vibrations. This

[21] Like the B_1 bands of propane, the A_u bands of *trans*-*n*-butane should exhibit weak, stubby *Q* branches, and *P* and *R* branches with ill defined shoulders. The B_u bands, on the other hand, should have well defined *P* and *R* branches, but the resolution of the spectrograph is not adequate to demonstrate this on the bands shown in Fig. 4.

follows from the fact that the 786-cm^{-1} line in *n*-butane is polarized and hence cannot be the B_g CH_2 rocking fundamental, and also that higher *n*-paraffins do not exhibit strong Raman lines in the 600 to 800-cm^{-1} region. As has been noted with propane, Raman lines associated with many HCC bending vibrations are not observed because of weakness.

The CH_2 twisting frequencies (propane: 1278 cm^{-1}) would be expected to be weak in the infra-red even though the over-all symmetry allows their appearance, since to a first approximation these motions involve no dipole changes. As mentioned above, the characteristic Raman shifts at 1300 cm^{-1} in *n*-paraffins[12b] may be ascribed to this type of vibration. In *n*-butane, the 1297-cm^{-1} band may be assigned to the infra-red active A_u twisting vibration, but in *n*-pentane (Fig. 7) and higher hydrocarbons[4] there are no obvious infra-red analogs of the 1300 cm^{-1} Raman lines, probably because of the weakness of the infra-red counterparts and because of the overlapping of the stronger CH_2 wagging types.

The CH_2 wagging frequencies (propane: 1338 cm^{-1}) should yield one infra-red band for *n*-butane and three for *n*-pentane. The observed spectra fit this expectation adequately; *n*-butane shows a band at 1340 cm^{-1}, and *n*-pentane shows three at 1350 cm^{-1}, 1313 cm^{-1}, and 1269 cm^{-1}. If this interpretation is accepted, it is clear that a reasonable spreading apart of the wagging frequencies has occurred, due to both kinetic and potential interactions.

Regarding the methyl rocking frequencies, two considerations are to be noted initially. Firstly, in *n*-butane and higher *n*-paraffins the end methyl groups are sufficiently separated that very little interaction between them is to be expected. Hence, the symmetric and antisymmetric combinations of which one would usually speak become indistinguishable, and very little separation in their frequencies will occur. Secondly, the assignment in propane indicates that the difference to be expected between methyl rocking frequencies for in-plane and out-of-plane rocking motions is small, of the order of only 20 cm^{-1} (the plane referred to is the carbon plane).

The only bands so far lacking assignment in the *n*-butane and *n*-pentane spectra are those in the 1140-cm^{-1} region (Fig. 7), and in view of the fact that some of the propane methyl-rocking frequencies occur near here, it becomes plausible to assign all the methyl rocking vibrations to this frequency region. Owing to lack of resolution, it is not possible to observe whether there are the correct number of infra-red bands in this region. The possibility cannot be excluded, however, that the 1140-cm^{-1} frequencies represent only one set of methyl rocking bands (in-plane or out-of-plane) and that the other occurs at lower frequencies, in among the skeletal stretching frequencies.

The *n*-butane and *n*-pentane assignments discussed above are recapitulated in Table VI.

VI. ISOPENTANE

The spectrum of this molecule can be interpreted in a satisfactory fashion in light of the considerations given above. Internal skeletal torsion is present here also, so that the same difficulties arise in interpreting the Raman spectrum of the liquid in the CC stretching vibration region as were noted for *n*-butane and *n*-pentane. Hence, no further attempt will be made to discuss these except to note that both Raman and infra-red spectra indicate a skeletal frequency near 800 cm^{-1}, close to the symmetrical (A_1) isobutane skeletal frequency and hence presumably representing an analogous motion in isopentane.

The CH_2 rocking vibration appears as a moderately strong infra-red band at 765 cm^{-1}. The Raman line occurring at this position (Fig.

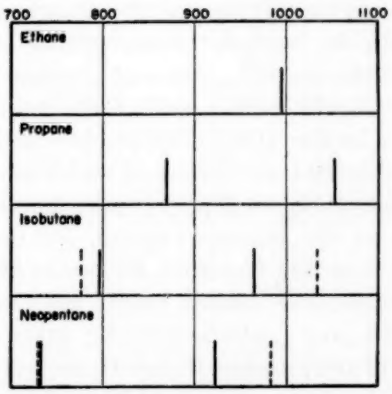

FIG. 8. Calculated (full line) and observed (broken line) skeletal stretching frequencies.

TABLE VI. Frequency assignments for paraffin hydrocarbons. Frequencies in cm^{-1} ( ) signifies estimated value.

Type vibration	Propane	Isobutane	Neopentane	*n*-Butane (*trans*)	*n*-Pentane (*trans*)	Isopentane	Higher paraffins
CC stretching	870 (A_1) 1053 (B_1)	799 (A_1) 965 (E)	731 (A_1) 924 (T_2)	(~865) (A_g) 962 (B_u) (~1070) (A_g)	864 (A_1) 916 (B_1) 1022 (A_1) 1075 (B_1)	800 3 at 850–1050	*n*-Paraffins and *n*-alkyl chains: one frequency per CC bond, filling the range 800–1100 cm^{-1}; branched structures, one or more $\leq$800 cm^{-1}
CH_2 rocking	748 (B_2)			740 (A_u) (~770) (B_g)	730 (B_2) (~760) (B_2) (~800) (A_2)	765	One per CH_2, 720–790 cm^{-1}
CH_2 twisting	1278 (A_2)			1297 (A_u) 1300 (B_g)	3 at 1300 ($2A_2+B_2$)	1300	One per CH_2, ~1300 cm^{-1}
CH_2 wagging	1338 (B_1)			1340 (B_u) (~1300) (A_g)	1350 1313 (A_2+2B_1) 1269	1270	One per CH_2, 1200–1350 cm^{-1}
CH wagging		1335 (E)				1334	Two per CH, 1300–1350 cm^{-1}
CH_3 rocking	922 (B_1) (~900) (A_2) 1160 (A_1) 1179 (B_2)	920 (E) (~900) (A_2) 1170 (A_1) 1179 (E)	(~900) (~1200) ($E+T_1$) 1257 (T_2)	1134 (~1140) (A_u+B_u) 1146 (~1140) (A_g+B_g)	4 at ~1140 ($A_1+A_2+B_1+B_2$)	(~900) 920 2 at ~1140 1164 1176	Terminal on ethyl or longer alkyl chain: two per CH_3, ~1150 cm^{-1}; methyl on tertiary carbon: two per CH_3, ~900 and ~1170 cm^{-1}; methyl on quaternary carbon: two per CH_3, 900–1250 cm^{-1}

7) is believed to represent one of the skeletal vibrations, since higher isoparaffins show no strong Raman lines in this region (600 to 800 cm^{-1}), whereas the strong infra-red bands, attributable to CH_2 rocking vibrations, persist. The CH_2 twisting and wagging vibrations may be reasonably assigned to the infra-red bands and Raman lines near 1270 cm^{-1} and 1300 cm^{-1}. By analogy with isobutane, the tertiary CH wagging vibration may be taken to be represented by the 1134-cm^{-1} frequency.

As to the methyl rock frequencies, the methyl of the ethyl group would be expected to be not greatly different from that of *n*-butane and to exhibit its rocking frequencies near 1150 cm^{-1}. The two methyl groups on the branched end of the molecule bear the same relation to each other as the methyl groups of propane and by analogy should exhibit two of the rocking frequencies in the 1150- to 1180-cm^{-1} region and two in the 900-cm^{-1} region, of which one should be unobservably weak. That such bands, attributable to the isopropyl group, are present is evident from the fact that all isoparaffins (i.e., 2-methylalkanes) exhibit bands near 920 cm^{-1} and 1175 cm^{-1}, which may be taken as the analogs of the propane B_1 and B_2 methyl rocking bands. The 920-cm^{-1} and 1176-cm^{-1} isopentane bands may then be ascribed to the same origin. This frequency assignment is recapitulated in Table VI.

VII. EXTENSION TO HIGHER PARAFFINS

As noted in various places above, several of the conclusions receive confirmation when the spectra of higher paraffins are examined.

In view of the ambiguities of structure of most higher paraffins due to possibilities of internal rotation of the carbon skeleton, little can be said regarding the skeletal vibrations. However, it is apparent from the richness of the Raman spectra in the region 800 to 1100 cm^{-1},[22] that most of the skeletal vibrations lie in this range. Infra-red spectra also (generally of the liquid state, as with the Raman work) show great complexity and lack of regularity in this region. Branched structures show one or more strong Raman lines near 800 cm^{-1} or lower, ascribable to low frequency skeletal vibrations analogous to those observed in the branched molecules isobutane (799 cm^{-1}) and neopentane (731 cm^{-1}).

In line with the interpretations given above for HCC bending vibrations, the strong infra-red bands in the 720- to 790-cm^{-1} range, which are an obvious feature of most paraffin spectra, are

[22] E.g., see reference 12b, and E. J. Rosenbaum, A. V. Grosse, and H. F. Jacobson, J. Am. Chem. Soc. **61**, 689 (1939).

TABLE VII. Force constants for skeletal frequency calculations of isobutane and neopentane.

Constant		Calculated value, 10^5 dynes/cm	Source of calculated value
K_c	C−C stretching	4.36[a]	Ethane C−C stretching frequency at 993 cm^{-1}
k_1	C−C stretching: C−C stretching interaction for adjacent bonds	0.20	From propane skeletal frequencies at 374, 870, and 1053 cm^{-1} (see Section III)
H_c	C−C−C bending	0.35[b]	
g_1	C−C stretching: C−C−C bending interaction for a C−C−C angle and an included C−C bond	0.35[b]	
h_1	C−C−C bending: C−C−C bending interaction for angles with a C−C bond in common	0.10[b]	Isobutane skeletal bending frequency at 434 cm^{-1}

[a] In order to allow for the known lowering in C−C bond strength in propane, isobutane, and neopentane over ethane, this value was decreased for these molecules proportionately to the decrease in total bond energy as determined from electron impact measurements. The values so obtained are: propane, $4.24 \cdot 10^5$; isobutane, $4.15 \cdot 10^5$; and neopentane, $4.10 \cdot 10^5$ dynes/cm. The decrease in force constants for this sequence of molecules was noted by Kohlrausch and Köppl (see reference 12b). The electron impact data from which the above adjustment was calculated are from D. P. Stevenson and J. A. Hipple, J. Am. Chem. Soc. 64, 1588 (1942).

[b] These constants refer to bending coordinates which are angular displacements multiplied by the equilibrium C−C distance, and hence carry the same units as linear displacement coordinates.

ascribed to CH_2 rocking vibrations, and, in fact, positions of the strongest bands in this region can be nicely correlated with the lengths of CH_2 chains present. The group of bands of moderate intensity found in the range 1200 to 1300 cm^{-1} is ascribable to CH_2 wagging and twisting and to tertiary CH wagging vibrations. In general, the simpler compounds show only a few bands in these regions (as with the assignments discussed in detail above), but as more complex compounds are considered (containing more CH_2 or CH groups) bands become more numerous and fill up the intervals.

Methyl rocking vibrations of higher paraffins are to be found, in accordance with the discussion given previously, in the region near 1150 cm^{-1}. This accords with the observed spectra[4] in that bands are found in this region which are, in general, stronger and more numerous for compounds with more methyl groups and whose positions can be correlated with various arrangements of methyl groups.[23] For those arrangements where methyl groups are adjacent, as two methyl groups on a tertiary carbon, some of the methyl rocking frequencies may be expected to occur also in the lower frequency region near 900 cm^{-1}, as typified by propane and isobutane.

An exception to the above methyl rocking positions occurs when two or more methyl groups are attached to a quaternary carbon. These compounds exhibit strong bands in the 1200- to 1250-cm^{-1} region, which from the assignment in neopentane are to be attributed to methyl rocking vibrations of the quaternary methyl groups. A qualitative explanation of this shift to higher frequencies is at hand in the fact that methyl groups attached to secondary or tertiary carbons can, by expansion of CCC angles, push themselves away from the remainder of the molecule. Quaternary methyl groups, on the other hand, are constrained to closer contact with adjacent groups and hence suffer increased repulsion, which results in increased methyl rocking frequencies. Two lines of evidence support this concept: the CCC angle in propane and isobutane is shown by electron diffraction studies to be greater than tetrahedral,[24] presumably due to methyl group repulsion, and the barrier to methyl torsion is greater in neopentane than in either propane or isobutane, arising from the increased interaction due to closer neighbors.[25]

VIII. CONCLUDING REMARKS

Table VI shows, along with the specific frequency assignments discussed earlier, the general

[23] A. Y. Mottlau, Serial No. 26, American Petroleum Institute Hydrocarbon Research Project, Ohio State University Research Foundation, Columbus, Ohio; the same correlations have been independently noted by Dr. G. B. B. M. Sutherland and Dr. H. W. Thompson in Great Britain (private communication) and by ourselves.

[24] L. Pauling and L. O. Brockway, J. Am. Chem. Soc. **59**, 1223 (1937); J. G. Beach and J. Walter, J. Chem. Phys. **8**, 303 (1940).

[25] E.g., see discussion given by F. A. French and R. S. Rasmussen, J. Chem. Phys. **14**, 389 (1946).

TABLE VIII. Force constants for HCC bending frequency calculations.

Constant	Type	Calculated value, 10^5 dynes/cm	Source of calculated value
K_c	Same as Table VII	4.45[b]	See reference a
k_1	Same as Table VII	0.20	See Table VII
H_c	Same as Table VII	0.35[c]	See Table VII
h_1	Same as Table VII	0.10[c]	See Table VII
g_1	Same as Table VII	0.35[c]	See Table VII
H_H	H−C−H bending	0.42[c]	From methane 1306 and 1500 cm^{-1} frequencies[d]
h_2	H−C−H bending: H−C−H bending interaction for angles with a C−H bond in common	−0.01[c]	
H_{CH}	H−C−C bending	0.43[c]	From ethane frequencies at 821, 993, 1374, 1379, and 1480 cm^{-1} [d]
h_3	H−C−H bending: H−C−C bending interaction for angles with a C−H bond in common	−0.05[c]	
h_4	H−C−C bending: H−C−C bending interaction for angles at the same end of a common C−C bond	−0.05[c]	
g_2	C−C stretching: H−C−C bending interaction for an H−C−C angle and included C−C bond	0.18[c]	Assumed equal to h_3 and h_4
h_5	H−C−C bending: H−C−C bending interaction for angles with a C−H bond in common	−0.05[c]	
h_6	C−C−C bending: H−C−C bending interaction for angles with a C−C bond in common	−0.05[c]	

[a] Taken as the average between the constant calculated from the full ethane treatment and that from the diatomic-molecule approximation. In the propane and isobutane models to which these constants are applied, one end of a C−C bond follows the diatomic approximation (i.e., the methyl is considered a point mass) while the other end follows the full treatment.
[b] For use in propane and isobutane, this value was modified in the fashion described in Table VII, footnote a.
[c] The constants refer to bending coordinates which are angular displacements multiplied by the equilibrium C−H distance (in the case of H−C−H and H−C−C angles) or by the equilibrium C−C distance (in the case of C−C−C angles). This procedure gives the coordinates and constants the same units as with linear displacement coordinates.
[d] Essentially the same values as given by Herzberg (reference 1).

regions in which various types of vibrations may be expected in more complicated molecules. These have been found of use in thermodynamic calculations, since they give a much more accurate distribution of vibrational levels than has hitherto been available. For this purpose they are also applicable, with sufficient accuracy for the purpose, to the hydrocarbon portions of nonhydrocarbon compounds. Further use has been made of the assignments in gaining some knowledge of the structures of complex molecules, or compositions of complex hydrocarbon mixtures, particularly by making use of the correlations mentioned in the preceding section.

It is realized that the considerations employed here represent to some extent a fitting of facts into an oversimplified scheme, particularly as regards the assignment of observed frequencies to single vibration types. The justification for this procedure is that a certain degree of order can be attained and useful correlations made. Further work is contemplated toward verifying the assignments given, mainly by examination of deuterated compounds, and toward extension of the same type of treatment to other classes of organic compounds.

ACKNOWLEDGMENTS

The author expresses his appreciation to Mr. P. S. Zucco for operation of the spectrograph and assistance with the calculations, to Mr. D. H. Merrill for assistance with the calculations, and to Mrs. L. B. Scharton for drawing the figures.

APPENDIX A

Skeletal Force Constant Calculations on Ethane Propane, Isobutane, and Neopentane

These calculations were made under the usual assumption that CH_3, CH_2, and CH groups could be treated as point masses, hydrogen vibrations being ignored. Tetrahedral carbon angles were assumed, the small error introduced in the cases of propane and isobutane being considered negligible.

The method of Wilson[7] was used for setting up the inverse kinetic energy matrices (G matrices) in terms of suitable symmetry coordinates. The matrix terms were evaluated numerically, and subsequent operations (ob-

taining, expanding, and solving the secular determinants) were carried out numerically.

The force constants given in Table VII were evaluated from known frequencies of ethane, propane, as shown in the table. The frequencies calculated from these force constants, which are discussed in Sections III and IV are:

Isobutane:	A_1	776 cm^{-1}
		(434)
	E	1034
		369
Neopentane:	A_1	729 cm^{-1}
	E	230
	T_2	983
		422

APPENDIX B

HCC Bending Force Constant Calculations on Propane and Isobutane

In the models used, the CH_3 groups were considered as point masses, but the secondary and tertiary hydrogens were included in the calculations. The methods used were the same as those described in Appendix A, with the additional simplification that the CH stretching force constants were set equal to infinity and the CH stretching vibrations were separated from the others and subsequently ignored, according to the procedure given by Wilson.[7]

In order to obtain suitable force constants for use with these models, calculations were made under similar assumptions on methane and ethane. The force constants used, and their sources, are given in Table VIII. The calculated frequencies, which are discussed in Sections III and IV, are:

Propane:	A_1	898 cm^{-1} (C−C stretching)
		1467 (HCH bending)
		427 (C−C−C bending)
	A_2	1175 (CH_2 twisting)
	B_1	998 (C−C stretching)
		1205 (CH_2 wagging)
	B_2	761 (CH_2 rocking)
Isobutane:	A_1	821 cm^{-1} (C−C stretching)
		571 (C−C−C bending)
	E	994 (C−C stretching)
		319 (C−C−C bending)
		1113 (CH wagging)

THE JOURNAL OF CHEMICAL PHYSICS VOLUME 16, NUMBER 7 JULY, 1948

The Nature of Bond Orbitals in Quadricovalent Complexes of Transition Elements*

HANS KUHN**
Gates and Crellin Laboratories, California Institute of Technology, Pasadena, California
(Received April 7, 1948)

In quadricovalent complexes of transition elements (Ni^{II}, Pd^{II}, Pt^{II}, Au^{III}, Ag^{II}, Cu^{II}) the central atom uses four s or d orbitals of its outer shell for unshared electron pairs and two s or d and two p orbitals for bond formation. The problem here is to find the strongest possible four hybrid bond orbitals obtained by combining the two $s-d$ and the two p orbitals available for bond formation. The strongest bond orbitals thus obtained are directed from the middle towards the four corners of a square, as it is expected from experimental evidence; they are composed of 4/9 s, 14/9 d, and two p orbitals, the strength being 2.943. These strongest possible orbitals are presumably used in complex of Ni^{II}, Pt^{II}, Au^{III}, and Cu^{II}, but probably not in complexes of Pd^{II} and Ag^{II}; in the latter two cases there must be assumed square bond orbitals of composition $s^n d^{2-n} p^2$ with n somewhere between 1 and 4/9, i.e., orbitals of character between that of the strongest square bond orbitals of composition $s^{4/9} d^{14/9} p^2$ mentioned above and that of sdp^2 square orbitals discovered by Pauling.

1. INTRODUCTION

THE problem of directed valence was first developed by Pauling[1] and Slater.[2] Pauling formulated a very simple method of discussing the bond-forming power of an atomic bond orbital. The fundamental assumption of this method is that in the case of bond orbitals with the same or nearly the same radial part of the wave function the magnitude of the angular part of a bond along the bond axis (that is, in the direction of the ligand) is a measure of its relative bond-forming power.

* Contribution No. 1187 from Gates and Crellin Laboratories.
** Present address: Institute of Physical Chemistry of the University of Basel, Basel, Switzerland.
[1] L. Pauling, J. Am. Chem. Soc. **53**, 1367 (1931); *The Nature of the Chemical Bond* (Cornell University Press, Ithaca, New York, 1945), second edition.
[2] J. C. Slater, Phys. Rev. **37**, 481 (1931).

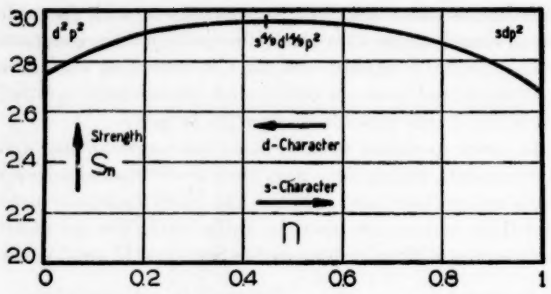

FIG. 1. Square bond orbitals. Plot of the strength, S_n, against the amount, n, of s orbitals involved. As there are exactly two p orbitals involved in each square arrangement, the amount of d orbitals is $2-n$, the arrangement thus being $s^n d^{2-n} p^2$.

The bond-forming power or strength S of an s orbital defined in this way is 1, that of a p orbital $\sqrt{3}$, and that of the best d orbital $(5)^{\frac{1}{2}}$.

Pauling has shown that it is possible, by combining s and p or s, p, and d orbitals, to obtain a number of strong bond orbitals (i.e., orbitals with large S). For example, he has found combinations of s and p orbitals which are directed towards the corners of a tetrahedron, combinations of s, p, and d orbitals which are directed toward the corners of a square, and other combinations which are directed towards the corners of an octahedron.

An important result of Pauling's approach is that the four sp orbitals in the directions of the corners of a regular tetrahedron are the strongest possible combinations of s and p orbitals. Thus the tetrahedral valence of carbon and similar elements has found a simple explanation.

In contrast to carbon are the B group elements such as Ni^{II}, Pd^{II}, Pt^{II}, Cu^{II}, and Au^{III}, surrounded by four electronegative atoms generally in a square, and not tetrahedral, arrangement. Pauling has shown that four rather strong bond orbitals with strength $S=2.694$ can be constructed for this square arrangement by hybridization of one s, one d, and two p orbitals.

The question as to whether or not the square bond orbitals discussed by Pauling are the strongest possible four hybrid orbitals has not before been answered. We may think of the possibility of constructing four stronger spd orbitals than the square orbitals; it must be decided whether or not the concept of bond strength enables us to exclude other arrangements as less stable, such as a tetrahedral or a tetragonal pyramidal arrangement.

2. ELECTRONIC STRUCTURE AND BOND ARRANGEMENT OF QUADRICOVALENT COMPLEXES OF TRANSITION ELEMENTS

a. Square Complexes of Ni^{II}, Pt^{II}, and Au^{III}

Let us look at a covalent complex of bivalent nickel, such as the nickel cyanide ion $[Ni(CN)_4]^{--}$. The twenty-six electrons of Ni^{II} can be placed in the following way: 18 electrons can be placed in the $1s$, $2s$, three $2p$, $3s$, and three $3p$ orbitals; for the other eight electrons six orbitals, namely, the five $3d$ orbitals and the almost equally stable $4s$ orbital, are available, and four of these orbitals may be occupied by electron pairs.[3]

This leaves available for use in bond formation two orbitals of the $3d$–$4s$ shell as well as the three $4p$ orbitals, which are somewhat less stable than the $3d$ and $4s$ orbitals.[4,5] As four bonds are to be formed, the smallest possible amount of unstable $4p$ orbitals, namely two, should be used. We are left with the problem of determining the geometric arrangement of the four strongest spd hybrid orbitals that can be formed from two p and two s–d orbitals and that are, at the same time, orthogonal to four orbitals with pure $4s$ and $3d$ character (these orbitals being filled with eight electrons of the nickel shell) and to a pure p orbital (this orbital being empty).

For this purpose we shall discuss several geometrical arrangements of four spd bond orbitals, and we shall find that of all arrangements of equivalent orbitals only square arrangements have, in fact, the property stated above of being orthogonal to four s–d orbitals and one p orbital. In Fig. 1 the strength, S_n, of these orbitals as ordinate is plotted against the amount, n, of involved s orbital as abscissa. The square orbitals

[3] The nearly equal stability of $3d$ and $4s$ follows from the position of atomic spectral terms in nickel. The ground state of nickel is a ^3F state corresponding to a configuration $3d^8 4s^2$; the lowest excited state ^3D, corresponding to a structure $3d^9 4s$, is only 0.58 kcal./mole above the ground state (see reference 4). As this energy difference is small compared to any covalent bond energy, it can be neglected in our treatment and $4s$ and $3d$ can be regarded as equally stable.

[4] The difference in stability of $4s$ and $4p$ orbitals may be seen from the spectral terms of nickel. The $^3P^\circ$ term corresponding to the electronic structure $3d^9 4p$ is 81 kcal./mole above the state $3d^9 4s\ ^3D$ (see reference 5).

[5] R. F. Bacher and S. Goudsmit, *Atomic Energy States* (McGraw-Hill Book Company, New York, 1932).

that must be assumed to be actually used in covalent complexes of bivalent nickel are the orbitals with maximum strength. These orbitals are composed of 0.44 s, 1.56 d, and 2.00 p orbitals, the strength of each orbital being 2.943.

These strongest square orbitals are presumably also used in covalent complexes of Pt^{II} and Au^{III}. There is the same number of electrons involved in the outmost $5d$–$6s$ shell of Pt^{II} and Au^{III} as in the $3d$–$4s$ shell of Ni^{II} and furthermore it can be assumed[6] that the $5d$ and $6s$ orbitals are nearly equal in stability, as are $3d$ and $4s$ in nickel; therefore, the same discussion is applicable.

b. Complexes of Pd^{II}

A somewhat different case is found in square complexes of Pd^{II}. The $4d$ and $5s$ orbitals in Pd cannot be assumed as equally stable. If we place 36 of the 44 electrons of Pd^{II} in the inner shells and the other 8 electrons in four of the five $4d$ orbitals, we obtain a state which is, by about 50 kcal./mole, more stable than the state containing the four electron pairs in the $5s$ and in three of the five $4d$ orbitals.[7] In bond formation, hence, there will be a tendency to use as much of the stable $4d$ orbitals as possible for unshared pairs, leaving the less stable $5s$ and $5p$ as well as one of the $4d$ orbitals for bond formation; this tendency by itself would lead to the sp^2d square arrangement found by Pauling.[1] On the other hand, there will be, as in the cases discussed above, a tendency to use the strongest possible bond orbitals, i.e., the $s^{0.44}d^{1.56}p^2$ square bond orbitals. In consequence a compromise will be reached; the bond orbitals will utilize less than one and more than 0.44 s orbital; we will thus have $s^nd^{2-n}p^2$ square bond orbitals with n somewhere between 1 and 0.44 (see Fig. 1).

The value of n in a given case can be found by the following treatment:

We shall first assume that sp^2d square orbitals are used for bond formation, then we shall replace these orbitals by $s^np^2d^{2-n}$ bond orbitals, n being arbitrary within the limits 0 and 1. The energy difference which is involved in this replacement produces the sum of two parts.

On one hand, the strength of the bond orbitals and therefore the covalent bond energy is changed. Let us denote by $W_{n=1}$ the energy of a bond between the central atom and one of its ligands in the case where the sp^2d square orbitals of strength $S_{n=1}=2.694$ are used in bond formation. The bond energy that has to be assumed in case that the central atom uses $s^np^2d^{2-n}$ bond orbitals of strength S_n is then equal to $W_n=W_{n=1}\cdot(S_n^2/S_{n=1}^2)$. This follows from a theorem by Pauling, according to which the energy of a bond is proportional to the product of the squares of the strengths of the orbitals of the two atoms involved. Hence, the change of bond energy in the replacement that we are considering (formation of four bonds involving $s^np^2d^{2-n}$ square orbitals instead of bonds involving sp^2d orbitals) is equal to $4W_{n=1}((S_n^2/S_{n=1}^2)-1)$.

On the other hand, the electronic energy is changed in the replacement under consideration. At first, when sp^2d orbitals are used in bond formation no unstable s orbital is used for unshared pairs. However, when $s^np^2d^{2-n}$ bond orbitals are used, an amount $(1-n)$ of an s orbital is needed for unshared pairs. The interaction energy of a shared pair is in the case of a pure covalent bond the same as that of a single unshared electron;[1] therefore, the energy required for the interchange of $(1-n)$ shared pairs and $(1-n)$ unshared pairs between s and d orbitals is equal to $(1-n)\Delta E$, ΔE being the $s-d$ separation energy, i.e., the energy required for the transport of one electron from the d into the less stable s orbital. Assuming, however, that there are not pure covalent bonds between the central atom and its ligands but bonds with, say, 100-P percent ionic character (the attached atoms being more electronegative than the central atom), the interaction energy of a shared pair with the central atom is equal to that of only P percent of a single electron. The energy required for the interchange of a shared and an unshared pair between s and d orbitals is thus equal to $(2-P/100)\Delta E$ and the energy required for interchanging $(1-n)$ shared and unshared pairs equal to $(1-n)(2-P/100)\Delta E$.

Therefore, the total energy increase ΔU in the replacement under consideration is given by

$$\Delta U=-4W_{n=1}((S_n^2/S_{n=0}^2)-1)+\Delta E(1-n)(2-P/100).$$

The n value actually used in bond orbital formation is obtained by minimizing ΔU in respect to n. We obtain:

$$(2-P/100)(\Delta E/W_{n=1})=-(8/S_{n=0}^2)S_n(dS_n/dn).$$

By substituting S_n from Eqs. (10) and (10a) mentioned later we obtain the following values of n for various values

---

[6] From the atomic spectra of platinum it can be seen (see reference 4) that the excited state $5d^96s\ ^3D$ is only 2.35 kcal./mole above the ground state $5d^86s^2\ ^3F$.

The difference in stability between $6s$ and $6p$ orbitals in Pt may be of interest. The state $5d^96p\ ^3P$ is not known in platinum, but it can be estimated that this state is, as in the case of nickel, about 80–90 kcal./mole less stable than the state $5d^96s\ ^3D$. (This is seen in the following way: the energy difference between the $d^9s\ ^3D$ and the $d^9p\ ^3P$ states in the sequence Ni, Cu^{+1}, Zn^{+2} are 81, 126, 170 kcal./mole, respectively; the corresponding energy values for Au^{+1} and Hg^{+2} are 137 and 173 kcal./mole, respectively (see reference 4); the value in the case of Pt, the element next to the left of Au in the periodic table, is thus found by extrapolation to be about 90 kcal./mole.)

[7] This can be concluded from the atomic spectral terms of Pd. The energy difference between the state $4d^95s\ ^3D$ and the higher state $4d^85s^2\ ^3F$ is 52.8 kcal./mole in Pd. (See reference 4.)

of $\Delta E/W_{n-1}\times(2-P/100)$:

$(\Delta E/W_{n-1})(2-P/100)$	n
0.0	4/9
0.27	5/9
0.58	6/9
1.0	7/9
1.8	8/9
∞	1

The bond energy of a single bond in complexes of transition elements may be of the order of 60 to 100 kcal./mole, and, according to Pauling,[8] these bonds are in most cases about 50 percent covalent in character, P thus being about equal to 50; furthermore, the s–d separation energy ΔE in the case of palladium is 50 kcal./mole, as has been mentioned above; the expression $\Delta E/W_{n-1}(2-P/100)$ hence will be between 0.7 and 1.4; therefore, n probably lies between 2/3 and 8/9 in palladium complexes.

c. Complexes of Cu^{II} and Ag^{II}

In bivalent copper conditions are similar to those in bivalent nickel. Bivalent copper has, however, one electron more than bivalent nickel; we might at first think that this electron would occupy the fifth $3d$ or the about equally stable $4s$ orbital, making it unavailable for bond formation; this would leave available one $3d$–$4s$ and three $4p$ orbitals for bond formation. However, as has been pointed out by Pauling,[1] placing the unshared electron in the third $4p$ orbital (or in a $4s4p3d$ hybrid orbital) and using the residual four orbitals for bond formation involves no loss of energy by the copper atom. Each of the five orbitals under discussion (two $4s$–$3d$ orbitals and three $4p$ orbitals) is occupied either by a shared pair or by the single unshared electron in either formulation, and the interaction energy of a shared pair with the copper atom is the same as that of a single unshared electron.[9]

These considerations leave us with the problem of determining the geometric arrangement of the four strongest spd hybrid orbitals that are orthogonal to four orbitals with pure s–d character (these orbitals being filled with unshared pairs) and to an orbital of arbitrary composition in s, p, and d (this orbital being filled with the single unshared electron).

We shall find in the following treatment that the best possible orbitals that can be constructed under this condition are again the best square bond orbitals with strength 2.943 described above. These orbitals thus must be assumed for Cu^{II} complexes, which are in fact found to have a square arrangement.

Quadricovalent complexes of bivalent silver, like those of bivalent copper, are found to be coplanar. The same number of electrons are involved in the outer shell of Ag^{II} as in the outer shell of Cu^{II}, and therefore a similar discussion is applicable. It must be assumed, however, that the $5s$ orbital in silver, as in palladium, is considerably less stable than the $4d$ orbitals (while the outer $3d$ and $4s$ orbitals in copper, as in nickel, must be assumed about equally stable). Consequently, there will be used in quadricovalent complexes of silver as in complexes of palladium $s^n d^{2-n} p^2$ square bond orbitals, with n somewhere between 1 and 0.44, the odd electron of silver being in the third $5p$ orbital.

3. THE DIFFERENT POSSIBLE ARRANGEMENTS OF FOUR *spd* BOND ORBITALS AND THEIR BOND-FORMING POWER

It has been shown by Kimball[10] by group theoretical considerations that it is possible to construct from s, p, and d orbitals four equivalent bond orbitals in either a tetragonal plane, a tetragonal pyramidal, a regular tetrahedral, or an irregular (trigonal axis deformed) tetrahedral arrangement, and no other. The geometrical arrangement of the strongest possible equivalent spd orbitals can thus be found by determining the angular dependence of orbitals in only these four arrangements and by determining which of the four arrangements is the best.

[8] L. Pauling, *The Valences of Transition Elements* (Victor Henri Memorial Volume, Liège, 1947).

[9] In Section 2b we have seen that the interaction energy of a shared pair with the central atom is only in the case of pure covalent bonds equal to that of a single unshared electron, and that these energies are somewhat different in the case of covalent bonds partially ionic in character. A consideration similar to that given in Section 2b, the details of which are omitted, has shown that the difference of these two interaction energies is in any reasonable case too small for effecting a change of the nature of the most stable bond orbitals, and shall be neglected here for reason of simplicity.

[10] G. Kimball, J. Chem. Phys. **8**, 188 (1940). See also R. Hultgren, Phys. Rev. **40**, 891 (1932).

a. Tetragonal Plane Bond Orbital Arrangement

The angular parts of the s, p, and d wave functions are:[1]

$$\begin{aligned} s &= 1, \\ p_x &= \sqrt{3}\sin\vartheta\cos\varphi, \\ p_y &= \sqrt{3}\sin\vartheta\sin\varphi, \\ p_z &= \sqrt{3}\cos\vartheta, \\ d_{xy} &= ((15)^{\frac{1}{2}}/2)\sin^2\vartheta\cos 2\varphi, \\ d_{x+y} &= ((15)^{\frac{1}{2}}/2)\sin^2\vartheta\sin 2\varphi, \\ d_z &= ((5)^{\frac{1}{2}}/2)(3\cos^2\vartheta - 1), \\ d_{x+z} &= (15)^{\frac{1}{2}}\sin\vartheta\cos\vartheta\cos\varphi, \\ d_{y+z} &= (15)^{\frac{1}{2}}\sin\vartheta\cos\vartheta\sin\varphi, \end{aligned} \tag{1}$$

ϑ and φ being the angles used in spherical polar coordinates.

The bond direction of a first square bond orbital will be chosen as the x direction. It is easily seen that inclusion of p_y, p_z, d_{x+y}, or d_{x+z} orbitals would cause the bond direction to be different from the x direction, so they are ignored. It can also be shown that d_{y+z} does not increase the strength of a square orbital in the x direction but decreases it, so it is ignored, too, the function thus assuming the form

$$\psi_1 = a_s s + a_p p_x + d_{dxy} d_{xy} + a_{dz} d_z. \tag{2a}$$

By rotating ψ_1 around the z axis through angles of rotation of 90°, 180°, and 270°, respectively, the other equivalent square bond orbitals are easily found to be

$$\psi_2 = a_s s + a_p p_y - a_{dxy} d_{xy} + a_{dz} d_z, \tag{2b}$$

$$\psi_3 = a_s s - a_p p_x + a_{dxy} d_{xy} + a_{dz} d_z, \tag{2c}$$

$$\psi_4 = a_s s - a_p p_y - a_{dxy} d_{xy} + a_{dz} d_z. \tag{2d}$$

The orthogonality and normalization conditions require that

$$a_s^2 + a_p^2 + a_{dxy}^2 + a_{dz}^2 = 1, \tag{3}$$

$$a_s^2 - a_p^2 + a_{dxy}^2 + a_{dz}^2 = 0, \tag{4}$$

$$a_s^2 - a_{dxy}^2 + a_{dz}^2 = 0. \tag{5}$$

We obtain from these equations the results

$$a_p^2 = \tfrac{1}{2}, \tag{6}$$

$$a_{dxy}^2 = \tfrac{1}{4}, \tag{7}$$

$$a_s^2 + a_{dz}^2 = \tfrac{1}{4}. \tag{8}$$

It is seen from (6) that there is always $\frac{1}{2}p$ orbital involved in a square bond orbital and thus exactly two p orbitals in each square arrangement. Furthermore, it follows from (7) that the d_{xy} orbital is used completely in each square arrangement.

We obtain, by introducing (6), (7), and (8) into (2a),

$$\psi_1 = a_s s + (1/\sqrt{2})p_x + \tfrac{1}{2}d_{xy} - (\tfrac{1}{4} - a_s^2)^{\frac{1}{2}} d_z. \tag{9}$$

Similar expressions are obtained from (2b), (2c), and (2d).

The strength S_n is easily found from (9) and (1):

$$S_n = a_s + \sqrt{3}/\sqrt{2} + ((15)^{\frac{1}{2}}/4) + ((5)^{\frac{1}{2}}/2)(\tfrac{1}{4} - a_s^2)^{\frac{1}{2}}. \tag{10}$$

The quantity S_n, as given by Eq. (10), is plotted in Fig. 1 against the amount

$$n = 4a_s^2 \tag{10a}$$

of involved s orbital.

The value of a_s corresponding to the maximum strength is found, by maximization of (10), to be $\frac{1}{3}$, the corresponding strength being $S = 2.943$. The angular wave functions of these strongest square bond orbitals are thus found to be

$$\psi_1 = \tfrac{1}{3}s + (1/\sqrt{2})p_x + \tfrac{1}{2}d_{xy} - ((5)^{\frac{1}{2}}/6)d_z, \tag{11a}$$

$$\psi_2 = \tfrac{1}{3}s + (1/\sqrt{2})p_y - \tfrac{1}{2}d_{xy} - ((5)^{\frac{1}{2}}/6)d_z, \tag{11b}$$

$$\psi_3 = \tfrac{1}{3}s - (1/\sqrt{2})p_x + \tfrac{1}{2}d_{xy} - ((5)^{\frac{1}{2}}/6)d_z, \tag{11c}$$

$$\psi_4 = \tfrac{1}{3}s - (1/\sqrt{2})p_y - \tfrac{1}{2}d_{xy} - ((5)^{\frac{1}{2}}/6)d_z. \tag{11d}$$

This strongest arrangement of square bond orbitals is thus composed of 4/9s, 14/9d, and two p orbitals.

It is of interest to determine the nature of the five remaining orbitals, which are orthogonal to the square bond orbitals and are not involved in bonds. There are, of course, the four orbitals p_z, d_{x+y}, d_{x+z}, and d_{y+z} that are not used in hybridization. The fifth is the orbital

$$\psi_5 = (1 - 4a_s^2)^{\frac{1}{2}}s + 2a_s d_z, \tag{12}$$

which is formed from the parts of s and d_z orbitals that are not needed in bond orbital formation. In the case of the strongest square bond orbitals (11a), (11b), (11c), (11d), ψ_5 is given by

$$\psi_5 = ((5)^{\frac{1}{2}}/3)s + \tfrac{2}{3}d_z = (5)^{\frac{1}{2}}\cos^2\vartheta, \tag{13}$$

which gives a strength of $(5)^{\frac{1}{2}}$, that is, just the strength of the best single d orbital. The possibility of using this orbital for a weak bond along the z axis is not excluded.

b. Regular Tetrahedral Bond Orbitals

We shall now look for spd hybrid orbitals for bonds directed from the central atom to the four corners of a regular tetrahedron. The bond direction of a first hybrid orbital will be chosen as the z direction. As we restrict ourselves for reasons of simplicity to cylindrical orbitals, the orbitals p_x, p_y, d_{xy}, d_{x+y}, d_{x+z}, and d_{y+z} are ignored, and the function assumes the form

$$\psi_1 = a_s s + a_p p_z + a_d d_z. \tag{14a}$$

The other three equivalent tetrahedral bond functions ψ_2, ψ_3, and ψ_4 are easily found by rotating ψ_1 first around the y axis through an angle of 109°28′ (tetrahedral angle) and then around the z axis through angles 0°, 120°, and 240°, respectively.

$$\psi_2 = a_s s - \tfrac{1}{3}a_p p_z + (2\sqrt{2}/3)a_p p_x - \tfrac{1}{3}a_d d_z + (4/3\sqrt{3})a_d d_{xy} - (2\sqrt{2}/3\sqrt{3})a_d d_{x+z}, \tag{14b}$$

$$\psi_3 = a_s s - \tfrac{1}{3}a_p p_z - (\sqrt{2}/3)a_p p_x - (\sqrt{2}/\sqrt{3})a_p p_y - \tfrac{1}{3}a_d d_z - (2/3\sqrt{3})a_d d_{xy} + (\sqrt{2}/3\sqrt{3})a_d d_{x+z} + (\sqrt{2}/3)a_d d_{y+z} + \tfrac{2}{3}a_d d_{x+y}, \tag{14c}$$

$$\psi_4 = a_s s - \tfrac{1}{3}a_p p_z - (\sqrt{2}/3)a_p p_x + (\sqrt{2}/\sqrt{3})a_p p_y - \tfrac{1}{3}a_d d_z - (2/3\sqrt{3})a_d d_{xy} + (\sqrt{2}/3\sqrt{3})a_d d_{x+z} - (\sqrt{2}/3)a_d d_{y+z} - \tfrac{2}{3}a_d d_{x+y}. \tag{14d}$$

We shall require that these functions be normalized to 4π and be mutually orthogonal. These conditions lead to the relations

$$a_s^2 + a_p^2 + a_d^2 = 1, \tag{15}$$

$$a_s^2 - \tfrac{1}{3}a_p^2 - \tfrac{1}{3}a_d^2 = 0. \tag{16}$$

We obtain from these equations the result

$$a_s^2 = \tfrac{1}{4}, \tag{17}$$

$$a_p^2 + a_d^2 = \tfrac{3}{4}. \tag{18}$$

It can be seen from (17) that there is always $\frac{1}{4}s$ orbital involved in a tetrahedral orbital and thus exactly one s orbital in each tetrahedral arrangement.

We obtain by introducing (17) and (18) into (14a) the expression

$$\psi_1 = \tfrac{1}{2}s + a_p p_z + (\tfrac{3}{4} - a_p^2)^{\frac{1}{2}} d_z. \tag{19}$$

Similar expressions for ψ_2, ψ_3, ψ_4 are obtained from (14b), (14c), and (14d). The strength of these orbitals,

$$S_m = \tfrac{1}{2} + \sqrt{3}a_p + (5)^{\frac{1}{2}}(\tfrac{3}{4} - a_p^2)^{\frac{1}{2}}, \tag{20}$$

is shown in Fig. 2 as a function of the number $m = 4a_p^2$ of involved p orbitals, i.e., of the p character of the arrangement. The maximum strength $S_m = 2.950$ is obtained with $a_p = 3/4\sqrt{2}$, corresponding to $sd^{15/8}p^{9/8}$ orbitals. Of these orbitals we write, for reason of brevity only ψ_1, which is

$$\psi_1 = \tfrac{1}{2}s + (3/4\sqrt{2})p_z + \tfrac{1}{4}(15/2)^{\frac{1}{2}} d_z. \tag{21}$$

The five non-bonding orbitals, which are orthogonal to the tetrahedral orbitals given by (14a), (14b), (14c), (14d), (17), and (18), may be given by the following expressions:

$$\psi_5 = (\tfrac{2}{3})^{\frac{1}{2}} d_{y+z} - (1/\sqrt{3})d_{x+y}, \tag{22a}$$

$$\psi_6 = (\tfrac{2}{3})^{\frac{1}{2}} d_{x+z} + (1/\sqrt{3})d_{xy}, \tag{22b}$$

$$\psi_7 = (2/3\sqrt{3})[(\tfrac{3}{4} - a_p^2)^{\frac{1}{2}}(-p_x + 2p_y - 2p_z) + a_p(2d_z + 2\{(\tfrac{2}{3})^{\frac{1}{2}} d_{x+y} + (1/\sqrt{3})d_{y+z}\} - \{(\tfrac{2}{3})^{\frac{1}{2}} d_{xy} - (1/\sqrt{3})d_{x+z}\})], \tag{22c}$$

$$\psi_8 = (2/3\sqrt{3})[(\tfrac{3}{4} - a_p^2)^{\frac{1}{2}}(2p_x - p_y - 2p_z) + a_p(2d_z - \{(\tfrac{2}{3})^{\frac{1}{2}} d_{x+y} + (1/\sqrt{3})d_{y+z}\} + 2\{(\tfrac{2}{3})^{\frac{1}{2}} d_{xy} - (1/\sqrt{3})d_{x+z}\})], \tag{22d}$$

$$\psi_9 = (2/3\sqrt{3})[(\tfrac{3}{4} - a_p^2)^{\frac{1}{2}}(2p_x + 2p_y + p_z) + a_p(-d_z + 2\{(\tfrac{2}{3})^{\frac{1}{2}} d_{x+y} + (1/\sqrt{3})d_{y+z}\} + 2\{(\tfrac{2}{3})^{\frac{1}{2}} d_{xy} - (1/\sqrt{3})d_{x+z}\})]. \tag{22e}$$

It is seen that only two of these orbitals are pure d orbitals. Furthermore, using the theorem

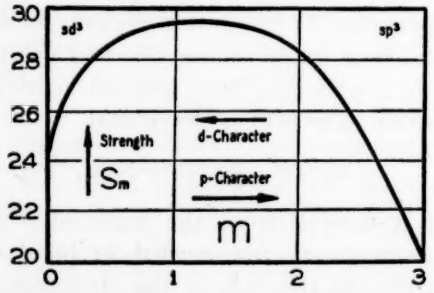

FIG. 2. Regular tetrahedral bond orbitals. Plot of the strength, S_m, against the amount, m, of p orbitals involved. As there is exactly one s orbital involved in each tetrahedral arrangement, the amount of d orbitals is $3-m$, the arrangement thus being $sp^m d^{3-m}$.

that the p content of any orbital is given by the sum of the squares of the coefficients of p_x, p_y, and p_z, it follows from (22c), (22d), and (22e) that each of the three dp non-bonding orbitals is composed of $(1-(4/3)a_p^2)p$ orbitals and $(4/3)a_p^2 d$ orbitals. In the case of the strongest tetrahedral orbitals ($a_p=3/4\sqrt{2}$) each of these three orthogonal dp non-bond orbitals becomes $5/8p$ and $3/8d$ in character.

c. Comparison of Suitability of the Different Possible Bond Orbital Arrangements

In Sections 2*a* and 2*b* we were looking for arrangements of four *spd* bond orbitals containing exactly two p functions and being at the same time orthogonal to four pure *s–d* orbitals. Both of these conditions are fulfilled by square bond orbital arrangements, as found in Section 3a.

These conditions, however, cannot be fulfilled simultaneously by tetrahedral orbitals (Section 3b). We can in that case fulfill the first condition by choosing $m=4a_p^2=2$, corresponding to a sp^2d tetrahedral bond orbital arrangement. Then we see, however, from Section 3b that there are two d and three $d^{\frac{1}{2}}p^{\frac{1}{2}}$ orbitals orthogonal to the tetrahedral bond orbitals thus obtained (and not four orbitals without p character), the second condition, therefore, being unsatisfied.

A consideration, the details of which will not be given here, of irregular (trigonal axis deformed) tetrahedral and tetragonal pyramidal bond orbital functions leads to the same result as in the case of a regular tetrahedral arrangement just discussed, namely, that the two conditions mentioned above cannot be fulfilled simultaneously. Thus the square arrangement is the only arrangement of four equal bond orbitals that can be used under the conditions of Sections 2a and 2b.

In Section 2c we were looking for the four strongest *spd* bond orbitals that fulfill the condition of orthogonality to four *s–d* or four pure d orbitals. On examination of the tetrahedral orbitals of Section 3*b* it is seen that this condition is fulfilled only in the case $m=4a_p^2=3$, corresponding to sp^3 tetrahedral orbitals of strength 2.00.

On the other hand, according to Section 3a, there can be constructed four square bond orbitals with strength 2.943 which fulfill the condition of being orthogonal to four *s–d* orbitals, and four square bond orbitals of strength 2.694 which are orthogonal to four pure d orbitals. The strengths of these square bond orbitals are both much larger than the value 2.00 of the possible tetrahedral arrangement; this circumstance makes the tetrahedral arrangement unfavorable.

A similar consideration concerning irregular tetrahedral and tetragonal pyramidal orbitals leads to the same conclusion as in the case of regular tetrahedral orbitals. The square bond orbitals are thus seen to be the strongest four equivalent orbitals that are possible under the conditions of Section 2.

The possibility of an arrangement of non-equivalent bond orbitals that are stronger than the bond orbitals in square arrangements remains to be considered. It is not probable, however, that such an arrangement is possible.[11]

ACKNOWLEDGMENTS

The author is greatful to Professor Linus Pauling for many helpful suggestions and discussions and for the kind hospitality that he extended to him during his stay in Pasadena. He also wishes to thank Dr. David P. Shoemaker for help in the preparation of the manuscript and to express his gratitude to the Swiss Foundation "Stiftung für Stipendien auf dem Gebiete der Chemie" for a fellowship.

[11] This conclusion can be drawn from a treatment, the details of which are omitted, concerning the four best *spd* orbitals that can be arranged in such a way that the strength vectors are directed from the center toward the corners of a rhombus. Such a treatment has shown that all bond orbital arrangements having the symmetry under discussion contain exactly two p orbitals and that the four bond orbitals are orthogonal to four *s–d* and one p orbital, just as in the limiting case of square bond orbitals. Furthermore, it can be shown that of all rhombus bond orbital arrangements of a given composition in s, p, and d, the square arrangement is the one for which the sum of the strengths (or the sum of the squares of the strengths) of the four bonding orbitals turns out to be a maximum. This circumstance makes the square arrangement favorable.

THE JOURNAL OF CHEMICAL PHYSICS VOLUME 16, NUMBER 7 JULY, 1948

General Theory of the Formation of Liquid Films

LAWRENCE BAYLOR ROBINSON
University of Chicago, Chicago, Illinois

(Received April 9, 1948)

Langmuir's theory of the formation of liquid films in narrow capillaries is developed for the general case of any electrolyte. The determination of the thicknesses of such films involves hyperelliptic integrals. By suitable transformations one can represent the integrand as the the product of binomial series and Legendre's series. No attempt is made to evaluate the thicknesses of the film numerically, because of the complexity of the necessary computations.

INTRODUCTION

IN discussing the problem of measuring the surface tension of solutions of electrolytes in narrow capillaries, Langmuir[1] proposed a theory which has been extended by others.[2] Since the details have been discussed previously, they are not repeated here; only a brief mention is made here of the ideas involved. All adaptations of the theory so far published have been applicable only for 1–1 and 2–1 electrolytes; the presentation herein is an extension of the general theory given elsewhere by this author.[3]

Langmuir believes that the wetting film formed in the capillary can be large enough to decrease the effective diameter of the tube. Solutions will then rise to a greater height than corresponds to the measured diameter of the capillary. Hence the capillary would not be a measure of the surface tension alone. This film has varying thicknesses depending upon the solution studied. The experimental procedure of using narrow capillaries, according to Langmuir, corresponds to measuring surface tensions with tubes of different (unknown) diameters. The problem of Langmuir's theory is to calculate the wetting film thickness for different solutions so that there can be some basis for comparing the surface tensions in terms of the capillary rises observed. The thickness of the film depends upon the solution used, the height to which the liquid rises in the tube, the zeta-potential, and the potential at the air-solution interface.

In discussing the mathematics of the problem, Langmuir utilizes the Poisson-Boltzmann equation and does not introduce the usual Debye-Hueckel simplifying assumptions.

MATHEMATICAL FORMULATION

The Poisson-Boltzmann equation for the electrical potential in an electrolytic solution in the region of a charged plane is

$$\nabla^2\psi = -\frac{4\pi}{D}\sum_{i=1}^{s} n_i z_i \epsilon \exp\left(\frac{-z_i\epsilon\psi}{kT}\right). \tag{1}$$

$\nabla^2\psi = d^2\psi/dx^2$ in this case as the potential is assumed to vary only in the direction perpendicular to the planar interface. This equation can be applied to the capillary tube because the radius of the tube is so much larger than the thickness of the wetting film. The curvature of the tube is relatively slight, and the inside surface appears as a plane to the film.

A simplification of Eq. (1) is effected by using the following substitutions (generally adopted):

$$\left.\begin{aligned} \eta &\equiv \epsilon\psi/kT, \\ \theta &\equiv \kappa x, \\ \kappa &\equiv \left[(4\pi\epsilon^2/DkT)\sum_{i=1}^{s} n_i z_i^2\right]^{\frac{1}{2}}, \\ 1/A &\equiv \sum_{i=1}^{s} n_i z_i^2, \\ p &\equiv d\eta/d\theta, \end{aligned}\right\} \tag{2}$$

Equation (1) becomes

$$p\frac{dp}{d\eta} = -A\sum_{i=1}^{s} n_i z_i \exp(-z_i\eta), \tag{3}$$

[1] I. Langmuir, Science **88**, 430 (1938); J. Chem. Phys. **6**, 894 (1938).
[2] G. Jones and L. D. Frizzell, J. Chem. Phys. **8**, 986 (1940); L. A. Wood and L. B. Robinson, J. Chem. Phys. **14**, 258 (1946).
[3] L. B. Robinson, Ph.D. Thesis, Harvard University, Cambridge, Massachusetts, May 1946, pp. 193–195.

which, when integrated, yields

$$p^2=\left(2A\sum_{i=1}^{s}n_i\exp(-z_i\eta)\right)+C. \quad (4)$$

The constant of integration is evaluated in the same manner as has been done by Langmuir, by assuming that at the air interface of the film, where $\theta=0$, the potential has a minimum. The minimum value of η is called m; at this point $p=0$. Hence the value of C is given by

$$C=-2A\sum_{i=1}^{s}n_i\exp(-z_im). \quad (5)$$

From (4) and (5) the following equation is obtained:

$$\frac{d\theta}{d\eta}=\frac{1}{\left[2A\sum_{i=1}^{s}n_i\{\exp(-z_i\eta)-\exp(-z_im)\}\right]^{\frac{1}{2}}}. \quad (6)$$

The solution of (6) may be written as

$$\Delta r=R(c_1, c_2, \cdots; z_1, z_2, \cdots; \psi_m, \zeta), \quad (7)$$

where the R function involves elliptic functions for the case that $-2\leqslant z\leqslant+2$, but cannot be expressed in terms of known tabulated functions for the cases where $|z|\geqslant 3$. Δr is the thickness of the liquid film. ψ_m represents the minimum potential (at the air-solution interface according to Langmuir) and ζ is the zeta-potential. Equation (6) will be integrated for the general case.

It is apparent that the general solution of (6) will involve hyperelliptic functions. If one makes the transformation,

$$y=\exp(-\eta), \quad K=\exp(-m), \quad (8)$$

assuming positive potentials, Eq. (6) becomes

$$d\theta=\kappa dx=\frac{bdy}{(a_ny^n+a_{n-1}y^{n-1}+\cdots+a_0)^{\frac{1}{2}}}, \quad (9)$$

where one or more of the a's may be zero. Let the radicand in the denominator be written $Q(y)$ and let it be factored as

$$Q(y)=(y-K_1)(y-K_2)\cdots(y-K_r)Q_0(y), \quad (10)$$

where $Q_0(y)$ is the term containing the part of the expression with whatever complex roots that may result. Let the root between zero and positive unity be called K_1. It is apparent that this root fixes the value of the minimum potential. This point is discussed elsewhere in connection with the specific examples of Jones-Frizzell and Wood-Robinson.

F. R. Moulton[4] provided a general method whereby hyperelliptic integrals can be evaluated and E. G. Keller[5] has applied this method to non-linear circuit problems. The question of the periods of the integral does not need to be discussed here in that the problem herein is different from those of Moulton and Keller. They were interested in the inverse problem, namely, the equivalent of finding y as a function of Δr.

The transformation given immediately below is made so as to put $Q(y)$ in a form more suitable for integration. Let

$$y=\frac{K_1+K_2}{2}+\frac{K_2-K_1}{2}t. \quad (11)$$

K_1 is the lower limit of the integration sign. Equation (10) now becomes

$$Q(y)=\frac{(K_2-K_1)^2}{4}(1-t^2)\prod_{j=1}^{m}b_j\left[1+\frac{K_2-K_1}{2b_j}t\right], \quad (12)$$

where

$$\frac{K_2-K_1}{2b_j}=\frac{g}{b_j}=\left|\frac{K_2-K_1}{K_2+K_1-2K_j}\right|<1. \quad (13)$$

If

$$b_j\left(1+\frac{g}{b_j}t\right)$$

is a complex root, then its complex conjugate

$$b_{j+1}\left(1+\frac{g}{b_{j+1}}t\right)$$

is, of course, also a root. Then

$$b_jb_{j+1}\left(1+\frac{gt}{b_j}\right)\left(1+\frac{gt}{b_{j+1}}\right)=B^2(1+\alpha_jt+\beta_jt^2), \quad (14)$$

where α_j and β_j are real and $B^2>0$.

---

[4] F. R. Moulton, Am. J. Math. **34**, 177 (1912).

[5] E. G. Keller, J. Frank. Inst. **225**, 561 (1938); **228**, 319 (1939); *Mathematics of Modern Engineering* (John Wiley and Sons, Inc., New York, 1942), Vol. II, pp. 264–284.

The use of t instead of y transforms (9) into

$$\Delta r = M\int_{-1}^{t_1} \frac{dt}{[(1-t^2)(1+f_1 t)\cdots(1+f_q t)\cdots \times(1+\alpha_1 t+\beta_1 t^2)\cdots l(t)]^{\frac{1}{2}}}, \quad (15)$$

where all symbols, other than l and t, represent constants. The integration must be performed for many values of the upper limit in order to obtain sufficient points to insure a smooth curve representing Δr as a function of the potentials. It is convenient also to make a transformation so that the upper limit will become plus one. The transformation is

$$t=[(\lambda-1)/2]+[(\lambda+1)/2]\omega, \quad \text{or} \quad \omega=(2t-\lambda+1)/(\lambda+1). \quad (16)$$

It is apparent that a different value of the parameter λ must be selected to equal each value of the upper limit t_1. This transformation is made in order to assist in the study of the convergence conditions of the series generated by the terms in the denominator of (15). Actually, no worry need exist concerning this point since the physical nature of the problem will make it so that the series involved will be suitable. The maximum value which can assume is given by the zeta-potential.

The transformation (16) is an interesting one in that the lower limit retains the value -1 for every value of λ. This is because the t representing the lower limit is -1.

When this transformation is made, Eq. (15) becomes

$$\Delta r = M'\int_{-1}^{+1} \prod_{i=1}^{n}(1+h_i\omega)^{-\frac{1}{2}}(1+\omega)^{-\frac{1}{2}} \times \prod_{j=1}^{m}\left\{\sum_{l=0}^{\infty} P_l(\mu\gamma^{\frac{1}{2}})(\gamma^{\frac{1}{2}}\omega)^l\right\}_j d\omega, \quad (17)$$

where the source of the various terms is explained below. The term $(1-t^2)^{\frac{1}{2}}$ transforms[6] as

$$(1-t^2)^{\frac{1}{2}}=C(1+\omega)^{\frac{1}{2}}(1+h\omega)^{\frac{1}{2}}. \quad (18)$$

The terms in (15) of the general nature $(1+\alpha t+\beta t^2)^{-\frac{1}{2}}$ retain the corresponding powers of ω in the transformation, and the values of the coefficients of ω and ω^2 are such that each expression can be represented by a Legendre series, which converges rapidly.

$$(1+\alpha t+\beta t^2)^{-\frac{1}{2}}=E(1-2\mu\gamma^{\frac{1}{2}}\omega+\gamma\omega^2)^{-\frac{1}{2}}, \quad (19)$$

and

$$(1-2\mu\gamma^{\frac{1}{2}}\omega+\gamma\omega^2)^{-\frac{1}{2}}=\sum_{l=0}^{\infty} P_l(\mu\gamma^{\frac{1}{2}})(\gamma^{\frac{1}{2}}\omega)^l, \quad (20)$$

where $P_l(x)$, the Legendre polynomial, is given by

$$P_l(x)=\frac{(2l)!}{2^l(l!)^2}\left\{x^l-\frac{l(l-1)}{2(2l-1)}x^{l-2}+\frac{l(l-1)(l-2)(l-3)}{2\cdot 4(2l-1)(2l-3)}x^{l-4}-\cdots\right\}. \quad (21)$$

It is apparent now that (17) will be an integral involving powers of the variable ω which can be evaluated at once. However, numerical computations are too difficult to make.

REMARKS

A general theory of the formation of liquid films consistent with Langmuir's ideas is developed. This theory involves hyperelliptic integrals, and a method of evaluating these integrals is given. For the case of 1–1 and 2–1 electrolytes, the integrals become elliptic integrals.

APPENDIX

All of the mathematical transformations given in this paper are more or less immediately apparent with the exception of Eq. (18). The details of this transformation are given here.

$$\begin{aligned}(1-t^2)^{\frac{1}{2}}&=\left[1-\frac{(\lambda-1)^2}{4}-\frac{2(\lambda^2-1)}{4}\omega-\frac{(\lambda+1)^2}{4}\omega^2\right]^{\frac{1}{2}}\\&=-\left[\frac{(\lambda^2-2\lambda-3)+2(\lambda^2-1)\omega+(\lambda+1)^2\omega^2}{4}\right]^{\frac{1}{2}}\\&=-\tfrac{1}{2}[(\lambda-3)(\lambda+1)]^{\frac{1}{2}}\left[1+\frac{2(\lambda-1)}{(\lambda-3)}\omega+\frac{(\lambda+1)}{(\lambda-3)}\omega^2\right]^{\frac{1}{2}}\\&=-\tfrac{1}{2}[(\lambda-3)(\lambda+1)]^{\frac{1}{2}}\times\left[1+\left\{\frac{(\lambda+1)+(\lambda-3)}{(\lambda-3)}\right\}\omega+\frac{(\lambda+1)}{(\lambda-3)}\omega^2\right]^{\frac{1}{2}}\\&=-\tfrac{1}{2}[(\lambda-3)(\lambda+1)]^{\frac{1}{2}}\times\left[1+\left\{\frac{(\lambda+1)}{(\lambda-3)}+1\right\}\omega+\frac{(\lambda+1)}{(\lambda-3)}\omega^2\right]^{\frac{1}{2}}\\&=-\tfrac{1}{2}[(\lambda-3)(\lambda+1)]^{\frac{1}{2}}\left[1+\frac{(\lambda+1)}{(\lambda-3)}\omega\right]^{\frac{1}{2}}(1+\omega)^{\frac{1}{2}}\\&=C(1+\omega)^{\frac{1}{2}}(1+h\omega)^{\frac{1}{2}}.\end{aligned}$$

[6] See appendix.

THE JOURNAL OF CHEMICAL PHYSICS · VOLUME 16, NUMBER 7 JULY, 1948

Frequency Dependence of the Capacity of a Diffuse Double Layer

JOHN D. FERRY
Department of Physical Chemistry, Harvard Medical School, Boston, Massachusetts, and Department of Chemistry, University of Wisconsin, Madison, Wisconsin

(Received April 19, 1948)

The capacity of a diffuse double layer is calculated to be inversely proportional to the square root of the frequency at frequencies high compared with the reciprocal of the relaxation time of the ionic atmosphere. This dependence is observed experimentally with inert electrodes in very dilute solutions, but at considerably lower frequencies. The observed capacity is probably concerned with phenomena at the immediate vicinity of the electrode rather than the diffuse double layer.

IN measurements of conductance[1] or dielectric constants[2–4] of solutions containing ions, using inert electrodes, account must be taken of the polarization capacity at the electrode surface. For solutions of electrolytes such as potassium chloride of the order of 10^{-4} M, with smooth or sand-blasted platinum electrodes, the A.C. polarization capacity has often been found to be proportional to the inverse square root of the frequency;[1–3] although this relation fails[1–4] below frequencies of 25 kc for solutions with conductances of the order of 10^{-4} ohm^{-1} cm^{-1}, and the deviations appear to be particularly marked in the case of hydrogen ions.[5]

A theory of polarization capacity was given by Warburg,[6] who assumed that electrolysis occurred, and treated the diffusion of the products of hydrolysis away from the electrodes. Although this theory predicts the correct frequency dependence within a certain frequency range, it seems of dubious applicability to measurements at very low potentials, where perceptible electrolysis cannot be expected to occur.

A phenomenological theory by Fricke[7] showed that, if the polarization voltage followed a transient decay with time of the form $V_0 t^{-\frac{1}{2}}$, the polarization capacity measured with an alternating potential should be proportional to the inverse square root of the frequency. However, no physical interpretation of this decay relationship was offered.

More recent treatments of the differential polarization capacity (as measured with alternating current) at inert electrodes in dilute solutions of electrolytes have considered it as equivalent to two condensers in series, one representing an adsorbed layer of ions and the other a diffuse double layer.[8,9] While the magnitude of the former capacity cannot be predicted,[9] the latter has at low frequencies the well-known value[10] $D\kappa/4\pi$, where D is the dielectric constant and κ the Debye-Hückel parameter (for a univalent electrolyte $(8\pi\epsilon^2 n/DkT)^{\frac{1}{2}}$, ϵ being the electronic charge, n the number of each ionic species per cc, k Boltzmann's constant, and T the absolute temperature).

If the potential across the diffuse double layer is removed, the charge due to unequal concentrations of positive and negative ions decays as the inequality of concentration is destroyed by diffusion. Under an alternating potential, this picture leads to a dispersion of the polarization capacity, which falls to zero at frequencies too high to permit changes in ion distribution within the period of alternation. The expected form of this dispersion has been calculated, to determine whether the observed frequency dependence of the polarization capacity can be explained on this basis.

We follow the treatment given by Falkenhagen[11] for relaxation of the ionic atmosphere,

[1] G. Jones and S. M. Christian, J. Am. Chem. Soc. **57**, 272 (1935).
[2] J. L. Oncley, J. Am. Chem. Soc. **60**, 1115 (1938).
[3] J. D. Ferry and J. L. Oncley, J. Am. Chem. Soc. **63**, 272 (1941).
[4] T. M. Shaw, J. Chem. Phys. **10**, 609 (1942).
[5] W. G. Smiley and A. K. Smith, J. Am. Chem. Soc. **64**, 624 (1942).
[6] Warburg, Ann. Phys. **6**, 125 (1901).
[7] H. Fricke, Phil. Mag. (7) **14**, 310 (1932).
[8] M. A. Vorsina and A. N. Frumkin, Compt. rend. Acad. Sci. U.R.S.S., **24**, 918 (1939).
[9] D. C. Grahame, J. Am. Chem. Soc. **68**, 301 (1946).
[10] G. Gouy, Ann. Chim. phys. [7] **29**, 145 (1903).
[11] H. Falkenhagen, *Electrolytes* (Oxford University Press, Oxford, 1934), p. 176.

but treat a diffuse double layer at a plane surface instead of a spherical atmosphere around a single ion. Neglecting interionic effects, we obtain the differential equation (for a uni-univalent electrolyte with ions of equal mobility, *e.g.*, potassium chloride)

$$\partial f/\partial\tau = \partial^2 f/\partial s^2 - f(s, \tau).$$

Here $f\epsilon$ is the momentary excess charge density due to inequality of ionic concentrations, $s=\kappa x$ where x is the distance from the electrode surface, $\tau = t/\Theta$ where t is time and $\Theta = \rho/kT\kappa^2$, and ρ is the frictional constant for the ions (the force required to move an ion through the solvent at unit velocity).

The solution of this equation for the disappearance of net charge following removal of potential is

$$f = \frac{S}{(\pi)^{\frac{1}{2}}} e^{-\sigma} \int_{(\tau)^{\frac{1}{2}} - \sigma/2(\tau)^{\frac{1}{2}}}^{\infty} e^{-x^2} dx$$

where $S = -D\psi_a\kappa^2/4\pi\epsilon$, ψ_a being the potential between $x=a$ (the closest approach of an ion to the surface) and $x=\infty$, and $\sigma = \kappa(x-a)$. The excess charge per unit area throughout the diffuse double layer is

$$(\epsilon/\kappa)\int_0^{\infty} f d\sigma,$$

and the time derivative of this gives the current. Thus the transient current is

$$i_t = [S\epsilon/\kappa\Theta(\pi)^{\frac{1}{2}}]\partial/\partial\tau \int_0^{\infty} e^{-\sigma} \int_{(\tau)^{\frac{1}{2}} - \sigma/2(\tau)^{\frac{1}{2}}}^{\infty} e^{-x^2} dx d\sigma$$

$$= -(D\psi_a\kappa e^{-\tau}/8\pi\Theta)[1 + 1/(\pi\tau)^{\frac{1}{2}}].$$

According to the principle of superposition, the steady-state current produced by an alternating potential of the form $\psi = \psi_a \sin\theta\tau$ (where $\theta\tau = \omega t$, ω being the circular frequency) is

$$(D\kappa\theta\psi_a/8\pi\Theta)\left[\cos\theta\tau \int_0^{\infty} e^{-u}[1 + 1/(\pi u)^{\frac{1}{2}}] \cos\theta u du + \sin\theta\tau \int_0^{\infty} e^{-u}[1 + 1/(\pi u)^{\frac{1}{2}}] \sin\theta u du\right].$$

To calculate the apparent capacity, C, we are interested only in the quadrature component, which is $\omega C\psi_a \cos\theta\tau$. Equating the coefficients of $\cos\theta\tau$ in the last two expressions, we obtain

$$C = (D\kappa/8\pi)\left[\int_0^{\infty} e^{-u} \cos\theta u du + \int_0^{\infty} [e^{-u}/(\pi u)^{\frac{1}{2}}] \cos\theta u du\right]$$

$$= (D\kappa/8\pi)\left\{\frac{1}{1+\theta^2} + \frac{1}{\sqrt{2}}\left[\frac{(\theta^2+1)^{\frac{1}{2}}+1}{\theta^2+1}\right]^{\frac{1}{2}}\right\}.$$

At high frequencies ($\theta \gg 1$) this becomes

$$(D\kappa/8\pi)[1/(2\theta)^{\frac{1}{2}}] = [D(kT)^{\frac{1}{2}}\kappa^2/8\sqrt{2\pi}(\rho)^{\frac{1}{2}}]/\omega^{\frac{1}{2}},$$

giving the experimentally observed proportionality to the inverse square root of frequency. For low frequencies ($\theta \ll 1$), it reduces properly to $D\kappa/4\pi$.

For 10^{-4} M potassium chloride in water at 25°C, Θ, the relaxation time of the ionic atmosphere, is about 0.3×10^{-6} sec., so that according to the theory proportionality to $\omega^{-\frac{1}{2}}$ should be observed only for frequencies over 10^6 cycles; while at lower frequencies the capacities should be smaller than those calculated from the $\omega^{-\frac{1}{2}}$ law. Actually the observed deviations from the $\omega^{-\frac{1}{2}}$ law are in the right direction but appear at much lower frequencies, about 2×10^4 cycles.

The proportionality of polarization capacity to electrolyte concentration (measured by κ^2) predicted by the theory is roughly confirmed in potassium chloride solutions from 1.3 to 2.7×10^{-4} M, using electrodes of sand-blasted platinum.

For 10^{-4} M potassium chloride, the theory predicts that the polarization capacity at 25 kc should be less than 1 percent smaller than the maximum, or Gouy capacity, $D\kappa/4\pi = 2.3\mu f/\text{cm}^2$. Experimental values obtained in connection with previously reported studies[3] range from 0.1 to 1.0 $\mu f/\text{cm}^2$, depending on the electrodes used and their previous history. In a frequency range where the capacity follows the $\omega^{-\frac{1}{2}}$ law, the absolute value should be much less than the maximum value $D\kappa/4\pi$. However, the actual surface of sand-blasted metal is probably much greater than the geometrical surface, so that comparisons of absolute values of capacity are of doubtful significance.

Thus the dependence upon frequency and concentration of the capacity of a diffuse double layer is the same as that observed experimentally for the polarization capacity. However, the frequency range in which dispersion occurs would be expected to be higher by about two decades than that observed. The discrepancy might conceivably be attributed to a higher effective viscosity in the diffuse double layer, but this does not seem reasonable for a layer of thickness 300A, which is the value of $1/\kappa$ at this concentration. It appears likely that the observed effects cannot be explained in terms of the diffuse double layer; they may involve slow processes in the immediate vicinity of the electrodes, such as adsorption and desorption of the ions.

THE JOURNAL OF CHEMICAL PHYSICS VOLUME 16, NUMBER 7 JULY, 1948

Thermodynamic Calculations Concerning the Possible Participation of the Carbides of Iron as Intermediate in Fischer-Tropsch Synthesis*

J. T. KUMMER, L. C. BROWNING, AND P. H. EMMETT
Mellon Institute, Pittsburgh, Pennsylvania

(Received April 19, 1948)

SINCE the discovery of the synthesis of hydrocarbons from carbon monoxide and hydrogen over iron catalysts, the suggestion has often been made that one of the iron carbides is an intermediate in the reactions:

$$n\mathrm{CO}+2n\mathrm{H_2}=(\mathrm{CH_2})_n+n\mathrm{H_2O}, \quad (1)$$

$$n\mathrm{CO}+(2n+1)\mathrm{H_2}=\mathrm{C}_n\mathrm{H}_{2n+2}+n\mathrm{H_2O}. \quad (2)$$

Some evidence has been cited for the carbide being an intermediate;[1] other evidence has argued rather strongly against it.[2] During the past year we have obtained equilibrium data that enable us to conclude that the reduction of Fe_2C [3-5] by hydrogen at pressures up to ten atmospheres can form only negligible amounts of monoolefins in the temperature range 227 to 327°C. Furthermore, the formation of appreciable partial pressures of normal paraffin hydrocarbons for which n is greater than six by the reduction of Fe_2C is thermodynamically impossible at a hydrogen pressure of one atmosphere or less in the temperature range 227 to 327°C, and at as high as ten atmospheres pressure of hydrogen at about 327°C. Accordingly, since it is well known that both at atmospheric pressure and at pressures of about ten atmospheres large partial pressures of monoölefins and of higher hydrocarbons are built up at temperatures as high as 300 to 330°C, it follows that these are formed by some mechanism other than the reduction of bulk Fe_2C.

The free energy change ΔF for the reaction

$$\mathrm{CH_4}+2\mathrm{Fe}=\mathrm{Fe_2C}+2\mathrm{H_2} \quad (3)$$

has been found to be 9.014 kcal. at 327°C and is estimated by extrapolation to be 11.91 kcal. at 227°C. It follows from the known free energies of formation of CH_4 [6] at 327 and 227°C (−5.490 and −7.841 kcal. per mole, respectively) for the reaction

$$2\mathrm{Fe}+\mathrm{C}=\mathrm{Fe_2C} \quad (4)$$

that the ΔF value is 3.542 kcal. at 327° and 4.070 kcal. at 227°C. From these data and the known free energies of formation of the various hydrocarbons[6] one can calculate the equilibrium constants for the reactions

$$n\mathrm{Fe_2C}+n\mathrm{H_2}=\mathrm{C}_n\mathrm{H}_{2n}+2n\mathrm{Fe}, \quad (5)$$

and

$$n\mathrm{Fe_2C}+(n+1)\mathrm{H_2}=\mathrm{C}_n\mathrm{H}_{2n+2}+2n\mathrm{Fe}. \quad (6)$$

Plots of the logarithm of the equilibrium con-

* Contribution from Gulf Research and Development Company's Multiple Fellowship, Mellon Institute, Pittsburgh, Pennsylvania.

[1] Ya T. Eidus, Bull. de l'academie des Sciences de l'U.R.S.S. classe des sciences chimiques, p. 447 (1946).

[2] Kummer, DeWitt, and Emmett, J. Am. Chem. Soc. (to be published).

[3] Hägg, Zeits. f. Krist. 89, 92 (1934).

[4] Jacks, Nature 158, 60 (1946).

[5] Bahr and Jesson, Ber. 66, 1238 (1933).

[6] American Petroleum Institute, Research Project 44, National Bureau of Standards.

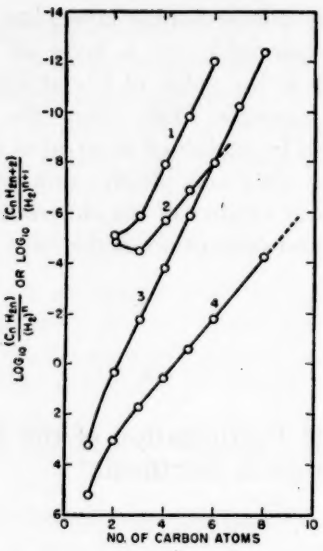

FIG. 1. Equilibrium constants for the synthesis of olefins (Eq. (4)) or paraffins (Eq. (5)) by the reduction of Fe_2C. Curves 1 and 2 are for the formation of normal 1-olefins at 327° and 227°C, respectively. Curves 3 and 4 are for the formation of normal paraffins at these two respective temperatures.

stant $[(C_nH_{2n}/(H_2)^n]$ for reaction 5 and of the constant $[(C_nH_{2n+2})/(H_2)^{(n+1)}]$ for reaction 6 are shown in Fig. 1 for the normal 1-monoölefins and for the normal paraffins.

It is apparent, from curves 1 and 2, that for all normal monoölefins with two or more carbon atoms the equilibrium constants are smaller than 3×10^{-5} in the temperature range 227° to 327°C. This means, for example, that at either 327° or 227°C the partial pressure of ethylene formed by reaction 5 from one atmosphere of hydrogen would be about 10^{-5} atmosphere. With ten atmospheres of hydrogen it would still be only 10^{-3} atmospheres. For C_4H_8 formation, the equilibrium calculations are even more startling, corresponding to about 2×10^{-6} atmosphere of C_4H_8 at 227°, and 10^{-8} atmosphere at 327° when the pressure of hydrogen is one atmosphere. At a partial pressure of ten atmospheres of hydrogen, the partial pressure of C_4H_8 would be 10^{-4} atmosphere at 327°, and 2×10^{-2} atmosphere at 227°C. Clearly, then, the large yields of olefins that are known to be obtained both at one atmosphere and in medium pressure Fischer-Tropsch synthesis over iron could not have been formed by the reduction of Fe_2C.

Curves 3 and 4 of Fig. 1 showing the logarithm of the equilibrium constants for the formation of the various normal paraffin hydrocarbons by reaction 6 indicate that products with n as high as six could, as far as thermodynamic limitations are concerned, be formed under Fischer-Tropsch synthesis conditions by reduction of the bulk Fe_2C by hydrogen. For higher paraffin hydrocarbons, however, the equilibrium of reaction 6 is unfavorable. For example, if $n=8$, $K=[C_8H_{18}/(H_2)^9]=5\times10^{-5}$ at 227° and 5×10^{-13} at 327°. This means that if $P_{H_2}=1$, $P_{C_8H_{18}}$ at equilibrium would be 5×10^{-5} atmosphere at 227° and 6×10^{-13} atmosphere at 327°. Yet it is well known that hydrocarbons with n values as large as 8 form over iron at temperatures of about 227°C even at one atmosphere pressure. Furthermore, at ten atmospheres pressure, large yields of such hydrocarbon are obtained at temperatures as high as 327°C. It appears, therefore, that these products could not have been formed by the reduction of the carbide Fe_2C.

The question naturally arises as to whether the well-known iron carbide Fe_3C or the "hexagonal" Fe_2C described by some of the German workers[7] might be intermediates. The data on Fe_3C; preclude** its being an intermediate for the same reasons advanced above for Fe_2C; the ΔF of formation of Fe_3C from iron and carbon is even smaller by a few hundred calories than that for Fe_2C formation. On the other hand, no data exist by which to judge with certainty the behavior of hexagonal Fe_2C. Since, however, the thermodynamic stability of a compound is not usually altered appreciably by a change in crystal structure, it seems very likely that the free energy of formation of hexagonal Fe_2C will be approximately the same as the free energy of formation or ordinary (Hägg) Fe_2C[3] and that, accordingly, the direct reduction by H_2 of either form of Fe_2C cannot account for the synthesis of normal 1-monoolefins or of higher paraffins from carbon monoxide and hydrogen over the temperature and pressure range commonly employed in the Fischer-Tropsch synthesis.

[7] T.O.M. Reel 26, Bag. 2463, Document 9, Forms 900000232–333 (March 31, 1943).

** Dr. C. W. Montgomery of the Gulf Research and Development Company has independently made calculations leading to this same conclusion for the Fe_3C phase.

Letters to the Editor

THIS section will accept reports of new work, provided these are terse and contain few figures, and especially few halftone cuts. The Editorial Board will not hold itself responsible for opinions expressed by the correspondents. Contributions to this section should not exceed 600 words in length and must reach the office of the Managing Editor not later than the first of the month preceding that of the issue in which the letter is to appear. No proof will be sent to the authors. The usual publication charge ($4.00 per page) will not be made and no reprints will be furnished free.

Metal-Ammonia Solutions

A. J. BIRCH AND D. K. C. MACDONALD
Dyson Perrins Laboratory and Clarendon Laboratory, University of Oxford, Oxford, England
May 10, 1948

RECENTLY Jaffe[1] has suggested, in analogy with lithium solutions, that the eutectic arising from a solution of sodium in ammonia is a compound (possibly $Na(NH_3)_5$ or perhaps non-stoichiometric) and thence he proposes an alternative explanation for our electrical conductivity measurements on solidified sodium-ammonia solutions.[2] Whilst we agree with Jaffe that lithium and ammonia almost certainly do form a compound,[3] probably $Li(NH_3)_4$, at low temperatures, which melts in contact with solid ammonia at −185°C (Jaffe gives −181°C) we do not believe that a compound is formed in the case of sodium. The obviously non-homogeneous mixture of metal and ammonia crystals constituting the solidified sodium-ammonia eutectic differs completely in appearance from the homogeneous lithium compound (and the analogous alkaline-earth metal derivatives).

That super-cooling can occur under favorable conditions is clearly indicated in the absence of a latent heat at −110°C (the m.p. of the sodium-ammonia eutectic) in some of our thermal measurements.[2] This is perhaps not so surprising as Jaffe seems to think because the composition of a saturated solution of sodium in ammonia is practically temperature independent, and the vapor-pressure:concentration curve in this region is almost vertical. There should thus be less tendency for either of the solid components (Na, NH_3) to separate from the saturated solution on cooling than in more familiar types of solution. Whether in fact at the very low temperatures (ca. −183°C) the super-cooled phase is a mobile liquid or a glass (i.e. a solid solution perhaps corresponding to Jaffe's non-stoichiometric compound) seems to us a distinction without a difference; the observed phenomenon is that a continuous network of conducting material is maintained. The contraction on slow cooling, and subsequent cracking with rupture of conducting material is due to the fact that metal-ammonia solutions have a far greater volume than their components, rather than to normal thermal contraction which would be small. On this view, the role of a super-cooled phase is thus to prevent this cracking, and the decrease in conductivity on warming is due to crystallization of the phase, which proceeds faster at higher temperatures still below −110°C.

A theoretical discussion of the constitution of metal-ammonia solutions and metal-ammoniates is to be published.[4]

[1] H. Jaffe, J. Chem. Phys. (to be published).
[2] A. J. Birch and D. K. C. MacDonald, Trans. Faraday Soc. **43**, 792 (1947).
[3] A. J. Birch and D. K. C. MacDonald, Nature **159**, 811 (1947); Trans. Faraday Soc. (to be published).
[4] A. J. Birch and D. K. C. MacDonald, Oxford Science (to be published).

A Reinvestigation of the Vibration Spectrum of Ozone

M. K. WILSON AND R. M. BADGER
Gates and Crellin Laboratories, California Institute of Technology, Pasadena, California
April 23, 1948

SEVERAL analyses of the vibration spectrum of ozone have been proposed in recent years,[1–5] all of which have been open to serious objection. Either they have failed to account for the observed structure of all the infrared bands, or if consistent with this structure have required an acute angled molecular model which is not in accord with the structure determination by electron diffraction.[6] These difficulties appear to have resulted in part from some misconceptions regarding the relative intensities of the ozone bands, but chiefly from the previous failure to recognize the fundamental band of the vibration ν_1.

The spectrum of ozone has recently been re-examined in this laboratory in the region 1.5–15μ, using a Beckman IR-2 spectrophotometer. Particular care was taken to avoid contamination by N_2O_5, and the possible effects of contamination by this gas, and by CO_2 and other impurities have been carefully considered. The concentration of ozone in the absorption tube was determined by chemical analysis and the "apparent" extinction coefficient at the maximum of each observed band was determined as shown in Table I.

Because of the limited resolution employed, and the discontinuous character of the absorption, these coefficients are appreciably dependent on pressure, but they approximately represent the pressure dependence of average absorption near the maximum, when the absorption lies between 10 and 30 percent, and they serve to indicate

TABLE I. Extinction coefficients[a] and assignments of the observed ozone bands.

ν (cm^{-1})	Observed type	Spacing (cm^{-1})	α	Assignment
705	doublet	~5.7	0.08	ν_2
1043	*Q*	~1	6.0	ν_3
1110	doublet	~5	0.05	ν_1
1740	?	—	0.04	$\nu_2+\nu_3$
2105	*Q*	~1	0.15	$\nu_1+\nu_3$
2800	?	—	0.005	$\nu_2+2\nu_3$
3050	*Q*	—	0.015	$3\nu_3$

[a] α (base 10) is expressed as cm^{-1} of pure ozone at S.T.P.

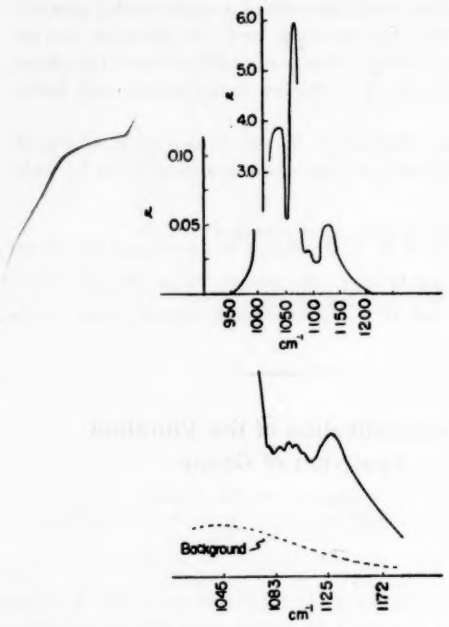

FIG. 1. Ozone bands near 1100 cm^{-1}.

relative intensities of the bands. In previous estimations of relative intensity the observations of Hettner, Pohlmann and Schumacher[2] appear to have been misinterpreted. It is now evident that in this earlier investigation about 5 percent of stray light was present at 10μ and that the 1043 cm^{-1} band is much more intense than was supposed.

The particularly new observation made in the course of this work was the discovery of a new fundamental band with center at about 1110 cm^{-1}, shown in Fig. 1. This band has nearly as great intensity as the fundamental at 705 cm^{-1}. It is suggested in several previously published tracings of the ozone spectrum but has apparently escaped special notice because of its proximity to the extremely intense band at 1043 cm^{-1}. Under conditions suitable for study of the latter band the former may easily escape detection. As shown in the lower tracing the new band shows no suggestion of a Q branch, but four lines with an average spacing of about 5 cm^{-1} have been resolved on the long wave-length side of the minimum. Evidently the new band is similar in structure to the fundamental at 705 cm^{-1}, recently investigated by Adel and Dennison, and these two bands are to be described as ν_1, and ν_2, respectively. The extremely intense band at 1043 cm^{-1} is then evidently the fundamental ν_3. There has been some question as to the structure of this band, and it has been suggested that the observed fine structure is due in part to CO_2 contamination. This may be possible in observations of atmospheric absorption, but our observations indicate that this is most unlikely under the laboratory conditions employed by Gerhardt.[1] The Q branch of this band is certainly not prominent, but the tracings of Gerhardt strongly suggest its presence, though somewhat displaced and "washed out" by convergence.

The new observations make possible the revised vibrational analysis presented in the table, which is in agreement with all observations on the band structures, and supports the approximate analysis of fine structure made by Miss Simpson on the basis of the obtuse angled model.[7] Some previous difficulties in the apparent divergence in band progressions and combination bands are now resolved, and the observed relative intensities of the bands support the proposed analysis.

The more accurate determination of the apex angle and internuclear distances of the ozone molecule must await better resolution of the fine structure of one or more of the B type bands which we propose to attempt in the near future.

[1] S. L. Gerhardt, Phys. Rev. **42**, 622 (1932).
[2] G. Hettner, R. Pohlmann, and H. J. Schumacher, Zeits. f. Physik. **91**, 372 (1934).
[3] W. G. Penney and G. B. B. M. Sutherland, Proc. Roy. Soc. **A156**, 654, 678 (1936).
[4] D. M. Simpson, Trans. Faraday Soc. **41**, 209 (1945).
[5] A. Adel and D. M. Dennison, J. Chem. Phys. **14**, 379 (1946).
[6] W. Shand and R. A. Spurr, J. Am. Chem. Soc. **65**, 179 (1943).
[7] D. M. Simpson, J. Chem. Phys. **15**, 846 (1947).

Joshi-Effect

K. R. DIXIT
Royal Institute of Science, Bombay, India
May 10, 1948

IN recent years a large number of papers have been published on the Joshi-effect.[1] The effect may be described as follows: An alternating field is applied to gases at low pressures and the gaseous current is measured. It is observed that the gaseous current diminishes when the discharge tube is exposed to light. The diminution in the gaseous current, which is an ionic current, is observed in a number of gases, and with light of different wavelengths. As the frequency of the incident light is generally not sufficient to produce photoelectrons in the gas, we shall be justified in excluding the photoelectric effect from the plausible agents which could reduce the ionic current. In addition "photo-ionization" or "resonance excitation" leading to ionization" may occur. Both these effects will lead to an increase in the gaseous current. Their mechanisms are well known and hence they are not considered here. But it is necessary to remember that unless the experimental conditions are isolated, both these effects are likely to occur along with the Joshi-effect and this may lead to an increase in the current occasionally observed.[3]

It is a well-known fact that the gaseous ionic current can be written as

$$Q=\Sigma nev,$$

where n is the number of charged particles carrying a charge e and moving with a velocity v. Or it can be written as

$$Q=\Sigma nekX,$$

where k is the ionic mobility and X the field strength. Joshi and others observe a diminution in Q. From the above equation it can be seen that Q can be reduced by changing n or e or k. That is, a change in the discharge current is

produced either by changing the number of charged particles or their average charge or their mobility. In the low pressure discharge as observed by Joshi and others, a large number of metastable ions will be formed.[4] It has been pointed out by the author in that paper that "the chemical effects can be produced more conveniently by means of a high frequency discharge in a gas enclosed in a chamber." This is the type of discharge used in the study of the Joshi-effect and chemical effects are very easily produced in such a discharge. As pointed out above, the frequency of the light used is inadequate to produce photoelectrons in the gas used in the discharge tube. Under the circumstances it is but natural to assume that the role of light is to modify the chemical action which takes place in such a discharge tube.

We are therefore led to believe that the Joshi-effect is probably due to the change in the number of particles as a result of complex molecular formation or change in the ionic mobility or both. If this assumption is correct, a systematic study of the Joshi-effect may enable us to understand the mechanism of low pressure discharge. All experimental papers about the Joshi-effect published so far refer to number of gases studied at different pressures and exposed to light of different frequencies. In all these experiments the change in gaseous current is measured. But it will be clear from the above hypothesis that, to understand clearly the mechanism of the Joshi-effect, experimental data are required about the following points and workers in this branch would do well to study these points first.

1. Accurate determination, to the order of at least a microsecond, of the time lag between the switching on or off of the radiation and the reduction or restoration of the ionic current.

2. Accurate measurement in the change of the number of particles after exposure to light. (The change may be measured by a relative change of pressure by a method like that of Hutchinson and Hinshelwood;[5] or it may be determined spectroscopically by the study of the formation of quasi-molecules.)

3. Determination of the changes in the values of e/m and the ionic mobility under the conditions of the experiment. (These quantities should be measured before and after exposing the discharge tube to light. The determination could be made if necessary, by taking a portion of the gas in another discharge tube. This method of isolating a beam is commonly used in all molecular ray work.)

In the end it may be pointed out that unless these experiments are performed, it will not be possible to understand the mechanism of the Joshi-effect. All experiments other than the crucial experiments given above and all experiments in which conditions are not isolated will only add to the available experimental data and in no way clarify the obscure problem of the chemical effects of electrical discharge.

[1] K. Venkateswara Rao, Proc. Ind. Acad. Sci. **27**, 72 (1948). (This paper gives references to previous papers on the subject.)
[2] K. J. Laidler, J. Chem. Phys. **15**, 712 (1947).
[3] S. S. Joshi, Curr. Sci. **16**, 19 (1947).
[4] K. R. Dixit, "Chemical effects of electrical discharge," Curr. Sci. **6**, 163–180 (1937).
[5] Hutchinson and Hinshelwood, Proc. Roy. Soc. **117**, 131 (1928).

Resistivity in the Systems Sodium-Ammonia and Lithium-Ammonia

HANS JAFFE
The Brush Development Company, Cleveland, Ohio
April 27, 1948

IN a recent paper, Birch and MacDonald[1] report measurements of the resistance of solutions of sodium in ammonia frozen in a short glass tube either by slow or by rapid cooling. These resistance measurements, as well as time-temperature curves on the slowly frozen system, confirm the solidification point near −110°C discovered by Ruff and Zedner.[2] To explain the low resistances, down to the order of one-tenth ohm, found in the range from −110 to −185°C, Birch and MacDonald assume (p. 795) "the persistence of a liquid phase due to supercooling of the eutectic" of sodium metal and ammonia.

The existence of a supercooled phase in contact with one solid component (ammonia) over a range of 70°C appears highly improbable. A more natural explanation of the observed phenomena can be based on the assumption that the solidification point of the concentrated solution is due to the formation of a solid sodium-ammonia compound, containing about 1 mole Na to 5 mole NH_3, a possibility already considered by Ruff and Zedner.[2] This compound may not have a simple stoichiometric composition. The very low and reproducible resistivity of the frozen concentrated solutions and the slight positive temperature coefficient of this resistivity then appears as a property of the solid compound; the fairly low resistance observed in quick-frozen solutions of about one mole Na in 50 moles NH_3 is due to a continuous network of the solid compound in solid ammonia; and the gradual increase of resistance of such systems kept below the solidification point is caused by recrystallization of this network tending to make it discontinuous.

The existence of a solid compound of sodium and ammonia here proposed provides an analogy to the case of lithium whose saturated solution in ammonia was found[3] to have a sharp and reversible melting point at −181°C, with a small but definite heat of fusion. The solid formed was proved not to be a eutectic of lithium and ammonia but a true compound. Among the points of evidence were the persistence of the characteristic bronze color and the extraordinarily low resistivity of $15 \cdot 10^{-6}$ ohms·cm, which is one-fourth of the resistivity of the saturated liquid phase. The equivalent conductivity per atom of Li in the solid compound was shown to be about the same as in compact lithium metal at the same temperature. Such a relationship would be impossible in an eutectic of lithium metal and solid ammonia.

X-ray diffraction studies would furnish the conclusive proof of the existence of a sodium-ammonia compound and would illuminate its structure.

[1] J. Birch and D. K. C. MacDonald, Trans. Faraday Soc. **43**, 792 (1947); see also MacDonald, Mendelssohn, and Birch, Phys. Rev. **71**, 563 (1947).
[2] O. Ruff and J. Zedner, Berichte **41**, 1948 (1908).
[3] Hans Jaffe, Zeits. f. Physik **93**, 741 (1935).

Note on the Specific Heat of Sulfur Hexafluoride[1]

E. GERALD MEYER AND C. E. BUELL
Research and Development Division, New Mexico School of Mines, Albuquerque, New Mexico
September 15, 1947

THE current interest in fluorine compounds has stimulated the compilation of data on the various physical and chemical properties of these substances. A recent report by Schumb[2] gives properties of sulfur hexafluoride; data on C_p at high temperature were not available, and inasmuch as this information is needed in free energy and heat of formation derivations, the following calculations were undertaken.

Using methods outlined by Fowler and Guggenheim,[3] the C_p values shown in Table I were obtained. Spectroscopic data of Yost, Steffens and Gross[4] were used. A plot of C_p *versus* temperature was made as shown in Fig. 1. A smooth curve passing through the points was found to have an empirical equation

$$C_p = 37.41 + 0.0876\times10^{-3}T - 18.78\times10^{5}T^{-2}.$$

Over a temperature range of 600 to 5000°K the points did not deviate over 0.5 percent from the calculated curve. The average deviation was 0.15 percent.

TABLE I. Calculated heat capacity data from 298 to 5000°K.

T°K	C_p cal/°K mole	T°K	C_p cal/°K mole
298	22.93	2400	37.33
500	30.51	2500	37.36
600	32.40	2600	37.39
700	33.65	2700	37.41
800	34.53	2800	37.43
900	35.14	2900	37.45
1000	35.58	3000	37.47
1100	35.93	3200	37.50
1200	36.21	3400	37.52
1300	36.41	3600	37.54
1400	36.59	3800	37.56
1500	36.72	4000	37.58
1600	36.85	4200	37.59
1700	36.95	4400	37.60
1800	37.03	4600	37.61
1900	37.10	4800	37.62
2000	37.16	5000	37.63
2100	37.22		
2200	37.26		
2300	37.30		

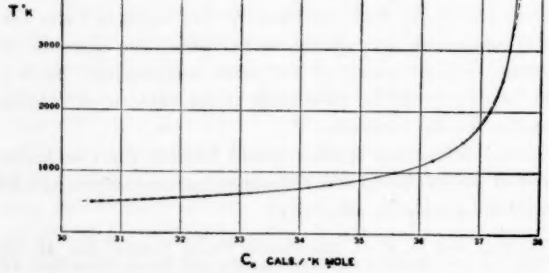

FIG. 1. Solid line represents a plot of the calculated heat capacity values. Dashed line is a plot of the empirical equation.

Using the foregoing equation with the data of Schumb[2] the following equations were computed for the free energy of formation and the heat of formation of the gas from $S_2(g)$ and $F_2(g)$.

$$\Delta F = -271{,}100 - 11.33T\ln T + 1.678\times10^{-3}T^2 + 9.39\times10^{5}T^{-1} + 171.2T$$

$$\Delta H = -271{,}100 + 11.33T - 1.678\times10^{-3}T^2 + 18.78\times10^{5}T^{-1}.$$

[1] This work was carried out in connection with the Applied Physics Laboratory of the Johns Hopkins University operating under Contract NOrd-9817, with the Navy Department, Bureau of Ordnance.
[2] W. C. Schumb, Ind. Eng. Chem. **39**, 421 (1947).
[3] Fowler and Guggenheim, *Statistical Thermodynamics* (The Macmillan Company, New York, New York, 1939).
[4] Yost, Steffens, and Gross, J. Chem. Phys. **2**, 311 (1934).

Thallium Bromide-Iodide Prism Spectroscopy in the Far Infra-Red†

W. LEWIS HYDE
Mallinckrodt Chemical Laboratory, Harvard University, Cambridge, Massachusetts
May 13, 1948

FOR some time exploratory measurements have been carried out in this laboratory on the infra-red absorption of various substances in the region 20 microns to 37 microns using a prism of thallium bromide-iodide[1] (KRS-5) similar to that employed by Plyler.[2]

The prism employed for most of the work had faces about 60 mm square and an apex angle of 18° 36′. The crystal was largely homogeneous and the surfaces were originally flat to within four fringes. Stray light was adequately eliminated by substituting a mirror of LiF for one of the Al-surfaced plane mirrors. Except as noted above, the spectrograph was that described by Gershinowitz and Wilson[3] with some later modifications.

By using gas cells 30 cm long with windows of 0.001″ polyethylene and 1 and 2 mm liquid cells with windows of 0.025″ polyethylene, the results listed in Table I were obtained.

The prism was maintained under a light clamp in our spectrometer for five months and then removed and reexamined. The faces were found to have deformed so as to

TABLE I.

Substance	Bands	Remarks
CH_3CCl_3	343 cm^{-1} very strong in vapor	Rubin *et al.* found Raman bands at 342 and 345 cm^{-1}.[a]
cis-$C_2H_2Cl_2$	405 cm^{-1} only 20% absorption in 2 mm liquid	Probably ν_7 assigned by Herzberg.[b] Raman band at 406 cm^{-1} seen by Paulsen[c]
CH_3OCH_3	407 cm^{-1}	Probably that seen by Crawford and Joyce[d] at 412 cm^{-1} in Raman
C_3H_8	No absorption. 5% between 270 and 410 cm^{-1}. 30 cm path, 76 cm pressure	

[a] Rubin, Levedahl, and Yost, J. Am. Chem. Soc. **66**, 279 (1944).
[b] G. Herzberg, *Infrared and Raman Spectra of Polyatomic Molecules* (D. Van Nostrand and Company, New York, 1945), p. 330.
[c] O. Paulsen, Zeits. Physik Chem. **B28**, 123 (1935).
[d] B. L. Crawford and L. Joyce, J. Chem. Phys. **7**, 307 (1939).

be about thirty fringes from flat. The angle was reduced 0.3 percent to 18° 33′ although the deviation for a given wave-length was almost the same as before, corresponding to a change in index ($\lambda = 5770$A) from 2.6396 to 2.6444. The quality of the visible spectrum was considerably reduced. This deterioration plus the wide slits used reduced the resolving power to about 10 wave numbers at 30 microns. The deterioration of KRS-5 certainly warrants further study if it is to be used extensively as a prism material.

† Assistance is gratefully acknowledged to the Engineer Research and Development Laboratories under a contract between them and the Baird Associates, and to the Office of Naval Research under Contract N5ori-76, T.O. V., with Harvard University. Our first prism was obtained through the kindness of Dr. P. H. Egli of the Naval Research Laboratory while the one currently in use, obtained from the Baird Associates, was cut and polished by F. Cooke (see J. Opt. Soc. Am. **37**, 984(A) (1947)) from ERDL Batch No. 23–2.

[1] O. F. Tuttle and P. H. Egli, J. Chem. Phys. **14**, 571 (1946).
[2] E. K. Plyler, J. Chem. Phys. **15**, 885 (1947).
[3] Gershinowitz and Wilson, J. Chem. Phys. **6**, 247 (1938).

The Isomerization of *n*-Butane-1-C^{13}

J. W. Otvos, D. P. Stevenson, C. D. Wagner, and O. Beeck
Shell Development Company, Emeryville, California
May 24, 1948

In a recent note,[1] data were presented showing that propane-1-C^{13} is reversibly converted into propane-2-C^{13} by an exclusively intramolecular mechanism in the presence of a water promoted aluminum bromide catalyst at *ca.* 25°C. An investigation of the reactions of *n*-butane-1-C^{13} in the presence of such a catalyst and at the same temperature has been carried out, using the same general methods previously outlined. The mass spectrometric analyses were supplemented, as needed, by low temperature distillation through a high efficiency Podbielniak column and infra-red spectrophotometric analyses.

The compositions of the initial normal butane and of the product after 12 and 1180 hours contact with the catalyst are given in Table 1. The product recovered after 12 hours reaction corresponds to 11.6 percent conversion of normal to isobutane, while that after 1180 hours corresponds approximately to the accepted equilibrium composition at 25°C.

It will be noted that the concentration of butane-C_2^{13} underwent no change in 1180 hours. Since at intermolecular redistribution equilibrium the concentration of butane-C_2^{13} would be 0.0131, it is apparent that, as was found to be the case for propane isomerization, the butane isomerization is exclusively intramolecular with respect to carbon atoms.

Comparison of the composition of the 12-hour product with the initial material reveals the *n*-butane-2-C^{13}, *i*-butane-1-C^{13}, and *i*-butane-2-C^{13} to have been formed from the *n*-butane-1-C^{13} in the ratios 2:3:1, respectively. These relative rates of formation of the three isomers of *n*-butane-1-C^{13} are in the ratio of their random statistical weights. Such rates of formation are most easily explained in terms of a single activated complex which may rearrange at random into the four butane-C^{13} isomers.

Table I. The isomerization of butane, catalyzed by aluminum bromide at 25°C.

Substance	Mole fraction $t=0$ hours	12 hours	1180 hours
n-C_4H_{10}-C_9^{13}	0.809	0.715	0.166
i-C_4H_{10}-C_9^{13}	0.000	0.094	0.643
n-C_4H_{10}-1-C_1^{13}	0.169_5	$.136_5$	0.020_4
n-C_4H_{10}-2-C_1^{13}	0.016_8	$.027_7$	0.017_8
i-C_4H_{10}-1-C_1^{13}	0.000_0	0.016_2	0.110_9
i-C_4H_{10}-2-C_1^{13}	0.000_0	0.005_4	0.036_9
C_4H_{10}-C_9^{13}	0.005_3	0.005_3	0.005_3

The results of these experiments provide no experimental basis for theories of the paraffin isomerization reaction which postulate attack of the molecule at a particular point, followed by the migration of a methyl group. Rather the experiments point toward a general activation of the molecule as a whole.

A comprehensive paper describing the synthesis of the various isotopic propanes and butanes, the analytical methods, and isomerization experiments is in preparation and will be submitted for publication in the near future.

[1] O. Beeck *et al.*, J. Chem. Phys. **16**, 255 (1948).

Free Volumes of the Metallic Elements at Their Melting Points

S. S. Penner
Jet Propulsion Laboratory, California Institute of Technology, Pasadena, California
May 17, 1948

The free volume model for the liquid and solid state has found application in various semi-empirical treatments of physico-chemical phenomena.[1–5] Eyring and co-workers[1,3,4] have given several equations for the free volume of a liquid, whereas Lennard-Jones[2] has derived an expression for the free volume of a solid in terms of the characteristic vibration frequency of the solid. The Kincaid-Eyring[4] formula for the free volume leads to results identical with those calculated from the Lennard-Jones equation[2] for a number of metallic elements at room temperature.[6]

It has been shown recently that the Lennard-Jones expression for the free volume can be obtained from a rate process treatment of melting by requiring that the free volume model for a liquid leads to the same result as a treatment based on the Einstein approximation of the solid.[6] This derivation of the Lennard-Jones formula for the free volume of a solid suggests application of this formula to a determination of the free volume at the melting point. Accordingly the free volumes v_f at the melting point have been calculated for a number of metallic elements by use of the relation

$$v_f = (RT/2\pi M\nu^2)^{\frac{1}{2}}, \qquad (1)$$

where R is the molar gas constant, T is the absolute temperature, M represents the atomic weight, and ν is the

TABLE I. The free volumes of the metallic elements at their melting points.

Element	Melting Point (°K)	$v_f \times 10^{27}$ (cc)	$v \times 10^{24}$ (cc)	$(v_f/v) \times 10^3$
Li	459	22.3*	21.7**	1.0**
Na	371	102	38.7	2.6
K	335	133	78.6	1.7
Cu	1356	16.7	13.3	1.3
Ag	1234	20.6	19.2	1.1
Au	1336	19.1	19.0	1.0
Be	1557	12.0	8.10**	1.5**
Mg	924	50.9	25.2	2.0
Ca	1083	61.2	42.9**	1.4**
Sr	1073	46.3	56.0**	0.83**
Zn	693	11.7	15.7	0.75
Cd	594	12.7	23.3	0.54
Hg	234	7.56	23.5	0.32
Cr	1888	10.2	12.5**	0.81**
Mn	1533	18.2	12.7**	1.4**
Fe	1808	13.2	13.4	0.98
Co	1753	15.1	11.0**	1.4**
Ni	1725	16.0	11.0**	1.5**
Mo	2893	16.0	15.6**	1.0**
Ru	>2223	>8.47	14.0**	>0.61**
Rh	2228	10.6	14.1**	0.75**
Pd	1828	18.1	16.1	1.1
Al	933	18.2	18.8	0.97
Ga	304	24.7	19.6**	1.3**
In	428	38.2	25.9**	1.5**
Tl	577	25.1	30.9	0.81
La	1099	35.0	37.5**	0.93**
Ti	2073	35.2	17.7**	2.0**
Zr	1973	24.3	23.7**	1.0**
Hf	>1975	>20.2	22.3**	>0.90**
Ge	1232	15.2	22.5**	0.68**
Pb	601	38.4	33.4	1.1
Sb	904	39.1	30.9	1.3
Bi	544	22.3	34.4	0.65
Ta	3123	25.9	18.1**	1.4**
W	3643	15.7	15.8**	0.99**
Re	3713	17.5	14.5	1.2
Os	2973	21.0	14.1**	1.5**
Ir	2623	11.5	14.3	0.80**
Pt	2028	15.6	17.1	0.91

* Since Seitz (See reference 7.) does not give the value for the characteristic vibration frequency of lithium, the value given in the Landolt-Börnstein *Tabellen* was used.
** Calculated by use of the room-temperature value for the density.

characteristic vibration frequency of the element under discussion. The value of ν was obtained from a compilation of the Debye characteristic temperatures given by Seitz.[7]

The total volume per molecule v, at the melting point, is given by the relation

$$v = M/N\rho \qquad (2)$$

where N is the Avogadro number and ρ is the density at the melting point. The calculated values of v_f, v, and the ratio v_f/v are summarized in Table I. For the elements for which the densities at the melting point were not readily available, the densities at room temperature were used. Use of room-temperature values for the density will yield values for v which are too small and values for v_f/v which are too large but will not alter the order of magnitude of the calculated results.

Reference to the values listed in Table I shows that the calculated free volumes at the melting point generally lie between 10×10^{-27} and 50×10^{-27} cc, whereas the free volumes per molecule at the melting point divided by the respective total volumes per molecule at the melting point are of the order of 10^{-3} for all of the elements listed. Some of the alkali metals have relatively large free volumes at the melting point, whereas mercury, cadmium, and germanium have relatively small free volumes at the melting point. A more detailed analysis indicates some regularities in the dependence of v_f/v on atomic number. Reference to Table I shows that for the elements of the first and second groups of the periodic system the ratio v_f/v decreases regularly with increasing atomic number except for the first member of each series. The behavior of the elements in the other groups of the periodic system appears to be less regular although some of the discrepancies may be removed if the densities at the melting points are used for each of the elements.

[1] S. Glasstone, K. J. Laidler, and H. Eyring, *The Theory of Rate Processes* (McGraw-Hill Book Company, Inc., New York, New York, 1941).
[2] J. E. Lennard-Jones and A. F. Devonshire, Proc. Roy. Soc. (London) **A163**, 53 (1937); *ibid.* **A165**, 1 (1938); *ibid.* **A169**, 317 (1939); *ibid.* **A170**, 464 (1939); J. E. Lennard-Jones, Proc. Phys. Soc. (London) **52**, 729 (1940).
[3] H. Eyring and J. O. Hirschfelder, J. Phys. Chem. **41**, 249 (1937).
[4] J. F. Kincaid and H. Eyring, J. Chem. Phys. **6**, 620 (1938).
[5] T. L. Hill, J. Phys. and Colloid Chem. **51**, 1219 (1947).
[6] S. S. Penner, to appear shortly in the Journal of Physical and Colloid Chemistry.
[7] F. Seitz, Table XXXIV, *The Modern Theory of Solids* (McGraw-Hill Book Company, Inc., New York, New York, 1940).